

Many-Body Approaches to Quantum Dots

by

Marte Hoel Jørgensen

THESIS
for the degree of
MASTER OF SCIENCE

(Master in Computational Physics)



Faculty of Mathematics and Natural Sciences
Department of Physics
University of Oslo

June 2011

Acknowledgements

First I would like to thank my supervisor Morten Hjorth-Jensen. During these two years I've come to know him by his enthusiasm and eagerness for his profession. It's been an inspiration and subject for admiration. Thank you for providing me with an interesting topic, and for your calmness and guidance along the way.

My gratitude also goes out to my fellow student and partly collaborator Yang Min Wang. Thank you for your propelling enthusiasm, always challenging my understanding.

My fellow students David Skålid Amundsen and Jørgen Trømborg deserve a thanks for great help when L^AT_EX would not cooperate with me.

To the former master students Magnus Pedersen Lohne and Lars Eivind Lervåg, thank you for sharing your knowledge and experience by answering my emails. Also, thank you Gustav Jansen for every now and then taking the time to answer questions, despite being in the final stages of your Ph.D.

Last but not least I thank my family. Mom, Dad, Magnus and Monne, thank you for being only a phonecall away with love and support. Thank you Jens Gaarder for looking out for my wellbeing during this time. It would not have been the same without your love, lunch-packages and attention.

Marte Hoel Jørgensen

Contents

Acknowledgements	3
Preface	7
I Theory	11
1 Quantum Mechanics	13
1.1 History of Quantum Mechanics	13
1.1.1 Black Body Radiation	14
1.1.2 The Photoelectric Effect	15
1.1.3 The Compton Effect	15
1.1.4 Summary	16
1.2 Theory of Quantum Mechanics	16
1.2.1 Postulates of Quantum Mechanics	17
1.2.2 The Time-Independent Schrödinger Equation	21
1.2.3 Quantum State Representation	22
1.2.4 Intrinsic Spin	25
1.2.5 Final Wave Function	27
2 Many-Body Theory	29
2.1 The Many-Body Problem	29
2.2 Identical Particles	30
2.3 Non-Interacting and Interacting Systems	34
2.4 Second Quantization	36
2.4.1 Creation and Annihilation Operators	36
2.4.2 Representation of Operators	38
2.4.3 Wick's Theorem	40
2.4.4 Quasi-Particle Formalism	43
3 Quantum Dots	45
3.1 Quantum Dots: structure and applications	45
3.2 Theoretical approximation of 2D Quantum Dots	46
3.2.1 Schrödinger Equation for Spherical Symmetric Potentials	47
3.2.2 One-Electron Parabolic Quantum Dot	49
3.2.3 Two-Electron Parabolic Quantum Dot	56
3.2.4 Hamiltonian of N-electron Quantum Dots	59

3.2.5	Dimensionality Scaling	60
4	Hartree-Fock Method	61
4.1	Introducing HF	61
4.2	HF equations	62
5	Coupled Cluster method	67
5.1	Introducing Coupled Cluster	67
5.2	Wave Function and Cluster-Operators	68
5.3	Formal Coupled Cluster Theory	71
5.4	Coupled Cluster Singles and Doubles	73
5.4.1	Normal-Ordering of the Hamiltonian	73
5.4.2	Energy equation: an Algebraic derivation	75
5.4.3	Diagrammatic approach	81
5.4.4	Diagrammatic CCSD Energy equation	85
5.4.5	Diagrammatic CCSD Amplitude equations	87
5.4.6	Diagram Rules	96
II	Implementation and Results	101
6	Implementation	103
6.1	Hartree-Fock Implementation	103
6.1.1	Code Structure and Algorithm	103
6.1.2	Code Validation	113
6.2	CCSD Implementation	113
6.2.1	Code Structure and Algorithm	113
6.2.2	CCSD With HF Basis	162
6.2.3	Code Validation	171
7	Computational Results	175
7.1	Standard Interaction	175
7.1.1	Standard Interaction Results: HMO basis	176
7.1.2	Standard Interaction Results: HF basis	188
7.2	Effective Interaction	192
7.2.1	Effective Interaction Results: HMO basis	193
7.2.2	Effective Interaction Results: HF basis	200
7.3	Frequency Analysis	204
7.4	The Wigner Crystal Limit	210
7.5	Tables	214
8	Conclusion	223

Preface

In this thesis we study the system of several interacting electrons in two dimensions. These systems are named quantum dots¹. In real life quantum dots are fabricated by confining electrons in small regions between layers of semiconductors. Theoretically we simulate what we call the parabolic quantum dots by confining electrons in a two-dimensional oscillator potential. Quantum dots are man-made devices, which during the last couples of decades have developed into a new research area in condensed-matter physics, and a popular field in solid state physics. The popularity of the quantum dots is due to their similarities with atoms, therefore quantum dots are known as "artificial atoms". The size of the quantum dots range from a couple of nanometres to the order of one micrometer, and they can hold a couple to several hundred or thousand electrons. Thus, quantum dots are much larger than real atoms, and this makes it possible to conduct experimental research on quantum dots not accessible at the atomic-scale. One can say that quantum dots constitute accessible laboratories of analogues to so far unexplored physics. The fact that we can explore quantum dots on a microscopic scale, and at the same time observe quantum effects, makes them excellent components in research studies. Quantum phenomena like tunneling, entanglement and magnetization are all observed in quantum dots. The applications of quantum dots are many. Especially, their electrical and optical properties make them attractive components for integration in electronic devices. Quantum dots also prove to be viable in both solar cells and biological applications. In order to develop and perhaps find new areas of application it is important to acquire the basic theory and behavior of quantum dots. In order to do acquire this knowledge, we can study quantum dots by utilizing different many-body methods. It is therefore important to have accurate methods where we know all advantages and disadvantages, and that is what this thesis aims at.

The aim of this thesis is to study quantum dots numerically by applying the ab initio method of Coupled Cluster Singles and Doubles (CCSD). The coupled cluster (CC) theory has over the last fifty years proved to be one of the most reliable and computationally affordable methods for solving the electronic Schrödinger equation [1]. We will study the parabolic quantum dots described in chapter 3, in order to investigate the reliability and accuracy of the CCSD method. Our main focus lies in applying the CCSD method on different sizes of the model space, when the confinement potential is relatively weak. In systems where the confinement potential is weak, the potential energy becomes dominant, and this leads to localization of the electrons. The weak confinement potential serves to undermine the CCSD assumption that the ground state wave function can be expressed by one Slater determinant only. It is therefore interesting to test the accuracy of the CCSD method for these confinement potentials. The drawback of wave function based

¹The quantum dots are discussed in detail in chapter 3.

methods like CC, is that the dimensionality scales almost exponentially with the number of particles in the system. The solution to this scaling problem is commonly to introduce a renormalized Coulomb interaction called an effective interaction. We have therefore conducted our calculations utilizing this effective interaction in addition to the standard Coulomb interaction. The last element to our studies is the choice of single-particle basis for our Slater determinants. We have used both a harmonic oscillator basis and a Hartree-Fock basis in our calculations.

In order to conduct the numerical analysis of quantum dots by applying the CCSD method, we have improved and extended the CCSD C++ code developed by Magnus P. Lohne in his thesis work [2]. By implementing a new memory-saving system for handling the interaction elements, and improving some of the calculation techniques, we obtained a significant speed-up of the CCSD code. In addition we developed our own Restricted Hartree-Fock C++ code. We have embedded this Hartree-Fock code in the CCSD program in order to enable the use of a Hartree-Fock basis.

Thesis Structure

The thesis is divided into two main parts *Theory* and *Implementation and Results*. The first part includes chapters 1-5, and presents the theoretical foundation of the thesis. The theory is organized as follows.

- Chapter 1 presents the theory of non-relativistic quantum mechanics. We give some historical aspects behind the developments and the discoveries which led to the theory of quantum mechanics. Further we introduce the fundamental postulates with focus on the single-particle theory. We cover some of the characteristic aspects like Schrödinger's equation and intrinsic spin.
- Chapter 2 introduces the non-relativistic many-body theory, i.e. quantum mechanics for systems consisting of more than one particle. We discuss basic quantum mechanical concepts like identical particles and properties of the wave function.
- Chapter 3 gives an introduction to quantum dots. We present the structure and applications of quantum dots. We also consider their theoretical description, where we discuss the Hamiltonian, and solve the Schrödinger equation for one and two electron quantum dots.
- Chapter 4 presents the theory behind the Hartree-Fock (HF) method. The basic idea of the theory is given, followed by the derivation of the HF equations.
- Chapter 5 introduces the Coupled Cluster theory. First the formal theoretical aspects of this theory is presented, before the focus is set on the Coupled Cluster Singles and Doubles (CCSD) method. For the CCSD method we derive the energy and amplitude equations, where we consider both an algebraic and a diagrammatic approach.

The second part of this thesis includes chapters 6-8, and presents the implementation of our computational effort and the obtained results.

- Chapter 6 contains the documentation of the CCSD code we have improved and extended, in addition to the documentation of the HF code we have developed. The documentation consists of both code examples and detailed description of the structure. The main focus lies on the CCSD method, for which we derive the implemented expressions in detail.
- Chapter 7 present our numerical results. We discuss and analyse the results in relation to corresponding results obtained by other many-body methods.
- Chapter 6 summarizes and concludes the work conducted in this thesis.

Part I

Theory

Chapter 1

Quantum Mechanics

The theory of quantum mechanics was founded in the beginning of the 20th century. Experiments conducted in the late 19th century suggested that the classical picture of mechanics, based on Newton's laws of motion, needed some reconsideration. From this grew the new theory of quantum mechanics concerning physical systems on the scale of atoms and subatomic particles.

In this chapter the history of quantum mechanics is presented. The first section gives a picture of how the theory came to be developed. The second section is devoted to the postulates constituting the theory of quantum mechanics.

1.1 History of Quantum Mechanics

Newton's formulation and publication in 1687 of the classical laws and equations of motion has had a tremendous effect on the development of the theory of physics. Until the end of the 19th century classical theoretical physics developed by exploring these equations of motion for different systems of matter. The knowledge from experiments was united with theory by introducing new equations and variables or modifying old ones. This scheme gave not only success, but seemed to progress towards simplicity and unity supporting the truth of the theory even more. The desire to unify the various branches of science has always been one important preoccupation of physicists. However, in the beginning of the 20th century it became clear that not all observed phenomena could be explained in terms of the classical mechanics and electromagnetic theory.

The experiments made in the early 20th century were not the first signs of inadequacy in classical theory. In 1752 the Scottish scientist Thomas Melvill discovered the sodium line, and with the measurements of the sunlight spectrum conducted by the German scientist Joseph von Fraunhofer in 1814, the foundation of spectroscopy was made. This phenomenon could not be explained by known theory. When the Swiss mathematician Johann Jacob Balmer proposed his empirical formula for the visible spectral lines of the hydrogen atom in 1885, the lack of theoretical explanation was obtrusive, but did not create a crisis.

In 1887 the Michelson-Morley experiment was conducted by the two American scientists who the experiment is named after. This experiment aimed at revealing the motion of earth relative to ether¹, and by this also verifying the very existence of ether. This exper-

¹Ether was thought to be the medium in which light propagates

iment failed. The lack of evidence on ether, along with the Scottish scientist James Clerk Maxwell's theory of electromagnetism, inspired the German scientist Albert Einstein in developing the *Theory of Relativity* around 1905. This theory rejected the notion of absolute time and proposed Newtonian Mechanics to be an approximation of Relativistic Mechanics valid only in the limit where the velocities of the particles are negligible compared to the velocity of light. This theory did not undermine the credibility of classical theory, but can be viewed as the start of a trend of new thinking.

At the turn of the century experimentalists followed two main fields of interest. One was to analyse the microscopic structure of matter, the other was to explore the mutual interaction of material and their interaction with the electromagnetic field. The search for microscopic structure of matter led to the discovery of the electron in 1897 by the British scientist J.J. Thomson. With this discovery came the theory of electron interaction with electromagnetic waves, where the Dutch scientist Lorentz made a great contribution.

Gradually the hypothesis of atoms and molecules got accepted much because of the studies of Brownian motion². The knowledge of microscopic structure grew with the discovery of radioactivity in 1896 done by the French scientists Becquerel, Marie and Pierre Curie. This was the first manifestation of the properties of atomic nuclei in addition to a great aid for investigation of atomic structure through alpha radiation. The British scientist Ernest Rutherford utilized this aid with studies of alpha scattered particles on different atoms. This led to the first modern picture of an atom.

New knowledge on the microscopic scale made scientists able to perform new experiments, where the first disagreements with classical theory became evident. These disagreements imposed a crisis which could not be disregarded. Examples of phenomena which could not be explained are, black body radiation, the photoelectric effect, and the Compton effect. The following sections give a short introduction to the three fields of experiments which possessed disagreements with classical theory.

1.1.1 Black Body Radiation

All matter is source of electromagnetic radiation, where intensity and frequency depends on the temperature of the matter. By definition a black body³ absorbs all received radiation and it emits radiation as a function of temperature only.

Experiments studying spectral distribution of electromagnetic radiation in thermodynamical equilibrium with matter, was conducted using a black body. From classical theory, which will not be encountered in detail here, one could assume that inside the cavity, approximating a black body, standing electromagnetic waves would occur. These waves behave like a mechanical harmonic oscillator for which classical statistical mechanics apply. This led to a radiation flux ω through the hole in the cavity given by

$$\omega = 2\pi \frac{\nu^2}{c^3} k_B T,$$

where k_B is Boltzmann's constant and c the velocity of light. This theoretical result did not agree with the experimental results, especially for high frequencies. It also meant

²Brownian motion is the disordered motion of particles suspended in water, named after R. Brown who first observed it in 1827

³One can achieve an approximate black body by making a cavity with a small entrance hole which will absorb all incoming radiation

that by integrating over all frequencies, the rate of radiation from a black body would be infinite.

In 1900 the German physicist Max Planck solved the discrepancy between theory and observation by renouncing classical ideas of matter-radiation interaction. He assumed that the energy exchange between matter and radiation is discrete given as energy quanta proportional to the frequency of the radiation.

$$E_\nu = nh\nu \quad n = 0, 1, 2, \dots$$

Here h is Planck's constant. This led to the radiation flux given by

$$\omega = 2\pi \frac{\nu^2}{c^3} \frac{h\nu}{\exp(\frac{h\nu}{k_B T}) - 1}.$$

Planck's result did coincide with experiments when Planck's constant was chosen to take the value $6.624 \cdot 10^{-34}$ Js. This theory of energy quantification was a revolutionary new idea, and it marks the beginning of quantum physics.

1.1.2 The Photoelectric Effect

The photoelectric effect is the phenomenon that electromagnetic radiation of matter, for example metal, causes emission of electrons. Observations made at the turn of the 19Th century showed that different matter had different threshold frequencies ν_0 at which emission occurred. Experiments also showed that the kinetic energy of the emitted electron did depend linearly on the frequency of radiation, not the intensity. The kinetic energy of the electron is given by

$$E_{kin} = h(\nu - \nu_0),$$

where ν is the frequency of the electromagnetic radiation. The fact that the intensity had no effect on the emission, could not be explained by classical theory.

After Planck introduced his theory on black body radiation, the general trend in the scientific community was to try and reconcile Planck's ad hoc hypothesis with the wave theory. Einstein took this further by assuming that electromagnetic radiation itself consisted of particles called photons with energy $h\nu$ and velocity c (equal velocity of light in vacuum). This assumption explained the relation between energy and frequency. When one electron absorbs a photon, some energy W is required to free the electron and the rest constitutes the kinetic energy of the electron given by

$$E_{kin} = h\nu - W,$$

where $W = h\nu_0$ and an increase of intensity would only result in more photons. This theory did coincide with experimental results, and the constant h turned out to be Planck's constant.

1.1.3 The Compton Effect

The Compton effect, observed by the American physicist Arthur H. Compton, might have been the indication of photon theory that won the skeptics over. In 1923 Compton conducted scattering experiments with high energy photons, found in X-rays among others.

These radiations caused a release of electrons in the target at the same time as the radiation experienced a shift in wavelength. The shift did depend on the angle of the incident radiation, and by this Compton showed that the effect was a result of a collision between two particles.

1.1.4 Summary

The failure of classical mechanics can be viewed in relation with two types of effects. The first effect is that a physical quantity according to a classical view could take on a continuous range of values, but through comparison with experiments was found to take on discrete values. Examples of these quantities are energies of electromagnetic waves and of lattice vibrations at given frequency, or the energies and angular momenta associated with electronic orbits in the hydrogen atom. The second effect is that of wave-particle duality. Through diffraction and interference effects the wave nature of light was apparent. At the same time the photoelectric and the Compton effects revealed the particle nature of light. This duality was not predicted by the classical theory.

In light of these discrepancies between classical theory and experimental results, quantum mechanics needed to encompass these effects. The next section will give an outline of how this was encountered in the theory of quantum mechanics. The historical facts rendered in this section, and more, can be found in [3], [4], [5] and [6]

1.2 Theory of Quantum Mechanics

The basic assumptions in quantum mechanics are radically different from those in classical mechanics, and they constitute a different way of considering nature. The basis of quantum mechanical theory is the postulates derived from intuition and analogy with classical concepts. The development from this basis resulted in predictions standing the test of both classical systems and systems indicating the inadequacy of classical theory.

The fundamental differences in quantum mechanics compared to classical mechanics can be outlined as follows:

- **Quantization:** Many physical quantities can take only certain discrete values.
- **Wave-Particle dualism:** Both electromagnetic radiation and particles possess wave-properties and particle-properties.
- **Probability interpretation:** The quantum mechanical description can only give the probability of finding a particle at a certain position.
- **Uncertainty principle:** The nature pose fundamental restrictions on the precision which a physical quantity can be measured by.
- **Creation and annihilation:** Any particle can be created and destroyed.

In the sections below we first give an outline of the fundamental postulates of quantum mechanics, and continue with some notions on basic execution.

1.2.1 Postulates of Quantum Mechanics

Every physical theory needs to be founded on some fundamental hypothesis or postulates⁴. The theory of quantum mechanics is no different. This section will present these postulates in a similar manner as presented in [6], [7] and [8].

Postulate 1: A quantum state of an isolated physical system is described by a vector in a complex and linear vector space, called Hilbert space \mathcal{H} .

The physical Hilbert space is an abstract complex vector space, finite or infinite, where an inner product is defined. The inner product associates a scalar value, complex or real, to each pair of vectors in the vector space. Note that the term vector space does not necessarily mean that we are dealing with vectors. In quantum mechanics the Hilbert space is defined as the space of functions that can be normalized either to unity or to the Dirac delta function. These functions are what we call state vectors or wave functions, and they are often denoted by ψ or in *bra-ket* notation $|\psi\rangle$. The interpretation of the quantum state is based on probability. Max Born stated in 1926 that the probability of finding a particle in the position x at time t is given by $|\psi(x, t)|^2$

The inner product of two functions is defined as follows:

$$\langle\psi_\alpha|\psi_\beta\rangle = \int \psi_\alpha^*(x)\psi_\beta(x)dx, \quad (1.1)$$

where $*$ is the complex conjugated function.

The *bra-ket* notation is a standard notation, developed by the physicist Paul Dirac, for describing quantum states. In this notation a quantum state is denoted by $|\alpha\rangle$, called a “ket”. For each quantum state in the Hilbert space there exists a dual state $\langle\alpha|$ in a dual vector space called a “bra”. The connection between two dual vectors is given by the inner product $\langle\alpha|\beta\rangle$. The properties read:

$$\langle\alpha|\beta\rangle = \langle\beta|\alpha\rangle^*, \quad (1.2)$$

$$\langle\alpha|(c_1|\beta\rangle + c_2|\gamma\rangle) = c_1\langle\alpha|\beta\rangle + c_2\langle\alpha|\gamma\rangle, \quad (1.3)$$

$$\langle\alpha|\alpha\rangle \geq 0, \quad (1.4)$$

where c_1 and c_2 are complex numbers and $*$ is the complex conjugate. Note that

$$(c|\alpha\rangle)^* = c^*\langle\alpha|. \quad (1.5)$$

A function is said to be *normalized* if its inner product with itself is one. Two functions are *orthogonal* if their inner product equals zero. A set of two or more functions is *orthonormal* if all of the functions are normalized and the inner product of all pairs equal zero.

Assume given a discrete orthonormal basis \mathcal{B} for the d -dimensional Hilbert space

$$\mathcal{B} = \{|i\rangle\}_{i=1}^d. \quad (1.6)$$

⁴A Postulate is like an Axiom, an assumption that does not need to be proved, but is considered to be self evident or a subsequent necessity

The orthonormal basis constitutes the following relation between its basis function

$$\langle i|j\rangle = \delta_{ij}, \quad (1.7)$$

and the completeness relation reads

$$\sum_i |i\rangle\langle i| = \mathbb{1}. \quad (1.8)$$

Here $\mathbb{1}$ the unity matrix and, δ_{ij} is the Kronecker delta, viz.

$$\delta_{ij} = \begin{cases} 0 & i \neq j \\ 1 & i = j \end{cases}. \quad (1.9)$$

The completeness relation is a necessity for the basis to be complete, meaning that any function in \mathcal{H} can be expressed as a linear combination of the basis vectors. By developing the quantum state $|\psi\rangle$ in this basis we obtain

$$|\psi\rangle = \sum_{i=1}^d |i\rangle\langle i|\psi\rangle = \sum_{i=1}^d c_i |i\rangle. \quad (1.10)$$

The set of basis vectors is not always discrete. In the case of continuous basis vectors the orthonormal relation is obtained by the Dirac-Delta function

$$\langle k|k'\rangle = \delta(k - k'). \quad (1.11)$$

The completeness relation is then given as an integration

$$\int dk |k\rangle\langle k|. \quad (1.12)$$

In similar manner the quantum state $|\psi\rangle$ can be written as

$$|\psi\rangle = \int |k\rangle\langle k|\psi\rangle dk = \int c(k) |k\rangle dk, \quad (1.13)$$

Postulate 2: Each physical observable A of a system is associated with a linear, Hermitian operator \hat{A} acting on the Hilbert space.

As postulated the operator of an observable is Hermitian i.e.

$$\hat{A} = \hat{A}^\dagger, \quad (1.14)$$

where \hat{A}^\dagger is the Hermitian conjugate of \hat{A} . Fundamental relations of the Hermitian conjugate reads:

$$(\hat{A}^\dagger)^\dagger = \hat{A}, \quad (1.15)$$

$$(c\hat{A})^\dagger = c^* \hat{A}^\dagger, \quad (1.16)$$

$$(\hat{A} + \hat{B})^\dagger = \hat{A}^\dagger + \hat{B}^\dagger, \quad (1.17)$$

$$(\hat{A}\hat{B})^\dagger = \hat{B}^\dagger \hat{A}^\dagger, \quad (1.18)$$

where $*$ is the complex conjugate.

The Hermitian conjugate is defined by the following relation, which has to be satisfied for all vectors α and β in \mathcal{H}

$$\langle \alpha | \hat{A}^\dagger | \beta \rangle = \langle \beta | \hat{A} | \alpha \rangle^*. \quad (1.19)$$

The Hermitian restriction on all operators comes from the fact that all expectation values must be real. When measuring an observable, a complex result makes no sense. The expectation value $\langle A \rangle$ of an observable A for a quantum state $|\psi\rangle$ therefore reads

$$\langle A \rangle = \langle \psi | \hat{A} \psi \rangle = \langle \hat{A} \psi | \psi \rangle = \langle \psi | \hat{A} | \psi \rangle = \int \psi^*(x) \hat{A} \psi(x) dx. \quad (1.20)$$

To demystify the concept of operators we give two examples. In the one dimensional case, the position operator \hat{x} in a position representation is given by

$$\hat{x} = x \quad (1.21)$$

Similar the momentum operator \hat{p} in the position representation reads

$$\hat{p} = \frac{\hbar}{i} \frac{d}{dx}, \quad (1.22)$$

where \hbar is the reduced Plank's constant $\hbar = \frac{h}{2\pi}$, and i is the imaginary unit number defined by $i = \sqrt{-1}$. For explanation on the representation comment see section 1.2.3. If the order in which two operators act on a wave function is indifferent, the two operators are said to *commute*, i.e.

$$[\hat{A}, \hat{B}] = \hat{A}\hat{B} - \hat{B}\hat{A} = 0. \quad (1.23)$$

The position and momentum operator do not commute, their commutation relation is given by

$$[\hat{x}, \hat{p}_x] = i\hbar. \quad (1.24)$$

Postulate 3: The only measurable values related to an observable \hat{A} are given by its eigenvalues. Since the operators of the observables satisfy the conditions given in postulate 2, the eigenvectors of such operators define a complete, orthonormal set of vectors.

The eigenvalues with corresponding eigenvectors are solutions of the eigenvalue equation given by

$$\hat{A}|a_i\rangle = a_i|a_i\rangle, \quad (1.25)$$

where a_i is the eigenvalue and $|a_i\rangle$ represent the corresponding eigenvector. The eigenvectors represent a complete set of vectors i.e.

$$\sum_{i=1}^d |a_i\rangle\langle a_i| = \mathbb{1}, \quad (1.26)$$

d is the dimension of \mathcal{H} . The Hermitian operator can then be written in terms of its spectral decomposition

$$\hat{A} = \sum_{i=1}^d a_i |a_i\rangle\langle a_i|. \quad (1.27)$$

If the system is in the state $|\psi\rangle$, and if the observable has a degeneracy⁵, the probability of measuring an eigenvalue a_i reads

$$p_i = \sum_{n=1}^g |\langle a_{in} | \psi \rangle|^2, \quad (1.28)$$

where g is the degree of degeneracy, meaning the number of eigenstates with the same eigenvalue. In the non-degenerated case $g = 1$

An ideal measurement of an observable A changes the state vector by leaving it in the state of the corresponding eigenvector of the measured eigenvalue. This is known as the *collapse of the wave function*. Note that the classical meaning of ideal measurement is when new information is collected without disturbance of the system. In the quantum mechanical case the *Heisenberg uncertainty principle* states that reducing the uncertainty of one observable by measurement, will necessarily increase the uncertainty of other observables. Thus, ideal measurements cannot be regarded as having no influence on the quantum system.

Postulate 4: The time evolution of the state vector $|\psi\rangle$ in the Schrödinger picture is defined by the Schrödinger equation of the form

$$i\hbar \frac{d}{dt} |\psi(t)\rangle = H |\psi(t)\rangle, \quad (1.29)$$

where H is the linear Hermitian operator called the Hamiltonian of the system. This operator is usually identified with the energy observable of the system.

Given the state vector at an initial time t_0 , the Schrödinger equation will determine the state vector at both earlier and later times t as long as the system stays isolated. The information about the dynamics of the system is contained in the Hamiltonian. The dynamical evolution of the state vector can be expressed by a time evolution operator, also called a propagator $\hat{U}(t, t_0)$. Thus a state vector at any time t can be expressed by the known state vector at time t_0 on the form

$$|\psi(t)\rangle = \hat{U}(t, t_0) |\psi(t_0)\rangle. \quad (1.30)$$

Assuming that H is independent of time, then the approach for finding an expression for the propagator is to find the eigenvalues and eigenvectors of H , and construct the propagator in terms of these (see [7] for more details). The result reads

$$\hat{U}(t, t_0) = e^{-\frac{i}{\hbar} \hat{H}(t-t_0)}. \quad (1.31)$$

Since H is Hermitian it follows that $\hat{U}(t, t_0)$ is unitary, i.e.

$$\hat{U} \hat{U}^\dagger = \hat{U}^\dagger \hat{U} = \mathbb{1}. \quad (1.32)$$

This result leads to the fact that the time evolution of a state vector $|\psi(t)\rangle$ can be viewed as a rotation in Hilbert space. Consequences of a rotational view is that the norm of the state vector $\langle \psi(t) | \psi(t) \rangle$ is invariant, thus a normalized state will stay normalized independent of the rotation. Another consequence is that by choosing a new basis, a new

⁵when two or more eigenvectors have the same eigenvalue

representation also called a picture is constructed. The calculation of physical entities will not be affected by this. As mentioned above, this derivation is made in the Schrödinger picture, but infinitely many pictures are possible, each labeled by how the basis is rotating. For a more elaborate derivation, see the chapter on postulates in [7].

To sum up, given an initial state $|\psi(t_0)\rangle$, the state at $t > t_0$, taken that the system is isolated and the Hamiltonian is time independent, reads

$$|\psi(t)\rangle = e^{-\frac{i}{\hbar}\hat{H}(t-t_0)}|\psi(t_0)\rangle. \quad (1.33)$$

The result for the time dependent Hamiltonian is somewhat more complex, see [7] and [8] for the derivation.

1.2.2 The Time-Independent Schrödinger Equation

In this section we consider the single particle system with the Hamiltonian

$$\hat{H} = \hat{T} + \hat{V}. \quad (1.34)$$

where \hat{T} is the kinetic energy and \hat{V} is the potential energy of the system. The dynamic of the system is governed by the Schrödinger equation, explicitly given in bra-ket notation in eq. (1.29). In the coordinate picture this equation reads

$$\begin{aligned} i\hbar \frac{\partial}{\partial t} \Psi &= H\Psi, \\ &= -\frac{\hbar^2}{2m} \nabla^2 \Psi + V\Psi, \end{aligned} \quad (1.35)$$

where ∇^2 is the Laplacian. The Schrödinger equation is a logically analogue to Newton's second law in classical mechanics. It determines the wave function $|\psi(t)\rangle$ for all future time (see postulate 4 in section 1.2.1), just as Newton's second law determines $x(t)$ for all future time.

In the case where the Hamiltonian is independent of time, the Schrödinger equation can be solved by *separation of variables*. The approach is to assume that the wave function is separated in position \vec{r} and time t

$$\Psi(\vec{r}, t) = \psi(\vec{r})\phi(t). \quad (1.36)$$

Inserted into the Schrödinger equation, this reduces the partial differential equation into two ordinary differential equations with the separation constant E , viz.

$$i\hbar \frac{1}{\phi} \frac{d\phi}{dt} = E, \quad (1.37)$$

$$\hat{H}\psi = E\psi. \quad (1.38)$$

The solution of eq. (1.37) is found by multiplying through with dt and integrating. The eq. (1.38) is called the *time-independent Schrödinger equation*. The final solution of the wave function is called *stationary states* and reads

$$\Psi(\vec{r}, t) = \psi(\vec{r})e^{-\frac{i}{\hbar}Et}. \quad (1.39)$$

The reason for this name has to do with the fact that the probability density, given by the wave function squared, is independent of time, see eq. (1.40). The same applies for every expectation value, which is constant in time.

$$|\Psi(\vec{r}, t)|^2 = \Psi^*(\vec{r}, t)\Psi(\vec{r}, t) = \psi^*(\vec{r})e^{\frac{i}{\hbar}Et}\psi(\vec{r})e^{-\frac{i}{\hbar}Et} = |\psi(\vec{r})|^2. \quad (1.40)$$

Another property of the separable solution is that every measurement of the total energy, represented by the Hamiltonian, is certain to return the value E , meaning that they are states of definite total energy.

The time-independent equation yields an collection of solutions $\psi_n(\vec{r})$ with associated vales of the separation constant E_n , thus there is a wave function for each allowed energy. This does not constitute a problem since the time-dependent Schrödinger equation has the property that any linear combination of solutions is also a solution. Once the separable solutions are determined, this gives rise to a general solution of the time dependent Schrödinger equation on the form

$$\Psi(\vec{r}, t) = \sum_n c_n \psi_n e^{-\frac{i}{\hbar}E_n t}, \quad (1.41)$$

where c_n needs to be determined so as to fit the initial conditions of the system.

Considering the unrealistic restriction made in eq. (1.36), it would not be strange if we were to assume that we would find only a small subset of all solutions. But in light of the properties of the separable solutions, construction of the most general solution as in eq. (1.41) turned out to be possible.

In terms of the bra-ket notation and the time propagator, see postulate 4 in section 1.2.1, the general solution takes the analytical form represented in eq. (1.44). The time independent Schrödinger equation reads in bra-ket notation:

$$\hat{H}|\theta_n\rangle = E_n|\theta_n\rangle. \quad (1.42)$$

Determination of the eigenvalues E_n and the corresponding eigenvectors $|\theta_n\rangle$ results in the following expression for the wave function at time t_0

$$|\psi(t_0)\rangle = \sum_{n=1}^d \langle\theta_n|\psi(t_0)\rangle|\theta_n\rangle = \sum_{n=1}^d c_n|\theta_n\rangle. \quad (1.43)$$

where d is the dimension of \mathcal{H} , see postulate 1 section 1.2.1. The wave function at time $t > t_0$ reads

$$|\psi(t)\rangle = e^{-\frac{i}{\hbar}H(t-t_0)}|\psi(t_0)\rangle = \sum_{n=1}^d \langle\theta_n|\psi(t_0)\rangle e^{-\frac{i}{\hbar}E_n(t-t_0)}|\theta_n\rangle. \quad (1.44)$$

To recapitulate this section; given a time independent Hamiltonian and an initial wave function at time t_0 , the wave function at time $t > t_0$ can be determined by solving the time-independent Schrödinger eqs. (1.38) and (1.42).

1.2.3 Quantum State Representation

Given an ordinary three dimensional vector \vec{V} , for most people the natural way of describing this vector is in terms of Cartesian coordinates as components of the axis x, y and

z . However two different persons could have chosen different axes in their description, thus obtaining different components, but that would not mean that the vectors was not the same. This also apply to the quantum mechanical system described by a function corresponding to a vector in Hilbert space. We denote this state vector by $|\xi\rangle$. The state vector can be expressed with respect to different bases, and thus appear as different state vectors. For instance the wave function in one dimension $\Psi(x, t)$ is the coefficient in the expansion of $|\xi\rangle$ in the basis of position eigenfunctions $|x\rangle$

$$\Psi(x, t) = \langle x|\xi\rangle, \quad (1.45)$$

where the eigenvalue equation of x reads

$$\hat{x}|x\rangle = x|x\rangle. \quad (1.46)$$

In this case the eigenvalues of eq. (1.46) take continuous values. This results in a completeness relation, corresponding to the discrete completeness relation in eq. (1.26), given by

$$\int dx |x\rangle \langle x| = \mathbb{1}. \quad (1.47)$$

Since the eigenvalue spectra is continuous the eigenvectors are normalized by the Dirac delta function

$$\langle x|x'\rangle = \delta(x - x'). \quad (1.48)$$

Similar the wave function $\Phi(p, t)$ is the coefficient in the expansion of $|\xi\rangle$ in the basis of momentum, thus

$$\Phi(p, t) = \langle p|\xi\rangle, \quad (1.49)$$

where the eigenvalue equation of p reads

$$\hat{p}|p\rangle = p|p\rangle, \quad (1.50)$$

and

$$\int dp |p\rangle \langle p| = \mathbb{1}. \quad (1.51)$$

As described in the section above, the wave function $|\xi\rangle$ can be expanded in energy eigenfunctions, i.e. eigenvectors of the eq. (1.42), where we here assume a discrete energy spectrum.

$$c_n = \langle \theta_n|\xi\rangle, \quad (1.52)$$

and completeness reads

$$\sum_n |\theta_n\rangle \langle \theta_n| = \mathbb{1}, \quad (1.53)$$

These three different representations all possess the same information of the system, and thus describe the same state vector. The expressions of the state vector $\Psi(x, t)$ is obtained by inserting the completeness relation of each representation into the eq. (1.45), e.g. the momentum representation is obtained by

$$\Psi(x, t) = \langle x|\xi\rangle = \int dp \langle x|p\rangle \langle p|\xi\rangle, \quad (1.54)$$

where we already defined $\langle p|\xi\rangle = \Phi(p, t)$. For derivation of $\langle x|p\rangle$ see [6]. The three representations read

$$\begin{aligned}\Psi(x, t) &= \int \Psi(x', t) \delta(x - x') dx', \\ &= \int \Phi(p, t) \frac{1}{\sqrt{2\pi\hbar}} e^{\frac{i}{\hbar} px} dp, \\ &= \sum_n c_n e^{-\frac{i}{\hbar} E_n t} \psi_n(x),\end{aligned}\tag{1.55}$$

where

$$\begin{aligned}\delta(x - x') &= \langle x|x'\rangle, \\ \frac{1}{\sqrt{2\pi\hbar}} e^{\frac{i}{\hbar} px} &= \langle x|p\rangle, \\ \psi_n(x) e^{-\frac{i}{\hbar} E_n t} &= \langle x|\theta_n\rangle.\end{aligned}\tag{1.56}$$

We now consider the time-independent Schrödinger equation (1.42) in the position representation. Note that we omit the indexing from here on. The energy eigenfunctions in terms of the position eigenfunctions of eq. (1.46) reads

$$|\theta\rangle = \int dx \theta(x) |x\rangle,\tag{1.57}$$

where

$$\theta(x) = \langle x|\theta\rangle,\tag{1.58}$$

By multiplying the time-independent Schrödinger equation from the left with $\langle x|$ and utilizing the completeness relation in eq. (1.47) we obtain

$$\langle x|\hat{H}|\theta\rangle = E\langle x|\theta\rangle,\tag{1.59}$$

equivalent to

$$\int dx' \langle x|\hat{H}|x'\rangle \langle x'|\theta\rangle = E\langle x|\theta\rangle,\tag{1.60}$$

and

$$\int dx' \langle x|\hat{H}|x'\rangle \theta(x') = E\theta(x),\tag{1.61}$$

Next we need to determine the expectation value $\langle x|\hat{H}|x'\rangle$. In [6] the following two relations are derived:

$$\langle x''|f(\hat{x})|x'\rangle = f(x')\delta(x'' - x'),\tag{1.62}$$

$$\langle x''|f(\hat{p})|x'\rangle = f\left(\frac{\hbar}{i} \frac{\partial}{\partial x''}\right) \delta(x'' - x'),\tag{1.63}$$

where f is a function of the position and momentum operators respectively. The Hamiltonian \hat{H} is the sum of the kinetic and potential energy of the system, see eq. (1.34). It

is a function of the position and the momentum operator given in eqs. (1.21) and (1.22) respectively, thus

$$\hat{H} = \hat{H}(\hat{x}, \hat{p}) = \hat{H}\left(x, \frac{\hbar}{i} \frac{\partial}{\partial x}\right). \quad (1.64)$$

From the relations in eqs. (1.62) and (1.63), we can determine the expectation value $\langle x | \hat{H} | x' \rangle$, viz.

$$\langle x | \hat{H}(\hat{x}, \hat{p}) | x' \rangle = \hat{H}\left(x, \frac{\hbar}{i} \frac{\partial}{\partial x}\right) \delta(x - x'). \quad (1.65)$$

Inserting this result into eq. (1.61) give us the time-independent Schrödinger equation in the position representation, i.e.

$$\hat{H}\left(x, \frac{\hbar}{i} \frac{\partial}{\partial x}\right) \theta(x) = E \theta(x). \quad (1.66)$$

From classical mechanics we have that the kinetic energy T is given by

$$T = \frac{1}{2} m v^2 = \frac{p^2}{2m}, \quad (1.67)$$

where m is the mass, v the velocity and $p = mv$ is the momentum of the system. In quantum mechanics, momentum operator is given as eq. (1.22), thus the kinetic energy in three dimensions reads

$$T = \frac{\hat{p}^2}{2m} = -\frac{\hbar^2}{2m} \nabla^2, \quad (1.68)$$

where ∇^2 is the Laplacian. The explicit time-independent Schrodinger equation in three dimensions in the position representation thus reads

$$\left(-\frac{\hbar^2}{2m} \nabla^2 + V(x, y, z) \right) \theta(x, y, z) = E \theta(x, y, z). \quad (1.69)$$

1.2.4 Intrinsic Spin

In classical mechanics an object is influenced by two types of angular momentum. One is the orbital momentum associated with the motion of the center of mass, defined as:

$$\vec{L} = \vec{r} \times \vec{p}, \quad (1.70)$$

where \vec{r} is the position vector, and \vec{p} is the momentum vector. Second is the spin associated with the motion about the center of mass, given by

$$\vec{S} = \vec{I} \vec{\omega}, \quad (1.71)$$

where \vec{I} is the moment of inertia, and $\vec{\omega}$ is the angular velocity. In quantum mechanics we have an analogous two-split of the angular momentum. Experimental results obtained in connection with the Zeemann effect from 1896, and the introduction of the fine-structure constant in 1916, showed the necessity of ascribing the particles an additional intrinsic angular momentum, named spin. Thus the elementary particles carry intrinsic angular momentum \mathbf{S} , in addition to their extrinsic angular momentum \mathbf{L} . The algebraic theory

of spin is analogous to the theory of angular momentum, (see angular momentum in [9]). The commutation relations are given by

$$[\hat{S}_X, \hat{S}_Y] = i\hbar\hat{S}_Z, \quad [\hat{S}_Z, \hat{S}_X] = i\hbar\hat{S}_Y, \quad [\hat{S}_Y, \hat{S}_Z] = i\hbar\hat{S}_X. \quad (1.72)$$

Eigenvectors of spin cannot be written as functions. They will in the following be denoted by $|\chi\rangle = |s, m_s\rangle$, where s is the principal spin quantum number, viz. the spin value, and m_s is the quantum number associated with the z-projection of the spin. The eigenvalue equation of $\hat{\mathbf{S}}^2$ and \hat{S}_z thus reads

$$\hat{\mathbf{S}}^2|s, m_s\rangle = s(s+1)\hbar^2|s, m_s\rangle, \quad (1.73)$$

$$\hat{S}_z|s, m_s\rangle = m_s\hbar|s, m_s\rangle. \quad (1.74)$$

The quantum mechanical spin has nothing to do with motion in space, and is therefore independent of the variables r , θ , and ϕ . This fact means that there are no reason, unlike in the case of angular momentum \mathbf{L} (see [9] for details), to assume that the spin value cannot take half-integer values, i.e.

$$s = 0, \frac{1}{2}, 1, \frac{3}{2}, \dots \quad m_s = -s, -s+1, \dots, s-1, s. \quad (1.75)$$

It turns out that every elementary particle has a specific and immutable value of \mathbf{S} . The most important value is $s = \frac{1}{2}$, not so surprising considered that this is the spin of particles like protons, neutrons, and electrons, in addition to quarks and leptons. In the coming of this thesis we consider the interaction of electrons, and naturally our interest lie in the spin-half system, viz;

$$s = \frac{1}{2}, \quad m_s = \pm\frac{1}{2}, \quad (1.76)$$

In this system there are only two eigenstates, *spin-up* represented by $|\frac{1}{2}, \frac{1}{2}\rangle = |+\rangle$, and *spin-down* represented by $|\frac{1}{2}, -\frac{1}{2}\rangle = |-\rangle$, thus Hilbert space \mathcal{H} in case of spin is two dimensional. Since \mathcal{H} is two dimensional we can express the state vectors in terms of two-dimensional vectors, and operators in terms of 2×2 matrices. The general state of a spin-half particle can as a result be expressed as;

$$|\chi\rangle = \alpha|+\rangle + \beta|-\rangle = \begin{pmatrix} \alpha \\ \beta \end{pmatrix}, \quad (1.77)$$

where $|\chi\rangle$ is called a *spinor*, with

$$|+\rangle = \begin{pmatrix} 1 \\ 0 \end{pmatrix}, \quad (1.78)$$

$$|-\rangle = \begin{pmatrix} 0 \\ 1 \end{pmatrix}, \quad (1.79)$$

representing spin up and spin down respectively. The probability of finding a particle in the spin up state is given by $|\alpha|^2$, and the corresponding probability of spin down is given by $|\beta|^2$. This requires that the spinor must be normalized, i.e.

$$|\alpha|^2 + |\beta|^2 = 1. \quad (1.80)$$

In the basis of $|+\rangle$ and $|-\rangle$ the operators $\hat{\mathbf{S}}^2$, \hat{S}_x , \hat{S}_y and \hat{S}_z are obtained in a matrix notation by evaluating the eigenvalue equations like the ones in eqs. (1.73) and (1.74), viz.

$$\hat{\mathbf{S}}^2 = \frac{3}{4}\hbar^2 \begin{pmatrix} 1 & 0 \\ 0 & 1 \end{pmatrix} \quad (1.81)$$

$$\hat{S}_x = \frac{\hbar}{2} \begin{pmatrix} 0 & 1 \\ 1 & 0 \end{pmatrix}, \quad \hat{S}_y = \frac{\hbar}{2} \begin{pmatrix} 0 & -i \\ i & 0 \end{pmatrix}, \quad \hat{S}_z = \frac{\hbar}{2} \begin{pmatrix} 1 & 0 \\ 0 & -1 \end{pmatrix}, \quad (1.82)$$

where the matrices in eq. (1.82) are referred to as the *Pauli spin matrices*, often denoted by σ_x , σ_y and σ_z respectively.

1.2.5 Final Wave Function

In the time-independent Schrödinger equation given by eq. (1.38), we observe that the wave function is given as a function of coordinates only. The wave function has several degrees of freedom, but none in which the spin degrees of freedom can be included. This is clear since the spin is independent of motion in space, and thus the spin degrees of freedom cannot be expressed in terms of space variables.

From section 1.2.1 we have established that the wave function is described by the energy eigenvectors (the solution of eq. (1.38)) in Hilbert space. The spin functions from section 1.2.4 do also make up a two-dimensional Hilbert space. These two Hilbert spaces are distinct. They can be combined by the tensor product to form one vector space, viz.

$$\mathcal{H} = \mathcal{H}_{\text{spatial}} \otimes \mathcal{H}_{\text{spin}}. \quad (1.83)$$

The tensor product is a construction that defines how to compose one vector space $V \otimes W$ with dimension kl , from two vector spaces V and W with dimension k and l respectively. A basis of $V \otimes W$ is then given by

$$|v_i\rangle \otimes |w_j\rangle = |v_i w_j\rangle; \quad 1 \leq i \leq k, 1 \leq j \leq l. \quad (1.84)$$

The final wave function of this system thus reads

$$\psi(\mathbf{x}) = \psi(\vec{r}) \otimes |\chi\rangle, \quad (1.85)$$

where \mathbf{x} denotes both the spin and coordinate degrees of freedom, $\psi(\vec{r})$ is the spatial part, and $|\chi\rangle$ is the spin part given in eq. (1.77).

The operators corresponding to the different spaces need to be modified so that they act on the space of their belonging. An operator acting on the spatial Hilbert space is thus given by

$$\hat{A} \otimes \mathbb{1}. \quad (1.86)$$

An operator acting on the spin Hilbert space is given by

$$\mathbb{1} \otimes \hat{B}. \quad (1.87)$$

The operators acting on the wave function reads

$$(\hat{A} \otimes \hat{B})\psi(\mathbf{x}) = \hat{A}\psi(\vec{r}) \otimes \hat{B}|\chi\rangle. \quad (1.88)$$

Usually the tensor product is omitted from the equation, especially when it is clear from context what space the operator is acting on.

Chapter 2

Many-Body Theory

The many-body problem may be defined as the study of the effects of interactions between bodies on the behavior of a many-body system [10]. The wide interest of many-body physics has survived the last 50 years, for which the reason is clear. Almost any real physical system consists of interacting particles. Examples of particles constituting many-body systems are nucleons in the nucleus, electrons in the atom, atoms in a molecule, or molecules in liquid, the list is long. The many-body problem is difficult much because of the intricate motion of the particles in an interacting system. In earlier days the preferred way of solving this problem was by ignoring the interactions all together. This surprisingly gave good results, but in the long run this technique was not adequate.

According to [11], the fundamental idea of many-particle systems is that they can be described approximately as a system of non-interacting quasi-particles, using second quantization and Feynman diagrams as building blocks. To recapitulate, many-body theory constitutes the framework for understanding the behavior of a system with many interacting particles. In this thesis the system of interest consists of interacting electrons, and the following sections will deal with this system. First we introduce the non-relativistic quantum mechanics of the many-body system of electrons, followed by an introduction to the technique of second quantization.

2.1 The Many-Body Problem

The description of the many-body system of N particles requires the solution of N coupled quantum mechanical equations of motion, namely the Schrödinger equations. These are not solvable for most encountered systems, but the theory of many-body physics offers concepts that approximately solve the many-body problem. The quantum mechanics of this problem will be outlined in this section.

In chapter 1, section 1.2.1, we stated that a physical system is described by a wave function in Hilbert space. For a system of N electrons this wave function reads

$$\Psi(\mathbf{r}_1, \mathbf{r}_2, \dots, \mathbf{r}_{N-1}, \mathbf{r}_N; \sigma_1, \sigma_2, \dots, \sigma_{N-1}, \sigma_N; t) \equiv \Psi(\mathbf{x}, t), \quad (2.1)$$

where \mathbf{x} denotes both the spatial \mathbf{r}_i , and spin σ_j degrees of freedom. The time-independent Schrödinger equation (see also eqs. (1.38) and (1.42) of chapter 1) is then given by

$$\hat{H}(\mathbf{x}_1, \mathbf{x}_2, \dots, \mathbf{x}_{N-1}, \mathbf{x}_N) \Psi_\lambda(\mathbf{x}_1, \mathbf{x}_2, \dots, \mathbf{x}_{N-1}, \mathbf{x}_N) = E_\lambda \Psi_\lambda(\mathbf{x}_1, \mathbf{x}_2, \dots, \mathbf{x}_{N-1}, \mathbf{x}_N), \quad (2.2)$$

where λ is the set of all quantum numbers necessary to classify a given N -particle state, and Ψ_λ is the eigenfunction. The Hamiltonian is defined as

$$\hat{H} = \hat{T} + \hat{V}, \quad (2.3)$$

where \hat{V} is the total potential energy, and \hat{T} is the total kinetic energy of the system. In the N -particle system, \hat{T} reads

$$\hat{T} = \sum_{i=1}^N t_i, \quad (2.4)$$

where t_i is the kinetic energy of particle i . The kinetic energy operator is a true one-body operator, unlike the N -body potential energy operator. The potential energy operator of the N -body system reads

$$\hat{V} = \sum_{i=1}^N V_i^{(1)} + \frac{1}{2!} \sum_{ij}^N V_{ij}^{(2)} + \frac{1}{3!} \sum_{ijk}^N V_{ijk}^{(3)} + \dots + \frac{1}{N!} \sum_{ijk\dots N}^N V_{ijk\dots N}^{(N)}, \quad (2.5)$$

where $V^{(n)}$ is the potential energy of the interaction between n particles. In our considerations of the N -electron system we only encounter two-body interactions. However, in nuclear physics one also encounter three-body interactions, exhibited by the fundamental strong interactions.

Thus, to concatenate the theory of the many-body problem we state the following. The time independent Schrödinger equation reads

$$\hat{H}|\Psi\rangle = E|\Psi\rangle, \quad (2.6)$$

where E is the energy, and $|\Psi\rangle$ is the eigenfunction of the Hamiltonian given in eq. (2.3). This equation is what we refer to as the quantum mechanical many-body problem. The equation has no exact solution, even when we consider the simple case where only the two-body interaction is included. In the same manner as outlined in chapter 1, section 1.2.1, postulate 4, the time evolution of this system is determined by the time-dependent Schrödinger eq. (1.29). The time evolution operator is given as before, in eq. (1.31). The wave function at time $t > t_0$ thus read:

$$|\Psi(\mathbf{x}, t)\rangle = e^{-\frac{i}{\hbar}\hat{H}(t-t_0)} \sum_{\lambda=1}^d \langle\psi_\lambda|\Psi(\mathbf{x}, t_0)\rangle |\psi_\lambda\rangle = \sum_{\lambda=1}^d C_\lambda |\psi_\lambda\rangle e^{-\frac{i}{\hbar}E_\lambda(t-t_0)}. \quad (2.7)$$

In the next section we consider the concept of identical particles in many-body theory, and as a result we derive the wave function of these N -body systems.

2.2 Identical Particles

In this section the concept of indistinguishability is presented in terms of the coordinate representation, see section 1.2.3.

Identical particles are particles which have all the same physical properties, e.g. mass and charge. In classical mechanics, and in terms of physical experience and intuitive

understanding, identical particles are distinguishable. In the quantum mechanical description however, the *principle of indistinguishability* is important. In quantum mechanics only identical particles far apart from each other can be viewed as distinguishable. Interacting identical particles are not distinguishable. This result has its origin in the uncertainty principle, stating that no sharply defined particle orbits exist. Thus the particle must be treated as a spreading wave packet, where the occupation probabilities of interacting particles overlap, making it impossible to identify the particles.

The measurable quantities of a stationary quantum mechanical system are the expectation values of the operators representing the observables of the system (See chapter 1, section 1.2.1). A consequence of the principle of indistinguishability is that the expectation values of the system cannot change when the coordinates of two particles in the wave function are interchanged, i.e.

$$\begin{aligned} & \int dx_1 \dots dx_N \Psi^*(x_1, \dots, x_i, \dots, x_j, \dots, x_N) \hat{A} \Psi(x_1, \dots, x_i, \dots, x_j, \dots, x_N), \\ &= \int dx_1 \dots dx_N \Psi^*(x_1, \dots, x_j, \dots, x_i, \dots, x_N) \hat{A} \Psi(x_1, \dots, x_j, \dots, x_i, \dots, x_N), \end{aligned} \quad (2.8)$$

where Ψ is the wave function, \hat{A} is the operator, and $x \equiv (r, \sigma)$ contains both spatial and spin degrees of freedom, thus meaning that $\int dx = \sum_{\sigma} \int d^3r$. Equation (2.8) has to be true for all pairs (i, j) , and for all operators. From eq. (2.8) one can derive properties of the wave function and the operators describing the many-body system of identical particles, see [11]. Next we outline this derivation.

The permutation operator P is expressed as a product of the interchanging of two particles denoted by P_{ij} , i.e.

$$\hat{P} = \prod \hat{P}_{ij}, \quad (2.9)$$

where \hat{P}_{ij} is the operator with the action

$$\hat{P}_{ij} \Psi(x_1, \dots, x_i, \dots, x_j, \dots, x_N) = \Psi(x_1, \dots, x_j, \dots, x_i, \dots, x_N). \quad (2.10)$$

Applying the permutation operator twice will then give back the original wave function, thus

$$\hat{P}_{ij} \hat{P}_{ij} = \mathbb{1} \quad \Rightarrow \quad \hat{P}_{ij}^{-1} = \hat{P}_{ij}. \quad (2.11)$$

This property makes it possible to rewrite eq. (2.8) such that we obtain the following operator identity for all pairs (i, j) :

$$\hat{A} = \hat{P}_{ij}^{\dagger} \hat{A} \hat{P}_{ij}. \quad (2.12)$$

See [11] for details. In the case where $\hat{A} = \mathbb{1}$ (the identity operator) the relation in the equation above reveals

$$\hat{P}_{ij}^{-1} = \hat{P}_{ij} = \hat{P}_{ij}^{\dagger}. \quad (2.13)$$

Thus the permutation operators corresponding to interchanging two particles are Hermitian when operating on the Hilbert space of identical particles. By multiplying eq. (2.12) from the left with \hat{P}_{ij} we obtain

$$\hat{P}_{ij} \hat{A} = \hat{A} \hat{P}_{ij} \quad \Rightarrow \quad [\hat{A}, \hat{P}_{ij}] = 0. \quad (2.14)$$

This result is valid for all pairs (i, j) , and tells us that the operators of the system of identical particles must commute with all the permutation operators. Hence operators of the system and the permutation operator have simultaneous eigenfunctions. The eigenvalue equation of the permutation operator \hat{P}_{ij} reads

$$\hat{P}_{ij}\Psi = \lambda_{ij}\Psi. \quad (2.15)$$

From this it follows

$$\Psi = \hat{P}_{ij}^2\Psi = \lambda_{ij}^2\Psi \quad \Rightarrow \quad \lambda_{ij}^2 = 1. \quad (2.16)$$

Since the permutation operator is Hermitian, the eigenvalues must be real

$$\lambda = \pm 1. \quad (2.17)$$

It can be proved that the eigenvalues of all the permutation operators \hat{P}_{ij} must be identical [11]. This makes it possible to stipulate the following definitions:

If $\hat{P}_{ij}\Psi = +1$ we say that Ψ is *symmetric*.

If $\hat{P}_{ij}\Psi = -1$ we say that Ψ is *antisymmetric*.

We denote the symmetric state by Ψ_S and the antisymmetric state by Ψ_{AS} . It is then given for any permutation \hat{P}

$$\begin{aligned} \hat{P}\Psi_S &= +\Psi_S, \\ \hat{P}\Psi_{AS} &= (-)^p\Psi_{AS}, \end{aligned}$$

where p is the number of permutations made by the permutation operator \hat{P} . Symmetric and antisymmetric functions are always orthogonal, which is shown by:

$$\langle \Psi_{AS} | \Psi_S \rangle = \langle \Psi_{AS} | \hat{P}_{ij} | \Psi_S \rangle = \langle \Psi_{AS} | \hat{P}_{ij}^\dagger | \Psi_S \rangle = \langle \hat{P}_{ij} \Psi_{AS} | \Psi_S \rangle = -\langle \Psi_{AS} | \Psi_S \rangle, \quad (2.18)$$

resulting in

$$\langle \Psi_{AS} | \Psi_S \rangle = 0. \quad (2.19)$$

These results give rise to the *symmetry postulate* which states:

The Hilbert space of wave functions of a system of identical particles contains either symmetric or antisymmetric functions, never both.

Particles with symmetric wave functions are named *bosons*, and those with an antisymmetric wave function are named *fermions*. According to spin-statistics bosons only have integer spin, while fermions only have spin equal half values of odd integers.

Now we consider the wave function of these non-interacting N -particle systems, consisting of both bosons and fermions. The wave functions of both symmetries can be constructed by defining a symmetrization operator \hat{S} and an antisymmetrization operator \hat{A} :

$$\hat{S} = \frac{1}{N!} \sum_p \hat{P}, \quad (2.20)$$

$$\hat{A} = \frac{1}{N!} \sum_p (-)^p \hat{P}, \quad (2.21)$$

where \hat{P} is the permutation operator defined above, and p is the number of permutations. By operating on a product state of single particle orbitals $\psi_\lambda(x)$ of the form

$$|\lambda_1 \lambda_2 \dots \lambda_N\rangle = |\lambda_1\rangle |\lambda_2\rangle \dots |\lambda_N\rangle = \psi_\lambda(x_1) \psi_{\lambda'}(x_2) \dots \psi_{\lambda''}(x_N), \quad (2.22)$$

the following normalized wave functions are obtained

$$\Psi_S(x_1, x_2 \dots x_N) = \sqrt{\frac{N!}{n_\lambda! n_{\lambda'}! \dots}} \hat{S} \psi_\lambda(x_1) \psi_{\lambda'}(x_2) \dots \psi_{\lambda''}(x_N) \quad (2.23)$$

$$\Psi_{AS}(x_1, x_2 \dots x_N) = \sqrt{N!} \hat{A} \psi_\lambda(x_1) \psi_{\lambda'}(x_2) \dots \psi_{\lambda''}(x_N), \quad (2.24)$$

where N is the number of particles in the system, and n_λ is the number of bosons which exists in the quantum state denoted by λ . The antisymmetric wave function can also be expressed as a determinant, known as the *Slater determinant*, viz.

$$\Psi_{AS}(x_1, x_2 \dots x_N) = \frac{1}{\sqrt{N!}} \begin{vmatrix} \psi_\lambda(x_1) & \psi_{\lambda'}(x_1) & \dots & \psi_{\lambda''}(x_1) \\ \psi_\lambda(x_2) & \psi_{\lambda'}(x_2) & \dots & \psi_{\lambda''}(x_2) \\ \vdots & \vdots & & \vdots \\ \psi_\lambda(x_N) & \psi_{\lambda'}(x_N) & \dots & \psi_{\lambda''}(x_N) \end{vmatrix}. \quad (2.25)$$

From the mathematical properties of the determinant, see [12], we know that the determinant equals zero if it has two rows or two column that are equal. This means that if two particles are in the same position, or if one quantum state λ equals another quantum state λ' , the antisymmetric wave function does not exist. This is exactly what the *Pauli exclusion principle* states, formulated by the Austrian physicist Wolfgang Pauli in 1925. It is impossible to have two fermions in the same quantum state, and it is impossible to place two electrons with the same spin projection in the same point. Note that there are no restrictions of this sort on the system of bosons. Also note that the order of the single particle orbitals in the Slater determinant is important to conserve in order for the Slater determinant to be unambiguously defined.

The system of electrons we study in this thesis constitutes a system of identical particles of fermions. Our main interest is therefore the antisymmetric wave functions. The eigenfunctions of eq. (2.2) can be expressed as in eq. (1.85)

$$\Psi_\lambda(x) = \psi(r) \otimes |\chi_\sigma\rangle, \quad (2.26)$$

the antisymmetric wave function then has two possible realizations, namely

$$\Psi_\lambda^{AS}(x) = \psi^{AS}(r) \otimes |\chi_\sigma\rangle^S, \quad (2.27)$$

$$\Psi_\lambda^{AS}(x) = \psi^S(r) \otimes |\chi_\sigma\rangle^{AS}. \quad (2.28)$$

Either the spatial part of the wave function is antisymmetric, hence the spin part is symmetric, or vice versa.

To recapitulate the properties of the system of identical particles outlined in this section, here is a short list:

- The principle of indistinguishability requires that the expectation values of the system are unaffected by the interchange of particles in the wave function.
- The operators of the system must commute with all permutation operators.
- The wave function of the system must be either *symmetric* or *antisymmetric* defined by the eigenvalue of the permutation operator being $+1$ and -1 respectively
- Particles with symmetric wave function are named *bosons*, and are recognized by integer spin values. Particles with antisymmetric wave functions are named *fermions*, and are recognized by half integer spin values.
- In a fermion system, two fermions cannot be in the same quantum state, and no fermions with same spin projection can be placed in the same position. No such restrictions apply for a boson system.

2.3 Non-Interacting and Interacting Systems

In the non-interacting system of N -particles the Hamiltonian reads

$$\hat{H}_0 = \hat{T} + \hat{V}, \quad (2.29)$$

where \hat{T} is the total kinetic energy, and \hat{V} is the total one-body potential energy originating from external influences. \hat{T} and \hat{V} are given as

$$\hat{T} = \sum_{i=1}^N \hat{t}_i \quad \hat{V} = \sum_{i=1}^N \hat{v}_i. \quad (2.30)$$

If we then define

$$\hat{h}_i = \hat{t}_i + \hat{v}_i, \quad (2.31)$$

the Hamiltonian can be expressed as

$$\hat{H}_0 = \sum_{i=1}^N \hat{h}_i. \quad (2.32)$$

The time-independent Schrödinger equation, see eq. (1.38), is given by

$$\hat{H}_0 |\Phi_a\rangle = E_a |\Phi_a\rangle, \quad (2.33)$$

and the associated one-particle problem reads

$$\hat{h} |\phi_\lambda\rangle = \epsilon_\lambda |\phi_\lambda\rangle, \quad (2.34)$$

where $|\Psi_a\rangle$ is the Hamiltonian eigenfunction of the N -body system, and $|\psi_\lambda\rangle$ is the single-particle orbital constituting the eigenfunction of the one-particle Hamiltonian. The energy relation reads

$$E_a = \sum_{\lambda} \epsilon_{\lambda}. \quad (2.35)$$

If we assume that the particles in this system are distinguishable, then the eigenfunctions of eq. (2.33) could be expressed as

$$|\Phi_a\rangle = |\phi_\lambda\rangle \otimes |\phi_{\lambda'}\rangle \otimes \dots \otimes |\phi_{\lambda''}\rangle. \quad (2.36)$$

Note that the subscript a denotes the set of quantum numbers $\lambda, \lambda', \dots, \lambda''$. However, if the particles are indistinguishable, as encountered in section 2.2, the solution of eq. (2.36) is not possible. The solution for indistinguishable particles must be constructed as a symmetric or antisymmetric sum of products of single particle orbits, as shown in eqs. (2.23) and (2.24) respectively. In our study of N -electron systems we consider only the antisymmetric wave function represented by the Slater determinant in eq. (2.25), viz..

$$\Phi_a^{AS} = \frac{1}{\sqrt{N!}} \begin{vmatrix} \phi_\lambda(x_1) & \dots & \psi_{\lambda''}(x_1) \\ \vdots & \ddots & \vdots \\ \psi_\lambda(x_N) & \dots & \psi_{\lambda''}(x_N) \end{vmatrix}. \quad (2.37)$$

The time-independent Schrödinger equation then reads

$$\hat{H}_0 \Phi_a^{AS} = E \Phi_a^{AS}, \quad (2.38)$$

with energy eigenvalues given as

$$E = \sum_{i=1}^N \epsilon_{\lambda_i}. \quad (2.39)$$

Note that often we are in search of the ground state of the many-body system. From our perspectives on the Slater determinant we conclude that the ground state of a N -body non-interacting system of fermions can be represented by one Slater determinant built up of the N single-particle orbitals with the lowest energy.

Next we consider the interacting N -fermion system. We start by defining the N -particle Hilbert space of symmetric and antisymmetric states \mathcal{H}_N^S and \mathcal{H}_N^{AS} . In general the N -particle Hilbert space reads

$$\mathcal{H} = \mathcal{H}_N^S \otimes \mathcal{H}_N^{AS}. \quad (2.40)$$

The Hamiltonian of the interacting N -fermion system is given in eq. 2.3, and the associated single-particle problem reads

$$\hat{h}|\phi_\lambda\rangle = \epsilon_\lambda|\phi_\lambda\rangle. \quad (2.41)$$

From single-particle quantum mechanics we have that the solution set $\{\phi_\lambda\}$ of eq. (2.41) constitutes a complete and orthonormal set of eigenvectors. In ref. [11], the following is given proof of

If the family $\{\phi_\lambda\}$ is complete, so too are the families $\{\Phi^{AS}\}$ and $\{\Phi^S\}$ of many-particle functions in the corresponding Hilbert space of antisymmetric and symmetric many-particle functions, respectively.

From earlier we know that an arbitrary product state can be expressed as an symmetric or antisymmetric state by applying the symmetrization and antisymmetrization operator

in eqs. (2.23) and (2.24) respectively. Thus, the wave function of the interacting N -fermion system can be expressed as a linear combination of the eigenfunctions of the non-interacting system in eq. (2.33), i.e.

$$\Psi_a(\mathbf{x}_1, \dots, \mathbf{x}_N) = \sum_{\alpha, \beta, \dots, \gamma} C_{\alpha, \beta, \dots, \gamma}^a \Phi_{\alpha, \beta, \dots, \gamma}(\mathbf{x}_1, \dots, \mathbf{x}_N), \quad (2.42)$$

where $C_{\alpha, \beta, \dots, \gamma}^a$ is the expansion coefficient, and $\Phi_{\alpha, \beta, \dots, \gamma}(\mathbf{x}_1, \dots, \mathbf{x}_N)$ is the Slater determinant given in eq. (2.37). Note that this solution is not trivial. There usually exists an infinite number of solutions to the single-particle problem, thus the basis of the Slater determinant is also infinite.

2.4 Second Quantization

The second quantization formalism is a significant tool in describing the many-body systems. It renders the Schrödinger equation in a simplified manner, but it does not represent a solution to the many-body problem. In this section we will present the technique of second quantization for systems of fermions.

2.4.1 Creation and Annihilation Operators

The second quantisation formalism is recognized by the introduction of the *creation* and the *annihilation* operators. These operators makes the construction of N -particle wave functions as symmetrized or antisymmetrized products of single particle functions unnecessary, since the symmetry properties are included in fundamental anticommutation relations [13]. This constitutes one of two prominent advantages of second quantization. The other advantage is that it enables a handling of systems containing a variable number of particles. In this section, the properties of the creation and the annihilation operators are presented.

The wave functions of a system of fermions are represented by Slater determinants, as outlined in section 2.2, see eqs. (2.24) and (2.25). This section also states that the order of the single particle orbitals contained in the Slater determinant must be conserved in order for the ambiguity of sign determination to be removed. We are free to choose the ordering any way we want, but an example could be an order of increasing one-electron energy. If the Slater determinant is denoted

$$\Psi_{\alpha_1, \alpha_2 \dots \alpha_N}^{AS} = |\alpha_1 \alpha_2 \dots \alpha_N\rangle, \quad (2.43)$$

where α_i denotes the single particle orbits, the following relation holds

$$|\alpha_1, \dots \alpha_i \dots \alpha_k \dots \alpha_N\rangle = -|\alpha_1, \dots \alpha_k \dots \alpha_i \dots \alpha_N\rangle. \quad (2.44)$$

The creation and annihilation operators are mappings between the many-particle Hilbert space of different particle numbers, and are respectively denoted by

$$a_{\alpha}^{\dagger} : \mathcal{H}_N \Rightarrow \mathcal{H}_{N+1}, \quad (2.45)$$

$$a_{\alpha} : \mathcal{H}_{N-1} \Rightarrow \mathcal{H}_N, \quad (2.46)$$

where \mathcal{H}_N is the Hilbert space of N particles. Note that we omit the operator symbol for these two operators. Also note that a_α^\dagger is the Hermitian conjugate of a_α , for a more elaborate explanation see ref. [14].

The space comprising all the many-particle Hilbert spaces of different particle numbers are named the *Fock space*. It is defined as the direct sum of tensor products of single-particle Hilbert spaces, i.e. the sum of the vacuum state (definition below), the single particle Hilbert space $\{|\alpha\rangle\}$, the two-particle Hilbert space $\{|\alpha_1\alpha_2\rangle\}$, and so on. The creation and annihilation operators thus operate on this Fock space. The advantage with the Fock space is its convenience with problems of variable particle numbers.

From the definition in eq. (2.45), we read that the creation operator a_α^\dagger adds a state ψ_α to the Slater determinant, thus creating a new antisymmetric $(N + 1)$ -particle state, viz.

$$a_\alpha^\dagger |\alpha_1\alpha_2 \dots \alpha_N\rangle = |\alpha\alpha_1\alpha_2 \dots \alpha_{N+1}\rangle. \quad (2.47)$$

Note that the result would be zero if the α -state already existed in the Slater determinant. Also, if the order of the single particle orbitals were different, this operation would acquire an additional sign. This sign is positive if the number of orbitals in the Slater determinant preceding α is even, and negative if the number is odd. See [14] for more details.

Similarly the annihilation operator a_α removes a state ψ_α from the Slater determinant, thus creating a new $(N - 1)$ -particle state, i.e.

$$a_{\alpha_1} |\alpha_1\alpha_2 \dots \alpha_N\rangle = |\alpha_2 \dots \alpha_{N-1}\rangle. \quad (2.48)$$

Note that the result would be zero if the α -state did not already exist in the Slater determinant. The same additional sign with the same conditions as for the creation operation would appear if the order of the single particle orbits were different.

The set of all possible α single particle states can be viewed as a finite or infinite, but predefined set of orbitals with a given order. The Slater determinant is therefore expressed as a state where some of these predefined orbitals are occupied and some are not. The Slater determinant can then be represented by an occupation number n_α , which takes the value one if occupied or zero if not occupied. We however, stick to the representation in eq. (2.43).

This occupation picture gives rise to an intuitive understanding and definition of the *vacuum state*. The vacuum state is the state where none of the orbitals are occupied, and it is denoted by $|0\rangle$. Any annihilation operator applied to this vacuum state will result in Zero.

$$a_\alpha |0\rangle = 0 \quad \text{for all possible } \alpha. \quad (2.49)$$

However, by applying the creation operator on the vacuum state, every possible N -particle state can be generated by a product of creation operators, i.e.

$$|\alpha_1\alpha_2 \dots \alpha_N\rangle = a_{\alpha_1}^\dagger a_{\alpha_2}^\dagger \dots a_{\alpha_N}^\dagger |0\rangle. \quad (2.50)$$

The anticommutation relations of the fermion creation and annihilation operators are of great importance since they include fundamental properties of the system. The anticommutator of two operators is defined by

$$\{\hat{A}, \hat{B}\} = \hat{A}\hat{B} + \hat{B}\hat{A}. \quad (2.51)$$

The relations read:

$$\{a_\alpha, a_\beta\} = 0, \quad (2.52)$$

$$\{a_\alpha^\dagger, a_\beta^\dagger\} = 0, \quad (2.53)$$

$$\{a_\alpha^\dagger, a_\beta\} = \delta_{\alpha\beta}, \quad (2.54)$$

where δ is the Kronecker delta. We will give a proof for the first relation. For similar derivations of the remaining two, see for example ref. [11].

The proof runs as follows; we have assumed that the two single particle orbits α and β are contained in the Slater determinant. If not, the equations below would all be zero. θ_k denotes the sign given by $(-1)^{\sum_{i < k} n_i}$, where n is the occupation number. Independent of the position ordering of orbital k , we have that $\tilde{\theta}_k = -\theta_k$.

$$\begin{aligned} a_\alpha a_\beta |\gamma \dots \alpha \dots \beta \dots\rangle &= \theta_\beta a_\alpha |\gamma \dots \alpha \dots\rangle, \\ &= \theta_\beta \theta_\alpha |\gamma \dots\rangle, \end{aligned} \quad (2.55)$$

When the operators change place, we notice that the state corresponding to α is removed before the state β is considered, hence the order position of β is changed such that $\tilde{\theta}_\beta$ is obtained, viz.

$$\begin{aligned} a_\beta a_\alpha |\gamma \dots \alpha \dots \beta \dots\rangle &= \theta_\alpha a_\beta |\gamma \dots \beta \dots\rangle, \\ &= \theta_\alpha \tilde{\theta}_\beta |\gamma \dots\rangle, \\ &= -\theta_\alpha \theta_\beta |\gamma \dots\rangle, \end{aligned} \quad (2.56)$$

The result is the anticommutation relation in eq. (2.52).

2.4.2 Representation of Operators

Operators in many-particle systems often contain the coordinates of one or two particles, and in rare cases of three particles. It is very useful to express these operators in terms of creation and annihilation operators. In this section we introduce the second quantization form of one-body and two-body operators.

For one-body operators, here represented by the Hamiltonian \hat{H}_0 of the non-interacting system in eq. (2.29), the second quantization representation reads

$$\begin{aligned} \hat{H}_0 &= \sum_{i=1}^N \hat{h}(x_i) = \sum_{ij}^\infty \langle i | \hat{h} | j \rangle a_i^\dagger a_j, \\ \langle i | \hat{h} | j \rangle &= \int \phi_i^*(x) \hat{h}(x) \phi_j(x) dx, \end{aligned} \quad (2.57)$$

where the set of vectors $\{|i\rangle\}_1^d$ constitutes a single-particle basis of the Hilbert space with dimension d . The interpretation of this expression is that the operator moves the particle from state $|j\rangle$ to state $|i\rangle$ with the transition probability given by $\langle i | \hat{h} | j \rangle$. Similarly, the two-body operators represented here by the two-body interaction operator in eq. (2.5),

have a second quantization representation given by

$$\hat{V} = \frac{1}{2} \sum_{\substack{i,j=1 \\ i \neq j}}^N \hat{v}(x_i, x_j) = \frac{1}{2} \sum_{ijkl}^{\infty} \langle ij | \hat{v} | kl \rangle a_i^\dagger a_j^\dagger a_l a_k, \quad (2.58)$$

$$\langle ij | \hat{v} | kl \rangle = \int \int \phi_i^*(x_1) \phi_j^*(x_2) \hat{v}(x_1, x_2) \phi_k(x_1) \phi_l(x_2) dx_1 dx_2.$$

Note the transposed order of the indices of the annihilation operators in eq. (2.58). The interpretation of this expression goes like this: a fermion is removed from state $|k\rangle$ and $|l\rangle$, and created in state $|i\rangle$ and $|j\rangle$ respectively, with the probability $\frac{1}{2} \langle ij | \hat{v} | kl \rangle$.

Note that the operators in second quantization representation can only be applied to a many-fermion wave function expressed as Slater determinants. To verify the second quantization representation we must show that the action of both representations on an arbitrary pair of N -electron Slater determinants Φ_a and Φ_b equals the same matrix element $\langle \Phi_a | \hat{A} | \Phi_b \rangle$, where \hat{A} is the operator of interest. In the following we will in a simple manner show the plausibility of the one-body operator representation. The plausibility check of the two-body operator is similar, see ref. [14]. For a more profound proof see ref. [11].

In the one-body operator case we consider the simplest Slater determinant, viz. the Slater determinant with only one single-particle orbital, corresponding to only one occupation number different from zero.

$$\Phi_a = |\alpha\rangle = \phi_\alpha(x), \quad (2.59)$$

$$\Phi_b = |\beta\rangle = \phi_\beta(x). \quad (2.60)$$

From the coordinate representation of eq. (2.57) we obtain

$$\begin{aligned} \langle \Phi_a | \hat{H}_0 | \Phi_b \rangle &= \langle \Phi_a | h(x) | \Phi_b \rangle, \\ &= \langle \alpha | h | \beta \rangle. \end{aligned} \quad (2.61)$$

From the second quantization representation of eq. (2.57) we obtain

$$\begin{aligned} \langle \Phi_a | \sum_{ij} \langle i | \hat{h} | j \rangle a_i^\dagger a_j | \Phi_b \rangle &= \sum_{ij} \langle i | \hat{h} | j \rangle \langle \Phi_a | a_i^\dagger a_j | \Phi_b \rangle, \\ &= \sum_{ij} \langle i | \hat{h} | j \rangle \int \phi_\alpha^* a_i^\dagger a_j \phi_\beta dx, \\ &= \langle \alpha | h | \beta \rangle. \end{aligned} \quad (2.62)$$

From eq. (2.49) we know that the annihilation of a vacuum state results in zero, thus the integral in the equation above necessarily requires that the indices i and j equals α and β respectively. This shows that the two representations of \hat{H}_0 results in the same matrix element, thus being equivalent.

We are now able to express both operators and Slater determinants in terms of second quantization. The problem of calculating expectation values and matrix elements is then reduced to a vacuum expectation value of products of creation and annihilation operators. As an example we consider the matrix element

$$\langle \alpha_1 \alpha_2 | \hat{V} | \alpha_3 \alpha_4 \rangle, \quad (2.63)$$

the second quantized form of the Slater determinants are given by

$$\langle \alpha_1 \alpha_2 | = \langle 0 | a_{\alpha_1} a_{\alpha_2}, \quad (2.64)$$

$$| \alpha_3 \alpha_4 \rangle = a_{\alpha_3}^\dagger a_{\alpha_4}^\dagger | 0 \rangle. \quad (2.65)$$

With \hat{V} in second quantized form as in eq. (2.58), the matrix element reads

$$\langle \alpha_1 \alpha_2 | \hat{V} | \alpha_3 \alpha_4 \rangle = \frac{1}{2} \sum_{\alpha \beta \gamma \delta} \langle \alpha \beta | \hat{v} | \gamma \delta \rangle \langle 0 | a_{\alpha_1} a_{\alpha_2} a_{\alpha}^\dagger a_{\beta}^\dagger a_{\gamma} a_{\delta} a_{\alpha_3}^\dagger a_{\alpha_4}^\dagger | 0 \rangle. \quad (2.66)$$

This means that we are able to calculate matrix elements and expectation values by evaluating the second quantized expression with the help of the anticommutation relations given in eqs. (2.52), (2.53) and (2.54). By utilizing the anticommutation relations, the product-string of arbitrarily ordered creation and annihilation operators can be reduced to a linear combination of normal ordered operator strings multiplied by Kronecker delta functions. The normal ordered string of second quantization operators is defined as the string where all annihilation operators are standing to the right of all creation operators, viz.

$$N[\hat{A}\hat{B}\hat{C}\dots] = (-1)^p a_a^\dagger a_b^\dagger \dots a_u a_v, \quad (2.67)$$

where $\hat{A}\hat{B}\dots$ represent various creation and annihilation operators, and p is the number of permutation made in order to obtain all creation operators to the left. As an example of the use of the anticommutation relations consider the operator string

$$\begin{aligned} a_\alpha a_\beta^\dagger a_\gamma a_\delta^\dagger &= \delta_{\alpha\beta} a_\gamma a_\delta^\dagger - a_\beta^\dagger a_\alpha a_\gamma a_\delta^\dagger, \\ &= \delta_{\alpha\beta} \delta_{\gamma\delta} - \delta_{\alpha\beta} a_\delta^\dagger a_\gamma - \delta_{\gamma\delta} a_\beta^\dagger a_\alpha + a_\beta^\dagger a_\alpha a_\delta^\dagger a_\gamma, \\ &= \delta_{\alpha\beta} \delta_{\gamma\delta} - \delta_{\alpha\beta} a_\delta^\dagger a_\gamma - \delta_{\gamma\delta} a_\beta^\dagger a_\alpha + \delta_{\alpha\delta} a_\beta^\dagger a_\gamma - a_\beta^\dagger a_\delta^\dagger a_\alpha a_\gamma, \end{aligned} \quad (2.68)$$

Here the anticommutator in eq. (2.54) is used repeatedly to obtain normal ordering of the operators. The strength of this technique becomes clear in the evaluation of the vacuum expectation value of this operator string. All the terms with operators remaining will not contribute to this value, and the result reads $\delta_{\alpha\beta} \delta_{\gamma\delta}$.

This technique of utilizing the anticommutation relations is powerful, but we can understand that the complexity of it manifests itself for operator strings with relative few operators. The process fast becomes tedious, and errors can easily appear. However, there is developed a technique named *Wick's theorem* that can solve this in an easier manner based on the normal-ordering and contractions. The concept of contractions and wick's theorem will be presented in next section.

2.4.3 Wick's Theorem

Wick's theorem is a theorem and technique enabling the computation of expectation values of general operator strings of creation and annihilation operators. The theorem is based on two fundamentals, namely *normal ordering* and *contractions*. Normal ordering is defined in the previous section, see eq. (2.67). We will in this section define the concept of contractions and present Wick's theorem.

A contraction of two arbitrary annihilation and/or creation operators is defined as the difference between their original ordering and normal ordering, i.e.

$$\hat{A}\hat{B} \equiv \hat{A}\hat{B} - N[\hat{A}\hat{B}]. \quad (2.69)$$

There are four possibilities of which two creation and/or annihilation operators can be contracted. Three of them result in zero contribution since they already are in a normal ordering, while one results in a Kronecker delta, viz.

$$\begin{aligned} \overline{a_\alpha a_\beta} &= a_\alpha a_\beta - N[a_\alpha a_\beta] = a_\alpha a_\beta - a_\alpha a_\beta = 0, \\ \overline{a_\alpha^\dagger a_\beta^\dagger} &= a_\alpha^\dagger a_\beta^\dagger - N[a_\alpha^\dagger a_\beta^\dagger] = a_\alpha^\dagger a_\beta^\dagger - a_\alpha^\dagger a_\beta^\dagger = 0, \\ \overline{a_\alpha^\dagger a_\beta} &= a_\alpha^\dagger a_\beta - N[a_\alpha^\dagger a_\beta] = a_\alpha^\dagger a_\beta - a_\alpha^\dagger a_\beta = 0, \\ \overline{a_\alpha a_\beta^\dagger} &= a_\alpha a_\beta^\dagger - N[a_\alpha a_\beta^\dagger] = a_\alpha a_\beta^\dagger + a_\beta^\dagger a_\alpha = \delta_{\alpha\beta}. \end{aligned}$$

Note, the fourth relation above is just the anticommutator in eq. (2.54). The contraction of two pairs of operators inside a normal ordered product is defined as

$$N[\overbrace{\hat{A}\hat{B} \dots \hat{M} \dots \hat{R} \dots \hat{U} \dots}] = (-1)^p N[\overbrace{\hat{A}\hat{M}} \overbrace{\hat{B}\hat{U}} \dots \hat{R} \dots], \quad (2.70)$$

where p is the total number of permutations made in order to bring both pair of contraction operators to the left. The result is either ± 1 or zero.

With these means in hand we can proceed to the definition of Wick's theorem. The theorem states

an arbitrary string of annihilation and creation operators equals its normal ordered product plus the sum of all possible contractions of the normal ordered product.

i.e. for operator strings the following equality holds:

$$\begin{aligned} \hat{A}\hat{B}\hat{C} \dots \hat{U}\hat{V}\hat{W} &= N[\hat{A}\hat{B}\hat{C} \dots \hat{U}\hat{V}\hat{W}] \\ &+ \sum_{(1)} N[\overbrace{\hat{A}\hat{B}} \hat{C} \dots \hat{U}\hat{V}\hat{W}] \\ &+ \sum_{(2)} N[\overbrace{\hat{A}\hat{B}} \overbrace{\hat{C}\hat{U}} \dots \hat{V}\hat{W}] \\ &\vdots \\ &+ \sum_{(N/2)} N[\overbrace{\hat{A}\hat{B}} \overbrace{\hat{C}\hat{U}} \overbrace{\hat{V}\hat{W}}], \end{aligned} \quad (2.71)$$

where $N/2$ equals the maximum number of simultaneously contractions, N is the number of operators in the product string. If the operator string contains an even number of operators we obtain fully contracted terms with $N/2$ contractions. In the calculation of the contractions above, we need to consider the sign originating from eq. (2.70). This sign

can be determined by counting the number c of crossings in the contraction lines. The sign is then given by $(-1)^c$.

We now see why Wick's theorem is so useful in the calculation of vacuum expectation values. When the original expectation value or matrix element is reduced to the corresponding vacuum expectation value as described in the previous section (see eq. (2.66)), the operator string can be expressed in terms of Wick's theorem. The result gets its contribution only from the fully contracted terms, since any annihilation operator acting on the vacuum state is zero. This also means that only even operator strings will be able to contribute when evaluated in a vacuum. In a schematic representation this reads:

$$\begin{aligned}
 \langle 0 | \hat{A} \hat{B} \hat{C} \dots \hat{U} \hat{V} \hat{W} | 0 \rangle &= \langle 0 | N[\hat{A} \hat{B} \hat{C} \dots \hat{U} \hat{V} \hat{W}] | 0 \rangle \\
 &+ \sum_{(1)} \langle 0 | N[\overbrace{\hat{A} \hat{B} \hat{C} \dots \hat{U} \hat{V} \hat{W}}^{(1)}] | 0 \rangle \\
 &+ \sum_{(2)} \langle 0 | N[\overbrace{\hat{A} \hat{B} \hat{C} \dots \hat{U} \hat{V} \hat{W}}^{(2)}] | 0 \rangle \\
 &\vdots \\
 &+ \sum_{(fc)} \langle 0 | N[\overbrace{\hat{A} \hat{B} \hat{C} \dots \hat{U} \hat{V} \hat{W}}^{(fc)}] | 0 \rangle \\
 &= \sum_{(fc)} \langle 0 | N[\overbrace{\hat{A} \hat{B} \hat{C} \dots \hat{U} \hat{V} \hat{W}}^{(fc)}] | 0 \rangle, \tag{2.72}
 \end{aligned}$$

where (fc) stands for fully contracted.

There also exists a *generalized Wick's theorem* stating

contractions need only to be evaluated between normal ordered strings of creation and annihilation operators, not within them.

The schematic representation reads:

$$\begin{aligned}
 N[\hat{A} \hat{B} \hat{C} \dots] N[\hat{U} \hat{V} \hat{W} \dots] &= N[\hat{A} \hat{B} \hat{C} \dots \hat{U} \hat{V} \hat{W} \dots] \\
 &+ \sum_{(1)} N[\overbrace{\hat{A} \hat{B} \hat{C} \dots \hat{U} \hat{V} \hat{W} \dots}^{(1)}] \\
 &\vdots \\
 &+ \sum_{(fc)} N[\overbrace{\hat{A} \hat{B} \hat{C} \dots \hat{U} \hat{V} \hat{W} \dots}^{(fc)}], \tag{2.73}
 \end{aligned}$$

Wick's theorem along with the generalized theorem constitutes a powerful method for determination of expectation values and matrix elements.

2.4.4 Quasi-Particle Formalism

In a system of many fermions, it is often more convenient to introduce a new N -fermion reference determinant $|\Phi_0\rangle$, instead of the vacuum reference state $|0\rangle$.

$$|\Phi_0\rangle = a_i^\dagger a_j^\dagger a_k^\dagger \dots |0\rangle. \quad (2.74)$$

The process of utilizing Wick's theorem in determining "vacuum expectation" values, or what we rather call reference expectation values, would be less tedious if we omitted the operators constructing the new reference determinant from the vacuum state. This new reference determinant is referred to as the *Fermi vacuum*. In this section we introduce the quasi particle formalism, which takes into account the changes necessary to enable the altering of the reference state.

The states occupied in the reference state $|\Phi_0\rangle$ are named *hole states*, and are said to lie below the Fermi level. The states unoccupied in the reference state are named *particle states*, and are said to lie above the Fermi level. The creation and annihilation operators acting on the new reference state must be changed to accompany this new particle-hole picture. These operators are in this picture called *quasi particle* construction operators.

A hole is created when an annihilation operator acts on an occupied state in the reference state. Creation of a particle requires a creation operator to act on an unoccupied state in the reference state. Destruction of a hole is carried through by a creation operator acting on an occupied state in reference, while destruction of a particle is made by an annihilation operator acting on an unoccupied state in reference. Hole states are indexed by the letters i, j, k, \dots , while particle states are indexed by the letters a, b, c, \dots . To recapitulate; if the quasi particle creation and annihilation operators are denoted b_α^\dagger and b_α respectively, they read:

$$b_\alpha^\dagger = \begin{cases} a_\alpha^\dagger & \alpha = a, b, c, \dots \\ a_\alpha & \alpha = i, j, k, \dots \end{cases} \quad b_\alpha = \begin{cases} a_\alpha & \alpha = a, b, c, \dots \\ a_\alpha^\dagger & \alpha = i, j, k, \dots \end{cases}. \quad (2.75)$$

A quasi particle state can now be expressed by

$$|abs \dots ijk \dots\rangle = b_a^\dagger b_b^\dagger b_c^\dagger \dots b_i^\dagger b_j^\dagger b_k^\dagger \dots |\Phi_0\rangle. \quad (2.76)$$

These operators, applied on the new reference Fermi state, give the same results as the ordinary creation and annihilation operators executed on the vacuum state. Hence, we obtain anticommutation relations for the quasi particle operators identical to those in eqs. (2.52), (2.53) and (2.54), viz.

$$\{b_\alpha, b_\beta\} = 0, \quad (2.77)$$

$$\{b_\alpha^\dagger, b_\beta^\dagger\} = 0, \quad (2.78)$$

$$\{b_\alpha^\dagger, b_\beta\} = \delta_{\alpha\beta}. \quad (2.79)$$

The modifications made in the quasi particle picture affects the concepts of normal ordering and contractions related to Wick's theorem. In the quasi particle picture where we use the b-labeled creation and annihilation operators, all the equations in section 2.4.3 holds by changing from a-labeled to b-labeled operators. It is in the translation from b-labeled to a-labeled operators the confusion can become complete.

A normal ordered operator string of creation and annihilation operators are still defined as the operator string where all creation operators lie to the left of all annihilation operators. However the twofold in the quasi particle construction operators eq. (2.75), lead to a more complex expression in terms of ordinary a-labeled operators. As an example we consider the following translation of a normal ordered operator string:

$$b_i^\dagger b_a^\dagger b_b^\dagger b_c b_j b_k = a_i a_a^\dagger a_b^\dagger a_c a_j^\dagger a_k^\dagger. \quad (2.80)$$

The contractions are also defined as before, see eq. (2.69), but the changes in the normal ordering implies corresponding changes in the contraction relations. In the quasi particle picture there are two contractions resulting in a non-zero result, viz.

$$\overline{b_i b_j^\dagger} = \overline{a_i^\dagger a_j} = a_i^\dagger a_j - N[a_i^\dagger a_j] = a_i^\dagger a_j + a_j a_i^\dagger = \delta_{ij}, \quad (2.81)$$

$$\overline{b_a b_b^\dagger} = \overline{a_a a_b^\dagger} = a_a a_b^\dagger - N[a_a a_b^\dagger] = a_a a_b^\dagger + a_b^\dagger a_a = \delta_{ab}. \quad (2.82)$$

All other contractions combinations results in zero.

Chapter 3

Quantum Dots

In this section we introduce the systems of confined interacting electrons, named quantum dots. First we give a small introduction on what quantum dots are, and depict some of their applications. Next, we consider the quantum dots from a theoretical aspect.

3.1 Quantum Dots: structure and applications

Quantum dots are man-made devices often referred to as *artificial atoms*. The devices contain a small droplet of free electrons fabricated in semiconductor materials. These droplets are obtained by confining electrons in three dimensions inside the semiconductors. The dimension of the droplets range from a few nanometres¹ to the size of a micrometer². The spatial extension of an atom is in the order of 0.1 \AA^3 . We thus conclude that the quantum dot is much bigger than the atom. Typically the size of the quantum dot corresponds to a number of ten to 100 thousands of atoms, and they contain anything from one electron to several thousand electrons[15].

Quantum dots hold many properties similar to those of the naturally occurring quantum system constituting the atom, hence the name artificial atom. Due to the confinement of the electrons in the quantum dot the energy levels become quantized, just like the atom. This analogue can be expanded by viewing two or more quantum dots as an artificial molecule, or a string of quantum dots as an artificial two-dimensional crystal. These analogues makes it possible to perform experiments revealing fundamental quantum theories otherwise not accessible due to the size limitations imposed by nature. An example of this is how the quantum dot can be connected to electrodes, making it possible to study atomic-like properties, while for real atoms this is not possible. Because of the size difference between the artificial and the real atom, in addition to the tunability of the number of electrons in the quantum dot, this device is well suited in a number of experiments. This is one reason why quantum dots have attracted much interest over the past thirty years. Recapitulated in the words of ref. [16];

Quantum dots can recreate many of the phenomena observed in atoms and nuclei, making it possible to explore new physics in the regimes that cannot otherwise be accessed in the laboratory.

¹nanometres $nm = 10^{-9}m$

²micrometer $\mu m = 10^{-6}m$

³ångström $\text{\AA} = 10^{-10}m$

The applications of quantum dots are versatile. The quantum dots possess excellent optical and electrical properties, and are therefore desirable components in electronic devices. In the work of realizing the idea of quantum computers, the quantum dots are considered as possible building components. Quantum dots are also suitable in the area of absorbing and emitting light at any wavelength. This property makes the quantum dot interesting in laser technology. Quantum dots are of interest also when it comes to research and application in medicine and solar cell technologies. For more details on the applications of quantum dots, we refer to [17].

3.2 Theoretical approximation of 2D Quantum Dots

In this section we will consider how the theoretical two-dimensional (2D) quantum dot is modeled. Theoretically the 2D semiconductor quantum dot represent a unique system, which enables the comparison of various quantum theories and methods with experimental results. The article of ref. [15] so delicately puts it:

2D semiconductor quantum dots are an ideal laboratory to investigate the interplay between confinement, magnetic field and electronic correlation effects.

In order to give a complete description of the system we must find its exact Hamiltonian. This however, is not straight forward because of the complexity of the quantum dot. Introduction of approximations is inevitable. The common approximations regarding the quantum dot can be summarized in three stages:

- The velocity of the electrons are considered to be exactly two-dimensional.
- The electrons are confined by a confining potential, which is given an approximate form.
- The interaction potential between the electrons is assumed to be the two-body Coulomb interaction.

The two-dimensionality approximation reduces the number of spatial dimensions from three to two, which leads to a two-dimensional confining potential. This approximation is realized with manufacturing techniques, however truly two-dimensionality is not obtained. According to ref. [18], this approximation will to some extent exaggerate the Coulomb repulsion between the electrons. According to ref. [19], the deviation from pure two-dimensionality is effectively an extra potential term, which can be both positive and negative. The deviation is small, but it is shown to affect some of the model predictions.

A common choice of confining potential is the *harmonic oscillator potential*. This potential is shown to be a good approximation when the particle number is low [20]. However, when the system is approaching a number of twenty electrons, this model is not optimal, and it is important to be aware of this limitation. The harmonic oscillator potential is given as follows, for the general three-dimensional case and the two-dimensional case respectively

$$u(r) = \frac{1}{2}m^*\omega^2r^2, \tag{3.1}$$

$$u(x, y) = \frac{1}{2}m^*\omega_x^2x^2 + \frac{1}{2}m^*\omega_y^2y^2, \tag{3.2}$$

where m^* is the effective mass of the electron, ω is the oscillator frequency, and r is the distance between the electron and the point in space where $V(r) = 0$. Accordingly ω_x and ω_y are the oscillator frequencies in their respective directions, and x and y are the distances between the electron and the point in space where $u(x, y) = 0$.

The two-body Coulomb interaction is given as follows:

$$V(r_{ij}) = \frac{e^2}{4\pi\epsilon_0\epsilon_r} \frac{1}{r_{ij}}, \quad (3.3)$$

where r_{ij} is the distance between electron i and electron j , e is the electron charge, ϵ_0 is the vacuum permittivity, and ϵ_r is the relative permittivity.

In the following we consider the spherically symmetric harmonic oscillator potential as our confining potential, meaning that $\omega_x = \omega_y = \omega_0$, which gives the potential:

$$u(x, y) = \frac{1}{2}m^*\omega_0^2(x^2 + y^2). \quad (3.4)$$

Quantum dots with this confining potential are named *parabolic quantum dots*. Next we consider the single-particle parabolic quantum dot problem, which can be solved exactly. We present the Hamiltonian both with and without the presence of an external perpendicular magnetic field $\mathbf{B} = (0, 0, B_0)$. We will solve the single-particle problem with the presence of an external perpendicular magnetic field. The effect of the external magnetic field is a modified harmonic oscillator frequency and a shift of energy proportional to the strength of the field. This inclusion of a perpendicular magnetic field is useful in order to explain experimental observation of shell structure in the 2D semiconductor quantum dot. We will demonstrate both the effect of the magnetic field and the shell structure in the following sections. First we derive the Schrödinger equation for spherical symmetric potentials in general.

3.2.1 Schrödinger Equation for Spherical Symmetric Potentials

Spherically symmetric potentials depend only on the distance $r = |\vec{r}|$ from a certain point in space (normally origin), viz

$$V = V(r). \quad (3.5)$$

The one-particle Hamiltonian with a spherical symmetric potential reads

$$\begin{aligned} \hat{H} &= \frac{\hat{P}^2}{2m} + V(r), \\ &= -\frac{\hbar^2}{2m}\nabla^2 + V(r), \end{aligned} \quad (3.6)$$

where $\hat{P} = -i\hbar\nabla$ is the momentum operator, m is the mass of the particle, and the Laplacian $\nabla^2 = \frac{\partial^2}{\partial x^2} + \frac{\partial^2}{\partial y^2} + \frac{\partial^2}{\partial z^2}$. When we are dealing with spherical symmetry it is convenient to introduce spherical coordinates (r, φ, θ) . The time-independent Schrödinger equation can then be separated in these new coordinates. We will further consider the two-dimensional case. From section 1.2.5 we have that the total wave function is a tensor product of one spatial part and one spin part. Our spherically symmetric potential does

not dependent on spin, and therefore we only consider the spatial part $\psi(\vec{r})$ of the total wave function.

The two-dimensional time-independent Schrödinger equation in Cartesian coordinates reads

$$-\frac{\hbar^2}{2m} \left(\frac{\partial^2}{\partial x^2} + \frac{\partial^2}{\partial y^2} \right) \psi(x, y) + u(\sqrt{x^2 + y^2}) \psi(x, y) = \epsilon \psi(x, y), \quad (3.7)$$

where $u(\sqrt{x^2 + y^2})$ is a spherically symmetric potential, ϵ is the energy eigenvalue corresponding to the wave function $\psi(x, y)$. If we change to spherical coordinates (r, φ) the two-dimensional momentum operator in second power is given by

$$-\hbar^2 \nabla^2 = -\hbar^2 \left(\frac{\partial^2}{\partial r^2} + \frac{1}{r} \frac{\partial}{\partial r} + \frac{1}{r^2} \frac{\partial^2}{\partial \varphi^2} \right). \quad (3.8)$$

The time-independent Schrödinger equation then yields

$$-\frac{\hbar^2}{2m} \left(\frac{\partial^2}{\partial r^2} + \frac{1}{r} \frac{\partial}{\partial r} + \frac{1}{r^2} \frac{\partial^2}{\partial \varphi^2} \right) \psi(r, \varphi) + u(r) \psi(r, \varphi) = \epsilon \psi(r, \varphi). \quad (3.9)$$

We separate this equation by assuming that the wave function is separable, viz.

$$\psi(r, \varphi) = R(r)Y(\varphi). \quad (3.10)$$

If we insert this into eq. (3.9), multiply by $-\frac{2mr^2}{\hbar R(r)Y(\varphi)}$ and gather the r -terms and φ -terms separately, we obtain

$$\left[\frac{r^2}{R(r)} \frac{\partial^2 R(r)}{\partial r^2} + \frac{r}{R(r)} \frac{\partial R(r)}{\partial r} - \frac{2mr^2}{\hbar^2} (u(r) - \epsilon) \right] + \left[\frac{1}{Y(\varphi)} \frac{\partial^2}{\partial \varphi^2} \right] = 0. \quad (3.11)$$

Since the two square brackets depend on different variables, the two expressions inside them must equal a constant. These two constants must sum up to zero, which means they are equal with opposite signs. Thus, we obtain two separate differential equations:

$$r^2 \frac{\partial^2 R(r)}{\partial r^2} + r \frac{\partial R(r)}{\partial r} - \frac{2mr^2 R(r)}{\hbar^2} (u(r) - \epsilon) = m_l^2 R(r), \quad (3.12)$$

$$\frac{1}{Y(\varphi)} \frac{\partial^2}{\partial \varphi^2} = -m_l^2 Y(\varphi), \quad (3.13)$$

where m_l is a constant.

The angular eq. (3.13) have a solution given by

$$Y(\varphi) = K e^{im_l \varphi}, \quad (3.14)$$

where K is a constant, and i is the imaginary unit. Normalization of the wave function requires that:

$$\int_0^{2\pi} |Y(\varphi)|^2 d\varphi = 1, \quad (3.15)$$

which yields the normalization

$$Y(\varphi) = \frac{1}{\sqrt{2\pi}} e^{im_l \varphi}. \quad (3.16)$$

The value of m_l is determined from the fact that the system is invariant under rotation, viz. $Y(\varphi + 2\pi) = Y(\varphi)$. This implies that

$$e^{im_l 2\pi} = 1, \quad (3.17)$$

thus

$$m_l = 0, \pm 1, \pm 2, \dots \quad (3.18)$$

The spatial eq. (3.12) can be simplified by introducing the substitution $\rho(r) = \sqrt{r}R(r)$. The spatial equation then reads

$$-\frac{\hbar^2}{2m^*} \frac{\partial^2 \rho(r)}{\partial r^2} + \left[u(r) + \frac{\hbar^2}{2m^*} \frac{m_l^2 - \frac{1}{4}}{r^2} \right] \rho(r) = \epsilon \rho(r). \quad (3.19)$$

This equation is named the *radial equation*, and it is identical to the one-dimensional Schrödinger equation with a potential equal the expression inside the square brackets. Normalization conditions for the solution of the radial eq. reads

$$\int_0^\infty |R(r)|^2 r dr = \int_0^\infty |\rho(r)|^2 dr = 1. \quad (3.20)$$

The final spatial solution is given by:

$$\psi(r, \varphi) = \frac{1}{\sqrt{2\pi}} R(r) e^{im_l \varphi}. \quad (3.21)$$

3.2.2 One-Electron Parabolic Quantum Dot

In this section we solve the time-independent Schrödinger equation for the single-particle parabolic quantum dot in two-dimensions, with the presence of an external magnetic field. In the absence of a magnetic field the Hamiltonian reads

$$\hat{H} = -\frac{\hat{P}^2}{2m^*} + \frac{1}{2} m^* \omega_0^2 (x^2 + y^2), \quad (3.22)$$

where

$$\hat{P} = -i\hbar \nabla = -i\hbar \left(\frac{\partial}{\partial x} \mathbf{i} + \frac{\partial}{\partial y} \mathbf{j} \right), \quad (3.23)$$

where \mathbf{i} and \mathbf{j} are the Cartesian unit vectors, \hat{P} is the momentum operator, m^* is the effective mass, ω_0 is the oscillator frequency, and x and y are the distances between the electron and the point in space where $u(x, y) = 0$.

The classical Hamiltonian of a charged particle in an electromagnetic field is given by:

$$\hat{H} = \frac{1}{2m} (\mathbf{p} - e\mathbf{A})^2 + e\Omega, \quad (3.24)$$

where m is the mass of the particle, e is the charge of the particle, Ω and \mathbf{A} are the electromagnetic potentials, and $\mathbf{p} = m\mathbf{v}$ is the classical momentum [21]. The electromagnetic potentials are connected to the electric and magnetic field by the relations:

$$\mathbf{E} = -\frac{\partial \mathbf{A}}{\partial t} - \nabla \Omega, \quad (3.25)$$

$$\mathbf{B} = \nabla \times \mathbf{A}, \quad (3.26)$$

where t is the time and $\nabla = \frac{\partial}{\partial x}\mathbf{i} + \frac{\partial}{\partial y}\mathbf{j} + \frac{\partial}{\partial z}\mathbf{k}$. In section 1.2.4 we learned that charged particles, like the electron, have intrinsic spin. This gives rise to an additional energy term arising from the magnetic moment μ . Thus the Hamiltonian of one electron confined by the spherical symmetric harmonic oscillator potential in a perpendicular magnetic field reads:

$$\hat{H} = \frac{1}{2m^*}(\hat{\mathbf{p}} - e\mathbf{A})^2 + \frac{1}{2}m^*\omega_0^2(x^2 + y^2) + e\Omega - \hat{\mu} \cdot \mathbf{B}. \quad (3.27)$$

The magnetic field is constant and perpendicular to the quantum dot, meaning $\mathbf{B} = B_0\mathbf{k}$. Where \mathbf{k} is the unit vector in z -direction. We assume that no external electric field affects the quantum dot. From eq. (3.26) we have that if \mathbf{B} is constant in time, then \mathbf{A} must be constant in time. From eq. (3.25) and the fact that no electric field is present we then have that

$$\nabla\Omega = 0, \quad (3.28)$$

which means that Ω is a constant, and $e\Omega$ is just a constant addition to the energy in eq. (3.27).

We have many degrees of freedom in the choice of determining the form of the potentials \mathbf{A} and Ω . Gauge transformations are transformations of the potentials that leave the electromagnetic fields unchanged. The purpose of performing these transformations is to handle the redundant degrees of freedom in the field variables. One can make specific gauge choices by defining conditions that the potentials should satisfy [21]. This is what we will do in order to express the Hamiltonian in a more convenient form. Consider the first term in eq. (3.27). By expanding this we obtain:

$$(\hat{\mathbf{p}} - e\mathbf{A})^2 = \hat{\mathbf{p}}^2 + e^2\mathbf{A}^2 - e(\hat{\mathbf{p}} \cdot \mathbf{A} + \mathbf{A} \cdot \hat{\mathbf{p}}). \quad (3.29)$$

We can make \mathbf{p} and \mathbf{A} commute by applying the Coulomb gauge, viz.

$$\nabla \cdot \mathbf{A} = 0. \quad (3.30)$$

In general \mathbf{A} is given by

$$\mathbf{A} = A_x(x, y, z)\mathbf{i} + A_y(x, y, z)\mathbf{j} + A_z(x, y, z)\mathbf{k}. \quad (3.31)$$

By applying the Coulomb gauge, \mathbf{A} reads

$$\mathbf{A} = A_x(y, z)\mathbf{i} + A_y(x, z)\mathbf{j} + A_z(x, y)\mathbf{k} \quad (3.32)$$

We now choose a vector potential \mathbf{A} with respect to the given limitations, one possibility reads

$$\mathbf{A} = \frac{B_0}{2}(-y\mathbf{i} + x\mathbf{j}), \quad (3.33)$$

If we insert this into eq. (3.29), we obtain:

$$(\hat{\mathbf{p}} - e\mathbf{A})^2 = \hat{\mathbf{p}}^2 + \frac{e^2 B_0^2}{4}(\hat{x}^2 + \hat{y}^2) - eB_0(\hat{x}\hat{p}_y - \hat{y}\hat{p}_x). \quad (3.34)$$

In books on quantum mechanics, for example ref. [6], the angular momentum operator reads

$$\begin{aligned} \hat{\mathbf{L}} &= \hat{\mathbf{r}} \times \hat{\mathbf{p}}, \\ &= \hat{L}_x\mathbf{i} + \hat{L}_y\mathbf{j} + \hat{L}_z\mathbf{k}, \\ &= (\hat{y}\hat{p}_z - \hat{z}\hat{p}_y)\mathbf{i} + (\hat{z}\hat{p}_x - \hat{x}\hat{p}_z)\mathbf{j} + (\hat{x}\hat{p}_y - \hat{y}\hat{p}_x)\mathbf{k}. \end{aligned} \quad (3.35)$$

We recognize the z -projection of the angular momentum \hat{L}_z in the last term of eq. (3.34). Inserting this into the Hamiltonian reads

$$\hat{H} = \frac{1}{2m^*} \left(\hat{\mathbf{p}}^2 + \frac{e^2 B_0^2}{4} (\hat{x}^2 + \hat{y}^2) - eB_0 \hat{L}_z \right) + \frac{1}{2} m^* \omega_0^2 (x^2 + y^2) + e\Omega - \hat{\mu} \cdot \mathbf{B}. \quad (3.36)$$

This expression can be simplified by defining

$$\omega_B = \frac{eB_0}{2m^*}, \quad (3.37)$$

$$\omega^2 = \omega_B^2 + \omega_0^2, \quad (3.38)$$

which yields the Hamiltonian

$$\hat{H} = \frac{1}{2m^*} \left(\hat{\mathbf{p}}^2 - eB_0 \hat{L}_z \right) + \frac{1}{2} m^* \omega^2 (x^2 + y^2) + e\Omega - \hat{\mu} \cdot \mathbf{B}. \quad (3.39)$$

We now solve the single-particle parabolic quantum dot problem by inserting the Hamiltonian into the time-independent Schrödinger equation, viz.

$$\left(\frac{1}{2m^*} \left(\hat{\mathbf{p}}^2 - eB_0 \hat{L}_z \right) + \frac{1}{2} m^* \omega^2 (x^2 + y^2) + e\Omega - \hat{\mu} \cdot \mathbf{B} \right) \psi(\mathbf{x}) = \epsilon \psi(\mathbf{x}), \quad (3.40)$$

where ϵ is the energy eigenvalue, and \mathbf{x} contains spatial and spin degrees of freedom. $\psi(\mathbf{x})$ is the total wave function of the system. In section 1.2.5 the total wave function was defined as

$$\psi(\mathbf{x}) = \psi(\vec{r}) \otimes |\chi\rangle, \quad (3.41)$$

where $\psi(\vec{r})$ is the spatial dependent part, and $|\chi\rangle$ is the spin dependent part. The Hamiltonian in eq. (3.39) contains one spin dependent part, and two spatial dependent parts, which leads to the time-independent Schrödinger equations

$$\left(\frac{1}{2m^*} \left(\hat{\mathbf{p}}^2 - eB_0 \hat{L}_z \right) + \frac{1}{2} m^* \omega^2 (x^2 + y^2) \right) \psi(x, y) = \epsilon_r \psi(x, y) \quad (3.42)$$

$$- (\hat{\mu} \cdot \mathbf{B}) |\chi\rangle = \epsilon_s |\chi\rangle, \quad (3.43)$$

where the total energy of the system reads

$$\epsilon = \epsilon_r + \epsilon_s + e\Omega. \quad (3.44)$$

We first consider the solution of the spatial wave function and corresponding energy from eq. (3.42). A solution is easier to find if we express this equation in spherical coordinates. The spherical expression for the momentum operator in second power is given in eq. (3.8). The z -projection operator of the angular moment in spherical coordinates reads

$$\hat{L}_z = -i\hbar \frac{\partial}{\partial \varphi}, \quad (3.45)$$

which result in the time-independent Schrödinger equation

$$-\frac{\hbar^2}{2m^*} \left(\frac{\partial^2}{\partial r^2} + \frac{1}{r} \frac{\partial}{\partial r} + \frac{1}{r^2} \frac{\partial^2}{\partial \varphi^2} - \frac{ieB_0}{\hbar} \frac{\partial}{\partial \varphi} \right) \psi(r, \varphi) + \frac{1}{2} m^* \omega^2 r^2 \psi(r, \varphi) = \epsilon_r \psi(r, \varphi). \quad (3.46)$$

Compared to the corresponding equation for general spherical symmetric potentials given in eq. (3.9), we observe that the only difference is the additional term $-\frac{ieB_0}{\hbar} \frac{\partial}{\partial \varphi}$ originating from the magnetic field. This additional term depends only on the angle φ , and the solution is therefore separable. We assume that we have the same solution of the angular part as given in eq. (3.16), thus the spatial wave function reads

$$\psi(r, \varphi) = \frac{1}{\sqrt{2\pi}} R(r) e^{im_l \varphi}, \quad (3.47)$$

where m_l takes the values in eq. (3.18), and we have demanded that $e^{im_l \varphi} = 1$. Inserting this into eq. (3.46) results in the time-independent Schrödinger equation:

$$\frac{1}{\sqrt{2\pi}} \left[-\frac{\hbar^2}{2m^*} \left(\frac{\partial^2}{\partial r^2} + \frac{1}{r} \frac{\partial}{\partial r} - \frac{m_l^2}{r^2} + \frac{em_l B_0}{\hbar} \right) + \frac{1}{2} m^* \omega^2 r^2 \right] R(r) = \epsilon_r \frac{R(r)}{\sqrt{2\pi}}. \quad (3.48)$$

The normalized solutions to this equation is given by

$$\psi_{nm_l}(r, \varphi) = \sqrt{\frac{n!}{\pi(n+|m_l|)!}} \beta^{\frac{1}{2}(1+|m_l|)} r^{|m_l|} e^{-\frac{1}{2}\beta r^2} L_n^{|m_l|}(\beta r^2) e^{im_l \varphi}, \quad (3.49)$$

where $L_n^{|m_l|}(\beta r^2)$ is the associated Laguerre polynomials, and β is defined as

$$\beta = \frac{m^* \omega}{\hbar}. \quad (3.50)$$

The energy eigenvalues are given as

$$\epsilon_r = (1 + |m_l| + 2n) \hbar \omega + m_l \hbar \omega_B, \quad (3.51)$$

where $n = 0, 1, 2, 3, \dots$ and ω_b is given in eq. (3.37). The derivation of eqs. (3.49) and (3.51) can be found in [2].

Next we consider the solution of the spin wave function and corresponding energy from eq. (3.43). The magnetic moment $\hat{\mu}$ reads

$$\hat{\mu} = g \frac{e}{2m^*} \hat{S}, \quad (3.52)$$

where m^* is the particle mass, e is the electron charge, \hat{S} is the spin operator, and g is the g-factor of the electron. In our case the magnetic field is constant and perpendicular to the quantum dot, viz. $\mathbf{B} = B_0 \mathbf{k}$. The Hamilton contribution thus reads

$$\begin{aligned} -\hat{\mu} \cdot \mathbf{B} &= -g \frac{e}{2m^*} \hat{S} \cdot B_0 \mathbf{k}, \\ &= -g \frac{e B_0}{2m^*} \hat{S}_z, \\ &= -g \omega_B \hat{S}_z. \end{aligned} \quad (3.53)$$

In section 1.2.4 we discussed the intrinsic spin of particles. We denoted the spin-state $|\chi\rangle$ by $|s, m_s\rangle$, where s is the eigenvalue of the spin operator \hat{S} , and m_s is the eigenvalue of

the z -projection \hat{S}_z of the spin. The effect of applying \hat{S}_z on the spin state is given in eq. (1.74). The solution of the spin Schrödinger eq. in (3.43) thus reads

$$-g\omega_B \hat{S}_z |\chi\rangle = -g\omega_B \hbar m_s |\chi\rangle = \epsilon_s |\chi\rangle. \quad (3.54)$$

The total wave function of the single-particle 2D parabolic quantum dot can now be expressed as follows

$$\psi_{nm_l m_s}(r, \varphi) = \sqrt{\frac{n!}{\pi(n+|m_l|)!}} \beta^{\frac{1}{2}(1+|m_l|)} r^{|m_l|} e^{-\frac{1}{2}\beta r^2} L_n^{|m_l|}(\beta r^2) e^{im_l \varphi} \otimes |\chi_{m_s}\rangle, \quad (3.55)$$

where $|\chi_{m_s}\rangle$ represent the spin states given in eqs. (1.78) and (1.79). This wave function is normalized. The corresponding energy eigenvalues are given as

$$\epsilon_{nm_l m_s} = (1 + |m_l| + 2n)\hbar\omega + m_l \hbar\omega_B - g m_s \hbar\omega_B + e\Omega. \quad (3.56)$$

If the magnetic field is removed, thus $\omega_B = 0$ and $\Omega = 0$, then the energy reads

$$\epsilon_{nm_l}^0 = (1 + |m_l| + 2n)\hbar\omega_0, \quad (3.57)$$

where the zero power denotes the absence of the magnetic field. This energy spectrum is the same as the one we would obtain if we solved the radial eq. (3.19) directly. The quantum numbers of the energy spectrum $\epsilon_{nm_l}^0$ take on the values:

$$\begin{aligned} n &= 0, 1, 2, 3, \dots, \\ m_l &= 0, \pm 1, \pm 2, \pm 3, \dots, \end{aligned}$$

which means that the degeneracy d of this energy spectrum, when included spin degeneracy (spin-up/spin-down), reads

$$D = 2d = 2(1 + |m_l| + 2n). \quad (3.58)$$

This is called the *shell structure* of the quantum dot. Shell structures similar to this one are often observed in nature. The shell number is defined as

$$R = (1 + |m_l| + 2n), \quad (3.59)$$

and is associated with the energy level without the factor $\hbar\omega_0$. This shell structure is illustrated in fig. 3.1. Table 3.1 lists the corresponding values of shell number, degeneracy, m_l and n , together with the *magic numbers* given by shell-fillings. The magic numbers are the numbers of non-interacting electrons, which is required in order to obtain a closed-shell ground state for the corresponding shell number. Thus, it is the sum of the the current shell-degeneracy and all lower shell-degeneracies.

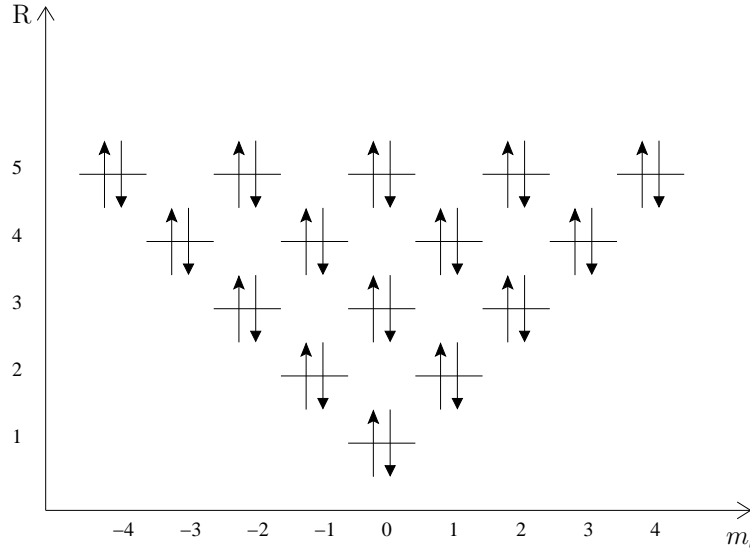


Figure 3.1: The figure illustrates the shell structure of the single-electron parabolic quantum dot in two dimensions. R is the shell number defined in eq. 3.59, m_l is the angular quantum number, while $\uparrow\downarrow$ represent orbitals with $m_s = \pm\frac{1}{2}$.

Shell number R	Degeneracy D	m_l	n	Shell-filling
1	2	0	0	2
2	4	± 1	0	6
3	6	$0, \pm 2$	1,0	12
4	8	$\pm 1, \pm 3$	1,0	20
5	10	$0, \pm 2, \pm 4$	2,1,0	30
6	12	$\pm 1, \pm 3, \pm 5$	2,1,0	42

Table 3.1: The table shows the shell structure of the single-electron parabolic quantum dot in two dimensions. The shell number (energy level) is given in the left most column, the degeneracy denotes how many particles it is possible to place in the corresponding shell, and the shell-filling represent the number of particles needed in order to fill all underlying shells including the corresponding shell. The quantum numbers m_l and n constituting the shell number are also given, note that they are listed in a corresponding order.

We now return to the case where a magnetic field is applied. From the energy spectrum given by eq. (3.56), we observe that the energy now depends on the signe of the quantum number m_l and m_s . We observe that by applying a magnetic field we obtain lifting of the angular degeneracies, present when no magnetic field is applied. This means that the energy levels with positive m_l -values are shifted downward, and energy levels with negative m_l -values are shifted upward. The term containing m_s would lift the spin-up/spin-down degeneracy and result in even more energy levels. The lifting of angular degeneracy can be illustrated by neglecting the m_s -term and the constant term $e\Omega$, which results in an

energy spectrum given by eq. (3.51). Substituting eq. (3.38) into this energy spectrum, and dividing by $\hbar\omega_0$ produces the energy spectra given as

$$\frac{\epsilon_{nm_l}}{\hbar\omega_0} = (1 + |m_l| + 2n) \sqrt{1 + \frac{\omega_B^2}{\omega_0^2}} + m_l \frac{\omega_B^2}{\omega_0^2}. \quad (3.60)$$

This energy spectrum can be illustrated in an energy vs. magnetic field diagram called a *Fock-Darwin Spectrum*. Characteristic for the Fock-Darwin spectrum is the criss-cross pattern of energy levels with positive and negative quantum number m_l . See the Fock-Darwin spectrum of this 2D parabolic quantum dot in fig. 3.2. In order to observe this

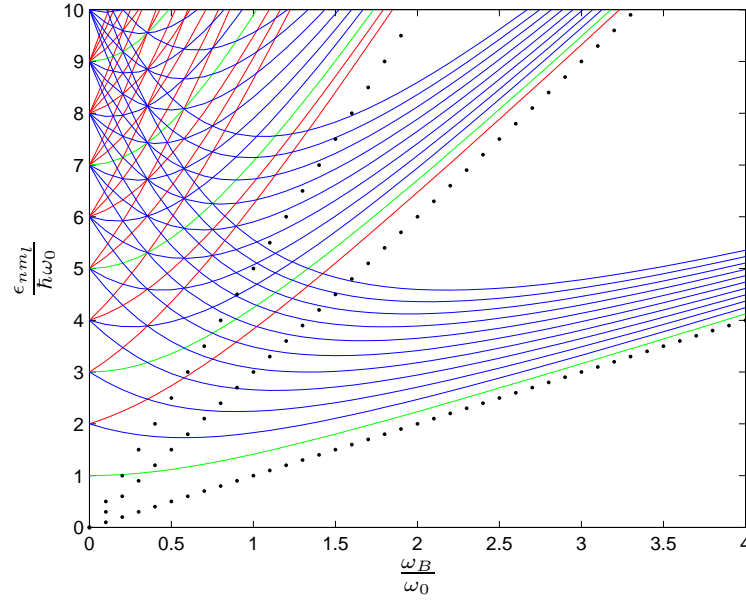


Figure 3.2: The two-dimensional Fock-Darwin spectrum illustrates how the angular degeneracies are lifted when a magnetic field is applied to the parabolic quantum dot. Levels of positive m_l -values (blue color) are shifted downwards, while levels of negative m_l -levels (red color) are shifted upwards. Levels with $m_l = 0$ have green color. This results in the characteristic criss-cross pattern of energy levels.

pattern for real atoms, magnetic fields in the order of hundreds to thousands of Tesla would be necessary. However in quantum dots these effects are observed with magnetic fields of a few to tens of Tesla. This is an example of how the quantum dot makes it easier to explore some physical phenomena. Interesting physical phenomena can be observed by increasing the strength of the magnetic field. By applying a high enough magnetic field, one can obtain degeneracies between positive angular moment states of lower levels, and negative angular moment states of higher levels. Thus, we obtain degeneracies with states of different shell numbers, which means that we have mixing of states that is not immediately obvious. Electrons in these degenerate states will choose to occupy the available states with most favorable energy, meaning the states with the lowest energy. Further increase in the magnetic field will give rise to new degeneracies. From Fig. 3.2 we observe that in the limit $\frac{\omega_B}{\omega_0} \rightarrow \infty$ the energy levels seems to form a band structure.

The energy spectrum in this limit reads

$$\lim_{\omega_B \rightarrow \infty} \epsilon_{nm_l} = (1 + |m_l| + 2n + m_l) \hbar \omega_B. \quad (3.61)$$

This spectrum takes two forms depending on the signed value of m_l . For positive values the spectrum reads

$$\lim_{\omega_B \rightarrow \infty} \epsilon_{nm_l} = (1 + 2(n + m_l)) \hbar \omega_B. \quad (3.62)$$

Negative m_l -values results in a spectrum independent of m_l , viz.

$$\lim_{\omega_B \rightarrow \infty} \epsilon_{nm_l} = (1 + 2n) \hbar \omega_B. \quad (3.63)$$

The band structure we observe for large field values are named *Landau bands* because the energy eigenvalues asymptotically approach the Landau levels [22]. Landau levels are given as

$$\epsilon_{N_L} = (1 + 2N_L) \hbar \omega_B, \quad (3.64)$$

where N_L is the Landau level index, which takes on values

$$N_L = 0, 1, 2, \dots \quad (3.65)$$

In fig. 3.2 we have plotted the three first Landau levels as dotted black lines. The asymptotic behavior is clearly illustrated by this.

3.2.3 Two-Electron Parabolic Quantum Dot

In this section we introduce the system of a two-electron parabolic quantum dot in two-dimensions. According to ref. [23], this system, where the electrons interact via the Coulomb interaction, have an analytic solution. The analytic solution provides a good benchmark, meaning that our computational programs must reproduce this result in order to obtain credibility.

The Hamiltonian of this 2-electron system reads

$$\hat{H} = \sum_{i=1}^2 \left\{ \frac{1}{2m^*} (\hat{\mathbf{p}}_i - e\mathbf{A}_i)^2 + \frac{1}{2} m^* \omega_0^2 r_i^2 \right\} + \frac{e^2}{4\pi\epsilon_0\epsilon_r r_{12}}, \quad (3.66)$$

where ϵ_0 is the vacuum permittivity, ϵ_r is the relative permittivity, $r_i^2 = x_i^2 + y_i^2$, and $r_{12} = |\vec{r}_2 - \vec{r}_1|$. We consider only the spatial part of the wave function. Inclusion of spin will produce the same addition to the wave function and the energy as in the section above, eqs. (3.55) and (3.56). We proceed by introducing the relative coordinate \vec{r} and the center-of-mass coordinate \vec{R} respectively

$$\vec{r} = \vec{r}_2 - \vec{r}_1, \quad (3.67)$$

$$\vec{R} = \frac{\vec{r}_1 + \vec{r}_2}{2}, \quad (3.68)$$

which enables the definition of two new momentum operators $\hat{\mathbf{p}}$ and $\hat{\mathbf{P}}$

$$\hat{\mathbf{p}} = \frac{\hat{\mathbf{p}}_2 - \hat{\mathbf{p}}_1}{2}, \quad (3.69)$$

$$\hat{\mathbf{P}} = \hat{\mathbf{p}}_1 + \hat{\mathbf{p}}_2. \quad (3.70)$$

The vector potential \mathbf{A} can be expressed as follows, given that the magnetic field has a perpendicular form $\mathbf{B} = B_0 \mathbf{k}$, where \mathbf{k} is the unit vector in z-direction.

$$\mathbf{A}(\vec{r}) = \mathbf{A}(\vec{r}_2) - \mathbf{A}(\vec{r}_1), \quad (3.71)$$

$$\mathbf{A}(\vec{R}) = \frac{\mathbf{A}(\vec{r}_1) + \mathbf{A}(\vec{r}_2)}{2}. \quad (3.72)$$

From these definitions it is clear that we have some useful relations, which reads:

$$\vec{r}_1^2 + \vec{r}_2^2 = \frac{1}{2}(4\vec{R}^2 + \vec{r}^2), \quad (3.73)$$

$$\hat{\mathbf{p}}_1^2 + \hat{\mathbf{p}}_2^2 = \frac{1}{2}(\hat{\mathbf{P}}^2 + 4\hat{\mathbf{p}}^2), \quad (3.74)$$

$$\mathbf{A}(\vec{r}_1)^2 + \mathbf{A}(\vec{r}_2)^2 = \frac{1}{2}\mathbf{A}(\vec{r})^2 + 2\mathbf{A}(\vec{R})^2. \quad (3.75)$$

Next we write out the explicit expression of the Hamiltonian eq. (3.66):

$$\begin{aligned} \hat{H} = & \frac{1}{2m^*} [\hat{\mathbf{p}}_1^2 + \hat{\mathbf{p}}_2^2 - 2e(\hat{\mathbf{p}}_1 \cdot \mathbf{A}(\vec{r}_1) + \hat{\mathbf{p}}_2 \cdot \mathbf{A}(\vec{r}_2)) + e^2(\mathbf{A}^2(\vec{r}_1) + \mathbf{A}^2(\vec{r}_2))] \\ & + \frac{1}{2}m^*\omega_0^2(r_1^2 + r_2^2) + \frac{e^2}{4\pi\epsilon_0\epsilon_r r_{12}} \end{aligned} \quad (3.76)$$

If we exploit the given relations and insert the relative and the center-of-mass coordinates, we obtain the Hamiltonian

$$\begin{aligned} \hat{H} = & \frac{1}{2m^*} \left[2\hat{\mathbf{p}}^2 + \frac{1}{2}\hat{\mathbf{P}}^2 - 2e(\hat{\mathbf{p}} \cdot \mathbf{A}(\vec{r}) + \hat{\mathbf{P}} \cdot \mathbf{A}(\vec{R})) + e^2 \left(\frac{1}{2}\mathbf{A}^2(\vec{r}) + 2\mathbf{A}^2(\vec{R}) \right) \right] \\ & + \frac{1}{2}m^*\omega_0^2(2\vec{R}^2 + \frac{1}{2}\vec{r}^2) + \frac{e^2}{4\pi\epsilon_0\epsilon_r r}. \end{aligned} \quad (3.77)$$

We introduce the relations

$$\begin{aligned} \mathbf{A}_r &= \frac{1}{2}\mathbf{A}(\vec{r}), \quad \mathbf{A}_R = 2\mathbf{A}(\vec{R}), \\ \omega_r &= \frac{1}{2}\omega_0, \quad \omega_R = 2\omega_0, \end{aligned}$$

which give rise to the Hamiltonian expressed as

$$\begin{aligned} \hat{H} &= \frac{1}{2} \left\{ \frac{1}{2m^*} [\hat{\mathbf{P}} - e\mathbf{A}_R]^2 + \frac{1}{2}m^*\omega_R^2\vec{R}^2 \right\} \\ &+ 2 \left\{ \frac{1}{2m^*} [\hat{\mathbf{p}} - e\mathbf{A}_r]^2 + \frac{1}{2}m^*\omega_r^2\vec{r}^2 + \frac{e^2}{4\pi\epsilon_0\epsilon_r r} \right\}, \\ &= \frac{1}{2}\hat{H}_R + 2\hat{H}_r. \end{aligned} \quad (3.78)$$

This illustrates the separability in the coordinates \vec{r} and \vec{R} , meaning that we can make a product ansatz for the wave function, viz.

$$\Psi(\vec{R}, \vec{r}) = \psi(\vec{R})\psi(\vec{r}), \quad (3.79)$$

These separated wave functions are eigenfunctions of the time-independent Schrödinger equation of the respective Hamiltonians, viz.

$$\hat{H}_R \psi_R(\vec{R}) = \epsilon_R \psi_R(\vec{R}), \quad (3.80)$$

$$\hat{H}_r \psi_r(\vec{r}) = \epsilon_r \psi_r(\vec{r}), \quad (3.81)$$

The total energy is therefore given as

$$\epsilon = \frac{1}{2} \epsilon_R + 2 \epsilon_r, \quad (3.82)$$

We now assume that we have the same magnetic field ($\mathbf{B} = B_0 \mathbf{k}$) and the same gauge potential field (eq. (3.33)) as for the single-particle problem in the previous section. In a similar manner as we defined ω in eq. (3.38), we now define $\bar{\omega}_R$ and $\bar{\omega}_r$, viz.

$$\bar{\omega}_R^2 = \omega_R^2 + 4\omega_B^2 = 2\omega, \quad (3.83)$$

$$\bar{\omega}_r^2 = \omega_r^2 + \frac{\omega_B^2}{4} = \frac{\omega}{2}, \quad (3.84)$$

From eq. (3.78), we observe that the center-of-mass Hamiltonian \hat{H}_R is identical to the single-particle Hamiltonian, only with modified parameters. The energy solution is thus the same as for the single-particle problem in eq. (3.51), viz.

$$\begin{aligned} \epsilon_R &= (2N + |M| + 1) \hbar \bar{\omega}_R + 2M \hbar \omega_B \\ &= 2(2N + |M| + 1) \hbar \omega + 2M \hbar \omega_B, \end{aligned} \quad (3.85)$$

where M and N are the quantum numbers, and ω and ω_B are defined as in the previous section. The ground state energy is obtained when $N = M = 0$, viz.

$$\epsilon_R^0 = 2\hbar\omega. \quad (3.86)$$

From eq. (3.78) we also observe that the relative Hamiltonian \hat{H}_r , unlike \hat{H}_R , contains an additional term proportional to $\frac{1}{r}$. This means that in general eq. (3.81) has no analytic solution. However, according to ref. [23], it is possible to obtain closed-form expressions for particular values of $\bar{\omega}_r$. We refer to ref. [23] for a full derivation of the technique of finding these closed-form solutions. Here we only list the results. The energy solutions of eq. (3.81) are given as

$$\begin{aligned} \epsilon_r &= (n + |m|) \hbar \bar{\omega}_r + \frac{1}{2} m \hbar \omega_B \\ &= \frac{1}{2} (n + |m|) \hbar \omega + \frac{1}{2} m \hbar \omega_B. \end{aligned} \quad (3.87)$$

The ground state is found by choosing $n = 2$ and $m = 0$, which results in $\omega = 1$ and the energy

$$\epsilon_r^0 = \hbar. \quad (3.88)$$

The total energy when $\omega = 1$ is found by eq. (3.82), and reads $3\hbar$.

3.2.4 Hamiltonian of N -electron Quantum Dots

The two previous sections show that only the single-electron quantum dot has an analytic solution, and that for the special case of an interacting two-electron quantum dot, one can obtain particular solutions. The N -electron quantum dot system must therefore be considered numerically. We will in this section present the Hamiltonian of this system.

We assume that we have a constant magnetic field pointing in the perpendicular z -direction relative to the quantum dot, thus $\mathbf{B} = B_0 \mathbf{k}$. We also assume that we use the Coulomb gauge with the potential field defined in eq. (3.33), and oscillator frequencies defined in eqs. (3.37) and (3.38). The Hamiltonian then reads

$$\begin{aligned} \hat{H} &= \sum_{i=1}^N \left(\frac{1}{2m^*} (\hat{\mathbf{p}}_i - e\mathbf{A}_i)^2 + \frac{1}{2} m^* \omega_0^2 (x_i^2 + y_i^2) + e\Omega - \hat{\mu}_i \cdot \mathbf{B} \right) + \frac{e^2}{4\pi\epsilon_0\epsilon_r} \sum_{i<j}^N \frac{1}{r_{ij}} \\ &= \sum_{i=1}^N \left(-\frac{\hbar^2}{2m^*} \nabla_i^2 - \omega_B \hat{L}_z^{(i)} + \frac{1}{2} m^* \omega^2 r_i^2 - g\omega_B \hat{S}_Z^{(i)} \right) + \frac{e^2}{4\pi\epsilon_0\epsilon_r} \sum_{i<j}^N \frac{1}{r_{ij}}, \end{aligned} \quad (3.89)$$

where we in the second equality assume $e\Omega = 0$. We can make this assumption since this term is a constant contribution to the energy. This Hamiltonian is similar to the single-electron Hamiltonian eq. (3.27), except for the added interaction term and the sum over all N -electrons. See section 3.2.2 for a more detailed derivation of the second equality. Both operators \hat{L}_z and \hat{S}_Z commute with the Hamiltonian, which means that calculations can be performed separately in subspaces given by \hat{L}_z and \hat{S}_Z [24]. The operators can therefore be replaced by the corresponding good quantum numbers. The Hamiltonian then reads

$$\hat{H} = \sum_{i=1}^N \left(-\frac{\hbar^2}{2m^*} \nabla_i^2 + \frac{1}{2} m^* \omega^2 r_i^2 - \omega_B (m_l^{(i)} + g m_s^{(i)}) \right) + \frac{e^2}{4\pi\epsilon_0\epsilon_r} \sum_{i<j}^N \frac{1}{r_{ij}}. \quad (3.90)$$

From this expression we observe that the angular and the spin part of the Hamiltonian constitute a constant addition to the energy. We remove this constant from the calculations in order to obtain the easiest solvable Hamiltonian, viz.

$$\hat{H} = \sum_{i=1}^N \left(-\frac{\hbar^2}{2m^*} \nabla_i^2 + \frac{1}{2} m^* \omega^2 r_i^2 \right) + \frac{e^2}{4\pi\epsilon_0\epsilon_r} \sum_{i<j}^N \frac{1}{r_{ij}}. \quad (3.91)$$

By solving this Hamiltonian numerically and adding the constant contribution from the angular part and the spin part, we obtain the energy of the N -electron system.

In the particular case where we are considering only closed-shell systems, i.e. systems of 2, 6, 12, 20, ... electrons, there is a symmetry in the angular and spin quantum numbers in the shell structure. The shell structure contains quantum numbers given as

$$m_l = 0, \pm 1, \pm 2, \dots, \pm m_{max}, \quad (3.92)$$

$$m_s = \pm \frac{1}{2}, \quad (3.93)$$

where m_{max} is determined by the relevant shell. When we add the constant angular and spin energy contribution, we sum over all these quantum numbers. Obviously the positive and the negative quantum numbers will cancel each other. Thus for closed-shell systems there is no angular or spin contribution to be added, and effectively the system with an external magnetic field is determined by tuning the oscillator frequency $\omega_o \rightarrow \omega$.

3.2.5 Dimensionality Scaling

The Hamiltonian in eq. (3.91) can be simplified by scaling it into a dimensionless form. The scaling will be introduced in this section.

We start by expressing the variables in terms of corresponding dimensionless variables, viz. we define

$$\omega \equiv \omega_c \omega', \quad (3.94)$$

$$\vec{r} \equiv l_0 \vec{r}' = l_0(x' \mathbf{i} + y' \mathbf{j} + z' \mathbf{k}), \quad (3.95)$$

$$\nabla^2 \equiv \frac{1}{l_0^2} \nabla'^2, \quad (3.96)$$

where ' denotes the dimensionless variables, and ω_c and l_0 are constants. We insert these expressions into eq. (3.91) and obtain

$$\hat{H} = -\frac{\hbar^2}{2m^* l_0^2} \sum_{i=1}^N \nabla_i'^2 + \frac{1}{2} m^* \omega_c^2 \omega'^2 l_0^2 \sum_{i=1}^N r_i'^2 + \frac{\hbar}{\kappa l_0} \sum_{i < j}^N \frac{1}{r_{ij}'}, \quad (3.97)$$

where κ is defined as

$$\kappa = \frac{4\pi\epsilon_0\epsilon_r\hbar}{e^2}. \quad (3.98)$$

In order to obtain a dimensionless Hamiltonian we multiply eq. (3.97) by $\frac{m^* l_0^2}{\hbar^2}$, viz.

$$\frac{m^* l_0^2}{\hbar^2} \hat{H} = -\frac{1}{2} \sum_{i=1}^N \nabla_i'^2 + \frac{1}{2} \left(\frac{m^* \omega_c \omega' l_0^2}{\hbar} \right)^2 \sum_{i=1}^N r_i'^2 + \frac{m^* l_0}{\kappa \hbar} \sum_{i < j}^N \frac{1}{r_{ij}'}. \quad (3.99)$$

Next we assume that

$$l_0 = \frac{\kappa \hbar}{m^*} \quad (3.100)$$

Inserting this into eq. (3.99) reads

$$\frac{\kappa^2}{m^*} \hat{H} = -\frac{1}{2} \sum_{i=1}^N \nabla_i'^2 + \frac{1}{2} \left(\frac{\hbar \kappa^2}{m^*} \right)^2 \omega_c^2 \omega'^2 \sum_{i=1}^N r_i'^2 + \sum_{i < j}^N \frac{1}{r_{ij}'}. \quad (3.101)$$

From the above expression we observe that a suitable choice of ω_c reads

$$\omega_c = \frac{m^*}{\hbar \kappa^2}. \quad (3.102)$$

This finally results in the dimensionless Hamiltonian

$$\begin{aligned} \hat{H}' &= \frac{1}{2} \sum_{i=1}^N (-\nabla_i'^2 + \omega'^2 r_i'^2) + \sum_{i < j}^N \frac{1}{r_{ij}'} \\ &= \sum_{i=1}^N \hat{h}'_i + \sum_{i < j}^N \hat{v}'_{ij}, \end{aligned} \quad (3.103)$$

where the dimensionless Hamiltonian \hat{H}' is defined as

$$\hat{H}' = \frac{\kappa^2}{m^*} \hat{H} = \frac{\hat{H}}{E_H}. \quad (3.104)$$

When applying the dimensionless Hamiltonian, the energy is measured in units of E_H , called Hartrees, and lengths are measured in units of l_0 .

Chapter 4

Hartree-Fock Method

In this chapter we introduce the theory of the Hartree-Fock (HF) method. This method is frequently used in disciplines like computational physics and computational chemistry for solving the many-body problem of fermions. In the first section we expose the idea of the method, and in the subsequent section the HF equations are derived.

4.1 Introducing HF

The Hartree Fock method is an *ab initio*¹ many-body method. The method is a simplification of the many-body problem of the system of interacting fermions encountered in chapter 2. Through simplifying approximations the method determines the ground state energy and wave function of the fermion system. The method is based on describing the interacting fermion system in terms of an effective single particle problem. By assuming that each particle in the system moves in a mean-field potential, produced by all the other particles in the system and possibly an external potential, we approximate the two-particle potential by an effective single particle potential, namely the Hartree-Fock potential. The HF potential is unknown, this makes it difficult to determine the single-particle orbitals in the Slater determinants, which constitute the wave function. The problem is solved by making an ansatz stipulating the exact many-body wave function as a single Slater determinant of single-particle orbitals. Ritz' variational theorem states that this ansatz is optimized by minimizing the total energy of the system [11]. Minimizing with respect to the single-particle orbitals yields the HF equations, see section 4.2.

The HF method is thus a variational method, which because of the coupling between the single-particle orbitals, via the HF potential, must be solved iteratively. The method is a result of the work of the English physicist Hartree and the Russian physicist Fock. Hartree developed the Hartree self-consistent field method in the late 1920s. In 1930 Fock contributed to the method by pointing out that Hartree's method did not obey Pauli's exclusion principle. Thus, the Hartree-Fock method is similar to the Hartree self consistent field method, except from the definition of the wave function. In the Hartree-Fock method the wave function, as already mentioned, takes into account Pauli's exclusion principle by taking shape as a Slater determinant containing single-particle orbitals.

¹Latin term meaning "from the beginning", indicates that the theory and calculations are based on first principles, not empirical results.

The HF method is one of the simplest approximation methods to the solution of the many-fermion Hamiltonian. The method does not precisely take into account the Coulomb repulsion between electrons. However, Pauli's exclusion principle, and hence the repulsion between particles with same spin, is accurately included. The method therefore gives useful information about the fermion system. For this reason it often serves as the starting point of more complex methods, which do address the Coulomb repulsion, e.g. the variational Monte Carlo method [25], and the coupled cluster method [1] and chapter 5.

4.2 HF equations

The procedure of deriving the HF equations is outlined in this section. First we approximate the wave function by one Slater determinant. Then we vary the single-particle orbitals constituting the Slater determinant in a manner such as to minimize the total energy of the system. The ansatz wave function given by Ψ_{HF} must therefore contain a set of adjustable variables which can be varied according to some constraints given by the system. The variational principle states that the expectation value of the Hamiltonian in the ansatz wave function always satisfies

$$\langle \Psi_{HF} | \hat{H} | \Psi_{HF} \rangle \geq E_0, \quad (4.1)$$

where E_0 is the ground state energy of the system. At best the energy of the ansatz wave function equals the ground state energy, otherwise it will overestimate it. Thus, we have to minimize the energy expectation value in order to find the best estimate of the ground state energy.

The exact Hamiltonian of the many-fermion system is given by

$$\hat{H} = \sum_i^N (\hat{t}_i + \hat{v}_i) + \frac{1}{2} \sum_{\substack{ij \\ i \neq j}}^N \hat{v}_{ij}, \quad (4.2)$$

where \hat{t}_i and \hat{v}_i are one-body operators of kinetic and potential energy respectively, while \hat{v}_{ij} is the two-body operator of potential energy. N is the number of particles. The HF Hamiltonian obtained by approximating the two-body operator by an effective one-body potential reads

$$\hat{H}_{HF} = \sum_i^N \hat{h}_i^{HF} = \sum_i^N (\hat{t}_i + \hat{v}_i^{HF}). \quad (4.3)$$

The HF potential \hat{v}_i^{HF} is unknown. The solution of the eigenvalue equation

$$\hat{H}_{HF} \Psi = E \Psi, \quad (4.4)$$

results in the fact that the wave function with correct symmetry properties, is given by Slater determinants. The HF ansatz, as mentioned, assumes that the wave function Ψ_{HF} is given by a single Slater determinant, thus

$$\Psi_{HF}(\mathbf{r}_1 \mathbf{r}_2 \dots \mathbf{r}_N) = \frac{1}{\sqrt{N!}} \sum_p (-1)^p \hat{P} \varphi_a(\mathbf{r}_1) \varphi_b(\mathbf{r}_2) \dots \varphi_g(\mathbf{r}_N), \quad (4.5)$$

where $\varphi(\mathbf{r}_i)$ are the HF orbitals, and \hat{P} is the permutation operator, see section 2.2 eq. (2.24). The HF orbitals satisfy

$$\hat{h}^{HF} \varphi_a = \tilde{\epsilon} \varphi_a. \quad (4.6)$$

The HF orbitals can be varied in at least two different ways in order to minimize the energy expectation value in eq. (4.1). One can vary the spatial part of the HF orbitals directly. Or as we will proceed in this derivation, the single-particle orbitals can be expanded in a known basis and then varied by varying the coefficients. The HF orbitals are thus defined as

$$\varphi_a(\mathbf{r}) = \sum_{\lambda}^d C_{a\lambda} \psi_{\lambda}(\mathbf{r}), \quad (4.7)$$

where $C_{a\lambda}$ is the expansion coefficient, and $\{\psi(\mathbf{r})\}_{\lambda}^d$ is the set of orthonormal single-particle functions spanning the chosen model space. The set of basis functions can in principle be chosen arbitrarily, and should in principle also have an infinite dimension, viz. $d = \infty$. Computationally, an infinite basis is unmanageable, and truncation is necessary. However, an advantage related to the expansion is that the matrix elements $\langle \alpha | \hat{h} | \beta \rangle$ and $\langle \alpha \beta | \hat{v} | \gamma \delta \rangle_{AS}$, occurring in the energy functional eq. (4.10), can be tabulated once and for all. This saves some computational effort.

The exact Hamiltonian expressed in the second quantization formalism (see section 2.4) is given by

$$\hat{H} = \sum_{ab}^N \langle a | \hat{h} | b \rangle a_a^{\dagger} a_b + \frac{1}{2} \sum_{abcd}^N \langle ab | v | cd \rangle a_a^{\dagger} a_b^{\dagger} a_d a_c, \quad (4.8)$$

where a is the annihilation operator and a^{\dagger} is the creation operator. The energy expectation value of the exact Hamiltonian, also known as the energy functional $E[\Psi_{HF}]$, is obtained by utilizing Wick's theorem (section 2.4.3), with Ψ_{HF} as the Fermi vacuum, i.e.

$$\begin{aligned} E[\Psi_{HF}] &= \langle \Psi_{HF} | \hat{H} | \Psi_{HF} \rangle \\ &= \sum_{ab}^N \langle a | \hat{h} | b \rangle \langle \Psi_{HF} | a_a^{\dagger} a_b | \Psi_{HF} \rangle + \frac{1}{2} \sum_{abcd}^N \langle ab | v | cd \rangle \langle \Psi_{HF} | a_a^{\dagger} a_b^{\dagger} a_d a_c | \Psi_{HF} \rangle \\ &= \sum_{ab}^N \langle a | \hat{h} | b \rangle \langle \Psi_{HF} | \overline{a_a^{\dagger} a_b} | \Psi_{HF} \rangle + \frac{1}{2} \sum_{abcd}^N \langle ab | v | cd \rangle \langle \Psi_{HF} | \overline{a_a^{\dagger} a_b^{\dagger} a_d a_c} | \Psi_{HF} \rangle \\ &= \sum_a^N \langle a | \hat{h} | a \rangle + \frac{1}{2} \sum_{ab}^N [\langle ab | v | ab \rangle - \langle ab | v | ba \rangle]. \end{aligned} \quad (4.9)$$

In the equation above, all possible contractions are illustrated. These contractions results in Kronecker delta relations as shown in the final expression. By inserting the expansion of the HF orbitals in eq. (4.7), into the expression of the energy expectation value in eq. (4.9), we obtain

$$E[\Psi_{HF}] = \sum_a^N \sum_{\alpha\beta}^d C_{a\alpha}^* C_{a\beta} \langle \alpha | \hat{h} | \beta \rangle + \frac{1}{2} \sum_{ab}^N \sum_{\alpha\beta\gamma\delta}^d C_{a\alpha}^* C_{b\beta}^* C_{a\gamma} C_{b\delta} [\langle \alpha\beta | \hat{v} | \gamma\delta \rangle - \langle \alpha\beta | \hat{v} | \delta\gamma \rangle]. \quad (4.10)$$

Note that Latin letters denote the HF orbitals, while Greek letters denote the chosen basis of expansion.

We now wish to minimize the energy functional with the constraint that the HF orbitals are normalized, viz.

$$\langle a|b \rangle = \delta_{ab}, \quad (4.11)$$

thus

$$\langle a|b \rangle = \sum_{\alpha\beta} C_{a\alpha}^* C_{b\beta} \langle \alpha|\beta \rangle = \sum_{\alpha} C_{a\alpha}^* C_{a\alpha}. \quad (4.12)$$

From calculus we have that in order to determine extreme values of a function $f(x, y, z, \dots)$, subject to one or more constraints of the form $g_i(x, y, z, \dots) = c_i$, where c_i is a constant, the technique of *Lagrange multipliers* is applied [26]. The technique is to define a new Lagrange function $L(x, y, z, \dots, \omega_1, \omega_2, \dots)$, where the Lagrange multipliers ω_i are introduced. The extremal values are then determined by calculating the extremal values of this new function instead. Thus, given N constraints the Lagrange function reads

$$L(x, y, z, \dots, \omega_1, \omega_2, \dots, \omega_N) = f(x, y, z, \dots) + \omega_1 g_1 + \dots + \omega_N g_N. \quad (4.13)$$

By solving the differential equations and the constraint equations, respectively given by

$$\frac{\partial L}{\partial x_i} = 0, \quad (4.14)$$

$$\frac{\partial L}{\partial \omega_i} = 0, \quad (4.15)$$

the extremal values of $f(x, y, z, \dots)$ are determined. In our case we define the Lagrange function as follows

$$L = E[\Psi_{HF}] - \sum_a^N \omega_a \sum_{\alpha}^d C_{a\alpha}^* C_{a\alpha}, \quad (4.16)$$

where N is the number of particles, and d is the dimension of the basis in which the expansion was made. Next, we take the derivative of L with respect to $C_{k\kappa}^*$, and obtain the following HF equation for each HF orbital k

$$\begin{aligned} 0 &= \frac{\partial}{\partial C_{k\kappa}^*} \left(E[\Psi_{HF}] - \sum_a^N \omega_a \sum_{\alpha}^d C_{a\alpha}^* C_{a\alpha} \right) \\ &= \frac{\partial}{\partial C_{k\kappa}^*} \left(\sum_a^N \sum_{\alpha\beta}^d C_{a\alpha}^* C_{a\beta} \langle \alpha|\hat{h}|\beta \rangle + \frac{1}{2} \sum_{ab}^N \sum_{\alpha\beta\gamma\delta}^d C_{a\alpha}^* C_{b\beta}^* C_{a\gamma} C_{b\delta} \langle \alpha\beta|\hat{v}|\gamma\delta \rangle_{AS} - \sum_a^N \omega_a \sum_{\alpha}^d C_{a\alpha}^* C_{a\alpha} \right) \\ &= \sum_{\alpha\beta}^d C_{k\beta} \langle \alpha|\hat{h}|\beta \rangle + \sum_a^N \sum_{\alpha\beta\gamma\delta}^d C_{a\beta}^* C_{k\gamma} C_{a\delta} \langle \alpha\beta|\hat{v}|\gamma\delta \rangle_{AS} - \omega_k \sum_{\alpha} C_{k\alpha}, \end{aligned} \quad (4.17)$$

where $\langle \alpha\beta|\hat{v}|\gamma\delta \rangle_{AS}$ is the *antisymmetrized matrix element* defined by

$$\langle \alpha\beta|\hat{v}|\gamma\delta \rangle_{AS} = \langle \alpha\beta|\hat{v}|\gamma\delta \rangle - \langle \alpha\beta|\hat{v}|\delta\gamma \rangle. \quad (4.18)$$

The expression in eq. (4.17) can be simplified by identifying the dummy index β in the first term with the corresponding dummy index γ in the second term, thus

$$\sum_{\alpha\gamma} \left(\langle \alpha | \hat{h} | \gamma \rangle + \sum_a \sum_{\beta\delta}^d C_{a\beta}^* C_{a\delta} \langle \alpha\beta | \hat{v} | \gamma\delta \rangle_{AS} \right) C_{k\gamma} = \omega_k \sum_{\alpha} C_{k\alpha}. \quad (4.19)$$

The Hartree Fock Hamiltonian is defined as

$$h_{\alpha\gamma}^{HF} = \langle \alpha | \hat{h} | \gamma \rangle + \sum_a \sum_{\beta\delta}^d C_{a\beta}^* C_{a\delta} \langle \alpha\beta | \hat{v} | \gamma\delta \rangle_{AS}, \quad (4.20)$$

and the Hartree Fock equations read

$$\sum_{\gamma} h_{\alpha\gamma}^{HF} C_{k\gamma} = \omega_k C_{k\alpha}. \quad (4.21)$$

The eigenvalues ω_k can be interpreted as the single-particle energy of the HF orbitals, but note that these values do not sum up to equal the HF energy. The HF energy is given in eq. (4.23). The HF equations are non-linear, and they must be solved iteratively since the HF Hamiltonian depends on the unknown coefficients. The procedure is to choose an initial coefficient matrix $C_{a\gamma}$, where one common choice is the initial values $\delta_{a\gamma}$. The solution of the eqs. (4.21), with the selected initial coefficient matrix is then determined. From the solution we select the N eigenvectors with the lowest eigenvalues ω_k , and conduct the calculation of eqs. (4.21) again with this new coefficient matrix. We repeat the procedure until the change in the eigenvalues and eigenvectors from one calculation to the next converge within a given tolerance. Note that when we have solved the HF equations, we have not only determined the occupied single-particle orbitals, but also the set of unoccupied single-particle orbitals, which altogether form the basis of the single-particle Hilbert space.

The total energy approximated with the HF method, is obtained by solving the HF equations and inserting the resulting Slater determinant, containing HF orbitals, into the energy functional of eq. (4.9). If we manipulate this functional expression by adding and subtracting the double sum, we recognize the HF equations such that we obtain

$$E_{HF} = \sum_a^N \omega_a - \frac{1}{2} \sum_{ab}^N [\langle ab | \hat{v} | ab \rangle - \langle ab | \hat{v} | ba \rangle]. \quad (4.22)$$

This expression can be simplified further in a similar manner by manipulating the simple sum instead of the double sum, for details see refs. [11] and [14]. The result is

$$E_{HF} = \frac{1}{2} \sum_a^N [\omega_a + \langle a | \hat{h} | a \rangle], \quad (4.23)$$

where $\hat{h} = \hat{t}_i + \hat{v}_i$ is equal to the one-body operator in eq. (4.2) and

$$\langle a | \hat{h} | a \rangle = \sum_{\alpha\beta}^d C_{a\alpha}^* C_{a\beta} \langle \alpha | \hat{h} | \beta \rangle, \quad (4.24)$$

where d is the dimension of the basis, viz. the number of basis functions. One could expect that the HF energy would equal the sum of the single-particle energies $\sum_k^N \omega_k$, obtained from the HF equations. This however, is not the result because the initial assumption of approximating the exact Hamiltonian by an effective single-particle operator was not made directly. The approximation was made by assuming that the basis, constituting the single Slater determinant, satisfy the effective single-particle operator in eq. (4.6), while the total wave function is acted upon by the exact Hamiltonian. Had the approximation been made directly, the result would be the sum of single-particle energies. In our case the sum of single-particle energies agrees only with the zeroth order perturbation solution of the problem. The solution we obtain with eq. (4.23) agrees with first order perturbation theory of the problem, see ref. [11].

Chapter 5

Coupled Cluster method

In this chapter we introduce the history and theory of the Coupled Cluster method. In the first section we give a description and a historical outline of the method. In the following sections we introduce the formal Coupled Cluster method, before we consider the specific realization of Coupled Cluster Singles and Doubles (CCSD). In the sections presenting the CCSD method, we derive programmable equations by using both an algebraic and a diagrammatic approach.

5.1 Introducing Coupled Cluster

The Coupled Cluster (CC) method is a numerical method for describing the many-body system. It is one of the most reliable, and at the same time computationally affordable methods for determining the approximate solution of the many-electron system [1]. The CC method is an *ab initio* method, and as mentioned in chapter 4 the method often is a post-Hartree-Fock method. Essentially the method exploits the HF results, extending it by reinstating considerations of the electron correlations in the wave function.

The method was initially introduced in the 1950s by the German physicists H. Kümmel and F. Coester, who were working in the field of nuclear physics. It was however in quantum chemistry that the CC method first was prevalent. The Czech-born scientist J. Čížek introduced the CC method into quantum chemistry in the mid-1960s [27, 28], and a few years later in collaboration with the Czech scientist J. Paldus [29]. The method did not attract attention in quantum chemistry until the late 1970s. This was much because of the use of sophisticated techniques like *Feynman-like diagrams* and second quantization, which were unfamiliar to the quantum chemists. In the mid-1970, the Australian scientist A. C. Hurley presented a re-derivation of the Coupled cluster doubles equations (CCD) in a more understandable manner to the quantum chemist [30]. After Hurley's publication the popularity of Coupled Cluster theory grew. The Dutch scientist H. J. Monkhorst then developed a CC response theory for calculating molecular properties [31], and at the turning of the decade computer implementations of spin-orbital CCD were developed by the groups of Pople and Bartlett [32, 33]. In 1982 Purvis and Bartlett derived the coupled cluster singles and doubles equations (CCSD), and implemented them in a computer program [34]. Beyond this point in history tremendous efforts have been made in development of high efficient CCSD implementations, determining the ground state energy of the system. One has also made efforts in investigating inclusion of higher excitations

like the coupled cluster singles doubles and triples (CCSDT), quadruples (CCSDTQ) and pentuples (CCSDTQP), see for example ref. [35]. In addition, considerably work lies in developing the *equation of motion coupled cluster* method for treating excited states.

5.2 Wave Function and Cluster-Operators

From chapter 4, Hartree Fock method, we have that the wave function of a N-particle system is modeled by a single slater determinant consisting of single-particle orbitals, viz.

$$\Phi_0 = \frac{1}{\sqrt{N!}} \begin{vmatrix} \phi_i(\mathbf{x}_1) & \phi_j(\mathbf{x}_1) & \dots & \phi_k(\mathbf{x}_1) \\ \phi_i(\mathbf{x}_2) & \phi_j(\mathbf{x}_2) & \dots & \phi_k(\mathbf{x}_2) \\ \vdots & \vdots & & \vdots \\ \phi_i(\mathbf{x}_N) & \phi_j(\mathbf{x}_N) & \dots & \phi_k(\mathbf{x}_N) \end{vmatrix} = |\phi_i(\mathbf{x}_1)\phi_j(\mathbf{x}_2)\dots\phi_k(\mathbf{x}_N)\rangle = |\phi_i\phi_j\dots\phi_k\rangle. \quad (5.1)$$

The single-particle orbitals provide a separate treatment of the motion of each electron. From HF theory we remember that this results in the failure to account for the Coulomb interaction between the electrons. The question is how to improve this “independent-motion” approximation such that it models the correlated motion of the electrons?

In HF theory we stated that the set of occupied single-particle orbitals constitutes the single-particle Hilbert space together with the set of unoccupied single-particle orbitals, also called virtual orbitals. Both these sets are determined when the HF eqs. (4.21) are solved. Throughout this thesis we will use the notation where the occupied single-particle orbitals are denoted by i, j, k, l, \dots , the virtual orbitals are denoted by a, b, c, d, \dots , while general single-particle orbitals are denoted by p, q, r, s, \dots .

We now consider a 4-particle determinant, viz.

$$\Phi_0 = |\phi_i\phi_j\phi_k\phi_l\rangle. \quad (5.2)$$

The single-particle orbitals are eigenfunctions of a one-body Hamiltonian. In principle the basis functions $\{\phi_i\}$ can be chosen arbitrary, however a common practice is to use the solutions of the HF calculation. In order to improve this wave function with respect to electron correlations, one include a two-particle function f_{ij} for electrons in state ϕ_i and ϕ_j . The wave function then takes the form

$$\Psi = |[\phi_i\phi_j + f_{ij}]\phi_k\phi_l\rangle. \quad (5.3)$$

If we assume that pair correlations of this form occur simultaneously, the wave function can be expressed as follows, with correlations between all possible pairs

$$\begin{aligned} \Psi = & |\phi_i\phi_j\phi_k\phi_l\rangle + |f_{ij}\phi_k\phi_l\rangle - |f_{ik}\phi_j\phi_l\rangle + |f_{il}\phi_j\phi_k\rangle + |\phi_i f_{jk}\phi_l\rangle \\ & - |\phi_i f_{jl}\phi_k\rangle + |\phi_i\phi_j f_{kl}\rangle + |f_{ij}f_{kl}\rangle - |f_{ik}f_{jl}\rangle + |f_{il}f_{jk}\rangle. \end{aligned} \quad (5.4)$$

In this manner we could also include one and three-body correlation functions, also called cluster functions, up to N-cluster functions on the form $f_i, f_{ijk}, \dots, f_{ijk\dots l}$ [36]. Including all N-clusters would give the exact wave function spanned in the space $\{\phi\}_p$ of both occupied and unoccupied single-particle orbitals. However, in practice these clusters are truncated with respect to the conditions of the system, e.g. our Hamiltonian contains

two-body interactions and it is therefore natural to include clusters of only one and two orbitals. The 4-particle wave function then reads

$$\begin{aligned}
 \Psi = & |\phi_i\phi_j\phi_k\phi_l\rangle + |f_i\phi_j\phi_k\phi_l\rangle + |\phi_i f_j\phi_k\phi_l\rangle + |\phi_i\phi_j f_k\phi_l\rangle + |\phi_i\phi_j\phi_k f_l\rangle \\
 & + |f_i f_j\phi_k\phi_l\rangle + |f_i\phi_j f_k\phi_l\rangle + |f_i\phi_j\phi_k f_l\rangle + |\phi_i f_j f_k\phi_l\rangle + |\phi_i f_j\phi_k f_l\rangle + |\phi_i\phi_j f_k f_l\rangle \\
 & + |f_i f_j f_k\phi_l\rangle + |f_i f_j\phi_k f_l\rangle + |f_i\phi_j f_k f_l\rangle + |\phi_i f_j f_k f_l\rangle + |f_{ij}\phi_k\phi_l\rangle - |f_{ik}\phi_j\phi_l\rangle \\
 & + |f_{il}\phi_j\phi_k\rangle + |\phi_i f_{jk}\phi_l\rangle - |\phi_i f_{jl}\phi_k\rangle + |\phi_i\phi_j f_{kl}\rangle + |f_{ij} f_{kl}\rangle - |f_{ik} f_{jl}\rangle \\
 & + |f_{il} f_{jk}\rangle + |f_i f_j f_k f_l\rangle + |f_{ij} f_k\phi_l\rangle + |f_{ij}\phi_k f_l\rangle + |f_{ij} f_k f_l\rangle - |f_{ik} f_j\phi_l\rangle \\
 & - |f_{ik}\phi_j f_l\rangle - |f_{ik} f_j f_l\rangle + |f_{il} f_j\phi_l\rangle + |f_{il}\phi_j f_l\rangle + |f_{il} f_j f_l\rangle + |f_i f_{jk}\phi_l\rangle \\
 & + |\phi_i f_{jk} f_l\rangle + |f_i f_{jk} f_l\rangle - |f_i f_{jl}\phi_k\rangle - |\phi_i f_{jl} f_k\rangle - |f_i f_{jl} f_k\rangle + |f_i\phi_j f_{kl}\rangle \\
 & + |\phi_i f_j f_{kl}\rangle + |f_i f_j f_{kl}\rangle.
 \end{aligned} \tag{5.5}$$

The expression of the cluster-expanded wave function above can be simplified if we express it as operators applied to the reference wave function $|\Phi_0\rangle$. We obtain a cluster operator by requiring that the cluster functions are antisymmetric under index permutation, and that they are orthogonal to the occupied single-particle orbitals, thus

$$f_{ij} = -f_{ji}, \tag{5.6}$$

$$\int \phi_k^*(x_1) f_{ij}(x_1, x_2) dx_1 = 0. \tag{5.7}$$

With these definitions we can express the cluster function as follows

$$\begin{aligned}
 f_{ij}(x_1, x_2) &= \frac{1}{2} \sum_{ab} t_{ij}^{ab} [\phi_a(x_1)\phi_b(x_2) - \phi_b(x_1)\phi_a(x_2)] \\
 &= \sum_{ab} t_{ij}^{ab} |\phi_a\phi_b\rangle,
 \end{aligned} \tag{5.8}$$

In section 2.4, we introduced the annihilation and creation operators. With these in mind, the cluster operator \hat{t}_{ij} , which replaces $|\phi_i\phi_j\rangle$ with the cluster function in eq. (5.8), is given by

$$\hat{t}_{ij} = \frac{1}{2} \sum_{ab} t_{ij}^{ab} a_a^\dagger a_b^\dagger a_j a_i, \tag{5.9}$$

where t_{ij}^{ab} are the cluster coefficients, also called (cluster) amplitudes. These amplitudes have the following relation

$$t_{ij}^{ab} = -t_{ji}^{ab} = -t_{ij}^{ba} = t_{ji}^{ba}. \tag{5.10}$$

The one-particle cluster operator in terms of second quantization reads

$$\hat{t}_i = \sum_a t_i^a a_a^\dagger a_i. \tag{5.11}$$

Note that for both \hat{t}_i and \hat{t}_{ij} the creation operators are restricted to act only on the virtual orbitals, while the annihilation operators act only on the occupied orbitals. This fact ensures that the creation and annihilation operators within cluster operators anti-commute. All cluster operators contain an even number of second quantized operators, which together with the anti-commutation relation means that the cluster operators \hat{t}_i

and \hat{t}_{ij} commute. With the definition of the cluster operators, we are able to simplify the expression of the wave function in eq- (5.5). The simplified expression reads

$$\Psi = \left[1 + \sum_i \hat{t}_i + \frac{1}{2!} \sum_{ij} \hat{t}_i \hat{t}_j + \frac{1}{3!} \sum_{ijk} \hat{t}_i \hat{t}_j \hat{t}_k + \frac{1}{4!} \sum_{ijkl} \hat{t}_i \hat{t}_j \hat{t}_k \hat{t}_l + \sum_{(ij)} \hat{t}_{ij} + \sum_{\substack{(ij) \\ k}} \hat{t}_{ij} \hat{t}_k + \frac{1}{2!} \sum_{\substack{(ij) \\ kl}} \hat{t}_{ij} \hat{t}_k \hat{t}_l + \frac{1}{2!} \sum_{\substack{(ij) \\ (kl)}} \hat{t}_{ij} \hat{t}_{kl} \right] |\Phi_0\rangle, \quad (5.12)$$

where the sum over (ij) denotes the sum over distinct pairs, this equals the free summation multiplied by $1/2$. Further simplification can be made by including the sum over holes into the cluster operators, thus

$$\hat{T}_1 = \sum_i \hat{t}_i = \sum_{ia} t_i^a a_a^\dagger a_i, \quad (5.13)$$

$$\hat{T}_2 = \sum_{(ij)} \hat{t}_{ij} = \sum_{\substack{(ij) \\ (ab)}} t_{ij}^{ab} a_a^\dagger a_b^\dagger a_j a_i. \quad (5.14)$$

The n -cluster operator is generally defined by

$$\hat{T}_n = \left(\frac{1}{n!} \right)^2 \sum_{a,b,\dots,i,j,\dots} t_{ij\dots}^{ab\dots} a_a^\dagger a_b^\dagger \dots a_j a_i. \quad (5.15)$$

Notice the free summation in the general n -cluster operator expression. The wave function in eq. (5.12) can with these new cluster operators be simplified as follows

$$\Psi = \left(1 + \hat{T}_1 + \frac{1}{2!} \hat{T}_1^2 + \frac{1}{3!} \hat{T}_1^3 + \frac{1}{4!} \hat{T}_1^4 + \hat{T}_2 + \hat{T}_2 \hat{T}_1 + \frac{1}{2!} \hat{T}_2 \hat{T}_1^2 + \frac{1}{2!} \hat{T}_2^2 \right) |\Phi_0\rangle. \quad (5.16)$$

In this expression we recognize the power series expansion of the exponential function, only with some discrepancies due to natural truncation caused by the limitation of particles (in this case we have only 4 particles). Since the cluster operators commute, we can in fact express the wave function as below

$$\Psi = e^{\hat{T}_1 + \hat{T}_2} |\Phi_0\rangle = e^{\hat{T}} |\Phi_0\rangle. \quad (5.17)$$

This *exponential ansatz* of the wave function is characteristic for the CC approach. This ansatz applied to the reference wave function produces a new wave function containing cluster functions. The cluster functions provide correlations between all the electrons in the system. As mentioned above, if all possible electron groupings T_1, T_2, \dots, T_N contributes to the exponential operator, then the exact wave function is obtained.

We will now recapitulate this section by clarifying some details of the cluster functions and operators. The action of the cluster operator, in eq. 5.17, creates a linear combination of Slater determinants, where occupied orbitals are replaced with virtual orbitals. The new Slater determinants in the linear combination, correspond to excited Slater determinants.

In section 2.4.4 we introduced the formalism of quasi-particles, where the occupied orbitals of a Fermi reference state are labeled as hole states, and virtual orbitals are labeled as particle states. Note that we are using this formalism here, where $|\Phi_0\rangle$ acts as the Fermi reference, and instead of using b-notation operators, we index hole operators by i, j, k, \dots and particle operators by a, b, c, \dots . In the case of a two-particle cluster operator \hat{T}_2 we obtain two-particle two-hole excitations, denoted 2p2h, where two occupied orbitals are exchanged by two virtual orbitals. Combinatorial the 2p2h excitation can be realized in 2 ways. In general an nph excitation can be realized in $n!$ different ways. Physically however, the interest lies in which orbitals are occupied by electrons, not how we moved the electrons to obtain the state.

The exact wave function in terms of excited Slater determinants $|\Phi_{ij\dots k}^{ab\dots c}\rangle$ reads

$$\Psi = C_0|\Phi_0\rangle + \sum_{ia} C_i^a |\Phi_i^a\rangle + \sum_{ijab} C_{ij}^{ab} |\Phi_{ij}^{ab}\rangle + \dots + \sum_{ijk\dots abc\dots} C_{ijk\dots abc\dots}^{ab\dots c} |\Phi_{ijk\dots abc\dots}^{ab\dots c}\rangle, \quad (5.18)$$

where $\{C\}$ are the expansion coefficients. The first sum represent all the contributions from 1p1h excitations, the second sum represent all the contributions from 2p2h excitations, and so on up to the sum of $NpNh$ excitation contributions. This linear expansion is naturally truncated after $NpNh$ excitations, where N is the number of electrons in the system. The sum is however infinite if the subspace of virtual orbitals is not truncated. The coefficients $\{C\}$ contain contributions from all the possible couplings between cluster operators, which produce the excitation level of interest. Let us consider the 3p3h coefficient C_{ijk}^{abc} .

$$C_{ijk}^{abc} = t_i^a t_j^b t_k^c + t_{ij}^{ab} t_k^c + t_i^a t_{jk}^{bc} + t_j^b t_{ik}^{ac} + t_{ijk}^{abc}. \quad (5.19)$$

The expansion coefficients of the determinants can all be divided into a sum of all possible couplings that produce the corresponding excitation level. From this expression the name coupled clusters becomes evident. The cluster operators \hat{T}_i are often denoted as excitation operators, and the truncation of the cluster operator \hat{T} at specific excitation levels give rise to a hierarchy of coupled cluster techniques, viz.

$$\begin{aligned} \hat{T} &= \hat{T}_1 + \hat{T}_2 &\Rightarrow & CCSD \quad \text{singles doubles} \\ \hat{T} &= \hat{T}_1 + \hat{T}_2 + \hat{T}_3 &\Rightarrow & CCSDT \quad \text{singles doubles triples} \end{aligned}$$

5.3 Formal Coupled Cluster Theory

One of the essentials of Coupled Cluster theory is the exponential wave function ansatz in eq (5.17). This ansatz however, does not give us the solution scheme of the amplitudes implicit in the cluster operator \hat{T} . In order to determine the amplitudes and eventually the wave function, we start by inserting the exponential ansatz into the time-independent Schrödinger equation, viz.

$$\hat{H}e^{\hat{T}}|\Phi_0\rangle = E_0 e^{\hat{T}}|\Phi_0\rangle, \quad (5.20)$$

where E_0 is the ground state energy. From this equation we wish to provide a solution of the energy and the unknown amplitudes $t_i^a, t_{ij}^{ab}, \dots$. We therefore proceed with a projective technique involving multiplication by Φ_0 from the left, thus the *energy equation* reads

$$\langle \Phi_0 | \hat{H} e^{\hat{T}} | \Phi_0 \rangle = E_0 \langle \Phi_0 | e^{\hat{T}} | \Phi_0 \rangle = E_0, \quad (5.21)$$

where $\langle \Phi_0 | e^{\hat{T}} | \Phi_0 \rangle = \langle \Phi_0 | \Psi_{CC} \rangle = 1$ from construction. The energy equation can be simplified by considering the expansion of the exponential term, and the form of the Hamiltonian. We have a Hamiltonian that include only one and two-body interactions. The exponential expansion inserted in the energy equation reads

$$\langle \Phi_0 | \hat{H} (1 + \hat{T} + \frac{1}{2!} \hat{T}^2 + \frac{1}{3!} \hat{T}^3 + \dots) | \Phi_0 \rangle = E_0. \quad (5.22)$$

Slater's rules states that the matrix element between Slater determinants that differ by more than two orbitals are zero [37]. The energy equation thus truncates naturally in the fourth term, due to the form of the Hamiltonian. The energy equation therefore simplifies as follows

$$\langle \Phi_0 | \hat{H} (1 + \hat{T} + \frac{1}{2!} \hat{T}^2) | \Phi_0 \rangle = E_0. \quad (5.23)$$

The amplitudes are obtained by left multiplying the energy-independent Schrödinger equation by the excited determinants, produced by the cluster operator acting on the reference, hence the general *amplitude equations* read

$$\langle \Phi_{ij\dots}^{ab\dots} | \hat{H} e^{\hat{T}} | \Phi_0 \rangle = E_0 \langle \Phi_{ij\dots}^{ab\dots} | e^{\hat{T}} | \Phi_0 \rangle = E_0. \quad (5.24)$$

Note, we obtain equations for the amplitude t_{ij}^{ab} by using the projecting determinant $|\Phi_{ij}^{ab}\rangle$. Due to the term $e^{\hat{T}}$, these equations are non-linear. Each amplitude depend on all the other amplitudes, and the equations must therefore be solved by an iterative procedure.

The energy eq. (5.23) and the amplitude eqs. (5.24) are both theoretical reasonable CC equations. However, in computational science they are impractical. In order to obtain programmable equations, we modify them by left-multiplying the time-independent Schrödinger equation by $e^{-\hat{T}}$ before the projective technique is applied. The modified energy and amplitude equations are given as

$$\langle \Phi_0 | e^{-\hat{T}} \hat{H} e^{\hat{T}} | \Phi_0 \rangle = E_0 \quad \text{Energy eq.} \quad (5.25)$$

$$\langle \Phi_{ij\dots}^{ab\dots} | e^{-\hat{T}} \hat{H} e^{\hat{T}} | \Phi_0 \rangle = 0 \quad \text{Amplitude eqs.} \quad (5.26)$$

These equations characterize the conventional Coupled Cluster method. They are equivalent to the eqs. in (5.23) and (5.24), but they hold two advantages. First the amplitude equations are decoupled from the energy equation, and second the similarity transformed Hamiltonian $e^{-\hat{T}} \hat{H} e^{\hat{T}}$ can be simplified by the *Campbell-Baker-Hausdorff* (CBH) formula [1]. The CBH formula states that operator expressions of the form $e^{-\hat{A}} \hat{B} e^{\hat{A}}$ are equal to a linear combination of nested commutators of the operator between the exponential functions with the operator in the exponent, i.e.

$$e^{-\hat{T}} \hat{H} e^{\hat{T}} = \hat{H} + [\hat{H}, \hat{T}] + \frac{1}{2!} [[\hat{H}, \hat{T}], \hat{T}] + \frac{1}{3!} [[[\hat{H}, \hat{T}], \hat{T}], \hat{T}] + \frac{1}{4!} [[[[\hat{H}, \hat{T}], \hat{T}], \hat{T}], \hat{T}] + \dots \quad (5.27)$$

The use of the CBH formula is a simplification because the expression above is naturally truncated after the first five terms. The truncation is a result of the two-body form of the Hamiltonian and the fact that the cluster operators commute.

5.4 Coupled Cluster Singles and Doubles

In this section we derive the Coupled Cluster Singles and Doubles equations in both an algebraic and a diagrammatic approach. The singles and doubles are, as mentioned earlier, a CC scheme where the cluster operator is truncated such as to include only \hat{T}_1 and \hat{T}_2 , viz.

$$\hat{T} = \hat{T}_1 + \hat{T}_2, \quad (5.28)$$

where

$$\hat{T}_1 = \sum_{ia} t_i^a a_a^\dagger a_i, \quad (5.29)$$

$$\hat{T}_2 = \frac{1}{4} \sum_{ijab} t_{ij}^{ab} a_a^\dagger a_b^\dagger a_j a_i. \quad (5.30)$$

Remember that the indices $ij \dots$ denotes the occupied single-particle space, $ab \dots$ denotes the virtual single-particle space, while $pq \dots$ denotes an arbitrary state in the single-particle space of occupied and virtual orbitals.

5.4.1 Normal-Ordering of the Hamiltonian

The Hamiltonian expressed in a second quantized form reads

$$\hat{H} = \sum_{pq} \langle p|h|q \rangle a_p^\dagger a_q + \frac{1}{4} \sum_{pqrs} \langle pq|v|rs \rangle^{AS} a_p^\dagger a_q^\dagger a_s a_r, \quad (5.31)$$

see for example section 2.4.2. Note that we are using the antisymmetrized matrix element, the label AS is omitted hereafter. Using Wick's theorem from section 2.4.3, we determine the normal ordered Hamiltonian in the following.

The operator strings in the Hamiltonian of eq. 5.31, can according to Wick's theorem be expressed as below.

$$\begin{aligned} a_p^\dagger a_q &= \{a_p^\dagger a_q\} + \{\overline{a_p^\dagger a_q}\} \\ &= \{a_p^\dagger a_q\} + \delta_{pq \in i}, \end{aligned} \quad (5.32)$$

$$\begin{aligned} a_p^\dagger a_q^\dagger a_s a_r &= \{a_p^\dagger a_q^\dagger a_s a_r\} + \{\overline{a_p^\dagger a_q^\dagger a_s a_r}\} + \{\overline{a_p^\dagger a_q^\dagger a_s a_r}\} + \{\overline{a_p^\dagger a_q^\dagger a_s a_r}\} \\ &\quad + \{\overline{a_p^\dagger a_q^\dagger a_s a_r}\} + \{\overline{a_p^\dagger a_q^\dagger a_s a_r}\} + \{\overline{a_p^\dagger a_q^\dagger a_s a_r}\} \\ &= \{a_p^\dagger a_q^\dagger a_s a_r\} - \delta_{ps \in i} \{a_q^\dagger a_r\} + \delta_{qs \in i} \{a_p^\dagger a_r\} + \delta_{pr \in i} \{a_q^\dagger a_s\} \\ &\quad - \delta_{qr \in i} \{a_p^\dagger a_s\} - \delta_{ps \in i} \delta_{qr \in j} + \delta_{pr \in i} \delta_{qs \in j}, \end{aligned} \quad (5.33)$$

where $\{ \}$ denotes the normal ordering of the operators, and $\in i$ means that the operators act on the hole space of occupied single-particle orbitals. If the criterion $\in i$ is not satisfied,

all the contractions above equals zero. By substituting these equations into eq. (5.31) we obtain

$$\begin{aligned}\hat{H} = & \sum_{pq} \langle p|h|q \rangle \{a_p^\dagger a_q\} + \sum_i \langle i|h|i \rangle + \frac{1}{4} \sum_{pqrs} \langle pq|v|rs \rangle \{a_p^\dagger a_q^\dagger a_s a_r\} - \frac{1}{4} \sum_{iqr} \langle iq|v|ri \rangle \{a_q^\dagger a_r\} \\ & + \frac{1}{4} \sum_{ipr} \langle pi|v|ri \rangle \{a_p^\dagger a_r\} + \frac{1}{4} \sum_{iqs} \langle iq|v|is \rangle \{a_q^\dagger a_s\} - \frac{1}{4} \sum_{ips} \langle pi|v|is \rangle \{a_p^\dagger a_s\} \\ & - \frac{1}{4} \sum_{ij} \langle ij|v|ji \rangle + \frac{1}{4} \sum_{ij} \langle ij|v|ij \rangle.\end{aligned}\quad (5.34)$$

This expression can be simplified by utilizing the relations of the antisymmetrized matrix elements, which read

$$\langle pq|v|rs \rangle = -\langle pq|v|sr \rangle = -\langle qp|v|rs \rangle = \langle qp|v|sr \rangle. \quad (5.35)$$

Thus, the complete Hamiltonian reads

$$\begin{aligned}\hat{H} = & \sum_{pq} \langle p|h|q \rangle \{a_p^\dagger a_q\} + \frac{1}{4} \sum_{pqrs} \langle pq|v|rs \rangle \{a_p^\dagger a_q^\dagger a_s a_r\} + \sum_{ipq} \langle pi|v|qi \rangle \{a_p^\dagger a_q\} \\ & + \sum_i \langle i|h|i \rangle + \frac{1}{2} \sum_{ij} \langle ij|v|ij \rangle.\end{aligned}\quad (5.36)$$

We recognize the Fermi-vacuum expectation value $\langle \Phi_0|\hat{H}|\Phi_0 \rangle$, given by the two last terms in the expression above, thus

$$\langle \Phi_0|\hat{H}|\Phi_0 \rangle = \sum_i \langle i|h|i \rangle + \frac{1}{2} \sum_{ij} \langle ij|v|ij \rangle, \quad (5.37)$$

and we define:

$$f_q^p = \langle p|h|q \rangle + \sum_i \langle pi|v|qi \rangle, \quad (5.38)$$

$$F_N = \sum_{pq} f_q^p \{a_p^\dagger a_q\}, \quad (5.39)$$

$$V_N = \frac{1}{4} \sum_{pqrs} \langle pq|v|rs \rangle \{a_p^\dagger a_q^\dagger a_s a_r\}, \quad (5.40)$$

where the subscript N is related to the normal ordering, not the number of particles in the system. The complete Hamiltonian can then be written as

$$\begin{aligned}\hat{H} &= F_N + V_N + \langle \Phi_0|\hat{H}|\Phi_0 \rangle \\ &= \hat{H}_N + \langle \Phi_0|\hat{H}|\Phi_0 \rangle.\end{aligned}\quad (5.41)$$

The normal ordered Hamiltonian \hat{H}_N is defined as

$$\begin{aligned}\hat{H}_N &= F_N + V_N \\ &= \hat{H} - \langle \Phi_0|\hat{H}|\Phi_0 \rangle.\end{aligned}\quad (5.42)$$

The normal ordered Hamiltonian is actually the Hamiltonian minus its reference expectation value. This is a general definition, the normal ordering of any operator equals the operator minus its reference expectation value.

The normal ordered Hamiltonian is a means for developing the programmable CC-equations. Inserting eq. (5.41) into the conventional CC-eqs. (5.25) and 5.26, we obtain the CC-equations for the CCSD method

$$E_0 = \langle \Phi_0 | e^{-\hat{T}} \hat{H}_N e^{\hat{T}} | \Phi_0 \rangle + \langle \Phi_0 | \hat{H} | \Phi_0 \rangle \quad \text{Energy eq.} \quad (5.43)$$

$$0 = \langle \Phi_i^a | e^{-\hat{T}} \hat{H}_N e^{\hat{T}} | \Phi_0 \rangle \quad \hat{T}_1\text{-amplitude eq.} \quad (5.44)$$

$$0 = \langle \Phi_{ij}^{ab} | e^{-\hat{T}} \hat{H}_N e^{\hat{T}} | \Phi_0 \rangle \quad \hat{T}_2\text{-amplitude eq.} \quad (5.45)$$

This gives rise to the definition of the CC-energy

$$E_{CC} = \langle \Phi_0 | e^{-\hat{T}} \hat{H}_N e^{\hat{T}} | \Phi_0 \rangle = E_0 - \langle \Phi_0 | \hat{H} | \Phi_0 \rangle. \quad (5.46)$$

The CC-problem is thus reduced to solving the amplitude eqs. (5.44) and (5.45), and the energy eq. (5.46), which all contains the similarity-transformed normal-ordered Hamiltonian $\bar{H} = e^{-\hat{T}} \hat{H}_N e^{\hat{T}}$. From the truncation of the cluster operator \hat{T} , and the CBH formula in eq. (5.27), we obtain the similarity-transformed normal ordered Hamiltonian \bar{H} given by

$$\begin{aligned} \bar{H} = & \hat{H}_N + [\hat{H}_N, \hat{T}_1] + [\hat{H}_N, \hat{T}_2] + \frac{1}{2!} [[\hat{H}_N, \hat{T}_1], \hat{T}_1] \\ & + \frac{1}{2!} [[\hat{H}_N, \hat{T}_2], \hat{T}_2] + [[\hat{H}_N, \hat{T}_1], \hat{T}_2] + \dots \end{aligned} \quad (5.47)$$

In order to construct the programmable CCSD equations we must determine the second quantized expression for each term above, and evaluate them when inserted into the amplitude eqs. (5.44), (5.45) and the energy eq. (5.46). In the subsequent section we derive the programmable energy equation corresponding to eq. (5.46), by using the algebraic approach of Wick's theorem.

5.4.2 Energy equation: an Algebraic derivation

In this section we derive the algebraic expression of the programmable energy equation (5.46). In doing so, we uncover an important generalization regarding the commutators in eq. (5.47).

In the following we determine the energy contribution from each term of the similarity-transformed normal-ordered Hamiltonian \bar{H} , in eq. (5.47). The CC-energy contribution from the matrix element $\langle \Phi_0 | \hat{\mathcal{O}} | \Phi_0 \rangle$ is denoted

$$E_{CC} \leftarrow \langle \Phi_0 | \hat{\mathcal{O}} | \Phi_0 \rangle. \quad (5.48)$$

Note that in this section we denote the normal-ordered form of an operator string by the brackets $\{ \}$. The creation and annihilation operators in the excitation operators \hat{T}_i are already in a normal ordered form, however we emphasize this by using the brackets.

Term 1

The Fermi-vacuum expectation value of the first term in \bar{H} is zero by construction, viz.

$$E_{CC} \leftarrow \langle \Phi_0 | \hat{H}_N | \Phi_0 \rangle = 0. \quad (5.49)$$

Term 2

The second term in \bar{H} contributes as follows

$$E_{CC} \leftarrow \langle \Phi_0 | [\hat{H}_N, \hat{T}_1] | \Phi_0 \rangle = \langle \Phi_0 | [\hat{F}_N, \hat{T}_1] | \Phi_0 \rangle + \langle \Phi_0 | [\hat{V}_N, \hat{T}_1] | \Phi_0 \rangle. \quad (5.50)$$

The terms in the \hat{F}_N -commutator is obtained by combining eqs. (5.29) and (5.39), i.e.

$$\hat{F}_N \hat{T}_1 = \sum_{pqia} f_q^p t_i^a \{a_p^\dagger a_q\} \{a_a^\dagger a_i\}, \quad (5.51)$$

$$\hat{T}_1 \hat{F}_N = \sum_{pqia} f_q^p t_i^a \{a_a^\dagger a_i\} \{a_p^\dagger a_q\}, \quad (5.52)$$

Applying Wick's generalized theorem (section 2.4.3 and 2.4.4) on the operator strings above result in

$$\begin{aligned} \{a_p^\dagger a_q\} \{a_a^\dagger a_i\} &= \{a_p^\dagger a_q a_a^\dagger a_i\} + \overline{\{a_p^\dagger a_q a_a^\dagger a_i\}} + \{a_p^\dagger a_q \overline{a_a^\dagger a_i}\} + \overline{\{a_p^\dagger a_q \overline{a_a^\dagger a_i}\}} \\ &= \{a_p^\dagger a_q a_a^\dagger a_i\} + \delta_{pi} \{a_q a_a^\dagger\} + \delta_{qa} \{a_p^\dagger a_i\} + \delta_{pi} \delta_{qa}, \end{aligned} \quad (5.53)$$

$$\{a_a^\dagger a_i\} \{a_p^\dagger a_q\} = \{a_a^\dagger a_i a_p^\dagger a_q\} = \{a_p^\dagger a_q a_a^\dagger a_i\}. \quad (5.54)$$

All the contractions between the operators in eq. (5.54) are zero, see eqs. (2.81) and (2.82). The last equality in eq. (5.54) holds due to the constructed property that all creation and annihilation operators within the excitation operators anticommute, see section 5.2. Inserting these expressions into eqs. (5.51) and (5.52) yields the commutator

$$\begin{aligned} [\hat{F}_N, \hat{T}_1] &= \hat{F}_N \hat{T}_1 - \hat{T}_1 \hat{F}_N \\ &= \sum_{pqia} f_q^p t_i^a (\delta_{pi} \{a_q a_a^\dagger\} + \delta_{qa} \{a_p^\dagger a_i\} + \delta_{pi} \delta_{qa}) \\ &= \sum_{qia} f_q^i t_i^a \{a_q a_a^\dagger\} + \sum_{pia} f_a^p t_i^a \{a_p^\dagger a_i\} + \sum_{ia} f_a^i t_i^a. \end{aligned} \quad (5.55)$$

Finally, we obtain the energy contribution by calculating the reference expectation value of the commutator expression above, viz.

$$E_{CC} \leftarrow \langle \Phi_0 | [\hat{F}_N, \hat{T}_1] | \Phi_0 \rangle = \sum_{ia} f_a^i t_i^a. \quad (5.56)$$

Notice that only terms with fully contracted operators contribute to the energy. This is due to the fact that reference expectation values of normal-ordered strings with creation and annihilation operators are zero.

In a similar manner we determine the energy contribution from the \hat{V}_N -commutator in eq. (5.50). We evaluate the commutator terms obtained from eqs. (5.29) and (5.40), viz.

$$\hat{V}_N \hat{T}_1 = \frac{1}{4} \sum_{pqrsia} \langle pq|v|rs \rangle t_i^a \{a_p^\dagger a_q^\dagger a_s a_r\} \{a_a^\dagger a_i\}, \quad (5.57)$$

$$\hat{T}_1 \hat{V}_N = \frac{1}{4} \sum_{pqrsia} \langle pq|v|rs \rangle t_i^a \{a_a^\dagger a_i\} \{a_p^\dagger a_q^\dagger a_s a_r\}. \quad (5.58)$$

From these operator strings we observe that fully contracted terms are not obtainable, since the number of creation and annihilation operators in \hat{V}_N and \hat{T}_1 differ. The contribution to the energy is therefore zero, i.e.

$$E_{CC} \leftarrow \langle \Phi_0 | [\hat{V}_N, \hat{T}_1] | \Phi_0 \rangle = 0. \quad (5.59)$$

Term 3

Next, we evaluate the energy contribution from the third term of eq. (5.47)

$$E_{CC} \leftarrow \langle \Phi_0 | [\hat{H}_N, \hat{T}_2] | \Phi_0 \rangle = \langle \Phi_0 | [\hat{F}_N, \hat{T}_2] | \Phi_0 \rangle + \langle \Phi_0 | [\hat{V}_N, \hat{T}_2] | \Phi_0 \rangle. \quad (5.60)$$

The \hat{F}_N -commutator expressions are obtained from eqs. (5.30) and (5.39), and read

$$\hat{F}_N \hat{T}_2 = \frac{1}{4} \sum_{pqrsia} \langle pq|v|rs \rangle t_i^a \{a_p^\dagger a_q^\dagger a_s a_r\} \{a_a^\dagger a_i\}, \quad (5.61)$$

$$\hat{T}_2 \hat{F}_N = \frac{1}{4} \sum_{pqrsia} \langle pq|v|rs \rangle t_{ij}^{ab} \{a_a^\dagger a_i\} \{a_p^\dagger a_q^\dagger a_s a_r\}. \quad (5.62)$$

For the same reason that the contribution from the \hat{V}_N -commutator in **term2** was zero, the contribution from the \hat{F}_N -commutator in this term is zero, i.e.

$$E_{CC} \leftarrow \langle \Phi_0 | [\hat{F}_N, \hat{T}_2] | \Phi_0 \rangle = 0. \quad (5.63)$$

In order to contribute to the energy, the operator strings must be fully contracted. Full contractions are not possible for the two operator strings in eqs. (5.61) and (5.62).

The \hat{V}_N -commutator, however, obtains fully contracted operator strings. From eqs. (5.30) and (5.40) we obtain the commutator expressions

$$\hat{V}_N \hat{T}_2 = \frac{1}{16} \sum_{pqrsijab} \langle pq|v|rs \rangle t_{ij}^{ab} \{a_p^\dagger a_q^\dagger a_s a_r\} \{a_a^\dagger a_b^\dagger a_j a_i\}, \quad (5.64)$$

$$\hat{T}_2 \hat{V}_N = \frac{1}{16} \sum_{pqrsijab} \langle pq|v|rs \rangle t_{ij}^{ab} \{a_a^\dagger a_b^\dagger a_j a_i\} \{a_p^\dagger a_q^\dagger a_s a_r\}. \quad (5.65)$$

Evaluating these operator strings by Wick's generalized theorem yields

$$\begin{aligned}
 \{a_p^\dagger a_q^\dagger a_s a_r\} \{a_a^\dagger a_b^\dagger a_j a_i\} &= \{a_p^\dagger a_q^\dagger a_s a_r a_a^\dagger a_b^\dagger a_j a_i\} + \overbrace{\{a_p^\dagger a_q^\dagger a_s a_r a_a^\dagger a_b^\dagger a_j a_i\}}^{\text{contraction}} + \overbrace{\{a_p^\dagger a_q^\dagger a_s a_r a_a^\dagger a_b^\dagger a_j a_i\}}^{\text{contraction}} \\
 &+ \overbrace{\{a_p^\dagger a_q^\dagger a_s a_r a_a^\dagger a_b^\dagger a_j a_i\}}^{\text{contraction}} + \overbrace{\{a_p^\dagger a_q^\dagger a_s a_r a_a^\dagger a_b^\dagger a_j a_i\}}^{\text{contraction}} + \dots \\
 &= \{a_p^\dagger a_q^\dagger a_s a_r a_a^\dagger a_b^\dagger a_j a_i\} + \delta_{pi} \delta_{qj} \delta_{sb} \delta_{ra} + \delta_{pj} \delta_{qi} \delta_{sa} \delta_{rb} \\
 &- \delta_{pj} \delta_{qi} \delta_{sb} \delta_{ra} - \delta_{pi} \delta_{qj} \delta_{sa} \delta_{rb} + \dots
 \end{aligned} \tag{5.66}$$

$$\{a_a^\dagger a_b^\dagger a_j a_i\} \{a_p^\dagger a_q^\dagger a_s a_r\} = \{a_a^\dagger a_b^\dagger a_j a_i a_p^\dagger a_q^\dagger a_s a_r\} = \{a_p^\dagger a_q^\dagger a_s a_r a_a^\dagger a_b^\dagger a_j a_i\}. \tag{5.67}$$

Note that only full contractions are written explicitly in eq. (5.66). The operator string in eq. (5.67) produce only zero-contractions of the form $\overline{a_i^\dagger a_p^\dagger}$ and $\overline{a_a^\dagger a_s}$ (see section 2.4.4 for justification). Thus the energy contribution is given by

$$\begin{aligned}
 E_{CC} &\leftarrow \langle \Phi_0 | [\hat{V}_N, \hat{T}_2] | \Phi_0 \rangle = \langle \Phi_0 | \hat{V}_N \hat{T}_2 - \hat{T}_2 \hat{V}_N | \Phi_0 \rangle \\
 &= \langle \Phi_0 | \frac{1}{16} \sum_{pqrsijab} \langle pq | v | rs \rangle t_{ij}^{ab} \left(\{a_p^\dagger a_q^\dagger a_s a_r a_a^\dagger a_b^\dagger a_j a_i\} \right. \\
 &\quad + \delta_{pi} \delta_{qj} \delta_{sb} \delta_{ra} + \delta_{pj} \delta_{qi} \delta_{sa} \delta_{rb} - \delta_{pj} \delta_{qi} \delta_{sb} \delta_{ra} \\
 &\quad \left. - \delta_{pi} \delta_{qj} \delta_{sa} \delta_{rb} + \dots - \{a_p^\dagger a_q^\dagger a_s a_r a_a^\dagger a_b^\dagger a_j a_i\} \right) | \Phi_0 \rangle \\
 &= \frac{1}{4} \sum_{ijab} \langle ij | v | ab \rangle t_{ij}^{ab}.
 \end{aligned} \tag{5.68}$$

Term 4

The contribution from the fourth term of \bar{H} in eq. (5.47) reads

$$E_{CC} \leftarrow \langle \Phi_0 | \frac{1}{2} [[\hat{H}_N, \hat{T}_1], \hat{T}_1] | \Phi_0 \rangle = \frac{1}{2} \langle \Phi_0 | [[\hat{F}_N, \hat{T}_1], \hat{T}_1] + [[\hat{V}_N, \hat{T}_1], \hat{T}_1] | \Phi_0 \rangle. \tag{5.69}$$

From the expressions of \hat{T}_1 and $[\hat{F}_N, \hat{T}_1]$ in eqs. (5.29) and (5.55), respectively, we obtain the following commutator expressions

$$[\hat{F}_N, \hat{T}_1] \hat{T}_1 = \sum_{qijab} f_q^i t_j^{ab} \{a_q a_a^\dagger\} \{a_b^\dagger a_j\} + \sum_{pijab} f_a^p t_i^{ab} \{a_p^\dagger a_i\} \{a_b^\dagger a_j\} + \sum_{ijab} f_a^i t_j^{ab} \{a_b^\dagger a_j\}, \tag{5.70}$$

$$\hat{T}_1 [\hat{F}_N, \hat{T}_1] = \sum_{qijab} f_q^i t_j^{ab} \{a_b^\dagger a_j\} \{a_q a_a^\dagger\} + \sum_{pijab} f_a^p t_i^{ab} \{a_b^\dagger a_j\} \{a_p^\dagger a_i\} + \sum_{ijab} f_a^i t_j^{ab} \{a_b^\dagger a_j\}. \tag{5.71}$$

We observe that the third term on the right hand side of both eqs. (5.70) and (5.71), cancel each other in the commutator. We also observe that fully contracted terms are not obtainable because one of the contractions always ends up as a zero-contraction on the form $\overline{a_i^\dagger a_p^\dagger}$ or $\overline{a_a^\dagger a_s}$. The energy contribution is therefore zero, viz

$$E_{CC} \leftarrow \langle \Phi_0 | \frac{1}{2} [[\hat{F}_N, \hat{T}_1], \hat{T}_1] | \Phi_0 \rangle = 0. \tag{5.72}$$

From eqs. (5.29), (5.57) and (5.58) we obtain the expressions of the commutator involving \hat{V}_N , i.e.

$$\begin{aligned} [\hat{V}_N, \hat{T}_1] \hat{T}_1 &= \hat{V}_N \hat{T}_1^2 - \hat{T}_1 \hat{V}_N \hat{T}_1 \\ &= \frac{1}{4} \sum_{\substack{pqrs \\ ijab}} \langle pq|v|rs \rangle t_i^a t_j^b \{a_p^\dagger a_q^\dagger a_s a_r\} \{a_a^\dagger a_i\} \{a_b^\dagger a_j\} \\ &\quad - \frac{1}{4} \sum_{\substack{pqrs \\ ijab}} \langle pq|v|rs \rangle t_i^a t_j^b \{a_a^\dagger a_i\} \{a_p^\dagger a_q^\dagger a_s a_r\} \{a_b^\dagger a_j\}, \end{aligned} \quad (5.73)$$

$$\begin{aligned} \hat{T}_1 [\hat{V}_N, \hat{T}_1] &= \hat{T}_1 \hat{V}_N \hat{T}_1 - \hat{T}_1^2 \hat{V}_N \\ &= \frac{1}{4} \sum_{\substack{pqrs \\ ijab}} \langle pq|v|rs \rangle t_i^a t_j^b \{a_b^\dagger a_j\} \{a_p^\dagger a_q^\dagger a_s a_r\} \{a_a^\dagger a_i\} \\ &\quad - \frac{1}{4} \sum_{\substack{pqrs \\ ijab}} \langle pq|v|rs \rangle t_i^a t_j^b \{a_b^\dagger a_j\} \{a_a^\dagger a_i\} \{a_p^\dagger a_q^\dagger a_s a_r\}. \end{aligned} \quad (5.74)$$

By applying Wick's generalized theorem on the operator strings above, we obtain

$$\begin{aligned} [[\hat{V}_N, \hat{T}_1], \hat{T}_1] &= \frac{1}{4} \sum_{\substack{pqrs \\ ijab}} \langle pq|v|rs \rangle t_i^a t_j^b \\ &\quad \times (\delta_{pi} \delta_{qj} \delta_{sb} \delta_{ra} - \delta_{pi} \delta_{qj} \delta_{sa} \delta_{rb} + \delta_{pj} \delta_{qi} \delta_{sa} \delta_{rb} - \delta_{pj} \delta_{qi} \delta_{sb} \delta_{ra} + \dots) \\ &= \frac{1}{4} \sum_{ijab} (\langle ij|v|ab \rangle - \langle ij|v|ba \rangle + \langle ji|v|ba \rangle - \langle ji|v|ab \rangle) t_i^a t_j^b + \dots \\ &= \sum_{ijab} \langle ij|v|ab \rangle t_i^a t_j^b + \dots \end{aligned} \quad (5.75)$$

Only terms that contribute to the energy are shown explicitly above. These four terms arise from the full contractions of the first term in eq. (5.73). The other terms in eqs. (5.73) and (5.74) do not produce full contractions. Thus, the energy contribution reads

$$E_{CC} \leftarrow \frac{1}{2} \langle \Phi_0 | [[\hat{V}_N, \hat{T}_1], \hat{T}_1] | \Phi_0 \rangle = \frac{1}{2} \sum_{ijab} \langle ij|v|ab \rangle t_i^a t_j^b. \quad (5.76)$$

The explicit examples given above determine the energy contribution from the terms of the similarity-transformed normal-ordered Hamiltonian \bar{H} in eq. (5.47). These examples reveal that simplification is possible for performing the calculations. The examples show that the only nonzero terms in the CBH expansion, are those where the normal-ordered Hamiltonian \hat{H}_N has at least one contraction with every cluster operator \hat{T}_i on its right. This is the *connected cluster* theorem, which leads to a simplified CBH expansion. The CBH expansion eq. (5.27) takes the simplified form given by

$$\bar{H} = \left[\hat{H}_N + \hat{H}_N \hat{T} + \frac{1}{2!} \hat{H}_N \hat{T}^2 + \frac{1}{3!} \hat{H}_N \hat{T}^3 + \frac{1}{4!} \hat{H}_N \hat{T}^4 + \dots \right]_c, \quad (5.77)$$

where the subscript c indicates that only connected terms are included. This connected cluster theorem also clarifies the natural truncation of the CBH expansion at the quartic term. The two-body Hamiltonian contains at most four creation and annihilation

operators, thus it can connect to a maximum of four cluster operators at once. If the Hamiltonian includes a three-body operator, the CBH expansion would truncate after the term $\frac{1}{3!}\hat{H}_N\hat{T}^3$. In our case of CCSD and a two-body Hamiltonian, the simplified CBH expansion reads

$$\begin{aligned}\bar{H} = & \left[\hat{H}_N + \hat{H}_N\hat{T}_1 + \hat{H}_N\hat{T}_2 + \frac{1}{2}\hat{H}_N\hat{T}_1^2 + \frac{1}{2}\hat{H}_N\hat{T}_2^2 + \hat{H}_N\hat{T}_1\hat{T}_2 \right. \\ & + \frac{1}{6}\hat{H}_N\hat{T}_1^3 + \frac{1}{2}\hat{H}_N\hat{T}_1^2\hat{T}_2 + \frac{1}{2}\hat{H}_N\hat{T}_1\hat{T}_2^2 + \frac{1}{6}\hat{H}_N\hat{T}_2^3 \\ & \left. + \frac{1}{24}\hat{H}_N\hat{T}_1^4 + \frac{1}{6}\hat{H}_N\hat{T}_1^3\hat{T}_2 + \frac{1}{4}\hat{H}_N\hat{T}_1^2\hat{T}_2^2 + \frac{1}{6}\hat{H}_N\hat{T}_1\hat{T}_2^3 + \frac{1}{24}\hat{H}_N\hat{T}_2^4 \right]_c.\end{aligned}\quad (5.78)$$

When calculating the energy we observed that the condition of full contractions must be satisfied in order to get a nonzero contribution. If we include this condition in the energy equation we obtain

$$E_{CC} = \langle \Phi_0 | \bar{H} | \Phi_0 \rangle = \langle \Phi_0 | (\hat{H}_N\hat{T}_1 + \hat{H}_N\hat{T}_2 + \frac{1}{2}\hat{H}_N\hat{T}_1^2)_{fc} | \Phi_0 \rangle. \quad (5.79)$$

The fc -subscript indicates that only full contractions are included. These are the only terms of eq. (5.78), that makes contributions to the energy. This is clear since the cluster operators of the other terms contribute with more creation-annihilation operator pairs than the Hamiltonian. For example in the term $\hat{H}_N\hat{T}_2^2$, the cluster operators contribute with four pairs while the Hamiltonian contributes with only two. Full contractions are therefore not obtainable since contractions between excitation operators involve contractions of virtual and occupied orbitals, which is zero. If we write \hat{H}_N in terms of \hat{F}_N and \hat{V}_N the energy equation reads

$$E_{CC} = \langle \Phi_0 | \bar{H} | \Phi_0 \rangle = \langle \Phi_0 | (\hat{F}_N\hat{T}_1 + \hat{V}_N\hat{T}_2 + \frac{1}{2}\hat{V}_N\hat{T}_1^2)_{fc} | \Phi_0 \rangle. \quad (5.80)$$

These terms are calculated above. The explicit energy expression is thus given by

$$E_{CC} = \sum_{ia} f_a^i t_i^a + \frac{1}{4} \sum_{ijab} \langle ij | v | ab \rangle t_{ij}^{ab} + \frac{1}{2} \sum_{ijab} \langle ij | v | ab \rangle t_i^a t_j^b. \quad (5.81)$$

This energy equation holds for all CC-schemes, given that the Hamiltonian contains at most a two-body interaction. Thus the CCSD, CCSDT, CCSDTQ and so forth, would all have the same energy expression given by eq. (5.81). As pointed out, higher excitation operators such as \hat{T}_3 and \hat{T}_4 will not contribute to the energy since they are not able to produce full contractions with the Hamiltonian. However, higher order excitation operators contribute to the energy indirectly through the amplitudes t_i^a and t_{ij}^{ab} . In section 5.3 we concluded that all the amplitudes are coupled, such that they all depend on each other. Thus the amplitudes t_i^a and t_{ij}^{ab} are affected by all the other amplitudes $t_{ijk}^{abc}, t_{ijkl}^{abcd}, \dots$ in the scheme.

The CCSD amplitude eqs. (5.44) and (5.45) can in principle be solved in the same manner as the energy equation above. By expressing the excited amplitude states $\langle \Phi_i^a |$ and $\langle \Phi_{ij}^{ab} |$ in terms of the reference state as follows

$$\langle \Phi_i^a | = \langle \Phi_0 | a_i^\dagger a_a, \quad (5.82)$$

$$\langle \Phi_{ij}^{ab} | = \langle \Phi_0 | a_i^\dagger a_j^\dagger a_b a_a, \quad (5.83)$$

the contributions to the amplitude equations are determined by using Wick's generalized theorem on the operator strings produced by the terms in \bar{H} eq. (5.77). We have to demand full contraction of the operator strings in order to obtain contribution, but it is important to note that the connected cluster condition must be satisfied. We can obtain fully contracted operator strings with nonzero contributions that violate the connected cluster property. These cannot contribute to the amplitude equations. Even though the derivation of these amplitude contributions are straight forward, they are also tedious and prone of errors. The diagrammatic approach is a technique that offers a far more sophisticated and simpler way of determining the contributions of the coupled cluster equations. In the next section we will introduce the basics of this technique.

5.4.3 Diagrammatic approach

Diagrammatic notation originated in quantum field theory with the *Feynman diagrams*. The notation found applications in different areas of physics and quantum chemistry, e.g. the notation is used in both Rayleigh-Schrödinger perturbation theory and in coupled cluster theory [35]. Depending on the context, the diagrammatic notation can represent wave functions, operators or matrix elements. The diagrammatic notation outlined in this section enables us to interpret diagrams algebraically. In this section we give a brief introduction to the interpretation rules as preparation to the derivation of the diagrammatic coupled cluster equations in the two subsequent sections. In section 5.4.6 we give a proper introduction on how the coupled cluster diagrams are interpreted in order to obtain accurate algebraic expressions. These interpretation rules apply only to the matrix element representation of the Coupled Cluster diagrams.

Diagrammatic Slater Determinants

Slater determinants (SD) are represented by vertical arrow lines. These arrow lines implement the particle-hole formalism (section 2.4.4). Downward directed lines represent hole states, i.e. the occupied single-particle orbitals in the reference SD. Upward directed lines represent particle states, i.e. the virtual orbitals in excited SDs. This for example, means that excited SD $|\Phi_{ij,\dots}^{ab,\dots}\rangle$ are represented by a combination of hole and particle lines. Naturally this convention implies that the reference SD $|\Phi_0\rangle$ is represented by empty space. See fig. 5.1 for examples of diagrammatic ways to represent SDs.

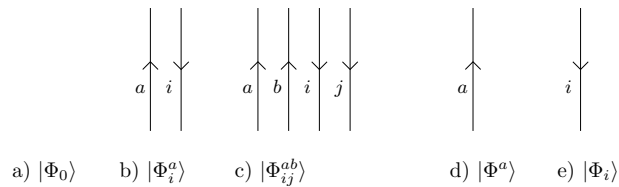


Figure 5.1: Diagrammatic representation of Slater determinants (SDs): a) represents the reference SD, b) depicts a single-excited (1p1h) SD, c) represents a doubly-excited (2p2h) SD, d) represents a reference SD with an added particle, e) depicts a reference SD with a particle removed

Diagrammatic Operators

Operators are depicted in diagrammatic notation by horizontal interaction lines connected with directed lines. Different operators have different types of interaction lines. Operators constituting the Hamiltonian are represented by dashed lines. Excitation operators are represented by solid lines, see illustration in fig. 5.2 The interaction lines have so called vertices, which represent the action of the operator. Each operator has at least one vertex, viz. one-body operators have one vertex, two-body operators have two vertices, three-body operators have three vertices etc. Every vertex is attached to two directed lines. The directed lines are associated with the annihilation and creation operators in the corresponding algebraic operator expressions. From section 2.4.2 we have that one-body operator expressions contain one pair of creation-annihilation operators, while two-body operator expressions contain two pairs. Each pair gives rise to two directed lines, viz. one-body operator diagrams contain two directed lines, two-body operator diagrams contain four directed lines, three-body operator diagrams contain six, etc. In general the n -body operator diagram contains n vertices and $2n$ directed lines. The direction of the lines depends on the subspace in which the operators act, namely the occupied hole space or the virtual particle space. Operators acting on hole states are directed downwards, while operators acting on particle states point upwards. Creation operators of both holes and particles lie above the interaction line, while accordingly annihilation operators lie below the interaction line. The hole- and particle-creation operators, which are found above interaction lines, are collectively called quasi-creation operators. Similarly the hole- and particle-annihilation operators, which are found below interaction lines, are collectively called quasi-annihilation operators [1].

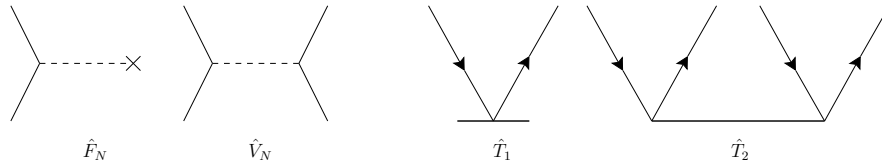


Figure 5.2: Illustration of different interaction representations. The two dashed line operators to the left represent the one-body and two-body interactions contained in the Hamiltonian. Interaction lines representing actions of the Hamiltonian are always illustrated as dashed lines. The two solid line operators to the left represent the \hat{T}_1 and \hat{T}_2 cluster operator action. The action of cluster operators are always represented by solid lines

We will concretize this operator representation by expressing the components \hat{F}_N and \hat{V}_N , of the normal-ordered Hamiltonian, in a diagrammatic notation. We start with the one-body operator \hat{F}_N given explicitly in eq. (5.39). The sum in \hat{F}_N runs over two indices contained in both subspaces (holes and particles). We can therefore divide the sum into

four terms according to which subspace the two indices exist in, viz.

$$\begin{aligned}
 \hat{F}_N &= \sum_{ab} f_b^a \{a_a^\dagger a_b\} + \sum_{ij} f_j^i \{a_i^\dagger a_j\} + \sum_{ai} f_a^i \{a_i^\dagger a_a\} + \sum_{ai} f_i^a \{a_a^\dagger a_i\} \\
 &= \text{diagram 1} + \text{diagram 2} + \text{diagram 3} + \text{diagram 4} . \quad (5.84)
 \end{aligned}$$

In the following we consider the first term and the third term of eq. (5.84). We explain how we express the different components of the algebraic expressions, in the corresponding diagrammatic expressions. In general we have that the vertex of a one-body operator is denoted by an \times . The first algebraic term in eq. (5.84) involves only particle space. The particle-creation operator a_a^\dagger , is in diagrammatic notation represented by the directed line above the interaction line. The upward direction indicates the particle nature of this creation operator. The particle-annihilation operator a_b , is in diagrammatic notation represented by a particle line below the interaction line. This representation is general for all particle annihilation and creation operators. In term three both subspaces are involved in the interaction. The interaction annihilates a particle state, illustrated by the upward directed line, and it annihilates a hole state illustrated by the downward directed line. Note that these two lines represent the quasi-annihilation operators, thus there are no lines present above the interaction line.

The two-body operator \hat{V}_N given explicitly in eq. (5.40), has a sum over four indices in both subspaces. This gives rise to 2^4 possible terms when dividing the sum according to which subspace the four indices exist in. However, many of these terms are equivalent and the sum reduces to nine distinct terms. This becomes evident by the different factors accompanying the sums illustrated in the expression below. See for example ref. [1] for more details. The diagrammatic expression of the \hat{V}_N operator thus reads

$$\begin{aligned}
 \hat{V}_N &= \frac{1}{4} \sum_{abcd} \langle ab|V|cd \rangle \{a_a^\dagger a_b^\dagger a_d a_c\} + \frac{1}{4} \sum_{ijkl} \langle ij|V|kl \rangle \{a_i^\dagger a_j^\dagger a_l a_k\} + \sum_{iajb} \langle ia|V|bj \rangle \{a_i^\dagger a_a^\dagger a_j a_b\} \\
 &+ \frac{1}{2} \sum_{aibcl} \langle ai|V|bc \rangle \{a_a^\dagger a_i^\dagger a_c a_b\} + \frac{1}{2} \sum_{ijka} \langle ij|V|ka \rangle \{a_i^\dagger a_j^\dagger a_a a_k\} + \frac{1}{2} \sum_{abci} \langle ab|V|ci \rangle \{a_a^\dagger a_b^\dagger a_i a_c\} \\
 &+ \frac{1}{2} \sum_{iajk} \langle ia|V|jk \rangle \{a_i^\dagger a_a^\dagger a_k a_j\} + \frac{1}{4} \sum_{abij} \langle ab|V|ij \rangle \{a_a^\dagger a_b^\dagger a_j a_i\} + \frac{1}{4} \sum_{ijab} \langle ij|V|ab \rangle \{a_i^\dagger a_j^\dagger a_b a_a\}
 \end{aligned} \quad (5.85)$$

(5.86)

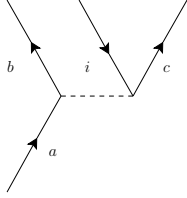
Diagrammatic Matrix Elements

Diagrams as the ones given above can also be interpreted as matrix elements of operators between Slater determinants. Diagrams interpreted from bottom to top, correspond to matrix elements read from right to left. Diagrams of this sort is convenient in CC-theory since the CC-equations constitute matrix elements of operators between the reference determinant $|\Phi_0\rangle$ to the right, and the reference determinant or excited reference determinants $\langle\Phi_{ij\ldots}^{ab}\rangle$ to the left. In the following we give some examples to illustrate the interpretation technique.

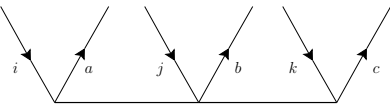
The first example is given by considering the fourth term of \hat{F}_N in eq. (5.84). Below the interaction line we have empty space. From fig. 5.1 this represents the reference determinant. Above the interaction line we have two quasi-creation lines creating a single excited reference determinant. The diagram is thus interpreted as

$$\langle\Phi_i^a|\hat{F}_N|\Phi_0\rangle = \text{diagram} \quad (5.87)$$

Second we can consider the sixth term of \hat{V}_N in eq. (5.86). Below the interaction line there is one particle line corresponding to the reference determinant with one added particle. Above the interaction line there are two particle lines and one hole line corresponding to the determinant with one added particle and one excited particle. Thus we obtain

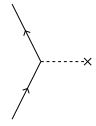
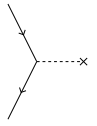


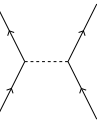
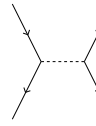


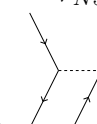


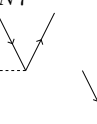

$$\langle \Phi_i^{bc} | \hat{V}_N | \Phi^a \rangle =$$

(5.88)

We also give an illustrative example of the cluster operator \hat{T}_3 . Below all cluster operator lines are empty space, which represents the reference determinant. Above the cluster operator line we have pairs of particle-hole creation lines. One pair for \hat{T}_1 , two pairs for \hat{T}_2 , etc. In the case of \hat{T}_3 , we have three pairs corresponding to the triple excited reference determinant, viz.

$$\langle \Phi_{ijk}^{abc} | \hat{T}_3 | \Phi_0 \rangle =$$

(5.89)

Excitation levels

It is practical to introduce the *excitation level* of the operator diagrams. This level is determined by subtracting the number of quasi-annihilation lines (below the interaction line) from the number of quasi-creation lines (above the interaction line), and divide by two [1]. This means that the excitation operator \hat{T}_3 above, has an excitation level of +3. From fig. 5.2 we observe that \hat{T}_1 and \hat{T}_2 have excitation level +1 and +2, respectively. See the excitation levels of the diagrams constituting the normal-ordered Hamiltonian in eq. (5.90). Excitation levels become useful when we have to combine diagrams with specific excitation numbers in order to obtain contributions to the CC-equations.

\hat{F}_{N1}	\hat{F}_{N2}	\hat{F}_{N3}	\hat{F}_{N4}	\hat{V}_{N1}	\hat{V}_{N2}	\hat{V}_{N3}
						
0	0	-1	+1	0	0	0
\hat{V}_{N4}	\hat{V}_{N5}	\hat{V}_{N6}	\hat{V}_{N7}	\hat{V}_{N8}	\hat{V}_{N9}	
						
-1	-1	+1	+1	+2	-2	

(5.90)

5.4.4 Diagrammatic CCSD Energy equation

In this section we illustrate how the coupled cluster energy equation can be solved by utilizing the diagrammatic matrix representation. Diagrams provide a straightforward technique that makes the determination of energy contributions easy and concise. The

complexity of the algebraic technique of Wick's theorem escalates with the size of the operator string, and it produces redundant information which we avoid using diagrams. The advantage of the diagrams will become clear in the following derivation.

The energy equation, which was derived earlier, reads

$$E_{CC} = \langle \Phi_0 | (\hat{H}_N + \hat{H}_N \hat{T} + \frac{1}{2!} \hat{H}_N \hat{T}^2 + \frac{1}{3!} \hat{H}_N \hat{T}^3 + \frac{1}{4!} \hat{H}_N \hat{T}^4 + \dots)_c | \Phi_0 \rangle. \quad (5.91)$$

The subscript c denotes that the connected cluster theorem must be satisfied, meaning that the Hamiltonian must have at least one contraction with each excitation operator on its right. We now translate this equation term by term into diagrammatic matrix elements. We are considering the truncation $\hat{T} = \hat{T}_1 + \hat{T}_2$. These excitation operators take the diagrammatic form given in fig. 5.2. The normal-ordered Hamiltonian consists of \hat{F}_N and \hat{V}_N , which have the diagrammatic form given in eqs. (5.84) and (5.86), respectively. From the energy equation we have that the matrix elements consist of the reference determinant on both left and right side. The reference state is represented by empty space, hence the energy diagrams cannot contain directed lines extending above or below the interaction lines. These extended lines are called *external lines*, and without them the excitation level of the diagram is zero. We observe that the diagrams constituting \hat{H}_N all have external lines, resulting in zero contribution to the energy. This we already knew from construction, see eq. (5.42). All the other terms in the energy equation are nested operators of \hat{H}_N , \hat{T}_1 and \hat{T}_2 . In the diagrammatic representation of such operator products, the interaction line of the rightmost operator is placed at the bottom, and the leftmost operator has its interaction line placed at the top. In order to avoid external lines the diagram lines of the operators in the product must be merged together, which is analogous to contractions in Wick's theorem. When the particle or hole creation and annihilation operator lines of two diagrams are merged together, the diagrams are connected. The total excitation level of the operator product is the sum of each excitation level of the operators involved. The excitation level of the normal-ordered Hamiltonian has a range from -2 to $+2$, see eq. (5.90). Therefor the energy receives only a limited number of contributions from the terms in eq. (5.91). The energy expectation value has excitation level zero, therefor only terms of eq. (5.91) with excitation level zero can contribute to the energy. Remembering that the Hamiltonian must obey the connected cluster theorem, we obtain the following contributing terms, and the reduced energy equation reads

$$E_{CC} = \langle \Phi_0 | (\hat{H}_N \hat{T}_1 + \hat{H}_N \hat{T}_2 + \frac{1}{2} \hat{H}_N \hat{T}_1^2)_c | \Phi_0 \rangle, \quad (5.92)$$

This is the same result obtained algebraically in eq. (5.79). Next, we consider the diagrams of each term in eq. (5.92).

The first term $\langle \Phi_0 | \hat{H}_N \hat{T}_1 | \Phi_0 \rangle$, contains the excitation operator \hat{T}_1 with excitation level $+1$. The diagram of the Hamiltonian must therefore have an excitation level of -1 , in addition to produce the reference determinant on the top. From eq. (5.90), we observe that the only diagram that fulfills the conditions is \hat{F}_{N3} . Thus the energy diagram reads

$$(5.93)$$

The second term $\langle \Phi_0 | (\hat{H}_N \hat{T}_2 | \Phi_0 \rangle$, contains the excitation operator \hat{T}_2 with excitation level +2. The Hamiltonian must therefore have an excitation level -2, and as before, produce the reference determinant on the top. One diagram fits the conditions, namely \hat{V}_{N9} in eq. (5.90). Thus, we obtain the energy contribution

$$(5.94)$$

The third term $\langle \Phi_0 | (\hat{H}_N \hat{T}_1^2 | \Phi_0 \rangle$, contains two excitation operators \hat{T}_1 with excitation level +1. This sum up to an excitation level of +2, which leaves only one option for the Hamiltonian diagram, viz. \hat{V}_{N9} . Note that since the excitation operators commute with each other, their vertical ordering in the diagram is irrelevant. The energy diagram is therefore given as

$$(5.95)$$

The final diagrammatic energy expression reads

$$(5.96)$$

We shall see that this is identical to the result obtained utilizing Wick's theorem. The diagrams can be translated into algebraic expressions by defining some diagrammatic interpretation rules. We will consider these rules after deriving the diagrams of the amplitude equations.

5.4.5 Diagrammatic CCSD Amplitude equations

The amplitude diagrams are derived, in the same manner as the energy diagrams, by combining Hamiltonian diagrams with cluster diagrams. Some additional considerations must however be made since the matrix elements of the amplitude eqs. (5.44) and (5.45) produce single and double excited reference determinants Φ_i^a and Φ_{ij}^{ab} on the left side. In

this section we determine the diagram contribution to the amplitude equations from each term in the similarity transformed normal-ordered Hamiltonian \bar{H} given by

$$\bar{H} = \left[\hat{H}_N + \hat{H}_N \hat{T} + \frac{1}{2!} \hat{H}_N \hat{T}^2 + \frac{1}{3!} \hat{H}_N \hat{T}^3 + \frac{1}{4!} \hat{H}_N \hat{T}^4 \right]_c. \quad (5.97)$$

We remember that $\hat{T} = \hat{T}_1 + \hat{T}_2$ and that the natural truncation at \hat{T}^4 is caused by the two-body form of the Hamiltonian. \bar{H} for CCSD is explicit given in eq. (5.78). We start with deriving the \hat{T}_1 -amplitude equation, and follow up with the \hat{T}_2 -amplitude equation.

\hat{T}_1 -amplitude equation

The \hat{T}_1 -amplitude equation explicitly reads

$$\langle \Phi_i^a | \left[\hat{H}_N + \hat{H}_N \hat{T} + \frac{1}{2!} \hat{H}_N \hat{T}^2 + \frac{1}{3!} \hat{H}_N \hat{T}^3 + \frac{1}{4!} \hat{H}_N \hat{T}^4 \right]_c | \Phi_0 \rangle = 0. \quad (5.98)$$

We will now determine the diagram contribution from each term above. In order to do that there are two conditions we must obey, viz.

- The total excitation level of the diagram must be +1, viz. there must be two external creation lines (one hole, one particle) at the top of the diagram, corresponding to the 1p1h excited reference determinant.
- The reference determinant must be present in the bottom of the diagram.

Term1

The first term of the \hat{T}_1 -amplitude equation is the normal-ordered Hamiltonian $\hat{H}_N = \hat{F}_N + \hat{V}_N$. Considering the diagrams of \hat{F}_N and \hat{V}_N in eqs. (5.90) we find only one diagram that fulfills the two conditions above, namely \hat{F}_{N4} . Thus we have one contribution to the amplitude equation from this term:

$$\langle \Phi_i^a | \bar{H} | \Phi_0 \rangle \leftarrow \begin{array}{c} \diagup \quad \diagdown \\ \quad \times \end{array} \quad (5.99)$$

Term2

The second term of eq. (5.98) receives contribution from both \hat{T}_1 and \hat{T}_2 . The term $\langle \Phi_i^a | \hat{H}_N \hat{T}_1 | \Phi_0 \rangle$, requires that the Hamiltonian diagram have an excitation level 0 in order to fulfill the two conditions. Considering the diagrams of \hat{F}_N and \hat{V}_N in eq. (5.90), we

observe that only diagrams \hat{F}_{N1} , \hat{F}_{N2} and \hat{V}_{N3} contribute as given respectively:

$$\begin{array}{ccc}
 \begin{array}{c} \text{Diagram 1} \\ \text{Diagram 2} \end{array} & \rightarrow & \begin{array}{c} \text{Diagram 3} \\ \text{Diagram 4} \end{array} \rightarrow \langle \Phi_i^a | \hat{H}_N \hat{T}_1 | \Phi_0 \rangle \quad (5.100)
 \end{array}$$

$$\begin{array}{ccc}
 \begin{array}{c} \text{Diagram 5} \\ \text{Diagram 6} \end{array} & \rightarrow & \begin{array}{c} \text{Diagram 7} \\ \text{Diagram 8} \end{array} \rightarrow \langle \Phi_i^a | \hat{H}_N \hat{T}_1 | \Phi_0 \rangle \quad (5.101)
 \end{array}$$

$$\begin{array}{ccc}
 \begin{array}{c} \text{Diagram 9} \\ \text{Diagram 10} \end{array} & \rightarrow & \begin{array}{c} \text{Diagram 11} \\ \text{Diagram 12} \end{array} \rightarrow \langle \Phi_i^a | \hat{H}_N \hat{T}_1 | \Phi_0 \rangle \quad (5.102)
 \end{array}$$

In term $\langle \Phi_i^a | \hat{H}_N \hat{T}_2 | \Phi_0 \rangle$, the excitation level of the Hamiltonian must balance the +2 excitation originating from \hat{T}_2 . This requires Hamiltonian diagrams with excitation level -1. The Hamiltonian diagrams which satisfy all conditions are \hat{F}_{N3} , \hat{V}_{N4} and \hat{V}_{N5} ,

$$\begin{array}{ccc}
 \begin{array}{c} \text{Diagram 13} \\ \text{Diagram 14} \end{array} & \rightarrow & \begin{array}{c} \text{Diagram 15} \\ \text{Diagram 16} \end{array} \rightarrow \langle \Phi_i^a | \hat{H}_N \hat{T}_2 | \Phi_0 \rangle \quad (5.103)
 \end{array}$$

$$\begin{array}{ccc}
 \begin{array}{c} \text{Diagram 17} \\ \text{Diagram 18} \end{array} & \rightarrow & \begin{array}{c} \text{Diagram 19} \\ \text{Diagram 20} \end{array} \rightarrow \langle \Phi_i^a | \hat{H}_N \hat{T}_2 | \Phi_0 \rangle \quad (5.104)
 \end{array}$$

$$\begin{array}{ccc}
 \begin{array}{c} \text{Diagram 21} \\ \text{Diagram 22} \end{array} & \rightarrow & \begin{array}{c} \text{Diagram 23} \\ \text{Diagram 24} \end{array} \rightarrow \langle \Phi_i^a | \hat{H}_N \hat{T}_2 | \Phi_0 \rangle \quad (5.105)
 \end{array}$$

Term3

The third term of eq. (5.98) give rise to three new terms $\langle \Phi_i^a | \frac{1}{2} \hat{H}_N \hat{T}_1^2 | \Phi_0 \rangle$, $\langle \Phi_i^a | \frac{1}{2} \hat{H}_N \hat{T}_2^2 | \Phi_0 \rangle$, and $\langle \Phi_i^a | \hat{H}_N \hat{T}_1 \hat{T}_2 | \Phi_0 \rangle$. We can neglect the term involving \hat{T}_2^2 since this results in an excitation level of +4, which cannot be balanced to +1 by the Hamiltonian. The two other terms will produce a contribution.

Term $\langle \Phi_i^a | \frac{1}{2} \hat{H}_N \hat{T}_1^2 | \Phi_0 \rangle$, requires Hamilton diagrams with excitation level -1 . This is acquired by \hat{F}_{N3} , \hat{V}_{N4} and \hat{V}_{N5} , which results in the diagram contributions:

$$\begin{array}{c} \text{Diagram 1} \end{array} \rightarrow \begin{array}{c} \text{Diagram 2} \end{array} \rightarrow \langle \Phi_i^a | \frac{1}{2} \hat{H}_N \hat{T}_1^2 | \Phi_0 \rangle \quad (5.106)$$

$$\begin{array}{c} \text{Diagram 3} \end{array} \rightarrow \begin{array}{c} \text{Diagram 4} \end{array} \rightarrow \langle \Phi_i^a | \hat{H}_N \hat{T}_1^2 | \Phi_0 \rangle \quad (5.107)$$

$$\begin{array}{c} \text{Diagram 5} \end{array} \rightarrow \begin{array}{c} \text{Diagram 6} \end{array} \rightarrow \langle \Phi_i^a | \hat{H}_N \hat{T}_1^2 | \Phi_0 \rangle \quad (5.108)$$

Term $\langle \Phi_i^a | \hat{H}_N \hat{T}_1 \hat{T}_2 | \Phi_0 \rangle$, requires Hamilton diagrams with excitation level -2 , since $\hat{T}_1 \hat{T}_2$ contribute with a level $+3$. \hat{V}_{N9} is the only Hamilton diagram fulfilling this requirement. However this one diagram will give rise to three distinct amplitude diagrams. A technique that ensures construction of all possible and unique diagrams, was developed by Kucharski and Bartlett [38]. Construction of diagrams can be quite complicated. One can construct diagrams that from the looks of it are different, but in reality are the same diagram. The technique of Kucharski and Bartlett is an easy and powerful method making the construction somewhat easier. We call the method the *sign-table technique*. The method is based on assigning a $+$ sign to the particle lines and a $-$ sign to the hole lines, which are situated below the interaction line of the Hamiltonian and above the interaction line of the excitation operators. The method of obtaining all diagrams is to divide the signs of the Hamiltonian diagram between the excitation operators in all possible ways. We illustrate this with an example of how we obtain all three diagrams of $\langle \Phi_i^a | \hat{H}_N \hat{T}_1 \hat{T}_2 | \Phi_0 \rangle$.

First we label the directed lines with signs as shown in fig. 5.3 We take the signs of

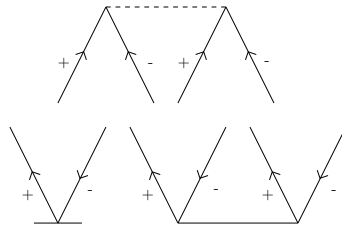


Figure 5.3

the Hamiltonian and place them side by side. Next we partition these signs between the excitation operators using the notation $\hat{T}_1 | \hat{T}_2$. In order to determine all the diagrams, the signs must be partitioned in all possible ways. The signs labeling the excitation operators help us decide which partitions that are allowed. For example, \hat{T}_1 have one $+$ and one $-$

sign, and can at most be coupled to one + and one - sign from the Hamiltonian operator. We also have to obey the connected cluster theorem, such that each excitation operator must have at least one sign in its partition. Thus the partition possibilities of $\hat{T}_1\hat{T}_2$ are

	\hat{T}_1		\hat{T}_2	
(1)	+		+ - -	(5.109)
(2)	-		+ + -	
(3)	+-		+-	

Note that the ordering of the signs on each side of the partition | is irrelevant. The diagrams are obtained by merging the lines of the Hamiltonian and the excitation operator corresponding to the sign in the table of eq. (5.109). The diagrams are given respectively:

$$\begin{array}{c} \text{Diagram 1} \end{array} \rightarrow \begin{array}{c} \text{Diagram 2} \end{array} \rightarrow \langle \Phi_i^a | \frac{1}{2} \hat{H}_N \hat{T}_1 \hat{T}_2 | \Phi_0 \rangle \quad (5.110)$$

$$\begin{array}{c} \text{Diagram 3} \end{array} \rightarrow \begin{array}{c} \text{Diagram 4} \end{array} \rightarrow \langle \Phi_i^a | \hat{H}_N \hat{T}_1 \hat{T}_2 | \Phi_0 \rangle \quad (5.111)$$

$$\begin{array}{c} \text{Diagram 5} \end{array} \rightarrow \begin{array}{c} \text{Diagram 6} \end{array} \rightarrow \langle \Phi_i^a | \hat{H}_N \hat{T}_1 \hat{T}_2 | \Phi_0 \rangle \quad (5.112)$$

Term4

The fourth term of eq. (5.98) produces four matrix elements with the operator strings $(\hat{H}_N \hat{T}_1^3)$, $(\hat{H}_N \hat{T}_1^2 \hat{T}_2)$, $(\hat{H}_N \hat{T}_1 \hat{T}_2^2)$ and $(\hat{H}_N \hat{T}_2^3)$. Only the operator string $\hat{H}_N \hat{T}_1^3$ can produce the excitation level +1, we therefore consider only the matrix element $\langle \Phi_i^a | \frac{1}{6} \hat{H}_N \hat{T}_1^3 | \Phi_0 \rangle$. The Hamiltonian must have an excitation level of -2, and as before the only diagram that satisfies this is \hat{V}_{N9} of eq. (5.90). We can construct one distinct diagram from this operator string. One might think that there were more than one by considering the sign-technique table, viz.

\hat{T}_1		\hat{T}_1		\hat{T}_1	
+		-		+-	(5.113)
-		+		+-	
-		+-		+	
⋮					

However, all these partitions are equal, since the excitation operators commute with each other. Thus, the diagram contribution to the \hat{T}_1 -amplitude equation reads

$$\begin{array}{c} \text{Diagram 7} \end{array} \rightarrow \begin{array}{c} \text{Diagram 8} \end{array} \rightarrow \langle \Phi_i^a | \frac{1}{6} \hat{H}_N \hat{T}_1^3 | \Phi_0 \rangle \quad (5.114)$$

The fifth term of eq. (5.98) will not contribute with any diagrams to the \hat{T}_1 -amplitude equation, because the excitation level +1 is not obtainable from \hat{T} raised to the fourth power. We recapitulate this section by writing out the explicit diagrammatic form of the \hat{T}_1 -amplitude equation:

$$\begin{aligned}
 0 = & \text{Diagram 1} + \text{Diagram 2} + \text{Diagram 3} + \text{Diagram 4} \\
 & + \text{Diagram 5} + \text{Diagram 6} + \text{Diagram 7} + \text{Diagram 8} \\
 & + \text{Diagram 9} + \text{Diagram 10} + \text{Diagram 11} + \text{Diagram 12} \\
 & + \text{Diagram 13} + \text{Diagram 14}
 \end{aligned} \tag{5.115}$$

\hat{T}_2 -amplitude equation

The \hat{T}_2 -amplitude equation reads

$$\langle \Phi_{ij}^{ab} | \left[\hat{H}_N + \hat{H}_N \hat{T} + \frac{1}{2!} \hat{H}_N \hat{T}^2 + \frac{1}{3!} \hat{H}_N \hat{T}^3 + \frac{1}{4!} \hat{H}_N \hat{T}^4 \right]_c | \Phi_0 \rangle = 0. \tag{5.116}$$

We start by deriving the diagrams of some selected terms in eq. (5.116). The final diagrams of the equation is presented at the end of this section. The diagrams of the \hat{T}_2 -amplitude equation must satisfy the following conditions:

- The excitation level of the diagram must equal +2, viz. there is four external creation lines (2hole, 2 particle) at the top of the diagram, corresponding to the 2p2h excited reference determinant.
- The reference determinant constitutes the bottom of the diagram, i.e. no external annihilation lines.

Term $\langle \Phi_{ij}^{ab} | (\hat{H}_N \hat{T}_1)_c | \Phi_0 \rangle$

The term $\langle \Phi_{ij}^{ab} | (\hat{H}_N \hat{T}_1)_c | \Phi_0 \rangle$ gives two diagram contributions. The excitation level of the Hamiltonian must equal +1 in order to obtain a total excitation level +2. The diagrams that satisfy all conditions, are derived from the diagrams \hat{V}_{N6} and \hat{V}_{N7} in eq. (5.90),

and the \hat{T}_1 diagram in fig. 5.2, viz.

$$\begin{array}{c} \text{Diagram 1} \end{array} \rightarrow \begin{array}{c} \text{Diagram 2} \end{array} \rightarrow \langle \Phi_{ij}^{ab} | (\frac{1}{2} \hat{H}_N \hat{T}_1)_c | \Phi_0 \rangle \quad (5.117)$$

$$\begin{array}{c} \text{Diagram 3} \end{array} \rightarrow \begin{array}{c} \text{Diagram 4} \end{array} \rightarrow \langle \Phi_{ij}^{ab} | (\frac{1}{2} \hat{H}_N \hat{T}_1)_c | \Phi_0 \rangle \quad (5.118)$$

Term $\langle \Phi_{ij}^{ab} | (\hat{H}_N \hat{T}_1 \hat{T}_2)_c | \Phi_0 \rangle$

This term requires that the Hamiltonian diagrams have an excitation level -1 . Three diagrams satisfy all the conditions, namely \hat{F}_{N3} , \hat{V}_{N4} and \hat{V}_{N5} in eq. (5.90). We use the sign-table technique in order to determine all the distinct diagrams from each Hamiltonian diagram.

Diagram \hat{F}_{N3} produce one $+$ and one $-$ sign to divide between the two operators \hat{T}_1 and \hat{T}_2 . This results in the sign-table eq. (5.119), which give two diagram contributions as obtained in eq. (5.120) and (5.121)

$$\begin{array}{c|c} \hat{T}_1 & \hat{T}_2 \\ \hline + & - \\ - & + \end{array} \quad (5.119)$$

$$\begin{array}{c} \text{Diagram 5} \end{array} \rightarrow \begin{array}{c} \text{Diagram 6} \end{array} \rightarrow \langle \Phi_{ij}^{ab} | (\hat{H}_N \hat{T}_1 \hat{T}_2)_c | \Phi_0 \rangle \quad (5.120)$$

$$\begin{array}{c} \text{Diagram 7} \end{array} \rightarrow \begin{array}{c} \text{Diagram 8} \end{array} \rightarrow \langle \Phi_{ij}^{ab} | (\hat{H}_N \hat{T}_1 \hat{T}_2)_c | \Phi_0 \rangle \quad (5.121)$$

Diagram \hat{V}_{N4} produce two $+$ and one $-$ sign, which we partition between the excitation operators in a sign-table. The resulting rows of the sign-table in eq. (5.122), give rise to the three diagrams shown in eq. (5.123), (5.124) and (5.125), respectively.

$$\begin{array}{c|c} \hat{T}_1 & \hat{T}_2 \\ \hline + & +- \\ - & ++ \\ +- & + \end{array} \quad (5.122)$$

$$\rightarrow \langle \Phi_{ij}^{ab} | (\hat{H}_N \hat{T}_1 \hat{T}_2)_c | \Phi_0 \rangle \quad (5.123)$$

$$\rightarrow \langle \Phi_{ij}^{ab} | (\hat{H}_N \hat{T}_1 \hat{T}_2)_c | \Phi_0 \rangle \quad (5.124)$$

$$\rightarrow \langle \Phi_{ij}^{ab} | (\hat{H}_N \hat{T}_1 \hat{T}_2)_c | \Phi_0 \rangle \quad (5.125)$$

Diagram \hat{V}_{N5} produces one + and two - sign, which we partition between the excitation operators in a sign-table. The resulting rows of the sign-table in eq. (5.126), give rise to three diagrams shown in eq. (5.127), (5.128) and (5.129), respectively.

\hat{T}_1		\hat{T}_2	
+		--	(5.126)
-		+-	
+-		-	

$$\rightarrow \langle \Phi_{ij}^{ab} | (\hat{H}_N \hat{T}_1 \hat{T}_2)_c | \Phi_0 \rangle \quad (5.127)$$

$$\rightarrow \langle \Phi_{ij}^{ab} | (\hat{H}_N \hat{T}_1 \hat{T}_2)_c | \Phi_0 \rangle \quad (5.128)$$

$$\rightarrow \langle \Phi_{ij}^{ab} | (\hat{H}_N \hat{T}_1 \hat{T}_2)_c | \Phi_0 \rangle \quad (5.129)$$

The final diagrammatic form of the \hat{T}_2 -amplitude equation is determined by evaluating each term in eq. (5.116), in a similar manner as for the two terms above. The final result

reads

$$\begin{aligned}
& 0 = \text{(diagram)} + \text{(diagram)} + \text{(diagram)} \\
& + \text{(diagram)} + \text{(diagram)} + \text{(diagram)} \\
& + \text{(diagram)} + \text{(diagram)} + \text{(diagram)} \\
& + \text{(diagram)} + \text{(diagram)} + \text{(diagram)} \\
& + \text{(diagram)} + \text{(diagram)} + \text{(diagram)} \\
& + \text{(diagram)} + \text{(diagram)} + \text{(diagram)} \\
& + \text{(diagram)} + \text{(diagram)} + \text{(diagram)} \\
& + \text{(diagram)} + \text{(diagram)} + \text{(diagram)} \\
& + \text{(diagram)} + \text{(diagram)} + \text{(diagram)} \\
& + \text{(diagram)} + \text{(diagram)} + \text{(diagram)} \\
& + \text{(diagram)} + \text{(diagram)} + \text{(diagram)}
\end{aligned}
\tag{5.130}$$

The diagrammatic equation (5.130) shows a sequence of 30 terms arranged in 10 rows and 3 columns. Each term consists of a Feynman diagram representing a process with four external legs (two incoming from the left, two outgoing to the right). The diagrams are connected by plus signs. The first row starts with '0 =' followed by three diagrams. Subsequent rows contain three diagrams each, separated by plus signs. The diagrams include various internal structures such as dashed lines, loops, and vertices, representing different contributions to a physical process.

5.4.6 Diagram Rules

In this section we present the diagram rules that enables the translation of diagrams into correct algebraic expressions. We start by listing the rules. Thereafter, we translate the energy diagrams into algebraic expressions, and see that these correspond with the expression obtained by the algebraic approach in eq. (5.81). We proceed by translating selected diagrams for the \hat{T}_1 and the \hat{T}_2 amplitude equations. We also list the complete algebraic expressions of \hat{T}_1 and \hat{T}_2 .

Interpretation Rules

1. Label all the directed lines in the diagram, $ijk\dots$ represent the hole states, and $abc\dots$ represent the particle states. Note that labels of external lines are those that occur in the bra part of the amplitude equations.
2. Each interaction line contributes with an integral or an amplitude to the algebraic expression, viz.

$$\begin{aligned}
 \hat{F}_N &= \text{diagram: a vertex with two incoming lines from the left and one outgoing line to the right ending in a cross} & : & \quad f_{in}^{out} \\
 \hat{V}_N &= \text{diagram: a vertex with two incoming lines from the left and two outgoing lines to the right} & : & \quad \langle \text{left-out right-out} | v | \text{left-in right-in} \rangle \\
 \hat{T}_1 &= \text{diagram: a vertex with one incoming line from the left labeled 'i' and one outgoing line to the right labeled 'a'} & : & \quad t_i^a \\
 \hat{T}_2 &= \text{diagram: a vertex with two incoming lines from the left labeled 'i' and 'j', and two outgoing lines to the right labeled 'a' and 'b'} & : & \quad t_{ij}^{ab}
 \end{aligned}$$

3. Include the sum over all internal indices, meaning indices associated with lines starting and ending in interaction lines.
4. The sign is given by a factor $(-1)^{h+l}$, where h is the number of hole lines and l is the number of loops. A loop is defined as a route along directed lines either returning to its beginning, or starting at one external line and ending at another external line.
5. Include a factor $\frac{1}{2}$ for each pair of *equivalent lines*, meaning directed lines which start in the same interaction line and end in the same interaction line, going in the same direction.
6. Include a factor $\frac{1}{2}$ for each *equivalent vertex*, meaning when two $\hat{T}_n, n = 1, 2, \dots$ operators have identical connections to the Hamiltonian interaction \hat{F}_N or \hat{V}_N .
7. Introduce a permutation function $\hat{P}_{(pq)}$ for each pair of *unique external lines* (holes or particles). Pairs of external lines (holes or particles, not both) that originate at different interaction lines are unique. The permutation function ensures antisymmetry and is defined as

$$\hat{P}_{(pq)} f(p, q) = f(p, q) - f(q, p). \quad (5.131)$$

Translation of the energy equation

The diagrammatic coupled cluster energy equation is given in eq. (5.96). We translate each diagram in this equation into an algebraic expression using the interpretation rules above.

The first diagram in eq. (5.132), contains one hole and one particle line which we label i and a respectively. The one-body part of the Hamiltonian contributes with a single particle integral f_i^a , while the \hat{T}_1 operator contributes with the amplitude t_i^a . Both directed lines are internal lines, which means we include the sum over i and a . We observe that the diagram has one loop and one hole line, which results in the positive sign $(-1)^2$. None of the other rules affect this diagram, thus

$$\text{Diagram 1} = \sum_{ai} f_i^a t_i^a. \quad (5.132)$$

The second diagram in eq. (5.133), contains two hole and two particle lines, which we label ij and ab respectively. The two-body part of the Hamiltonian contributes with a two-particle integral. This is given by $\langle \text{left-out right-out} | v | \text{left-in right-in} \rangle$, meaning that we place the labels of the two lines pointing into the vertices to the right, and those of the lines pointing out to the left, viz. $\langle ij | v | ab \rangle$. The operator \hat{T}_2 contributes with an amplitude t_{ij}^{ab} . All lines are internal and we therefore include the sum over all the indices. We observe that the two hole lines are equivalent lines, which also applies for the two particle lines, resulting in a factor $\frac{1}{4}$. The diagram holds two loops and two hole lines, which give a positive sign $(-1)^4$. The algebraic expression reads

$$\text{Diagram 2} = \frac{1}{4} \sum_{abij} \langle ij | v | ab \rangle t_{ij}^{ab}. \quad (5.133)$$

The third diagram in eq. (5.134), also contains two hole and two particle lines, which we label ij and ab respectively. The two-body contribution from the Hamiltonian equals that in the second diagram. The difference is in the presence of the two \hat{T}_1 operators, which contributes with two amplitudes $t_i^a t_j^b$ instead of one. We no longer have equivalent lines, but we observe that we have one pair of equivalent vertices contributing a factor $\frac{1}{2}$. The sign and sum equals the second diagram, viz. we obtain the expression:

$$\text{Diagram 3} = \frac{1}{2} \sum_{abij} \langle ij | v | ab \rangle t_i^a t_j^b. \quad (5.134)$$

The algebraic expression for the CC energy E_{CC} thus reads

$$E_{CC} = \sum_{ai} f_i^a t_i^a + \frac{1}{4} \sum_{abij} \langle ij | v | ab \rangle t_{ij}^{ab} + \frac{1}{2} \sum_{abij} \langle ij | v | ab \rangle t_i^a t_j^b, \quad (5.135)$$

which is the same answer as obtained using Wick's theorem in eq. (5.81).

Translation of the amplitude equations

By evaluating all fourteen diagrams of eq. (5.115) in the same manner as above, we obtain the following algebraic \hat{T}_1 -amplitude equation:

$$\begin{aligned}
 0 = & f_i^a + \sum_b f_b^a t_i^b - \sum_j f_i^j t_j^a + \sum_{bj} \langle ja|v|bi \rangle t_j^b + \sum_{bj} f_b^j t_{ij}^{ab} + \frac{1}{2} \sum_{bcj} \langle aj|v|bc \rangle t_{ij}^{bc} \\
 & - \frac{1}{2} \sum_{bjk} \langle jk|v|ib \rangle t_{jk}^{ab} - \sum_{bj} f_b^j t_j^a t_i^b + \sum_{bcj} \langle aj|v|bc \rangle t_i^b t_j^c - \sum_{bjk} \langle jk|v|ib \rangle t_j^a t_k^b - \frac{1}{2} \sum_{bcjk} \langle jk|v|bc \rangle t_i^b t_{jk}^{ac} \\
 & - \frac{1}{2} \sum_{bcjk} \langle jk|v|bc \rangle t_j^a t_{ik}^{bc} + \sum_{bcjk} \langle jk|v|bc \rangle t_j^b t_{ik}^{ac} - \sum_{bcjk} \langle jk|v|bc \rangle t_i^b t_j^a t_k^c. \tag{5.139}
 \end{aligned}$$

The terms in this equation agrees with the diagrams in eq. (5.115), which makes it easy to determine which diagram that belongs to which expression. Note that the sum-notation can be neglected. The indices we sum over are the indices which are common for the amplitudes and the Hamiltonian one-body or two-body integral/matrix-element. However, we include the sum for clarity.

\hat{T}_2 amplitude equation

We give one example of diagram translation concerning the \hat{T}_2 -amplitude equation. This example illustrates the effects of rule 6 and 7.

The 24. diagram in eq. (5.130) is derived from the operator string $\hat{H}_N \hat{T}_1^2 \hat{T}_2$. We observe four internal lines, which we label $cdkl$, and four external lines, which we label $abij$. The diagram have two loops and four hole lines, which yields a positive sign. We notice that the two \hat{T}_1 operators are connected to the two-body interaction in the exact same manner, which means we have one pair of equivalent vertices. We also notice that the two lines connecting the Hamiltonian and the \hat{T}_2 operator qualify as equivalent lines. We therefore include a factor $\frac{1}{4}$ as the contribution from one pair of equivalent vertices, and one pair of equivalent lines. The two external hole lines ij originate at different interaction lines, and thereby they constitute unique external lines. The permutation function $\hat{P}(ij)$ is therefore included. The final expression then reads

$$\text{Diagram} = \frac{1}{4} \hat{P}(ij) \sum_{cdkl} \langle kl|v|cd \rangle t_i^c t_{kl}^{ab} t_j^d. \tag{5.140}$$

By evaluating all 31 diagrams of eq. (5.130) we obtain the algebraic \hat{T}_2 -amplitude equation:

$$\begin{aligned}
 0 = \langle ij|v|ab\rangle & + \hat{P}_{(ij)} \sum_c \langle ab|v|cj\rangle t_i^c & - \hat{P}_{(ab)} \sum_k \langle kb|v|ij\rangle t_k^a \\
 & + \hat{P}_{(ab)} \sum_c f_c^b t_{ij}^{ac} & - \hat{P}_{(ij)} \sum_k f_j^k t_{ik}^{ab} & + \frac{1}{2} \sum_{cd} \langle ab|v|cd\rangle t_{ij}^{cd} \\
 & + \frac{1}{2} \sum_{kl} \langle kl|v|ij\rangle t_{kl}^{ab} & + \hat{P}_{(ab)} \hat{P}_{(ij)} \sum_{ck} \langle kb|v|cj\rangle t_{ik}^{ac} & + \frac{1}{2} \hat{P}_{(ij)} \sum_{cd} \langle ab|v|cd\rangle t_i^c t_j^d \\
 & + \frac{1}{2} \hat{P}_{(ab)} \sum_{kl} \langle kl|v|ij\rangle t_k^a t_l^b & - \hat{P}_{(ab)} \hat{P}_{(ij)} \sum_{ck} \langle kb|v|cj\rangle t_k^a t_i^c & - \hat{P}_{(ab)} \sum_{ck} f_c^k t_k^a t_{ij}^{cb} \\
 & - \hat{P}_{(ij)} \sum_{ck} f_c^k t_i^c t_{kj}^{ab} & + \hat{P}_{(ab)} \hat{P}_{(ij)} \sum_{cdk} \langle ak|v|dc\rangle t_i^d t_{jk}^{bc} & - \frac{1}{2} \hat{P}_{(ab)} \sum_{cdk} \langle kb|v|cd\rangle t_k^a t_{ij}^{cd} \\
 & + \hat{P}_{(ab)} \sum_{cdk} \langle ka|v|cd\rangle t_k^c t_{ij}^{db} & + \frac{1}{2} \hat{P}_{(ij)} \sum_{ckl} \langle kl|v|cj\rangle t_i^c t_{kl}^{ab} & - \hat{P}_{(ab)} \hat{P}_{(ij)} \sum_{ckl} \langle lk|v|ic\rangle t_l^a t_{kj}^{cb} \\
 & - \hat{P}_{(ij)} \sum_{ckl} \langle kl|v|ci\rangle t_k^c t_{jl}^{ba} & + \frac{1}{2} \hat{P}_{(ab)} \hat{P}_{(ij)} \sum_{cdkl} \langle kl|v|cd\rangle t_{ik}^{ac} t_{jl}^{bd} & - \frac{1}{2} \hat{P}_{(ab)} \hat{P}_{(ij)} \sum_{cdk} \langle kb|v|cd\rangle t_k^a t_i^c t_j^d \\
 & + \frac{1}{2} \hat{P}_{(ab)} \hat{P}_{(ij)} \sum_{ckl} \langle kl|v|cj\rangle t_k^a t_i^c t_l^b & + \hat{P}_{(ab)} \hat{P}_{(ij)} \sum_{cdkl} \langle kl|v|cd\rangle t_i^c t_k^a t_{jl}^{bd} & + \frac{1}{4} \hat{P}_{(ij)} \sum_{cdkl} \langle kl|v|cd\rangle t_i^c t_{kl}^{ab} t_j^d \\
 & + \frac{1}{4} \hat{P}_{(ab)} \sum_{cdkl} \langle kl|v|cd\rangle t_k^a t_{ij}^{cd} t_l^b & - \hat{P}_{(ab)} \sum_{cdkl} \langle kl|v|cd\rangle t_k^c t_l^a t_{ij}^{db} & - \hat{P}_{(ij)} \sum_{cdkl} \langle kl|v|cd\rangle t_k^c t_i^d t_{jl}^{ba} \\
 & + \frac{1}{4} \hat{P}_{(ab)} \hat{P}_{(ij)} \sum_{cdkl} \langle kl|v|cd\rangle t_k^a t_i^c t_l^b t_j^d & - \frac{1}{2} \hat{P}_{(ij)} \sum_{cdkl} \langle kl|v|cd\rangle t_{ki}^{cd} t_{lj}^{ab} & - \frac{1}{2} \hat{P}_{(ab)} \sum_{cdkl} \langle kl|v|cd\rangle t_{kl}^{ca} t_{ij}^{db} \\
 & + \frac{1}{4} \sum_{cdkl} \langle kl|v|cd\rangle t_{kl}^{ab} t_{ij}^{cd}. & &
 \end{aligned} \tag{5.141}$$

The terms in this equation agrees with the diagrams in eq. (5.130), which makes it easy to determine which diagram that belongs to which expression.

Part II

Implementation and Results

Chapter 6

Implementation

In this chapter we introduce the computational implementation of both the Hartree-Fock method (HF) and the Coupled Cluster Singles and Doubles method (CCSD). These methods are introduced in chapter 4 and 5, respectively. We discuss several essential parts of our HF and CCSD codes¹. In both programs we utilize C++ as programming language [39]. Our codes are object oriented and easy to extend to other physical systems. We have also developed several Python scripts [40], for efficient running of our C++ codes.

6.1 Hartree-Fock Implementation

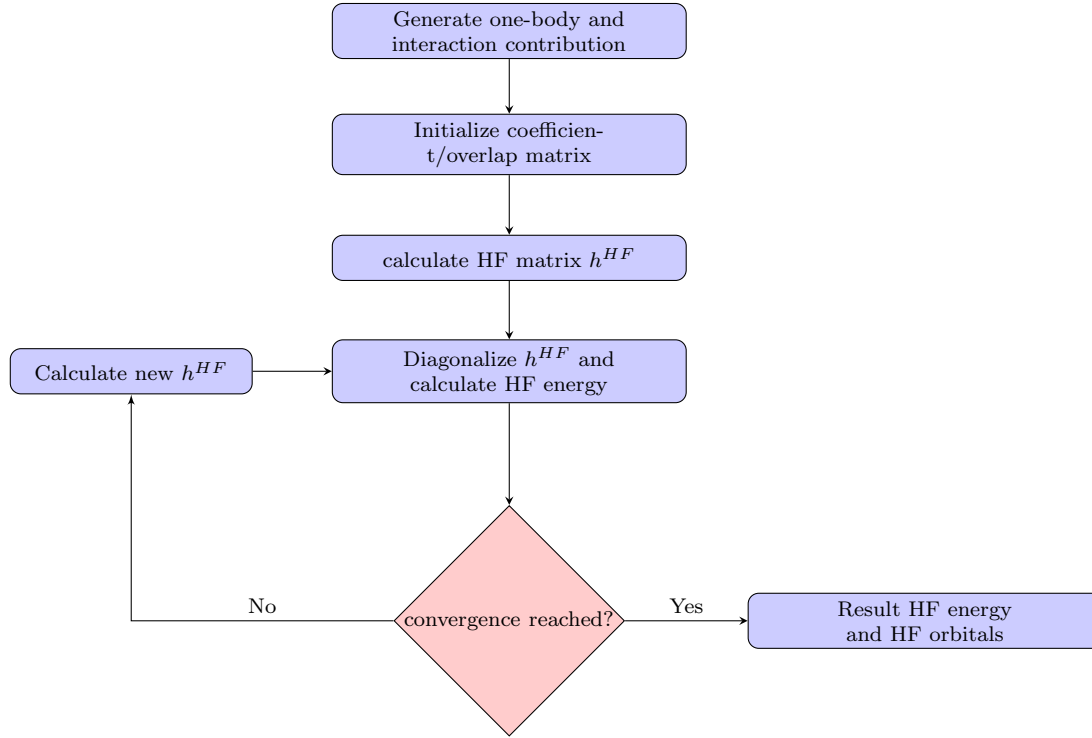
In this section we introduce the implementation of the Restricted Hartree-Fock method (RHF) for the two-dimensional closed-shell parabolic quantum dot. RHF implies that all single-particle orbitals up to a certain level, usually given by the Fermi level, must be occupied. This means that pair of electrons will have an identical spatial wave function, while the spin part of the wave function distinguish them with spin-up and spin-down. Utilizing RHF, we study the closed shell quantum dot, which means that the shell structure of the quantum dot described in chapter 3, is filled in our calculations. We start by introducing the algorithm and the code developed in this thesis, and follow up with some considerations on the validity of the code. Note that hereafter RHF is replaced by HF.

6.1.1 Code Structure and Algorithm

The implementations of the HF method follows the discussion of chapter 4. The HF orbitals, see eq. (4.7), are linear combinations of single-particle basis functions. In our case this single-particle basis is given by the harmonic oscillator basis (HMO). By varying the coefficients in the linear expansion we minimize the energy expectation value given in eq. (4.10). This minimization is accomplished by solving the HF eq. (4.21) iteratively, and as a result we can determine an approximate ground state energy of the system. We can also determine the HF orbitals through the coefficients we used in minimizing the energy.

The HF algorithm is illustrated in the top of fig. 6.1, and described in more detail below the illustration, but in the same figure. We will review this algorithm in the following. In order to calculate the energy of the system, we need to define its Hamiltonian. The

¹The code development in this thesis is done in collaboration with Yang Min Wang



Hartree-Fock Algorithm

1. Calculate the one-body energy contribution $\langle \alpha | \hat{h} | \gamma \rangle$ and the interaction contribution $\langle \alpha \beta | \hat{v} | \gamma \delta \rangle$
2. Initialize the coefficient vectors $\{C_a\}$ constituting the coefficient matrix $C_{a\lambda}$. $a \in [1, 2, \dots, N]$, where N is the number of electrons and $\lambda \in \{\alpha\}$. The identity matrix $\mathbb{1}$ is a common choice, or in the case where $C_{a\lambda}$ is not square $C_k[k] = 1$.
3. while not converged:
 - 3a calculate HF-matrix (h^{HF} HF-Hamiltonian)
 - 3b By diagonalizing the HF-matrix, determine eigenvalues and eigenvectors.
 - 3c Select the N eigenvectors with the lowest eigenvalues, where N is the number of electrons in the system. Let these represent the coefficient vectors.
 - 3d Calculate the new HF energy
 - 3e Calculate the difference between the HF energy of current and previous iteration.
4. Result: HF energy and expansion coefficients.

Figure 6.1: Illustration and description of the HF algorithm

Hamiltonian of the two-dimensional parabolic quantum dot is given in eq. (3.103). The HF calculation requires knowledge of the systems single-particle matrix elements (hereafter sp-

elements) and the two-particle interaction matrix elements (hereafter tp-elements) given respectively:

$$sp : \quad \langle \alpha | \hat{h} | \gamma \rangle, \quad (6.1)$$

$$tp : \quad \langle \alpha \beta | \hat{v} | \gamma \delta \rangle, \quad (6.2)$$

where the set $\{\alpha\}$ of quantum numbers refers to the single-particle basis in which the HF-orbitals are expanded. From the Hamiltonian in eq. (3.103) we have that the single-particle Hamiltonian \hat{h} is given by the sum of kinetic energy and the harmonic oscillator potential, while the interaction is given by the Coulomb interaction.

In the HF code developed in this thesis, the sp-elements are calculated given the information of how many shell one wishes to initialize in the calculation. The shell encountered here corresponds to the shell structure of the quantum dot in chapter 3. Therefore, an important input parameter to our code is the so-called shells R . This quantity defines, for a quantum dot, the total number of single-particle states by the formula

$$R \cdot (R + 1). \quad (6.3)$$

Comparing this formula with the content of table 3.1, we observe that it is correct. Higher shell numbers yields more single-particle basis functions. More basis functions leads to more exact calculations. Ideally the number of basis functions should be infinite, however in computing this is not possible. Therefore truncation is necessary, but does not prevent us from obtaining converged results. The quantum numbers $\{\alpha\}$ in eqs. (6.1) and (6.2) are results of the mapping

$$|n, m, m_s\rangle \rightarrow |\alpha\rangle, \quad (6.4)$$

where n is the quantum number originating from the associated Laguerre Polynomials in eq. (3.49), m is the angular quantum number and m_s is the spin quantum number. The mapping is shown explicitly for a selected number of shells in table 6.1. By studying this table and the shell structure illustrated in table 3.1 one observes a pattern to which the mapping scheme is performed. We developed an algorithm for this mapping shown in listing 6.1. In this mapping-algorithm we create three vectors containing the quantum numbers n , m and m_s , where the indices of each vector represents the quantum numbers $\{\alpha\}$. In addition we create an energy-vector which collects the energy of each quantum number in $\{\alpha\}$. In our case we assume that no magnetic field is present, thus the energy is given by eq. (3.57). When the number of single-particle orbitals are known, and the mapping of the basis functions is performed, we have in fact calculated the sp-elements of eq. (6.1). The harmonic oscillator basis is orthonormal, thus

$$\langle \alpha | \hat{h} | \gamma \rangle = \epsilon_\alpha \delta_{\alpha\gamma}. \quad (6.5)$$

The energy vector created in the mapping algorithm therefore contains these sp-elements ϵ_α . Perhaps for large systems, reading these sp-elements from file would be faster, but the mapping is essential because it initialize the harmonic oscillator basis, which is of great use later in both the HF- and the CCSD- calculations.

```
//mapping algorithm |n,m,m_s> —> |alpha>
number_basis = shellnumb*(shellnumb+1);
```

α	n	m	m_s	α	n	m	m_s	α	n	m	m_s	α	n	m	m_s	α	n	m	m_s
0	0	0	-1	10	1	0	-1	20	0	-4	-1	30	0	-5	-1	40	2	1	-1
1	0	0	1	11	1	0	1	21	0	-4	1	31	0	-5	1	41	2	1	-1
2	0	-1	-1	12	0	-3	-1	22	0	4	-1	32	0	5	-1				
3	0	-1	1	13	0	-3	1	23	0	4	1	33	0	5	1				
4	0	1	-1	14	0	3	-1	24	1	-2	-1	34	1	-3	-1				
5	0	1	1	15	0	3	1	25	1	-2	1	35	1	-3	1				
6	0	-2	-1	16	1	-1	-1	26	1	2	-1	36	1	3	-1				
7	0	-2	1	17	1	-1	1	27	1	2	1	37	1	3	1				
8	0	2	-1	18	1	1	-1	28	2	0	-1	38	2	-1	-1				
9	0	2	1	19	1	1	1	29	2	0	1	39	2	-1	1				

Table 6.1: mapping overview of the harmonic oscillator basis for 6 shells. The mapping is between quantum numbers $\{\alpha\}$ and the three quantum numbers n , m , and m_s , which occur in the solution of eqs. (3.42) and (3.43). Allowed values are given by $n = 0, 1, 2, \dots$, $m = 0, \pm 1, \pm 2, \dots$ and $m_s = \pm \frac{1}{2}$. Note that in the table we have replaced $m_s = \pm \frac{1}{2}$ with $m_s = \pm 1$ for simplicity. See fig. 3.1 for an illustration of the shell structure and the basis functions.

```

n=new int [ number_basis ];      m=new int [ number_basis ];
ms=new double [ number_basis ];  energy=new int [ number_basis ];

int org=0;
for (int i=1; i<=shellnumb; i++){
  for (int j=(-i+1); j<=0; j+=2){
    if (j!=0){
      m[org] = m[org+1] = j;
      m[org+2] = m[org+3] = -j;
      n[org] = n[org+1] = n[org+2] = n[org+3]=int ((i-abs(m[org]))-1)*0.5);
      ms[org]= ms[org+2] = -0.5;
      ms[org+1]= ms[org+3] = 0.5;
      energy[org]=energy[org+1]=energy[org+2]=energy[org+3]=i;
      org+=4;
    }
    else{
      m[org] = m[org+1] = j;
      n[org] = n[org+1] = int ((i-abs(m[org]))-1)*0.5);
      ms[org]= -0.5;
      ms[org+1]= 0.5;
      energy[org]=energy[org+1]=i;
      org+=2;
    }
  }
}

```

Listing 6.1: Algorithm performing the mapping $|n, m, m_s\rangle \rightarrow |\alpha\rangle$. This algorithm is present in both the HF-code and the CCSD-code.

The tp-elements in eq. (6.2) must be provided as an input file in binary format with the structure

$$\alpha \quad \beta \quad \gamma \quad \delta \quad \langle \alpha\beta | \hat{v} | \gamma\delta \rangle. \quad (6.6)$$

Note that the quantum numbers are given in *short int* precision, while the matrix element is given in *double precision*. The reason for choosing short int was to save space in memory.

Given the fact that in this thesis we encounter at most 20 shells, corresponding to 420 basis functions, the precision of short int is sufficient for holding the quantum numbers. We produce the tp-file with a code² developed by Simen Kvaal [41]. The tp-elements are stored efficiently by using the symmetry properties of the antisymmetrized matrix elements given by

$$\langle\alpha\beta|\hat{v}|\gamma\delta\rangle = -\langle\beta\alpha|\hat{v}|\gamma\delta\rangle = -\langle\alpha\beta|\hat{v}|\delta\gamma\rangle = \langle\beta\alpha|\hat{v}|\delta\gamma\rangle. \quad (6.7)$$

S. Kvaal's code produces all non-zero antisymmetric tp-elements for a given shell number, frequency, and some additional options. Some of this options allow us to the bare or a renormalized Coulomb interaction. These interactions are reviewed in detail in chapter 7. The following discussion applies to both of them. Many of the tp-elements are zero because of the properties of the Coulomb interaction, which is spherically symmetric and does not depend on spin. These properties leads to the following condition on the tp-elements $\langle\alpha\beta|\hat{v}|\gamma\delta\rangle$. If we define M and M_s as below

$$M = m_\alpha + m_\beta, \quad (6.8)$$

$$M_s = m_{s\alpha} + m_{s\beta}, \quad (6.9)$$

we can express the tp-elements in terms of M and M_s :

$$\langle M, M_s | \hat{v} | M', M'_s \rangle. \quad (6.10)$$

The elements are different from zero only when

$$M = M' \quad \text{and} \quad M_s = M'_s. \quad (6.11)$$

This is because the coulomb interaction affects neither of these quantum numbers, thus the interaction cannot change these quantum numbers in the transition from the right quantum state to the left quantum state in tp-elements. The fact that the quantum numbers M and M_s must be conserved in the tp-element, give rise to a mapping from two quantum numbers to one quantum number, viz.

$$|\alpha\beta\rangle \rightarrow |q\rangle, \quad (6.12)$$

which results in a two-dimensional matrix $\langle q_1 | \hat{v} | q_2 \rangle$ and, what we call, a two-particle basis, instead of a four-dimensional matrix $\langle\alpha\beta|\hat{v}|\gamma\delta\rangle$ and a single-particle basis. By carrying out this transformation from a single-particle basis to a two-particle basis, we avoid storing all the zero matrix elements. The mapping is carried through by assigning each set of (M, M_s) -values a number λ , and for each λ tabulate all pairs of quantum numbers $\alpha\beta$ producing that same λ -value. This tabulation is done in a two-dimensional matrix, where λ represents the rows, and the corresponding pairs of quantum numbers are stored along this row, taking up two elements for each pair. See the algorithm for this mapping of a two-particle basis explicitly in listing 6.2.

This algorithm of the two-particle basis map needs some explanation: First we establish how many λ -values we have, given a shell number. This value is calculated from the

²Originally this code was not intended to produce binary files, but we have altered it to do so. We have also altered the program to return only one fourth of the tp-elements in order to save space in memory. This is possible because of the symmetry properties of the antisymmetrized matrix elements.

knowledge of the maximal M -value (M_{max}). By studying fig. 3.1 and table 3.1 we obtain the formula for calculating the maximal M -value for two particles:

$$M_{max} = 2 \cdot (R - 1). \quad (6.13)$$

We have that

$$M = 0, \pm 1, \pm 2, \dots, \pm M_{max}, \quad (6.14)$$

$$M_S = -1, 0, 1, \quad (6.15)$$

which leads to the number of λ -values given by

$$\lambda_dim = 2 * M_{max} * 3 + 3. \quad (6.16)$$

Note that in all code-examples λ is exchanged by *alpha*, which is not to be confused with the quantum number α . When these shell-dependent variables are established, we loop over all possible pairs of (M, M_S) and gather information about the number of new basis functions (pair of quantum numbers) which produce interaction contributions. Each pair with the same (M, M_S) -values as the loop indices are counted as one basis function. We do not store the quantum numbers initially, we only count the pairs. On the background of this counting we allocate the matrix *config* with a number of λ rows, and the number of columns equal the number of two-particle basis functions times two. Thereafter we loop over all possible pairs of (M, M_S) -values once more, always starting with the lowest value of bot M and M_S , and for each λ set we store all corresponding pairs of quantum numbers sequential with lowest quantum number first. When the two-particle basis is in order, we are ready to collect the tp-elements from file. The way we do this is by creating a dictionary. This dictionary stores the quantum numbers as key and the interaction contribution as key-value, when we loop through the file units $[\alpha \ \beta \ \gamma \ \delta \ \langle \alpha\beta | \hat{v} | \gamma\delta \rangle]$, See listing 6.3 for details. Note that the filename of the file we wish to read, must be provided as input to our code. Further, we allocate the three-dimensional matrix *coulomb*, for holding the interaction contributions. This matrix is three-dimensional because for each λ -value we must pair all the corresponding two-particle basis functions q , creating the contributing matrix elements $\langle q_\lambda | \hat{v} | q'_\lambda \rangle$. The interaction matrix is filled by looping over all λ -values, and by the use of the two-particle basis stored in the mapping matrix (*config*), it determines the quantum numbers of the contributing matrix elements. These quantum numbers are then used to search through the dictionary, and fetch the interaction elements. See listing 6.3 for illustration.

```

/* algorithm for creating a two-particle basis*/

/*initializing shell-dependent variables;
   Mmax=m1_max+m2_max, alphadim = #(M,Ms)-values;*/
number_basis = shellnumb*(shellnumb+1);
int Mmax=(shellnumb-1)*2;
int alphadim=2*Mmax*3+3;
/*allocating vector for counting # of two-particle basis functions
   for each alpha(M,MS) set*/
int *basiscount
basiscount = new int [alphadim];
//Filling basiscount
alpha=0;
for (int l=-Mmax; l<=Mmax; l++){
    Mvalue=l;
    for (MSvalue=-1; MSvalue<=1; MSvalue++){
        bsize=0;
        for (int i=0; i<number_basis-1;i++){
            for (int j=i+1; j<number_basis;j++){
                M = m[i]+m[j];
                MS = ms[i]+ms[j];
                if (M==Mvalue && MS==MSvalue){
                    bsize += 1;
                }
            }
        }
        basiscount [alpha]=bsize*2;
        alpha+=1;
    }
}
/*allocating config-matrix[alpha,basis-pairs]
   for tabulating all two-particle basis pairs */
config=new int *[alphadim];
for (int i=0; i<alphadim; i++)
    config[i]=new int [basiscount[i]];
//loop over M and MS values determining the 2particle basis
alpha=0;
for (int l=-Mmax; l<=Mmax; l++){
    Mvalue=l;
    for (MSvalue=-1; MSvalue<=1; MSvalue++){
        bsize=0;
        for (int i=0; i<number_basis-1;i++){
            for (int j=i+1; j<number_basis;j++){
                M = m[i]+m[j];
                MS = ms[i]+ms[j];
                if (M==Mvalue && MS==MSvalue){
                    config [alpha] [ bsize]=i;
                    config [alpha] [ bsize+1]=j;
                    bsize += 2;
                }
            }
        }
        alpha+=1;
    }
}
}

```

Listing 6.2: Mapping of a two-particle basis. See text for a detailed explanation.

```

//allocating interaction-dictionary for reading interaction elements
typedef map<string , double> MapType;
MapType v_dictionary;
MapType::iterator search_value;
char *key = new char[10];
char *qn_search = new char[10];

//prepare reading from binary-file
char* filename = argv[3];
short int q, r ,s,t;
double value;
struct stat filestat;
stat(filename,&filestat);
int fileunits = filestat.st_size/(sizeof(double)+4*sizeof(short int));
ifstream infile;
infile.open(filename , ios::in | ios::binary);
//reading from binary-file , and filling the dictionary
for(int i=0; i<fileunits; i++){
    infile.read((char*)&q, sizeof(short int));
    infile.read((char*)&r, sizeof(short int));
    infile.read((char*)&s, sizeof(short int));
    infile.read((char*)&t, sizeof(short int));
    infile.read((char*)&value, sizeof(double));
    sprintf(key, "%d %d %d %d", q, r, s, t);
    v_dictionary.insert(MapType::value_type(key, value));
}
infile.close();

//allocating coulomb[alpha][b1][b2]
coulomb=new double**[alphadim];
for(int i=0; i<alphadim; i++){
    coulomb[i]=new double*[basiscount[i]/2];
    for(int j=0;j<basiscount[i]/2; j++){
        coulomb[i][j]=new double[basiscount[i]/2];
    }
}
//initializing coulomb[alpha][b1][b2]
for(int i=0; i<alphadim; i++){
    map1=0;
    for(int j=0;j<basiscount[i]; j+=2){
        map2=0;
        for(int k=0;k<basiscount[i]; k+=2){
            sprintf(qn_search , "%d %d %d %d", config[i][j], config[i][j+1],
                config[i][k], config[i][k+1]);
            search_value = v_dictionary.find(qn_search);
            coulomb[i][map1][map2]=search_value->second;
            map2+=1;
        }
        map1+=1;
    }
}
}

```

Listing 6.3: Code-snippet illustrating the reading of tp-elements from file.

These code-snippets reviewed above completes the first step in the HF algorithm, see fig. 6.1. To summarize, our HF code needs as input parameters the number of shells (R), the number of electrons which defines the Fermi level, and the name of the file that contains the two-body interaction elements. The next step in the algorithm is to initialize the coefficient matrix $C_{a\gamma}$. This matrix has N rows, where N is the number of electrons, and each row represents the eigenvector in the HF eq. (4.21) corresponding to particle k . Thus, the HF matrix given by eq. (4.20) reads:

$$h^{HF} = \begin{pmatrix} h_{11} & h_{12} & h_{13} & \dots & h_{1n} \\ h_{21} & h_{22} & h_{23} & \dots & h_{2n} \\ \vdots & \vdots & \vdots & \ddots & \vdots \\ h_{n1} & h_{n2} & h_{n3} & \dots & h_{nn} \end{pmatrix}, \quad (6.17)$$

where n is the number of single-particle basis functions. The orbital of electron k have an coefficient vector C_k , equivalent to the row $C_{k\gamma}$, which contains the expansion coefficients, viz.

$$C_k = \begin{pmatrix} C_{k1} \\ C_{k2} \\ C_{k3} \\ \dots \\ C_{kn} \end{pmatrix}. \quad (6.18)$$

The HF equation for orbital k then reads

$$h^{HF} C_k = \omega_k C_k, \quad (6.19)$$

where ω_k is the eigenvalue of the eigenvector C_k . From eq. (4.20) we have that the HF matrix depends on all the coefficient vectors, resulting in an iterative solution of the HF eq. (4.21). This iterative process of solving the HF problem is described in step three of the HF algorithm in fig. 6.1. The coefficient matrix is set equal to the identity matrix $\mathbb{1}$ in the first iteration, see listing 6.4. Listing 6.5 presents a code-snippet of the iteration process. The diagonalizing functions tqli and tred2 are modified versions of corresponding functions in [42], written by my supervisor Morten Hjorth-Jensen. In the calculation of the HF matrix, note that the loop over the two-particle basis saves both space in memory in addition to time, since we only tabulate contributing interaction elements. Also note that for each contributing element, we have to permute the indices because of the simplification we made by using the symmetry properties of the antisymmetrized matrix elements in eq. (6.7). The HF energy is calculated from the eq. (4.10).

```
//z=number of electrons
double **C;
C = new double*[z];
for(int i=0; i<z; i++){
    C[i]=new double[number_basis];
    for(int j=0; j<number_basis; j++){
        C[i][j]=0.0;
    }
}
for(int i=0; i<z; i++)
    C[i][i]=1;
```

Listing 6.4: Implementation of the coefficient matrix

```

while(check){
    iter++;
    //calculating HF matrix (hHF)
    for(alpha=0; alpha<number_basis; alpha++){
        for(gamma=0; gamma<number_basis; gamma++){
            if(alpha==gamma)
                hHF[alpha][alpha] = energy[alpha];
            else
                hHF[alpha][gamma] = 0;
        }
    }
    for(int a=0; a<z; a++){
        for(int i=0; i<alphadim; i++){
            map1=0;
            for(int j=0; j<basiscount[i]; j+=2){
                alpha=config[i][j];
                beta=config[i][j+1];
                map2=0;
                for(int k=0; k<basiscount[i]; k+=2){
                    gamma=config[i][k];
                    delta=config[i][k+1];
                    hHF[alpha][gamma] += C[a][beta]*C[a][delta]
                                         *coulomb[i][map1][map2];
                    hHF[beta][gamma] -= C[a][alpha]*C[a][delta]
                                         *coulomb[i][map1][map2];
                    hHF[alpha][delta] -= C[a][beta]*C[a][gamma]
                                         *coulomb[i][map1][map2];
                    hHF[beta][delta] += C[a][alpha]*C[a][gamma]
                                         *coulomb[i][map1][map2];

                    map2+=1;
                }
                map1+=1;
            }
        }
    }
    //solving eigenvalue problem-> diagonalizing
    tred2(hHF,number_basis,d,e);
    tqli(d,e,number_basis,hHF);
    //Selecting eigenvectors with lowest eigenvalues
    sort(hHF,d,number_basis);
    //updating eigenvectors/coefficient-matrix C
    for(int i=0; i<z; i++){
        for(int j=0; j<number_basis; j++){
            C[i][j] = hHF[j][i];
        }
    }
    //energy check
    E_new = HFenergy(C,energy);
    if(abs(E_new-E_old)<1e-6)
        check=false;
    E_old=E_new;
} //end while

```

Listing 6.5: The implemented iterative process of the HF algorithm.

6.1.2 Code Validation

In order to validate the HF code, one test is to check if the code reproduces the non-interacting energy of the system. By summing up the energy of each orbital corresponding to the shell number, see illustration in table 3.1, we have that $N = 2, 6, 12, 20$ will respectively give an energy of $2\hbar\omega$, $10\hbar\omega$, $28\hbar\omega$, and $60\hbar\omega$. Our HF code reproduces these results. In addition the code reproduces the HF results of [2] and [43], which is another indication that the code is valid.

6.2 CCSD Implementation

In this section we present the implementation of the Coupled Cluster Singles and Doubles method (CCSD), followed up by a validation of the code. The CCSD code utilized in this thesis was originally written by Magnus Pedersen Lohne in collaboration with Morten Hjorth-Jensen and Gustav Jansen [2]. During our thesis-period we have been working on modifying M.P.Lohne's code, in order to obtain speed-up in the calculations of the two-dimensional parabolic quantum dot. The speed-up was necessary in order to expand the range in which the calculations was possible. Originally the program was able to handle 12 electrons with 10 shells (110 basis functions) in approximately 35 hours. The modified code does this calculation in 4 minutes and thirty seconds. This corresponds to a speed-up factor of 500

The code is a generalized m-scheme code, specialized for the calculation of the two-dimensional parabolic quantum dot. However, the code may in our opinion be applied to other electronic systems, with only a few modifications. The program handles only closed-shell systems, meaning that calculations can be made for the two-dimensional parabolic quantum dot with 2, 6, 12, 20, 30, 42, ... particles. These electron numbers are often referred to as the magic numbers. Currently the cluster operator \hat{T} , in the CC-wave function, acts on the ground state of the non-interacting system, represented by one single Slater determinant. The non-interacting ground state of an open-shell system is represented by a linear combination of Slater determinants. If the program was to calculate open-shell systems, the reference state must include a linear combination of Slater determinants. Altogether, the program calculates an approximation to the ground state energy, in addition to the excitation amplitudes \hat{t}_i^a and \hat{t}_{ij}^{ab} , which determines the CC wave function.

6.2.1 Code Structure and Algorithm

M. P. Lohne wrote his CCSD code using an object-orientated style. His reasoning for this was:

An object oriented programming style offers an amazing opportunity to structure the code in parts that are "independent". Such a programming style also enables us to generalize parts of the code that are identical for many systems. Moreover, when the original system changes the structure often require modifications at well-defined places.

The program is structured into classes, with base classes and derived classes. This offers the opportunity to divide parts of the code that are specified by

the system, and the parts that are identical for every system, into different fragments. ... This is the beauty of object-oriented computing.

We most definitely agree with this reasoning. The object-oriented style made it easy for us to implement changes by simply creating new classes, in addition to make changes to the classes already existing. One significant difference between M. P. Lohne's code and our code, is that Lohne uses the BLITZ++ library. We have removed the BLITZ++ implementation, and this resulted in a significant speed-up of our code. In addition, parts of our code are parallelized, and we use efficient LAPACK libraries. We proceed this section by first presenting the CCSD algorithm, and then we document how it is implemented in five classes.

Figure 6.2 illustrates the CCSD algorithm implemented in this thesis. The first step is referred to as setting the modelspace. The single-particle model space is given by the selected basis. The dimension of this basis, meaning the number of basis functions n_b reads

$$n_b = n_p + n_h, \quad (6.20)$$

where n_p is the number of particle states, i.e. unoccupied single-particle orbitals, and n_h is the number of hole states, i.e. occupied single-particle orbitals. The second step in the CCSD algorithm calculates the interaction elements $\langle pq|\hat{v}|rs\rangle$, and the f_p^q -elements defined in eq. (5.38). When this elements are determined, we are ready to perform the calculations. In step three and four of the algorithm, we calculate the reference energy $E_{ref} = \langle \Phi_0|\hat{H}|\Phi_0\rangle$, given in eq. (5.37), and we initialize the amplitudes and the energy variables. The amplitudes and E_{old} are initialized to zero, while E_{new} is set equal to E_{ref} . We then perform an iterative process of calculations until the difference between E_{new} and E_{old} is within a given tolerance limit, thus convergence is reached. This iterative process consists of calculating the intermediates, the amplitudes and the energy in the given order. The expressions of the intermediates and the amplitudes are derived from the \hat{T}_1 and \hat{T}_2 amplitude eqs. (5.139) and (5.141). These derived expressions are given explicitly further down in this section. When the amplitudes are determined, the energy E_{new} is calculated from the expression given in eq. (5.135). Finally, the energy difference between the current and the previous iteration is calculated in order to determine if convergence is reached. If the result is not converged, the current energy is saved in the E_{old} variable, and the iterative process continues.

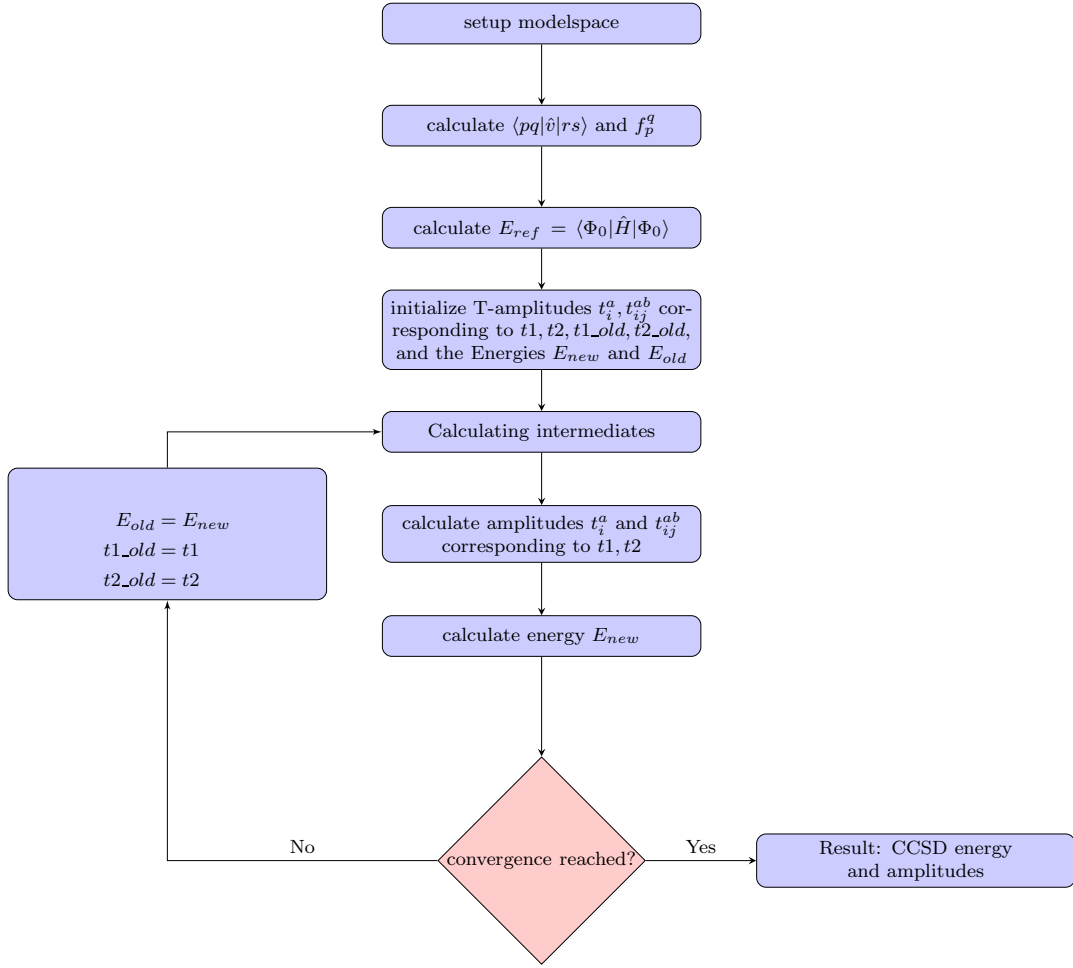


Figure 6.2: The CCSD algorithm - for detailed description, see the text above this figure.

The various stages of the CCSD algorithm are performed by five classes:

- **CCalgo:** CCSD algorithm class managing the algorithm.
- **Amplitudes:** Class for calculating the amplitudes t_i^a and t_{ij}^{ab} .
- **Fmatrix:** Class for calculating the F-matrix in eq. (5.38).
- **Interaction:** Class for providing the interaction elements $\langle pq|\hat{v}|rs\rangle$.
- **Basisconfig:** Class specialized for the two-dimensional parabolic quantum dot. This class sets up a two-particle basis divided in three types: $|pp\rangle$, $|hh\rangle$ and $|ph\rangle$, where p denotes the unoccupied particle orbitals, and h denotes the occupied hole orbitals. This new basis gives rise to simplifications.

The first four classes were created by M.P.Lohne. They are implemented as abstract base classes, meaning that the class operates only as a parent class from which child classes are derived. Their derived child classes are given respectively:

- **ccsd1:** Implementation of the CCSD algorithm.

- **amp1**: Implementation of the amplitude equations.
- **f1**: Tabulation of $\langle p|\hat{h}|q\rangle$, and calculation and tabulation of the F-matrix.
- **int1**: Tabulation of the interaction elements $\langle pq|\hat{v}|rs\rangle$.

In main.cpp these classes are initialized. In order to set up the model space, main.cpp needs n_p and n_h as input variables. This defines the number of holes n_h , and the number of particles n_p . However, the basis itself is determined by the sp-elements $\langle p|\hat{h}|q\rangle$ and the tp-elements $\langle pq|\hat{v}|rs\rangle$. The sp and tp elements are provided by files given as input to main.cpp. The tp-elements are provided in binary files, created with the same program and structure as for the HF code eq. (6.6). The sp-elements are provided in ordinary text files with the structure:

$$p \quad q \quad \langle p|\hat{h}|q\rangle. \quad (6.21)$$

Since our selected harmonic oscillator basis is orthonormal, this file contains only elements given by:

$$p \quad p \quad \langle p|\hat{h}|p\rangle. \quad (6.22)$$

To sum up, the main.cpp code needs as input parameters, the files which contains the sp and tp elements, but also a number of maximum iterations to perform, and a tolerance which determines when convergence is reached. The main features of main.cpp are rendered in listing 6.6. This listing illustrates the order in which the classes are required to be initiated, according to how they depend on each other. We now present the classes one by one in the order presented in main.cpp.

```
//main.cpp
int main(int argc, char* argv[]){
    int nh, np, max_iter;
    double tol;
    char* sp-energy_file; char* tp-energy_file;

    nh = atoi(argv[1]);
    np = atoi(argv[2]);
    max_iter = atoi(argv[3]);
    tol = atof(argv[4]);
    sp-energy_file = argv[5];
    tp-energy_file = argv[6];

    /* Basisconfig object */
    Basisconfig* B = new Basisconfig(nh,np);

    /* interaction object */
    Interaction* V = new int1(nh, np, B);
    // read interaction energy elements
    V->read_interaction(tp-energy_file);

    /* f-matrix object */
    Fmatrix* F = new f1(nh, np, B);
    // read single-particle energy elements
    F->read_sp-energy(sp-energy_file);
    // set up f-matrix
    F->set_up_fmatrix(V);
```

```

/* amplitude object */
Amplitudes* T = new Amplitudes(nh, np, B, F, V, write3, write4);

/* CCSD algorithm object */
CCalgo* simulator = new ccsd1(nh, np, max_iter, tol, B, F, V, T,
                               writel, write2);

//// — START SIMULATION — ////
simulator->ccsd_uncoupled_start();
}

```

Listing 6.6: central features of main.cpp. The classes and variables in this code are described in the text, except for the variables `write`. These four variables are irrelevant to the algorithm, they only decide practical questions regarding out-print of energy and amplitudes to file.

Basisconfig: CLASS implementation

The *Basisconfig* class tabulates the two-particle basis given by the map in eq. (6.12), which implements the restriction introduced in eq. (6.11). The class has no class-functions, all the necessary calculations are executed in the class constructor. The purpose of introducing a two-particle basis, is the advantages it brings when only pairs of quantum numbers producing non-zero matrix elements $\langle pq|\hat{v}|rs\rangle$ are tabulated. This practice reduces a four-dimensional tp-element $\langle pq|\hat{v}|rs\rangle$ into a two-dimensional element $\langle x|\hat{v}|y\rangle$.

The constructor of *Basisconfig* takes the input parameters n_h and n_p . The number of single-particle basis orbitals n_b is calculated from eq. (6.20). From these three parameters the class determines the shell-number and the Fermi-shell-number, referred to as *stage one* of this class. The shell number equals the highest filled shell given the number of single-particle basis orbitals. The Fermi-shell equals the highest shell, which is filled by hole orbitals only. Remember, we consider only closed shell systems, thus the shells are always filled. Both shell numbers are determined by using a while-loop. We know that each spatial orbital is occupied by one spin-up and one spin-down electron. From fig. 3.1 we observe that each spatial orbital is represented by a horizontal line, and the number of spatial orbitals in each shell equals the shell number. We can therefore determine the total number of spatial orbitals given a number of single-particle orbitals, by dividing the number of single-particle orbitals by two, and using this number in the while loop. In each loop made by the while-statement, the shell number is incremented by one, and a level-variable accumulates the current shell-number, which equals the number of spatial orbitals inside that shell. When the size of the level-variable equals or exceeds the number of single-particle functions divided by two, the while-loop terminates and the correct shell number is contained in the shell-number-variable. In a similar manner we determine the Fermi-shell. See listing 6.7. In what we call *stage two* of *Basisconfig*, we tabulate the single-particle basis, corresponding to the map described in eq. (6.4). This map is shown explicitly for a selected number of single-particle functions in table 6.1. The algorithm can be observed in listing 6.1, and is therefore not repeated in listing 6.7.

```

Basisconfig::Basisconfig(int nh, int np)
{
    num_sfunc=nh+np;
    //determine shellnumb
    shellnumb=0; level=0;
    while(level<(num_sfunc/2)){
        shellnumb+=1;
        level+=shellnumb;
    }
    //determine fermishell
    fermishell=0; level=0;
    while(level<(nh/2)){
        fermishell+=1;
        level += fermishell;
    }
    /* --calculating single-particle basis-- */
}

```

Listing 6.7: Stage one and two of the Basisconfig class. See text for explanation

When the single-particle basis is determined, one can proceed to what we call *stage three* of the *Basisconfig* class. *Stage three* tabulates the two-particle basis of eq. (6.12). The class tabulates the whole two-particle basis in a two-dimensional matrix *totbasis*, which is equivalent to the implementation in the HF calculations listing 6.2. However, we also create three two-dimensional matrices. Each of these three matrices contain different parts of the whole two-particle basis, corresponding to either of the pairs $|pp\rangle$, $|hh\rangle$, and $|ph\rangle$. The unoccupied particle orbitals are denoted p , and h denotes the occupied hole orbitals. The reason for this partitioning will become evident when we present the implementation of the *Interaction* and the *Amplitudes* class. Implementation of the $|ph\rangle$ -basis is illustrated in listing 6.8. The implementations of the $|pp\rangle$ and the $|hh\rangle$ basis is similar to the implementation of the $|ph\rangle$ -basis, only small changes in the loop over i and j distinguish them. The algorithm for finding the two-particle basis $|ph\rangle$ is almost identical to the algorithm for finding the whole two-particle basis in the HF calculations (listing 6.2). First we loop over the set of all (M, M_S) -values. For each value we count all pair of orbitals satisfying these (M, M_S) -values, and store the number in a vector $ph_bc[\lambda]$. Remember that in the code, λ is denoted by alpha. For the $|ph\rangle$ and the $|hh\rangle$ basis we also collect the information of the lowest and the highest λ -values containing pair of orbitals, see *alphamin* and *alphamax* respectively. This is due to the fact that for these two basis types the λ -values where contributing pairs of orbitals occur, are limited to a smaller interval. By collecting these limits we are able to loop more effectively through these two-dimensional basis-matrices later. One can convince oneself of these limited intervals of λ -values by studying the shell system illustrated in fig. 3.1, with respect to the number of holes and particles. Next we allocate the two-dimensional matrix *ph-basis* based on the collected knowledge of size stored in $ph_bc[\lambda]$. We fill the matrix by looping through all λ -values. For each λ we loop through all pairs of particle-hole orbitals (i and j loop), and store the pairs that satisfy λ . This summarizes the action of the *Basisconfig* class. The basis systems tabulated in this class constitutes the foundation for optimizing the CCSD equations with respect to the two-dimensional parabolic quantum dot.

```

Basisconfig::Basisconfig(int nh, int np)
{
    /* determining 2particle basis; |ph> */
    Mmax=(shellnumb-1)*2;
    //vector for counting basis size for each ph_alpha(M,MS) set
    ph_bc = new int[alphadim];
    //filling ph_bc (basiscount)
    counter=0; alpha=0;
    for(int l=-Mmax; l<=Mmax; l++){
        Mvalue=l;
        for( MSvalue=-1; MSvalue<=1; MSvalue++){
            bsize=0;
            for (int i=0; i<nh; i++){
                for(int j=nh; j<num_spfunc; j++){
                    M = m[i]+m[j];
                    MS = ms[i]+ms[j];
                    if(M==Mvalue && MS==MSvalue){
                        if(counter==0)
                            ph_alphamin=alpha;
                        bsize += 1;
                        ph_alphamax=alpha;
                        counter+=1;
                    }
                }
            }
            ph_bc[alpha]=2*bsize;
            alpha+=1;
        }
    }
    //allocating phbasis[alpha,basis-pair], tabulating 2particle basis-pairs
    phbasis = new int*[alphadim];
    for(int i=0; i<alphadim; i++){
        phbasis[i] = new int[ph_bc[i]];
        for(int j=0; j<ph_bc[i]; j++)
            phbasis[i][j]=0;
    }
    alpha=0;
    for(int l=-Mmax; l<=Mmax; l++){
        Mvalue=l;
        for( MSvalue=-1; MSvalue<=1; MSvalue++){
            bsize=0;
            for(int i=0; i<nh; i++){
                for(int j=nh; j<num_spfunc; j++){
                    M = m[i]+m[j];
                    MS = ms[i]+ms[j];
                    if(M==Mvalue && MS==MSvalue){
                        phbasis[alpha][bsize] = j-nh;
                        phbasis[alpha][bsize+1] = i;
                        bsize += 2;
                    }
                }
            }
        }
        alpha+=1;
    }
}

```

```

} /* determining 2particle basis; |pp> and |hh> */

```

Listing 6.8: Stage three of the Basisconfig class. See text above for explanation.

Interaction: CLASS implementation

Interaction is an abstract base class with one derived class, *int1*. This class handles the interaction matrix elements $\langle pq|\hat{v}|rs\rangle$, hereafter tp-elements. The tp-elements are provided by a binary file, which is read and tabulated in the *int1*-class function *read_interaction*. The task of this class is to read these elements from file, and store them in one of the six matrices **hhhh**, **phhh**, **pphh**, **phph**, **ppph** and **pppp**. As usual *p* denotes the unoccupied particle orbital, and *h* denotes the occupied hole orbital. The position of *h* and *p* reflects the corresponding position in the tp-element, viz.

$$\begin{aligned}
\mathbf{hhhh} &= \langle ij|\hat{v}|kl\rangle, \\
\mathbf{phhh} &= \langle aj|\hat{v}|kl\rangle, \\
\mathbf{pphh} &= \langle ab|\hat{v}|kl\rangle, \\
\mathbf{phph} &= \langle aj|\hat{v}|cl\rangle, \\
\mathbf{ppph} &= \langle ab|\hat{v}|cl\rangle, \\
\mathbf{pppp} &= \langle ab|\hat{v}|cd\rangle,
\end{aligned} \tag{6.23}$$

where *abc...* denote particle orbitals, and *ijk...* denote hole orbitals. This choice of structure is possible because of the symmetry properties of the antisymmetrized matrix element, viz

$$\langle pq|\hat{v}|rs\rangle = \langle qp|\hat{v}|sr\rangle = \langle rs|\hat{v}|pq\rangle = -\langle qp|\hat{v}|rs\rangle = -\langle pq|\hat{v}|sr\rangle. \tag{6.24}$$

These properties result in the matrix relation:

$$\begin{aligned}
&\mathbf{hhhh} \\
&\mathbf{phhh} = -\mathbf{hphh} = -\mathbf{hhhp} = \mathbf{hhph} \\
&\mathbf{pphh} = \mathbf{hhpp} \\
&\mathbf{phph} = -\mathbf{hpph} = -\mathbf{phhp} = \mathbf{hphp} \\
&\mathbf{ppph} = -\mathbf{pphp} = -\mathbf{hppp} = \mathbf{phpp} \\
&\mathbf{pppp},
\end{aligned} \tag{6.25}$$

which produces all possible combinations, 2^4 to be exact. Thus by tabulating only the six matrices in eq. (6.23), we have sufficient information for reproducing the whole specter of tp-elements. However, note that in the CCSD code these symmetries need no consideration. This is due to the fact that we implement CCSD equations, which are manipulated such that only the chosen six combinations occur, see implementation of the *Amplitudes* class.

This strategy leads to a significant reduction of space in memory, which is of great importance when the system is increasing. However, this reduction alone is not sufficient, if the goal is to perform CCSD calculations for more than a maximum of 10 shells. M. P.

Lohne implemented these six matrices as four-dimensional, containing all possible combinations of holes and particles corresponding to the matrix-configurations in eq. (6.23). Thus, he obtained matrices with size given as

$$\begin{aligned}
 \mathbf{hhhh} &= n_h^4 \\
 \mathbf{phhh} &= n_h^3 \cdot n_p \\
 \mathbf{pphh} &= n_h^2 \cdot n_p^2 \\
 \mathbf{phph} &= n_h^2 \cdot n_p^2 \\
 \mathbf{ppph} &= n_h \cdot n_p^3 \\
 \mathbf{pppp} &= n_p^4,
 \end{aligned} \tag{6.26}$$

where n_h and n_p are the number of holes and particles respectively. As an example consider the system of two holes and ten shells. Ten shells corresponds to a number of 110 single-particle basis orbitals, which means that with $n_h = 2$ we obtain $n_p = 108$. Thus, **pppp** would consist of $108^4 = 136,048,896$ elements. Each element are of type double, which uses 8 bytes in memory. The **pppp** matrix, corresponding to the system of two holes and ten shells, therefore requires 1.01GB in memory. Most of our computers have four nodes, each with RAM-memory of 2GB, Thus, we have 8GB RAM at our disposal. However, larger systems will quickly exceed this RAM limitation. The fact that it is very time consuming to look up values in these large matrices also contributes to the failure of this CCSD-implementation when larger systems are considered.

These limitations of the described CCSD-implementation make the need for improvement evident. In our development of the CCSD-code, we have reduced the dimension of the six matrices from four to three. This is done by implementing the two-particle basis of eq. (6.12). The implementation of the two-particle basis reduces the four-dimensional tp-element to two-dimensional matrix elements. However, this reduction would also produce many redundant zero elements if not the third dimension is introduced. The third dimension accounts for the (M, M_S) -values in eqs. (6.8) and (6.9). Only pairs with equal (M, M_S) values contribute to the interaction. Therefore, for each value of (M, M_S) we tabulate the interaction matrix which gives only non-zero contributions. In this way no zero elements are stored in memory.

In order to create the six three-dimensional matrices, we utilize the *Basisconfig* class. In this class we tabulated three types of basis pairs, namely $|pp\rangle$, $|hh\rangle$ and $|ph\rangle$. These basis pairs are stored in three two-dimensional matrices, one dimension corresponding to the possible (M, M_S) -value, and the other dimension corresponding to the number of paired orbitals belonging to the (M, M_S) -value. From these three types of basis pairs we are able to create all the six types of interaction elements in eq. (6.23). By combining two and two basis-sets, one representing the bra and one representing the ket of the matrix element, we construct all the interaction matrices. Thus, by combining the *pp*-basis and the *hh*-basis we obtain elements belonging to the **pphh**-matrix, or elements belonging to the **phph**-matrix is obtained by combining the *ph*-basis with itself. The implementation of this is shown in listing 6.9. First we create a dictionary, in which we store the elements we read from the binary tp-file. This code is identical with the corresponding code in listing 6.3, and is therefore not repeated here. When the dictionary is filled with all the tp-elements, we proceed by placing these elements in the matrix where they belong. This is accomplished by looping through the six interaction matrices one by one, and for each

loop we search the dictionary for the particular element given by the quantum numbers of that loop. If it exists, the interaction element is stored in the matrix. Note that in our case it always exists due to our construction, with the exception that the allowed matrix element equals zero. In that case the tp-file does not contain the element, but our basis configuration will, and the element is interpreted as zero.

In listing 6.9 we give two examples of how we fill the interaction matrices of type $pppp = \langle p_1 p_2 | \hat{v} | p_3 p_4 \rangle$ and $ppph = \langle p_1 p_2 | \hat{v} | p_3 h_1 \rangle$. We loop through the former matrix by combining the pp -basis with itself. For each (M, M_S) -value (alpha) the first loop represents the bra-side, and the second loop represents the ket-side of the matrix element. These loops run over the elements in the basis-count-vector (bc), corresponding to one of the three basis-types of the *Basisconfig* class. In this case pp_bc constitutes both loops. For each loop-index we fetch the quantum numbers stored in the corresponding basis, and are able to determine the quantum numbers of the contributing matrix element. By combining the basis-pairs of the bra-loop and the ket-loop in all possible ways, we obtain all the contributing matrix elements. The $ppph$ matrix is filled in a similar manner by combining the pp -basis as the bra-side, and the ph -basis as the ket-side of the matrix element, see the details below.

```
void int1::read_interaction(char* filename){
    /* creating interaction-dictionary */
    /* reading from binary-file, and filling dictionary */

    // filling pppp[alpha][i][j]
    int map1, map2;
    for(int alpha=0; alpha<alphadim; alpha++){
        map1=0;
        for(int i=0; i<pp_bc[alpha]; i+=2){
            map2=0;
            for(int j=0; j<pp_bc[alpha]; j+=2){
                sprintf(qn_search, "%d %d %d %d",
                    B->ppbasis[alpha][i], B->ppbasis[alpha][i+1],
                    B->ppbasis[alpha][j], B->ppbasis[alpha][j+1]);
                search_value = v_dictionary.find(qn_search);
                pppp[alpha][map1][map2] = search_value->second;
                map2+=1;
            }
            map1+=1;
        }
    }
    // filling ppph[alpha][i][j]
    for(int alpha=0; alpha<alphadim; alpha++){
        map1=0;
        for(int i=0; i<pp_bc[alpha]; i+=2){
            map2=0;
            for(int j=0; j<ph_bc[alpha]; j+=2){
                sprintf(qn_search, "%d %d %d %d",
                    B->ppbasis[alpha][i]+nh, B->phbasis[alpha][i+1]+nh,
                    B->phbasis[alpha][j+1], B->phbasis[alpha][j]+nh);
                search_value = v_dictionary.find(qn_search);
                phph[alpha][map1][map2] = search_value->second;
                map2+=1;
            }
        }
    }
}
```

```

        map1+=1;
    }
}
//filling hhhh,phhh,phph,pphh

```

Listing 6.9: Code-snippet illustrating the structure of the Interaction class. See text for explanation.

Similar loops are implemented in order to fill the remaining four matrices, where the form of the matrix decide whether to use the information stored in the *pp*-basis, *hh*-basis, or *ph*-basis of the *Basisconfig* class. Note that the implementation of the four-dimensional interaction matrices used by M. P. Lohne requires that the particle quantum numbers are rescaled accordingly

$$n_p \in [n_h, \dots, n_b] \rightarrow n_p \in [0, \dots, (n_b - n_h)],$$

where n_b is the number of all the single-particle basis orbitals, and n_h and n_p are the number of holes and particles respectively. An example of this rescaled relation of the matrix indices reads

$$\mathbf{phph}[a - nh, j, c - nh, l] = \langle aj | \hat{v} | cl \rangle.$$

This is the reason why we implemented rescaling of the particle indices in *Basisconfig*, see listing 6.8. However, the tp-file contains no such rescaling, therefore we add the number of holes to the particle indices when searching the dictionary, see listing 6.9. The new three-dimensional implementation of the six matrices suggests that this rescaling could be omitted, however in the *Amplitudes* class we depend on the rescaling when we create the matrices containing the amplitudes t_i^a and t_{ij}^{ab} . Therefore we keep this rescaling in all aspects of the code.

Fmatrix: CLASS implementation

Fmatrix is an abstract base class with one derived class *f1*. This class tabulates the single-particle matrix elements (sp) in eq. (6.1), and utilize them to calculate the F-matrix, or also called Fock matrix, in eq. (5.38).

The sp-elements are provided in a text file, which is read and tabulated in the *f1*-class function *read_sp_energy*. See listing 6.10. The class stores the sp-elements in different two-dimensional arrays according to the placement of holes and particles in the element. This give rise to four different arrays

$$\begin{aligned}
 \mathbf{s_hh} &= \langle i | \hat{h} | j \rangle, \\
 \mathbf{s_hp} &= \langle i | \hat{h} | a \rangle, \\
 \mathbf{s_ph} &= \langle a | \hat{h} | i \rangle, \\
 \mathbf{s_pp} &= \langle a | \hat{h} | b \rangle,
 \end{aligned} \tag{6.27}$$

where *h* and *ij*... denotes hole states, and *p* and *ab*... denotes particle states. In our case, where we are considering the diagonal basis of harmonic oscillator functions, we only obtain contribution on the form

$$\begin{aligned}
 \mathbf{s_hh} &= \langle i | \hat{h} | i \rangle, \\
 \mathbf{s_pp} &= \langle a | \hat{h} | a \rangle.
 \end{aligned}$$

```

void f1::read_sp_energy(char* filename){
    // open and reading from file
    ifstream file(filename, ios_base::in);
    while(!file.eof()){
        // read <bra| = <q|
        file >> q;
        // read |ket> = |r>
        file >> r;
        // read single-particle energy <q|h_0|r>
        file >> value;

        if(q<(nh+np) && r<(nh+np)){
            if(q<nh && r<nh){
                s_hh[q][r] = value;
            }
            else if(q<nh && r>=nh){
                s_hp[q][r-nh] = value;
            }
            else if(q>=nh && r<nh){
                s_ph[q-nh][r] = value;
            }
            else if(q>=nh && r>=nh){
                s_pp[q-nh][r-nh] = value;
            }
        }
    }
    file.close();
} // end read_sp_energy

```

Listing 6.10: Illustration of the implemented Fmatrix class function `read_sp_energy`. See the text for description.

However all possibilities are implemented making the code more general. Note that the rescaling of particles encountered in the implementation of the *Interaction* class, is a necessary implementation also for this class.

The `f1`-class function *set_up_fmatrix* calculates the F-matrix defined as follows

$$f_q^p = \langle p|h|q\rangle + \sum_i^d \langle pi|v|qi\rangle, \quad (6.28)$$

where $pq \dots$ denotes both particle and hole states, i denotes hole states, d is the number of hole states, and the interaction elements are antisymmetrized. Listing 6.11 illustrates the implementation of *set_up_fmatrix*.

```

void f1::set_up_fmatrix(Interaction* interaction){
    // set up f_hh = <i|h_0|j> + SUM_k <i k||j k>
    for(i=0; i<nh; i++){
        for(j=0; j<nh; j++){
            f_hh[i][j] = s_hh[i][j];
        }
    }
    for(a=0; a<alphadim; a++){

```

```

map1=0;
for (i=0; i<hh_bc[a]; i+=2){
    k=B->hhbasis[a][i];
    l=B->hhbasis[a][i+1];
    map2=0;
    for (j=0; j<hh_bc[a]; j+=2){
        m=B->hhbasis[a][j];
        n=B->hhbasis[a][j+1];
        if (l==n)
            f_hh[k][m] += interaction->hhhh[a][map1][map2];
        if (l==m)
            f_hh[k][n] -= interaction->hhhh[a][map1][map2];
        if (k==n)
            f_hh[l][m] -= interaction->hhhh[a][map1][map2];
        if (k==m)
            f_hh[l][n] += interaction->hhhh[a][map1][map2];
        map2+=1;
    }
    map1+=1;
}
}
// set up f_pp = <a|h_0|b> + SUM_k <a k|| b k>
for (a=0; a<np; a++){
    for (b=0; b<np; b++){
        f_pp[a][b] = s_pp[a][b];
    }
}
for (int a=0; a<alphadim; a++){
    map1=0;
    for (int i=0; i<ph_bc[a]; i+=2){
        map2=0;
        for (int j=0; j<ph_bc[a]; j+=2){
            if (B->phbasis[a][i+1]==B->phbasis[a][j+1]){
                f_pp[B->phbasis[a][i]][B->phbasis[a][j]]+=
                    interaction->phph[a][map1][map2];
            }
            map2+=1;
        }
        map1+=1;
    }
}
}

/* set up f_hp, f_ph */
} // end set_up_fmatrix

```

Listing 6.11: code-snippet illustrating the implementation of the Fmatrix calculation. See the text for description.

The F-matrix is also tabulated according to the placement of holes and particles, thus we obtain four arrays

$$\begin{aligned}
 \mathbf{f_hh} &= f_i^j, \\
 \mathbf{f_hp} &= f_i^a, \\
 \mathbf{f_ph} &= f_a^i, \\
 \mathbf{f_pp} &= f_a^b.
 \end{aligned} \tag{6.29}$$

In listing 6.11 the implementation of **f_hh** and **f_pp** is shown explicitly. The implementation of the two-particle basis in *Basisconfig*, and the subsequent implementation of three-dimensional matrices containing the interaction elements in *Interaction*, entails the consequence that the F-matrix cannot be calculated straightforwardly as in the expression of eq. (6.28). The first term in this equation equals the sp-elements tabulated in the four matrices of eq. (6.27). These terms are therefore included just by assigning the values stored in the **s**-matrices to the corresponding **f**-matrices. Further the sum over the interaction elements is calculated by looping through the contributing interaction elements, and adding them to the corresponding **f**-matrix element. Only interaction elements fulfilling the requirement of eq. (6.28) are considered, thus only **hhhh**, **phhh** and **phph** contains contributing elements. In the case of **f_hh** we consider only the elements in the **hhhh**-matrix. We loop through this matrix by combining two loops over the *hh*-basis in *Basisconfig*. For each element we test if the two quantum numbers representing the sum-index in eq. (6.28) are equal, and if they are, we add this interaction element to the **f_hh** element represented by the two remaining quantum numbers. Remember that we store only one fourth of the interaction elements, and therefore we permute the matrix elements according to eq. (6.7). In the case of **f_pp** we consider matrix elements stored in the **phph**-matrix. We loop through this matrix by combining two loops over the *ph*-basis in *Basisconfig*. As before, we test for equality of the two quantum numbers representing the sum-index, and add the element to the belonging **f_pp** element. We do not permute in this case, because such an element would not satisfy eq. (6.28). The two remaining **f**-matrices are filled in the same manner by considering the interaction elements in the **phhh**-matrix.

Amplitudes: CLASS implementation

Amplitudes is an abstract base class with the derived class *amp1*. This class implements the amplitude equations for both \hat{T}_1 and \hat{T}_2 . In this section we present the implementation of the \hat{T}_1 and \hat{T}_2 amplitude equations given respectively in eqs. (5.44) and (5.45). In eqs. (5.115) and (5.130), these amplitude equations are given in a diagrammatic form, and the corresponding algebraic form is presented in eqs. (5.139) and (5.141). The algebraic expressions of the amplitude equations provide a starting point for implementing these equations. However, some manipulation is necessary. We start by modifying the \hat{T}_1 -amplitude equation and illustrating the corresponding implementation, before proceeding with the \hat{T}_2 -amplitude equation.

\hat{T}_1 -amplitude equation

Consider the \hat{T}_1 -amplitude equation in eq. (5.139), note that the summation-notation is omitted. We rearrange this eq. as follows:

$$\begin{aligned}
0 = & f_i^a + \langle ja|v|bi\rangle t_j^b + \frac{1}{2} \langle aj|v|bc\rangle t_{ij}^{bc} + (f_b^a t_i^b + \langle aj|v|bc\rangle t_i^b t_j^c) \\
& + \left(-f_i^j t_j^a - f_b^j t_j^a t_i^b - \langle jk|v|ib\rangle t_j^a t_k^b - \langle jk|v|bc\rangle t_i^b t_j^a t_k^c - \frac{1}{2} \langle jk|v|bc\rangle t_j^a t_{ik}^{bc} \right) \\
& + \left(-\frac{1}{2} \langle jk|v|ib\rangle t_{jk}^{ab} - \frac{1}{2} \langle jk|v|bc\rangle t_i^b t_{jk}^{ac} \right) + (f_b^j t_{ij}^{ab} + \langle jk|v|bc\rangle t_j^b t_{ik}^{ac}), \quad (6.30)
\end{aligned}$$

which is equivalent to

$$\begin{aligned}
0 = & f_i^a + \langle ja|v|bi\rangle t_j^b + \frac{1}{2}\langle aj|v|bc\rangle t_{ij}^{bc} + (f_b^a + \langle aj|v|bc\rangle t_j^c) t_i^b \\
& - \left(f_i^j + f_b^j t_i^b + \langle jk|v|ib\rangle t_k^b + \langle jk|v|bc\rangle t_i^b t_k^c + \frac{1}{2}\langle jk|v|bc\rangle t_{ik}^{bc} \right) t_j^a \\
& + \frac{1}{2} (\langle jk|v|ic\rangle + \langle jk|v|bc\rangle t_i^b) t_{jk}^{ca} + (f_c^k + \langle jk|v|bc\rangle t_j^b) t_{ik}^{ac}.
\end{aligned} \tag{6.31}$$

In the above equation we have relabeled some of the indices in the last line, in order to extract a common amplitude from the parenthesis. We simplify this expression further by defining the parenthesis in eq. (6.31) as intermediates. These intermediates are manipulated such that the matrix elements fit the ordering of the six matrices implemented in the *Interaction* class.

$$\begin{aligned}
[I1]_b^a &= f_b^a + \langle aj|v|bc\rangle t_j^c \\
&= f_b^a + \langle bc|v|aj\rangle t_j^c,
\end{aligned} \tag{6.32}$$

$$\begin{aligned}
[I2]_c^k &= f_c^k + \langle jk|v|bc\rangle t_j^b \\
&= f_c^k + \langle bc|v|jk\rangle t_j^b,
\end{aligned} \tag{6.33}$$

$$\begin{aligned}
[I3]_i^j &= f_i^j + f_b^j t_i^b + \langle jk|v|ib\rangle t_k^b + \langle jk|v|bc\rangle t_i^b t_k^c + \frac{1}{2}\langle jk|v|bc\rangle t_{ik}^{bc} \\
&= f_i^j + \langle jk|v|ib\rangle t_k^b + \frac{1}{2}\langle jk|v|bc\rangle t_{ik}^{bc} + (f_b^j + \langle cb|v|kj\rangle t_k^c) t_i^b \\
&= f_i^j - \langle bi|v|jk\rangle t_k^b + \frac{1}{2}\langle bc|v|jk\rangle t_{ik}^{bc} + [I2]_b^j t_i^b,
\end{aligned} \tag{6.34}$$

$$\begin{aligned}
[I4]_{ic}^{jk} &= \langle jk|v|ic\rangle + \langle jk|v|bc\rangle t_i^b \\
&= -\langle ci|v|jk\rangle + \frac{1}{2}\langle bc|v|jk\rangle t_i^b + \frac{1}{2}\langle bc|v|jk\rangle t_i^b \\
&= [I5]_{ic}^{jk} + \frac{1}{2}\langle bc|v|jk\rangle t_i^b,
\end{aligned} \tag{6.35}$$

$$[I5]_{ic}^{jk} = -\langle ci|v|jk\rangle + \frac{1}{2}\langle bc|v|jk\rangle t_i^b. \tag{6.36}$$

We insert these definitions into eq. (6.31), and obtain the \hat{T}_1 amplitude equation:

$$\begin{aligned}
0 = & f_i^a - \langle aj|v|bi\rangle t_j^b + \frac{1}{2}\langle bc|v|aj\rangle t_{ij}^{bc} + [I1]_b^a t_i^b \\
& - [I3]_i^j t_j^a + \frac{1}{2}[I4]_{ic}^{jk} t_{jk}^{ca} + [I2]_c^k t_{ik}^{ac}.
\end{aligned} \tag{6.37}$$

Next, we wish to obtain an equation for the \hat{T}_1 amplitude t_i^a . We accomplish this by performing the trick of adding and subtracting the t_i^a amplitude inside eq. (6.37). Each

term containing a t_x^y amplitude is expressed in terms of the t_i^a amplitude, and added to the equation. This added term is then subtracted by including the original expression multiplied by one or more delta-function. Thus we obtain

$$\begin{aligned}
 0 = & f_i^a - \langle ai|v|ai \rangle t_i^a - (1 - \delta_{ab}\delta_{ij}) \langle aj|v|bi \rangle t_j^b + \frac{1}{2} \langle bc|v|aj \rangle t_{ij}^{bc} \\
 & + [I1]_a^a t_i^a + (1 - \delta_{ab}) [I1]_b^b t_i^b - [I3]_i^i t_i^a - (1 - \delta_{ij}) [I3]_i^j t_j^a \\
 & + \frac{1}{2} [I4]_{ic}^{jk} t_{jk}^{ca} + [I2]_c^k t_{ik}^{ac}.
 \end{aligned} \tag{6.38}$$

We are now able to extract an equation for the amplitude t_i^a , which reads

$$\begin{aligned}
 t_i^a = & \frac{1}{D_i^a} \left(f_i^a + \frac{1}{2} \langle bc|v|aj \rangle t_{ij}^{bc} - (1 - \delta_{ab}\delta_{ij}) \langle aj|v|bi \rangle t_j^b \right. \\
 & \left. + (1 - \delta_{ab}) [I1]_b^a t_i^b - (1 - \delta_{ij}) [I3]_i^j t_j^a + \frac{1}{2} [I4]_{ic}^{jk} t_{jk}^{ca} + [I2]_c^k t_{ik}^{ac} \right),
 \end{aligned} \tag{6.39}$$

where D_i^a is given as

$$D_i^a = \langle ai|v|ai \rangle - [I1]_a^a + [I3]_i^i. \tag{6.40}$$

The eq. (6.39) is implemented in the class function *t1_uncoupled_calc*, which is illustrated in listing 6.12. The implementation of the intermediates will be presented after the derivation of the \hat{T}_2 amplitude equation.

```

void Amplitudes::t1_uncoupled_calc(){
    // calculate t1 intermediates
    t1_uncoupled_intermediates();

    // f_i^a
    for(i=0; i<np; i++){
        for(j=0; j<nh; j++){
            t1[i][j] = F->f_ph[i][j];
        }
    }

    // -(1-delta_{ab})delta_{ij}<aj|v|bi>t_{j}^b
    t1_uncoupled_term2(t1);

    // (1-delta_{ab})[I1]_{-}{b}^a t_{-}{i}^b
    t1_uncoupled_term3(t1);

    // -(1-delta_{ij})[I3]_{-}{i}^j t_{-}{j}^a
    t1_uncoupled_term4(t1);

    // 0.5<bc|v|aj>t_{ij}^{bc}
    t1_uncoupled_term5(t1);

    // 0.5[I4]_{-}{ic}^jk t_{jk}^{ca}
    t1_uncoupled_term6(t1);

    // [I2]_{-}{c}^k t_{ik}^{ac}
    t1_uncoupled_term7(t1);

    // calculate t1 denominator

```



```

    t1_uncoupled_denom(t1);
} //end t1_uncoupled_calc

```

Listing 6.12: Implementation of the amp1 class function t1_uncoupled_calc()

In listing 6.12, $t1$ represents a two-dimensional array with dimension (np, nh) , containing all possible t_i^a amplitudes. We proceed by showing the implementation of the $t1_uncoupled_term$ -functions in $t1_uncoupled_calc$, which represents the terms of eq. (6.39). First the algebraic expression is given, followed by its implementation. Note how we in these implementations, loop effectively over contributing interaction elements only. This technique saves much cpu-time compared with the brute force technique of looping over all interaction elements, not only those that satisfy eq. (6.11). Also note that the intermediates are calculated prior to the t_1 calculations. These intermediates are tabulated in matrices carrying names which include *barh*. These names do not correspond with the algebraic notation utilized above, however the connections are seen from the algebraic expressions above the implementation.

$$t_i^a D_i^a \leftarrow -(1 - \delta_{ab} \delta_{ij}) \langle aj | v | bi \rangle t_j^b$$

```

void Amplitudes::t1_uncoupled_term2(double **t1){
    for(alpha=ph_alphamin; alpha<ph_alphamax; alpha++){
        map1=0;
        for(ph=0; ph<phbcount[alpha]; ph+=2){
            a = B->phbasis[alpha][ph];
            j = B->phbasis[alpha][ph+1];
            map2=0;
            for(ph2=0; ph2<phbcount[alpha]; ph2+=2){
                b = B->phbasis[alpha][ph2];
                i = B->phbasis[alpha][ph2+1];
                if(j!=i || b!=a){
                    t1[a][i] = t1[a][i] - V->phph[alpha][map1][map2]*t1_old[b][j];
                }
                map2+=1;
            }
            map1+=1;
        }
    }
} // end t1_uncoupled_term2

```

Listing 6.13: implementation of the amp1 class function t1_uncoupled_term2()

$$t_i^a D_i^a \leftarrow (1 - \delta_{ab}) [I1]_b^a t_i^b$$

```

void Amplitudes::t1_uncoupled_term3(double **t1){
    for(a=0; a<np; a++){
        for(i=0; i<nh; i++){
            temp = 0.0;
            for(b=0; b<np; b++){
                if(b!=a){
                    temp = temp + barh_i02a[a][b]*t1_old[b][i];
                }
            }
            t1[a][i] = t1[a][i] + temp;
        }
    }
} // end t1_uncoupled_term3

```

Listing 6.14: implementation of the amp1 class function t1_uncoupled_term3()

$$t_i^a D_i^a \leftarrow -(1 - \delta_{ij}) [I3]_i^j t_j^a$$

```

void Amplitudes::t1_uncoupled_term4(double **t1){
    for(a=0; a<np; a++){
        for(i=0; i<nh; i++){
            temp = 0.0;
            for(j=0; j<nh; j++){
                if(j!=i){
                    temp = temp + barh_03[j][i]*t1_old[a][j];
                }
            }
            t1[a][i] = t1[a][i] - temp;
        }
    }
} // end t1_uncoupled_term4

```

Listing 6.15: implementation of the amp1 class function t1_uncoupled_term4()

$$t_i^a D_i^a \leftarrow \frac{1}{2} \langle bc|v|aj \rangle t_{ij}^{bc}$$

```

void Amplitudes::t1_uncoupled_term5(double **t1){
    for (alpha=ph_alphamin; alpha<ph_alphamax; alpha++){
        for (i=0; i<nh; i++){
            map1=0;
            for (p=0; p<ppbcount[alpha]; p+=2){
                b = B->ppbasis[alpha][p];
                c = B->ppbasis[alpha][p+1];
                map2=0;
                for (ph=0; ph<phbcount[alpha]; ph+=2){
                    a = B->phbasis[alpha][ph];
                    j = B->phbasis[alpha][ph+1];
                    t1[a][i] += 0.5*V->ppph[alpha][map1][map2]*t2_old[b][c][i][j];
                    t1[a][i] -= 0.5*V->ppph[alpha][map1][map2]*t2_old[c][b][i][j];
                    map2+=1;
                }
                map1+=1;
            }
        }
    }
} // end t1_uncoupled_term5

```

Listing 6.16: implementation of the amp1 class function t1_uncoupled_term5()

$$t_i^a D_i^a \leftarrow \frac{1}{2} [I4]_{ic}^{jk} t_{jk}^{ca}$$

```

void Amplitudes::t1_uncoupled_term6(double **t1){
    for (a=0; a<np; a++){
        for (i=0; i<nh; i++){
            temp = 0.0;
            for (j=0; j<nh; j++){
                for (k=0; k<nh; k++){
                    for (c=0; c<np; c++){
                        temp = temp + barh_07[j][k][i][c]*t2_old[c][a][j][k];
                    }
                }
            }
            t1[a][i] = t1[a][i] + 0.5*temp;
        }
    }
} // end t1_uncoupled_term6

```

Listing 6.17: implementation of the amp1 class function t1_uncoupled_term6()

$$t_i^a D_i^a \leftarrow [I2]_c^k t_{ik}^{ac}$$

```

void Amplitudes::t1_uncoupled_term7(double **t1){
    for(a=0; a<np; a++){
        for(i=0; i<nh; i++){
            temp = 0.0;
            for(k=0; k<nh; k++){
                for(c=0; c<np; c++){
                    temp = temp + barh_01[k][c]*t2_old[a][c][i][k];
                }
            }
            t1[a][i] = t1[a][i] + temp;
        }
    }
} // end t1_uncoupled_term7

```

Listing 6.18: implementation of the amp1 class function t1_uncoupled_term7()

$$t_i^a \leftarrow \frac{t_i^a}{D_i^a} = t_i^a / (\langle ai|v|ai \rangle - [I1]_a^a + [I3]_i^i)$$

```

void Amplitudes::t1_uncoupled_denom(double **t1){
    /* allocating C[np][nh] */
    //C = [I3]-[I1]
    for(i=0; i<nh; i++){
        for(a=0; a<np; a++){
            C[a][i] = barh_03[i][i] - barh_i02a[a][a];
        }
    }
    //C += <ai|v|ai>
    for(int alpha=0; alpha<alphadim; alpha++){
        map1=0;
        for(ph=0; ph<phbcount[alpha]; ph+=2){
            a = B->phbasis[alpha][ph];
            i = B->phbasis[alpha][ph+1];
            C[a][i] += V->phph[alpha][map1][map1];
            map1+=1;
        }
    }
    //t_i^a/D_i^a
    for(i=0; i<nh; i++){
        for(a=0; a<np; a++){
            t1[a][i] = t1[a][i]/C[a][i];
        }
    }
    /* deallocating C[np][nh] */
} // end t1_uncoupled_denom

```

Listing 6.19: implementation of the amp1 class function t1_uncoupled_denom()

\hat{T}_2 -amplitude equation

Consider the \hat{T}_2 -amplitude equation in eq. (5.141). Note that the summation-notation is omitted. We rearrange this equation as follows:

$$\begin{aligned}
0 = & \langle ij|v|ab\rangle + \frac{1}{2}\langle ab|v|cd\rangle t_{ij}^{cd} \\
& - \left(\hat{P}_{(ij)} f_j^k t_{ik}^{ab} + \hat{P}_{(ij)} f_c^k t_i^c t_{kj}^{ab} + \hat{P}_{(ij)} \langle kl|v|ci\rangle t_k^c t_{jl}^{ba} + \hat{P}_{(ij)} \langle kl|v|cd\rangle t_k^c t_i^d t_{jl}^{ba} \right. \\
& \quad \left. + \frac{1}{2} \hat{P}_{(ij)} \langle kl|v|cd\rangle t_{ki}^{cd} t_{lj}^{ab} \right) \\
& + \frac{1}{2} \left(\langle kl|v|ij\rangle t_{kl}^{ab} + \hat{P}_{(ij)} \langle kl|v|cj\rangle t_i^c t_{kl}^{ab} + \frac{1}{2} \langle kl|v|cd\rangle t_{kl}^{ab} t_{ij}^{cd} + \frac{1}{2} \hat{P}_{(ij)} \langle kl|v|cd\rangle t_i^c t_{kl}^{ab} t_j^d \right) \\
& + \left(\hat{P}_{(ab)} f_c^b t_{ij}^{ac} - \hat{P}_{(ab)} f_c^k t_k^a t_{ij}^{cb} + \hat{P}_{(ab)} \langle ka|v|cd\rangle t_k^c t_{ij}^{db} - \hat{P}_{(ab)} \langle kl|v|cd\rangle t_k^c t_l^a t_{ij}^{db} \right. \\
& \quad \left. - \frac{1}{2} \hat{P}_{(ab)} \langle kl|v|cd\rangle t_{kl}^{ca} t_{ij}^{db} \right) \\
& + \left(\hat{P}_{(ab)} \hat{P}_{(ij)} \langle kb|v|cj\rangle t_{ik}^{ac} + \hat{P}_{(ab)} \hat{P}_{(ij)} \langle ak|v|dc\rangle t_i^d t_{jk}^{bc} - \hat{P}_{(ab)} \hat{P}_{(ij)} \langle lk|v|ic\rangle t_l^a t_{kj}^{cb} \right. \\
& \quad \left. + \hat{P}_{(ab)} \hat{P}_{(ij)} \langle kl|v|cd\rangle t_i^c t_k^a t_{jl}^{bd} + \frac{1}{2} \hat{P}_{(ab)} \hat{P}_{(ij)} \langle kl|v|cd\rangle t_{ik}^{ac} t_{jl}^{bd} \right) \\
& + \left(-\hat{P}_{(ab)} \langle kb|v|ij\rangle t_k^a - \frac{1}{2} \hat{P}_{(ab)} \langle kb|v|cd\rangle t_k^a t_{ij}^{cd} - \hat{P}_{(ab)} \hat{P}_{(ij)} \langle kb|v|cj\rangle t_k^a t_i^c \right. \\
& \quad - \frac{1}{2} \hat{P}_{(ab)} \hat{P}_{(ij)} \langle kb|v|cd\rangle t_k^a t_i^c t_j^d + \frac{1}{2} \hat{P}_{(ab)} \langle kl|v|ij\rangle t_k^a t_l^b + \frac{1}{4} \hat{P}_{(ab)} \langle kl|v|cd\rangle t_k^a t_{ij}^{cd} t_l^b \\
& \quad \left. + \frac{1}{2} \hat{P}_{(ab)} \hat{P}_{(ij)} \langle kl|v|cj\rangle t_k^a t_i^c t_l^b + \frac{1}{4} \hat{P}_{(ab)} \hat{P}_{(ij)} \langle kl|v|cd\rangle t_k^a t_i^c t_l^b t_j^d \right) \\
& + \left(\hat{P}_{(ij)} \langle ab|v|cj\rangle t_i^c + \frac{1}{2} \hat{P}_{(ij)} \langle ab|v|cd\rangle t_i^c t_j^d \right). \tag{6.41}
\end{aligned}$$

This is equivalent to:

$$\begin{aligned}
0 = & \langle ij|v|ab\rangle + \frac{1}{2}\langle ab|v|cd\rangle t_{ij}^{cd} \\
& - \hat{P}_{(ij)} \left(f_i^l + f_c^l t_i^c + \langle kl|v|ci\rangle t_k^c + \langle kl|v|cd\rangle t_k^c t_i^d + \frac{1}{2} \langle kl|v|cd\rangle t_{ki}^{cd} \right) t_{lj}^{ab} \\
& + \frac{1}{2} \left(\langle kl|v|ij\rangle + \hat{P}_{(ij)} \langle lk|v|jc\rangle t_i^c + \frac{1}{2} \langle kl|v|cd\rangle t_{ij}^{cd} + \frac{1}{2} \hat{P}_{(ij)} \langle kl|v|cd\rangle t_i^c t_j^d \right) t_{kl}^{ab} \\
& + \hat{P}_{(ab)} \left(f_d^a - f_d^k t_k^a + \langle ka|v|cd\rangle t_k^c - \langle lk|v|cd\rangle t_l^c t_k^a - \frac{1}{2} \langle kl|v|cd\rangle t_{kl}^{ca} \right) t_{ij}^{db} \\
& + \hat{P}_{(ab)} \hat{P}_{(ij)} \left(\langle kb|v|cj\rangle + \langle bk|v|dc\rangle t_j^d - \langle lk|v|jc\rangle t_l^b - \langle kl|v|cd\rangle t_j^d t_l^b + \frac{1}{2} \langle kl|v|cd\rangle t_{jl}^{bd} \right) t_{ik}^{ac}
\end{aligned}$$

$$\begin{aligned}
 & -\hat{P}_{(ab)} \left(\langle kb|v|ij\rangle + \frac{1}{2}\langle kb|v|cd\rangle t_{ij}^{cd} + \hat{P}_{(ij)}\langle kb|v|cj\rangle t_i^c + \frac{1}{2}\hat{P}_{(ij)}\langle kb|v|cd\rangle t_i^c t_j^d \right. \\
 & \quad \left. - \frac{1}{2}\langle kl|v|ij\rangle t_l^b - \frac{1}{4}\langle kl|v|cd\rangle t_{ij}^{cd} t_l^b - \frac{1}{2}\hat{P}_{(ij)}\langle kl|v|cj\rangle t_i^c t_l^b - \frac{1}{4}\hat{P}_{(ij)}\langle kl|v|cd\rangle t_i^c t_l^b t_j^d \right) t_k^a \\
 & + \hat{P}_{(ij)} \left(\langle ab|v|cj\rangle + \frac{1}{2}\langle ab|v|cd\rangle t_j^d \right) t_i^c,
 \end{aligned} \tag{6.42}$$

where we have relabeled some indices in the first, third and fourth parenthesis in order to extract common factors. We simplify this equation in a similar manner as for \hat{T}_1 , by defining intermediates. The intermediates corresponding to \hat{T}_2 are given explicitly below. Note that we manipulate these expressions so that they correspond to the six matrices defined in the *Interaction* class.

We recognize the first parenthesis of eq. (6.42) as the intermediate $[I3]$, already defined for the \hat{T}_1 amplitude eq. (6.34), viz.

$$\begin{aligned}
 [I3]_i^l &= f_i^l + f_c^l t_i^c + \langle kl|v|ci\rangle t_k^c + \langle kl|v|cd\rangle t_k^c t_i^d + \frac{1}{2}\langle kl|v|cd\rangle t_{ki}^{cd} \\
 &= f_i^l + \langle ci|v|kl\rangle t_k^c + \frac{1}{2}\langle cd|v|kl\rangle t_{ki}^{cd} + (f_c^l + \langle dc|v|kl\rangle t_k^d) t_i^c \\
 &= f_i^l - \langle ci|v|lk\rangle t_k^c + \frac{1}{2}\langle cd|v|lk\rangle t_{ik}^{cd} + (f_c^l + \langle cd|v|lk\rangle t_k^d) t_i^c \\
 &= f_i^l - \langle ci|v|lk\rangle t_k^c + \frac{1}{2}\langle cd|v|lk\rangle t_{ik}^{cd} + [I2]_c^l t_i^c.
 \end{aligned} \tag{6.43}$$

The second parenthesis reads

$$\begin{aligned}
 [I6]_{ij}^{kl} &= \langle kl|v|ij\rangle + \hat{P}_{(ij)}\langle lk|v|jc\rangle t_i^c + \frac{1}{2}\langle kl|v|cd\rangle t_{ij}^{cd} + \frac{1}{2}\hat{P}_{(ij)}\langle kl|v|cd\rangle t_i^c t_j^d \\
 &= \langle kl|v|ij\rangle + \frac{1}{2}\langle cd|v|kl\rangle t_{ij}^{cd} + \hat{P}_{(ij)} \left(-\langle cj|v|lk\rangle + \frac{1}{2}\langle cd|v|kl\rangle t_j^d \right) t_i^c \\
 &= \langle lk|v|ji\rangle + \frac{1}{2}\langle dc|v|lk\rangle t_{ij}^{cd} + \hat{P}_{(ij)} \left(-\langle cj|v|lk\rangle + \frac{1}{2}\langle dc|v|lk\rangle t_j^d \right) t_i^c \\
 &= \langle lk|v|ji\rangle + \frac{1}{2}\langle dc|v|lk\rangle t_{ij}^{cd} + \hat{P}_{(ij)} [I5]_{jc}^{lk} t_i^c \\
 &= \langle kl|v|ij\rangle + \frac{1}{2}\langle cd|v|kl\rangle t_{ij}^{cd} + \hat{P}_{(ij)} [I5]_{ic}^{kl} t_j^c,
 \end{aligned} \tag{6.44}$$

where the intermediate $[I5]$ is defined in eq. (6.36). The third parenthesis reads

$$\begin{aligned}
 [I7]_d^a &= f_d^a - f_d^k t_k^a + \langle ka|v|cd\rangle t_k^c - \langle lk|v|cd\rangle t_l^c t_k^a - \frac{1}{2}\langle kl|v|cd\rangle t_{kl}^{ca} \\
 &= (f_d^a + \langle dc|v|ak\rangle t_k^c) - (f_d^k + \langle cd|v|lk\rangle t_l^c) t_k^a - \frac{1}{2}\langle cd|v|kl\rangle t_{kl}^{ca} \\
 &= [I1]_d^a - [I2]_d^k t_k^a - \frac{1}{2}\langle dc|v|kl\rangle t_{kl}^{ac},
 \end{aligned} \tag{6.45}$$

where the intermediates $[I1]$ and $[I2]$ are defined in eqs. (6.32) and (6.33), respectively.

The fourth parenthesis reads

$$\begin{aligned}
[I8]_{cj}^{kb} &= \langle kb|v|cj\rangle + \langle bk|v|dc\rangle t_j^d - \langle lk|v|jc\rangle t_l^b - \langle kl|v|cd\rangle t_j^d t_l^b + \frac{1}{2}\langle kl|v|cd\rangle t_{jl}^{bd} \\
&= \left(-\langle bk|v|cj\rangle + \frac{1}{2}\langle dc|v|bk\rangle t_j^d \right) + \frac{1}{2}\langle dc|v|bk\rangle t_j^d \\
&\quad - \left(-\langle cj|v|lk\rangle + \frac{1}{2}\langle cd|v|kl\rangle t_j^d + \frac{1}{2}\langle cd|v|kl\rangle t_j^d \right) t_l^b \\
&\quad + \frac{1}{2}\langle cd|v|kl\rangle t_{jl}^{bd} \\
&= [I9]_{cj}^{kb} + \frac{1}{2}\langle dc|v|bk\rangle t_j^d - [I4]_{jc}^{lk} t_l^b + \frac{1}{2}\langle cd|v|kl\rangle t_{jl}^{bd},
\end{aligned} \tag{6.46}$$

where $[I4]$ corresponds to eq. (6.35) and $[I9]$ reads

$$[I9]_{cj}^{kb} = -\langle bk|v|cj\rangle + \frac{1}{2}\langle dc|v|bk\rangle t_j^d. \tag{6.47}$$

The fifth parenthesis yields

$$\begin{aligned}
[I10]_{ij}^{kb} &= \langle kb|v|ij\rangle + \frac{1}{2}\langle kb|v|cd\rangle t_{ij}^{cd} + \hat{P}_{(ij)}\langle kb|v|cj\rangle t_i^c + \frac{1}{2}\hat{P}_{(ij)}\langle kb|v|cd\rangle t_i^c t_j^d \\
&\quad - \frac{1}{2}\langle kl|v|ij\rangle t_l^b - \frac{1}{4}\langle kl|v|cd\rangle t_{ij}^{cd} t_l^b - \frac{1}{2}\hat{P}_{(ij)}\langle kl|v|cj\rangle t_i^c t_l^b - \frac{1}{4}\hat{P}_{(ij)}\langle kl|v|cd\rangle t_i^c t_l^b t_j^d \\
&= -\langle bk|v|ij\rangle - \frac{1}{2}\langle cd|v|bk\rangle t_{ij}^{cd} + \hat{P}_{(ij)}\left(-\langle bk|v|cj\rangle + \frac{1}{2}\langle dc|v|bk\rangle t_j^d \right) t_i^c \\
&\quad - \frac{1}{2}\left(\langle kl|v|ij\rangle + \frac{1}{2}\langle cd|v|kl\rangle t_{ij}^{cd} + \hat{P}_{(ij)}\left(\langle cj|v|kl\rangle + \frac{1}{2}\langle cd|v|kl\rangle t_j^d \right) t_i^c \right) t_l^b \\
&= -\langle bk|v|ij\rangle - \frac{1}{2}\langle cd|v|bk\rangle t_{ij}^{cd} + \hat{P}_{(ij)}[I9]_{cj}^{kb} t_i^c \\
&\quad - \frac{1}{2}\left(\langle lk|v|ji\rangle + \frac{1}{2}\langle dc|v|lk\rangle t_{ij}^{cd} + \hat{P}_{(ij)}\left(-\langle cj|v|lk\rangle + \frac{1}{2}\langle dc|v|lk\rangle t_j^d \right) t_i^c \right) t_l^b \\
&= -\langle bk|v|ij\rangle - \frac{1}{2}\langle cd|v|bk\rangle t_{ij}^{cd} + \hat{P}_{(ij)}[I9]_{cj}^{kb} t_i^c - \frac{1}{2}[I6]_{ij}^{kl} t_l^b.
\end{aligned} \tag{6.48}$$

Finally the sixth parenthesis yields

$$[I11]_{cj}^{ab} = \langle ab|v|cj\rangle + \frac{1}{2}\langle ab|v|cd\rangle t_j^d. \tag{6.49}$$

We now reinsert these definitions into eq. (6.42), and obtain the \hat{T}_2 amplitude equation

$$\begin{aligned}
0 &= \langle ab|v|ij\rangle + \frac{1}{2}\langle ab|v|cd\rangle t_{ij}^{cd} - \hat{P}_{(ij)}[I3]_i^l t_{lj}^{ab} + \frac{1}{2}[I6]_{ij}^{kl} t_{kl}^{ab} \\
&\quad + \hat{P}_{(ab)}[I7]_d^a t_{ij}^{db} + \hat{P}_{(ab)}\hat{P}_{(ij)}[I8]_{cj}^{kb} t_{ik}^{ac} - \hat{P}_{(ab)}[I10]_{ij}^{kb} t_k^a + \hat{P}_{(ij)}[I11]_{cj}^{ab} t_i^c.
\end{aligned} \tag{6.50}$$

Similar as for the \hat{T}_1 amplitude, we wish to obtain an equation for the \hat{T}_2 amplitude t_{ij}^{ab} .

This is obtained by using the same technique as in the case of \hat{T}_1 , thus

$$\begin{aligned}
0 = & \langle ab|v|ij\rangle + \frac{1}{2}\langle ab|v|ab\rangle t_{ij}^{ab} + \frac{1}{2}(1 - \delta_{ca}\delta_{db})\langle ab|v|cd\rangle t_{ij}^{cd} \\
& - \hat{P}_{(ij)}[I3]_i^i t_{ij}^{ab} - (1 - \delta_{il})\hat{P}_{(ij)}[I3]_i^l t_{lj}^{ab} + \frac{1}{2}[I6]_{ij}^{ij} t_{ij}^{ab} \\
& + \frac{1}{2}(1 - \delta_{ki}\delta_{lj})[I6]_{ij}^{kl} t_{kl}^{ab} + \hat{P}_{(ab)}[I7]_a^a t_{ij}^{ab} + \hat{P}_{(ab)}(1 - \delta_{da})[I7]_d^a t_{ij}^{db} \\
& + \hat{P}_{(ab)}\hat{P}_{(ij)}[I8]_{cj}^{kb} t_{ik}^{ac} - \hat{P}_{(ab)}[I10]_{ij}^{kb} t_k^a + \hat{P}_{(ij)}[I11]_{cj}^{ab} t_i^c.
\end{aligned} \tag{6.51}$$

We extract the t_{ij}^{ab} amplitudes and obtain the t_{ij}^{ab} -amplitude equation

$$\begin{aligned}
t_{ij}^{ab} = & \frac{1}{D_{ij}^{ab}} \left(\langle ab|v|ij\rangle + \frac{1}{2}(1 - \delta_{ca}\delta_{db})\langle ab|v|cd\rangle t_{ij}^{cd} - \hat{P}_{(ij)}(1 - \delta_{il})[I3]_i^l t_{lj}^{ab} \right. \\
& + \frac{1}{2}(1 - \delta_{ki}\delta_{lj})[I6]_{ij}^{kl} t_{kl}^{ab} + \hat{P}_{(ab)}(1 - \delta_{da})[I7]_d^a t_{ij}^{db} + \hat{P}_{(ab)}\hat{P}_{(ij)}[I8]_{cj}^{kb} t_{ik}^{ac} \\
& \left. - \hat{P}_{(ab)}[I10]_{ij}^{kb} t_k^a + \hat{P}_{(ij)}[I11]_{cj}^{ab} t_i^c \right),
\end{aligned} \tag{6.52}$$

where

$$D_{ij}^{ab} = \hat{P}_{(ij)}[I3]_i^i - \frac{1}{2}\langle ab|v|ab\rangle - \frac{1}{2}[I6]_{ij}^{ij} - \hat{P}_{(ab)}[I7]_a^a. \tag{6.53}$$

Equation (6.52) is implemented in the *amp1* class function *t2_uncoupled_calc*, which is illustrated in listing 6.20. In listing 6.20, *t2* represents the four-dimensional array with dimension (np,np,nh,nh), containing all possible t_{ij}^{ab} amplitudes. Note how we are utilizing the class *Basisconfig* (B) and *Interaction* (V) to get the hold of the interaction elements in question. We proceed by showing the implementation of each *t2_uncoupled_term*-function in *t2_uncoupled_calc*, corresponding to the terms of eq. (6.52). In order to limit the implementation scope, standard procedures, like allocating arrays, are replaced by explanatory comments. The implementations are first presented in listings 6.21-6.28, followed by a more detailed description of *t2_uncoupled_term2* and *t2_uncoupled_term4*.


```

void Amplitudes::t2_uncoupled_calc(){
    //calculating t2 intermediates
    t2_uncoupled_intermediates();

    // <ab|v|ij>
    for(a=0; a<np; a++)
        for(b=0; b<np; b++)
            for(i=0; i<nh; i++)
                for(j=0; j<nh; j++)
                    t2[a][b][i][j] = 0.0;
    for(int alpha=hh_alphamin; alpha<hh_alphamax; alpha++){
        map1=0;
        for(i=0; i<ppbcount[alpha]; i+=2){
            a=B->ppbasis[alpha][i];
            b=B->ppbasis[alpha][i+1];
            map2=0;
            for(j=0; j<hhbcount[alpha]; j+=2){
                m=B->hhbasis[alpha][j];
                n=B->hhbasis[alpha][j+1];
                t2[a][b][m][n] = V->pphh[alpha][map1][map2];
                t2[b][a][m][n] = -V->pphh[alpha][map1][map2];
                t2[a][b][n][m] = -V->pphh[alpha][map1][map2];
                t2[b][a][n][m] = V->pphh[alpha][map1][map2];
                map2+=1;
            }
            map1+=1;
        }
    }

    // 0.5(1-delta-{ca}delta-{db}) <ab|v|cd> t- {ij} ^{cd}
    t2_uncoupled_term2(t2);

    // -P-(ij)(1-delta-{il})[I3]-{i} ^{l} t- {lj} ^{ab}
    t2_uncoupled_term3(t2);

    // 0.5(1-delta-{ki}delta-{lj})[I6]-{ij} ^{kl} t- {kl} ^{ab}
    t2_uncoupled_term4(t2);

    // P-(ab)(1-delta-{da})[I7]-{d} ^{a} t- {ij} ^{db}
    t2_uncoupled_term5(t2);

    // P-(ab)P-(ij)[I8]-{cj} ^{kb} t- {ik} ^{ac}
    t2_uncoupled_term6(t2);

    // -P-(ab)[I10]-{ij} ^{kb} t- {k} ^{a}
    t2_uncoupled_term7(t2);

    // P-(ij)[I11]-{cj} ^{ab} t- {i} ^{c}
    t2_uncoupled_term8(t2);

    // calculating t2 denominator
    t2_uncoupled_denom(t2);
} // end t2_uncoupled_calc

```

Listing 6.20: Implementation of the amp1 class function t2_uncoupled_calc()

$$t_{ij}^{ab} D_{ij}^{ab} \leftarrow \frac{1}{2} (1 - \delta_{ca} \delta_{db}) \langle ab|v|cd \rangle t_{ij}^{cd}$$

```

void Amplitudes::t2_uncoupled_term2(double ****t2){

    /* allocate matrix C[alphadim][ppbcount[alpha]][nh*(nh-1)] */

    //filling of t2_pppp matrix = 2dimensional t2-old
    t2pppp_fill();

    //matrix multiplication
    for(alpha=0; alpha<alphadim; alpha++){
#pragma omp parallel default(shared) private(v,u,w)
    {
        nthreads = omp_get_num_threads();
#pragma omp for schedule (static)
        for(ab=0; ab<ppbcount[alpha]; ab++){
            for(ij=0; ij<temp; ij++){
                for(cd=0; cd<ppbcount[alpha]; cd++){
                    C[alpha][ab][ij] += 0.5*v_pppp[alpha][ab][cd]
                                     *t2_pppp[alpha][cd][ij];
                }
            }
        }
    }
}

//translation from 2dim to 4dim
translste(t2,C);

/* deallocate matrix C */
} // end t2_uncoupled_term2

void Amplitudes::t2pppp_fill()
{
    for(int a=0; a<alphadim ; a++){
        for(int cd=0; cd<ppbcount[a]; cd+=2){
            map2=0;
            for(int ij=0; ij<2*nh*(nh-1); ij+=2){
                t2_pppp[a][cd][map2] =t2_old[B->ppbasis[a][cd]][B->ppbasis[a][cd+1]]
                                         [ij_map[ij]][ij_map[ij+1]];
                t2_pppp[a][cd+1][map2]=t2_old[B->ppbasis[a][cd+1]][B->ppbasis[a][cd]]
                                         [ij_map[ij]][ij_map[ij+1]];
                map2+=1;
            }
        }
    }
} //end fill

void Amplitudes::translste(double ****t2, double*** C)
{
    for(int alpha=0; alpha<alphadim; alpha++){
        for(int ab=0; ab<ppbcount[alpha]; ab+=2){
            map1=0;
            for(int ij=0; ij<2*nh*(nh-1); ij+=2){

```

```

        t2[B->ppbasis[alpha][ab]][B->ppbasis[alpha][ab+1]]
        [ij_map[ij]][ij_map[ij+1]] += C[alpha][ab][map1];
        t2[B->ppbasis[alpha][ab+1]][B->ppbasis[alpha][ab]]
        [ij_map[ij]][ij_map[ij+1]] += C[alpha][ab+1][map1];
        map1+=1;
    }
}
}
} //end translate

```

Listing 6.21: implementation of the amp1 class function t2_uncoupled_term2()

$$t_{ij}^{ab} D_{ij}^{ab} \leftarrow -\hat{P}_{(ij)}(1 - \delta_{il})[I3]_i^l t_{lj}^{ab}$$

```

void Amplitudes::t2_uncoupled_term3(double ****t2){
    /*allocating new matrix barh03[nh][nh], where if(i!=l)
    is implemented in form of zero elements along the diagonal*/
    for(i=0; i<nh-1; i++){
        for(l=i+1; l<nh; l++){
            barh03[i][l] = barh03[l][i];
            barh03[l][i] = barh03[l][i];
        }
    }
    for(i=0; i<nh; i++)
        barh03[i][i]=0.0;

    for(a=0; a<np-1; a++){
        for(b=a+1; b<np; b++){
            for(i=0; i<nh-1; i++){
                for(j=i+1; j<nh; j++){
                    temp=0.0;
                    for(l=0; l<nh; l++){
                        temp -= barh03[l][i]*t2_old[a][b][l][j]
                        -barh03[l][j]*t2_old[a][b][l][i];
                    }
                    t2[a][b][i][j] += temp;
                    t2[b][a][i][j] -= temp;
                    t2[a][b][j][i] -= temp;
                    t2[b][a][j][i] += temp;
                }
            }
        }
    }

    //deallocating matrix barh03
} // end t2_uncoupled_term3

```

Listing 6.22: implementation of the amp1 class function t2_uncoupled_term3()

$$t_{ij}^{ab} D_{ij}^{ab} \leftarrow \frac{1}{2}(1 - \delta_{ki} \delta_{lj}) [I6]_{ij}^{kl} t_{kl}^{ab}$$

```

void Amplitudes::t2_uncoupled_term4(double ****t2){

    /* allocating matrix: A[np^2][nh^2], barh[nh^2][nh^2], C[np^2][nh^2] */
    //filling matrices A, barh:
    for(a=0; a<np; a++)
        for(b=0; b<np; b++)
            for(k=0; k<nh; k++)
                for(l=0; l<nh; l++)
                    A[a*np+b][k*nh+l] = t2_old[a][b][k][l];
    for(k=0; k<nh; k++)
        for(l=0; l<nh; l++)
            for(i=0; i<nh; i++)
                for(j=0; j<nh; j++)
                    if(i!=k || j!=l)
                        barh[k*nh+l][i*nh+j] = barh_09[k][l][i][j];

    //matrix multiplication
#pragma omp parallel default(shared) private(v,u,w)
    {
        nthreads = omp_get_num_threads();
#pragma omp for schedule (static)
        for(ab=0; ab<np*np; ab++){
            for(ij=0; ij<nh*nh; ij++){
                for(kl=0; kl<nh*nh; kl++){
                    C[ab][ij] += 0.5*A[ab][kl]*barh[kl][ij];
                }
            }
        }
    }

    //translate
    for(a=0; a<np; a++){
        for(b=0; b<np; b++){
            for(i=0; i<nh; i++){
                for(j=0; j<nh; j++){
                    t2[a][b][i][j] = t2[a][b][i][j]+C[a*np+b][i*nh+j];
                }
            }
        }
    }

    //deallocating matrix A,barh,C
} // end t2_uncoupled_term4

```

Listing 6.23: implementation of the amp1 class function t2_uncoupled_term4()

$$t_{ij}^{ab} D_{ij}^{ab} \leftarrow \hat{P}_{(ab)} (1 - \delta_{da}) [I7]_d^a t_{ij}^{db}$$

```

void Amplitudes::t2_uncoupled_term5(double ****t2){

    /* allocating new matrix barh02[np][np], which implement
    if(a!=d) by introducing zero elements along the diagonal*/
    for (a=0; a<np-1; a++){
        for (d=a+1; d<np; d++){
            barh02[a][d] = barh_02[a][d];
            barh02[d][a] = barh_02[d][a];
        }
    }
    for (a=0; a<np; a++)
        barh02[a][a]=0.0;

    for (a=0; a<np-1; a++){
        for (b=a+1; b<np; b++){
            for (i=0; i<nh-1; i++){
                for (j=i+1; j<nh; j++){
                    temp = 0.0;
                    for (d=0; d<np; d++){
                        temp += barh02[a][d]*t2_old[b][d][i][j]
                            -barh02[b][d]*t2_old[a][d][i][j];
                    }
                    t2[a][b][i][j] += temp;
                    t2[b][a][i][j] -= temp;
                    t2[a][b][j][i] -= temp;
                    t2[b][a][j][i] += temp;
                }
            }
        }
    }

    //deallocating barh02
} // end t2_uncoupled_term5

```

Listing 6.24: implementation of the amp1 class function t2_uncoupled_term5()

$$t_{ij}^{ab} D_{ij}^{ab} \leftarrow \hat{P}_{(ab)} \hat{P}_{(ij)} [I8]_{cj}^{kb} t_{ik}^{ac}$$

```

void Amplitudes::t2_uncoupled_term6(double ****t2){

    /* allocating matrix: A[np*nh][np*nh], I[np*nh][np*nh], C[np*nh][np*nh] */

    //filling the matrices
    for(j=0; j<nh; j++)
        for(b=0; b<np; b++)
            for(c=0; c<np; c++)
                for(k=0; k<nh; k++)
                    I[k*np+c][j*np+b]= barh_i10c[k][b][c][j];

    for(i=0; i<nh; i++)
        for(a=0; a<np; a++)
            for(c=0; c<np; c++)
                for(k=0; k<nh; k++)
                    A[i*np+a][k*np+c] = t2_old[a][c][i][k];

    //multiplication
    #pragma omp parallel default(shared) private(v,u,w)
    {
        nthreads = omp_get_num_threads();
    #pragma omp for schedule (static)
        for(u=0; u<np*nh; u++){
            for(v=0; v<np*nh; v++){
                for(w=0; w<np*nh; w++){
                    C[u][v]+=A[u][w]*I[w][v];
                }
            }
        }

    //translate
    for(a=0; a<np; a++){
        for(b=0; b<np; b++){
            for(i=0; i<nh; i++){
                for(j=0; j<nh; j++){
                    t2[a][b][i][j] += C[i*np+a][j*np+b];
                    t2[a][b][i][j] -= C[i*np+b][j*np+a];
                    t2[a][b][i][j] -= C[j*np+a][i*np+b];
                    t2[a][b][i][j] += C[j*np+b][i*np+a];
                }
            }
        }
    }

    //deallocate matrix: A, I, C
} // end t2_uncoupled_term6

```

Listing 6.25: implementation of the amp1 class function t2_uncoupled_term6()

$$t_{ij}^{ab} D_{ij}^{ab} \leftarrow -\hat{P}_{(ab)}[I10]_{ij}^{kb} t_k^a$$

```

void Amplitudes::t2_uncoupled_term7(double ****t2){

    /* t1 used instead if t1_old for a quicker convergence */
    for (a=0; a<np-1; a++){
        for (b=a+1; b<np; b++){
            for (i=0; i<nh-1; i++){
                for (j=i+1; j<nh; j++){
                    temp = 0.0;
                    for (k=0; k<nh; k++){
                        temp = temp + (barh_i12a[k][b][i][j]*t1[a][k]
                        - barh_i12a[k][a][i][j]*t1[b][k]);
                    }
                    t2[a][b][i][j] -= temp;
                    t2[b][a][i][j] += temp;
                    t2[a][b][j][i] += temp;
                    t2[b][a][j][i] -= temp;
                }
            }
        }
    }
} // end t2_uncoupled_term7

```

Listing 6.26: implementation of the amp1 class function t2_uncoupled_term7()

$$t_{ij}^{ab} D_{ij}^{ab} \leftarrow \hat{P}_{(ij)}[I11]_{cj}^{ab} t_i^c$$

```

void Amplitudes::t2_uncoupled_term8(double ****t2){

    /* t1 used instead if t1_old for a quicker convergence*/
    for (alpha=0; alpha<alphadim; alpha++){
        for (p=0; p<ppbcount[alpha]; p+=2){
            a=B->ppbasis[alpha][p];
            b=B->ppbasis[alpha][p+1];
            for (j=0; j<nh; j++){
                for (i=0; i<nh; i++){
                    temp1=0.0;
                    temp2=0.0;
                    for (c=0; c<np; c++){
                        temp1 += (barh_i11a[a][b][c][j]*t1[c][i]
                        - barh_i11a[a][b][c][i]*t1[c][j]);
                    }
                    t2[a][b][i][j] +=temp1;
                    t2[b][a][i][j] -=temp1;
                }
            }
        }
    }
} // end t2_uncoupled_term8

```

Listing 6.27: implementation of the amp1 class function t2_uncoupled_term8()

$$t_{ij}^{ab} \leftarrow \frac{t_{ij}^{ab}}{D_{ij}^{ab}} = t_{ij}^{ab} / \left(\hat{P}_{(ij)}[I3]_i^i - \frac{1}{2}\langle ab|v|ab\rangle - \frac{1}{2}[I6]_{ij}^{ij} - \hat{P}_{(ab)}[I7]_a^a \right)$$

```

void Amplitudes::t2_uncoupled_denom(double ****t2){

    /* allocating matrix C[np][np][nh][nh] */

    for(a=0; a<np; a++){
        for(b=0; b<np; b++){
            h2ab = barh_02[a][a] + barh_02[b][b];
            for(j=0; j<nh; j++){
                for(i=0; i<nh; i++){
                    h3ij = barh_03[i][i] + barh_03[j][j];
                    h9ijij = 0.5*barh_09[i][j][i][j];
                    C[a][b][i][j] = h3ij - h2ab - h9ijij;
                }
            }
        }
    }

    double temp;
    for(alpha=0; alpha<alphadim; alpha++){
        map1=0;
        for(p=0; p<ppbcount[alpha]; p+=2){
            a= B->ppbasis[alpha][p];
            b= B->ppbasis[alpha][p+1];
            temp=0.5*V->pppp[alpha][map1][map1];
            for(i=0; i<nh; i++){
                for(j=0; j<nh; j++){
                    C[a][b][i][j]-= temp;
                    C[b][a][i][j]-= temp;
                }
            }
            map1+=1;
        }
    }

    for(b=0; b<np-1; b++){
        for(a=b+1; a<np; a++){
            for(j=0; j<nh-1; j++){
                for(i=j+1; i<nh; i++){
                    t2[b][a][j][i] = t2[b][a][j][i]/C[b][a][j][i];
                    t2[a][b][j][i] = -t2[b][a][j][i];
                    t2[b][a][i][j] = -t2[b][a][j][i];
                    t2[a][b][i][j] = t2[b][a][j][i];
                }
            }
        }
    }

    //deallocate matrix C
} // end t2_uncoupled_denom

```

Listing 6.28: implementation of the amp1 class function t2_uncoupled_denom()

Let us review the class function *t2_uncoupled_term2* and *t2_uncoupled_term4* in detail. We start with the former. The expression calculated in this function reads

$$\frac{1}{2}(1 - \delta_{ca}\delta_{db})\langle ab|v|cd\rangle t_{ij}^{cd}. \quad (6.54)$$

Originally this calculation was implemented by M. P. Lohne using brute force, see code-snippet in listing 6.29.

```
void Amplitudes::t2_uncoupled_term2(Array<double,4> ans){
    for(j=0; j<nh; j++){
        for(i=0; i<nh; i++){
            for(b=0; b<np; b++){
                for(a=0; a<np; a++){
                    temp = 0.0;
                    for(d=0; d<np; d++){
                        for(c=0; c<np; c++){
                            if(a!=c || b!=d){
                                temp = temp + V->pppp(a,b,c,d)*t2_old(c,d,i,j);
                            }
                        }
                    }
                    ans(a,b,i,j) = 0.5*temp;
                }
            }
        }
    }
} // end t2_uncoupled_term2
```

Listing 6.29: M.P.Lohne's brute force implementation of amp1 class function *t2_uncoupled_term2*

The first simplification we make, is to utilize the two-particle basis embedded in the class *Basisconfig* (B), and the corresponding interaction matrices in the class *Interaction* (V). By coupling the *a*-loop and the *b*-loop into one loop over the *pp*-basis in *Basisconfig*, and repeating this for the *c*-loop and the *d*-loop, we obtain the simplification illustrated in listing 6.30

```
void Amplitudes::t2_uncoupled_term2(double ****t2){
    for(alpha=0; alpha<alphadim; alpha++){
        for(j=0; j<nh; j++){
            for(i=0; i<nh; i++){
                map1=0;
                for(p=0; p<ppbcount[alpha]; p+=2){
                    a = B->ppbasis[alpha][p];
                    b = B->ppbasis[alpha][p+1];
                    map2=0;
                    for(p2=0; p2<ppbcount[alpha]; p2+=2){
                        c = B->ppbasis[alpha][p2];
                        d = B->ppbasis[alpha][p2+1];
                        if(a!=c || b!=d){
                            t2[a][b][i][j] = ans[a][b][i][j]
                                + 0.5*V->pppp[alpha][map1][map2]*t2_old[c][d][i][j];
                            t2[b][a][i][j] = ans[b][a][i][j]

```

```

        + 0.5*V->pppp[alpha][map1][map2]*t2_old[d][c][i][j];
    }
    if(b!=e || a!=f){
        t2[b][a][i][j] = ans[b][a][i][j]
        - 0.5*V->pppp[alpha][map1][map2]*t2_old[c][d][i][j];
        t2[a][b][i][j] = ans[a][b][i][j]
        - 0.5*V->pppp[alpha][map1][map2]*t2_old[d][c][i][j];
    }
    map2+=1;
}
map1+=1;
}
}
}
} // end t2_uncoupled_term2

```

Listing 6.30: illustrates the first simplification of M. P. Lohne’s implementation of `amp1` class function `t2_uncoupled_term2`

Next we notice in listing 6.29 that the interaction matrix *pppp* have two common indices with the four-dimensional matrix *t2_old*. Remember that *t2_old* holds the *t2*-amplitudes from the previous iteration (see the CCSD algorithm fig. 6.2). Thus, this multiplication is in reality a matrix multiplication. Therefore, by mapping the four-dimensional *t2_old* into a two-dimensional matrix *t2_pppp*, we can replace these loops by a matrix multiplication. This matrix multiplication results in a significant speed-up of our code. The new matrix *t2_pppp* is created in correspondence with the three-dimensional interaction matrix *pppp*. For each possible (M, M_S) -value (see Interaction: class implementation), we create a two-dimensional *t2_pppp*-matrix with dimension $[cd, ij]$. The common dimension $[cd]$ is determined by the *pp*-basis in *Basisconfig*, while the dimension of $[ij]$ reads

$$ij = nh * (nh - 1). \quad (6.55)$$

This dimension equals the number of all pairs of *i* and *j*, where *i* and *j* are different. If *i* and *j* are equal it violates the Pauli exclusion principle. The mapping of *i* and *j* into one variable is obtained as illustrated in listing 6.31. We create an array *ij_map* with twice the size of the $[ij]$ dimension eq. (6.55), and tabulate the pairs of *i* and *j* values constituting the new *ij* values. This mapping is performed once in the *Amplitudes* constructor.

```

//mapping i, j -> ij
int ij_map = new int[2*nh*(nh-1)];
temp=0;
for(int i=0; i<nh; i++){
    for(int j=0; j<nh; j++){
        if(i!=j){
            ij_map[temp]=i;
            ij_map[temp+1]=j;
            temp+=2;
        }
    }
}
}

```

Listing 6.31: illustrates the map of the two quantum numbers *i,j* into one number *ij*

We utilize this mapping when we fill $t2_pppp$, and when we translate the new two-dimensional system back into the four-dimensional system of $t2$, see the functions $t2_pppp_fill$ and $translate$ respectively, in listing 6.21. The matrix multiplication however, is not straight forward because of the if-statements in both listing 6.29 and 6.30. We therefore create a new interaction matrix v_pppp , where these if-statements are incorporated. We incorporate the if-statements by implementing the unwanted matrix elements as zero. The matrix multiplication between $t2_pppp$ and v_pppp is then carried out, and $t2$ is obtained by translating back into a four-dimensional system, see listing 6.21.

Next we consider the class function $t2_uncoupled_term4$. This function performs the calculation of the following expression

$$\frac{1}{2}(1 - \delta_{ki}\delta_{lj})[I6]_{ij}^{kl} t_{kl}^{ab}. \quad (6.56)$$

Originally this expression was implemented with brute force by M. P. Lohne, see illustration in listing 6.32

```
void Amplitudes::t2_uncoupled_term4(Array<double,4> ans){
    for(j=0; j<nh; j++){
        for(i=0; i<nh; i++){
            for(b=0; b<np; b++){
                for(a=0; a<np; a++){
                    temp = 0.0;
                    for(l=0; l<nh; l++){
                        for(k=0; k<nh; k++){
                            if(i!=k || j!=l){
                                temp = temp + barh_09(k,l,i,j)*t2_old(a,b,k,l);
                            }
                        }
                    }
                    ans(a,b,i,j) = 0.5*temp;
                }
            }
        }
    }
} // end t2_uncoupled_term4
```

Listing 6.32: M. P. Lohne's brute force implementation of amp1 class function $t2_uncoupled_term4$

In this implementation there is no direct connections to an interaction element, thus simplification utilizing the two-particle basis embedded in the class *Basisconfig* is not obtainable. However, we observe that the four-dimensional matrices $barh_09$ and $t2_old$ have two common indices k and l . This means that by mapping the matrices into a two-dimensional form, the performed calculation is equivalent to a matrix multiplication between $barh_09[kl][ij]$ and $t2_old[ab][kl]$, which results in a matrix with dimension $[ab][ij]$. We create three new two-dimensional matrices, $barh$ representing $barh_09[kl][ij]$, A representing $t2_old[ab][kl]$, and C for performing the multiplication. The mapping from four to two dimensions is performed in a brute force way when we fill the matrices A and

barh in listing 6.23. The dimensions thus read

$$\begin{aligned} ab &= a * b = np^2, \\ ij &= i * j = nh^2, \\ kl &= k * l = nh^2. \end{aligned}$$

Note how the if-statement is incorporated in the new matrix *barh*. From here the matrix multiplication is straightforward, and the final result for *t2* is obtained by mapping back into the four-dimensional system, in the same manner which we mapped into the two-dimensional system.

In both listing 6.21 and 6.23 we are utilizing Open Multi-Processing (OMP), which is an application for parallelizing programs in a shared memory environment. OMP provides tools which create and manage threads automatically, and this makes parallelizing a much easier job. Parallel computing refers to computations where many calculations are carried out simultaneously, such that large and time consuming problems can be divided between threads into smaller ones, and then solved concurrently. Pragmas are special compiler commands, providing the compiler with additional information. OMP contains a set of pragmas which instructs the compiler to parallelize the code, but only if the compiler support OMP. The most basic pragma is the "`#pragma omp parallel`", which denotes the region one wish to parallelize. OMP is thereby a source to speed-up of our code. However, it is worth noticing that OMP cannot run on different remote machines, like in a cluster of machines. This means that the speed-up is limited by the number of processors on the single machine performing the calculation. OMP is a widely accepted application, and it is supported by the big vendors like Sun and Intel. For complementary details on OMP we refer to the websites of these vendors.

Intermediates

In the following we present the implementation of the intermediates for both amplitudes \hat{T}_1 and \hat{T}_2 . We are not utilizing matrix multiplication when calculating the intermediates, even though this is possible in some of the calculations. We did not prioritize this implementation, because the time expenditure of calculating the intermediates did not imply that this would constitute a great speed-up of our code. We have implemented the intermediates using the technique of considering only the contributing matrix elements, which satisfy eq. (6.11). Therefor we present the implementations without further explanation.

$$[I1]_b^a = f_b^a + \langle bc|v|aj\rangle t_j^c$$

```
void Amplitudes::ccsd_uncoupled_barh_i02a_store(){
    //initializing barh_i02a ([I1]) by including f_{b}^{a}
    for(int a=0; a<np; a++){
        for(int b=a; b<np; b++){
            barh_i02a[a][b] = F->f_pp[a][b];
            barh_i02a[b][a] = F->f_pp[b][a];
        }
    }
}
```

```

// calculating second term of [I1]
for (alpha=ph_alphamin; alpha<ph_alphamax; alpha++){
  map1=0;
  for (p=0; p<ppbcount[alpha]; p+=2){
    b = B->ppbasis[alpha][p];
    c = B->ppbasis[alpha][p+1];
    map2=0;
    for (ph=0; ph<phbcount[alpha]; ph+=2){
      a = B->phbasis[alpha][ph];
      j = B->phbasis[alpha][ph+1];
      barh_i02a[a][b] += V->ppph[alpha][map1][map2]*t1[c][j];
      barh_i02a[a][c] -= V->ppph[alpha][map1][map2]*t1[b][j];
      map2+=1;
    }
    map1+=1;
  }
}
//end [I1]

```

Listing 6.33: implementation of I1 in the amp1 class function ccscd_uncoupled_barh_i02a_store

$$[I2]_c^k = f_c^k + \langle bc|v|jk\rangle t_j^b$$

```

void Amplitudes::ccscd_uncoupled_barh_01_store(){
  //initializing barh_01 ([I2]) by including f- {c} ^{k}
  for (int c=0; c<nh; c++){
    for (int k=0; k<np; k++){
      barh_01[c][k] = F->f_hp[c][k];
    }
  }
  //calculating second term of [I2]
  for (alpha=hh_alphamin; alpha<hh_alphamax; alpha++){
    map1=0;
    for (p=0; p<ppbcount[alpha]; p+=2){
      c = B->ppbasis[alpha][p];
      b = B->ppbasis[alpha][p+1];
      map2=0;
      for (h=0; h<hhbcount[alpha]; h+=2){
        k = B->hhbasis[alpha][h];
        j = B->hhbasis[alpha][h+1];
        barh_01[k][c] += V->pphh[alpha][map1][map2]*t1[b][j];
        barh_01[k][b] -= V->pphh[alpha][map1][map2]*t1[c][j];
        barh_01[j][c] -= V->pphh[alpha][map1][map2]*t1[b][k];
        barh_01[j][b] += V->pphh[alpha][map1][map2]*t1[c][k];
        map2+=1;
      }
      map1+=1;
    }
  }
}
//end [I2]

```

Listing 6.34: implementation of I2 in the amp1 class function ccscd_uncoupled_barh_01_store

$$[I3]_i^j = f_i^j - \langle bi|v|jk\rangle t_k^b + \frac{1}{2} \langle bc|v|jk\rangle t_{ik}^{bc} + [I2]_b^j t_i^b$$

```

void Amplitudes::ccsd_uncoupled_barh_03_store(){

    //initializing barh_03 ([I3]) by including f- $\{i\}^{\{j\}}$ 
    for(int i=0; i<nh; i++){
        for(int j=i; j<nh; j++){
            barh_03[i][j] = F->f_hh[i][j];
            barh_03[j][i] = F->f_hh[j][i];
        }
    }

    //calculating [I2]
    for(j=0; j<nh; j++){
        for(i=0; i<nh; i++){
            for(b=0; b<np; b++){
                barh_03[j][i] = barh_03[j][i] + barh_01[j][b]*t1[b][i];
            }
        }
    }

    //calculating second term of [I3]
    for(alpha=hh_alphamin; alpha<hh_alphamax; alpha++){
        map1=0;
        for(ph=0; ph<phbcount[alpha]; ph+=2){
            b = B->phbasis[alpha][ph];
            i = B->phbasis[alpha][ph+1];
            map2=0;
            for(h=0; h<hhbcount[alpha]; h+=2){
                j = B->hhbasis[alpha][h];
                k = B->hhbasis[alpha][h+1];
                barh_03[j][i] -= V->p_hhh[alpha][map1][map2]*t1[b][k];
                barh_03[k][i] += V->p_hhh[alpha][map1][map2]*t1[b][j];
                map2+=1;
            }
            map1+=1;
        }
    }

    //calculating third term of [I3]
    for(alpha=hh_alphamin; alpha<hh_alphamax; alpha++){
        map1=0;
        for(p=0; p<ppbcount[alpha]; p+=2){
            b = B->ppbasis[alpha][p];
            c = B->ppbasis[alpha][p+1];
            map2=0;
            for(h=0; h<hhbcount[alpha]; h+=2){
                j = B->hhbasis[alpha][h];
                k = B->hhbasis[alpha][h+1];
                for(i=0; i<nh; i++){
                    barh_03[j][i] += V->p_phh[alpha][map1][map2]*t2[b][c][i][k];
                    barh_03[k][i] -= V->p_phh[alpha][map1][map2]*t2[b][c][i][j];
                }
                map2+=1;
            }
            map1+=1;
        }
    }
}

```

```
} //end [I3]
```

Listing 6.35: implementation of I3 in the amp1 class function ccscd_uncoupled_barh_03_store

$$[I4]_{ic}^{jk} = [I5]_{ic}^{jk} + \frac{1}{2} \langle bc|v|jk \rangle t_i^b$$

```
void Amplitudes::ccsd_uncoupled_barh_07_store(){
    //initializing barh_07 ([I4]) by including [I5]-{ic}^{jk}
    for(int j=0; j<nh; j++){
        for(int k=j; k<nh; k++){
            for(int i=0; i<nh; i++){
                for(int c=0; c<np; c++){
                    barh_07[j][k][i][c] = barh_i07a[j][k][i][c];
                    barh_07[k][j][i][c] = barh_i07a[k][j][i][c];
                }
            }
        }
    }
    //calculating second term of [I4]
    for(alpha=hh_alphamin; alpha<hh_alphamax; alpha++){
        map1=0;
        for(p=0; p<ppbcount[alpha]; p+=2){
            b = B->ppbasis[alpha][p];
            c = B->ppbasis[alpha][p+1];
            map2=0;
            for(h=0; h<hhbcount[alpha]; h+=2){
                j = B->hhbasis[alpha][h];
                k = B->hhbasis[alpha][h+1];
                temp3 = 0.5 * V->pphh[alpha][map1][map2];
                for(i=0; i<nh; i++){
                    temp1 = temp3*t1[f][i];
                    temp2 = temp3*t1[e][i];
                    barh_07[j][k][i][c] += temp1;
                    barh_07[j][k][i][b] -= temp2;
                    barh_07[k][j][i][c] -= temp1;
                    barh_07[k][j][i][b] += temp2;
                }
                map2+=1;
            }
            map1+=1;
        }
    }
} //end[I4]
```

Listing 6.36: implementation of I4 in the amp1 class function ccscd_uncoupled_barh_07_store

$$[I5]_{ic}^{jk} = -\langle ci|v|jk \rangle + \frac{1}{2} \langle bc|v|jk \rangle t_i^b$$

```
void Amplitudes::ccsd_uncoupled_barh_i07a_store(){
    //calculating first term of [I5] (barh_i07a)
    for(alpha=hh_alphamin; alpha<hh_alphamax; alpha++){
        map1=0;
```

```

    for(ph=0; ph<phbcount[alpha]; ph+=2){
        c = B->phbasis[alpha][ph];
        i = B->phbasis[alpha][ph+1];
        map2=0;
        for(h=0; h<hhbcount[alpha]; h+=2){
            j = B->hhbasis[alpha][h];
            k = B->hhbasis[alpha][h+1];
            barh_i07a[j][k][i][c] = -V->phhh[alpha][map1][map2];
            barh_i07a[k][j][i][c] = +V->phhh[alpha][map1][map2];
            map2+=1;
        }
        map1+=1;
    }
}
//calculating second term of [I5]
for(alpha=hh_alphamin; alpha<hh_alphamax; alpha++){
    map1=0;
    for(p=0; p<ppbcount[alpha]; p+=2){
        b = B->ppbasis[alpha][p];
        c = B->ppbasis[alpha][p+1];
        map2=0;
        for(h=0; h<hhbcount[alpha]; h+=2){
            j = B->hhbasis[alpha][h];
            k = B->hhbasis[alpha][h+1];
            temp3 = 0.5*V->pphh[alpha][map1][map2];
            for(i=0; i<nh; i++){
                temp1 = temp3*t1[b][i];
                temp2 = temp3*t1[c][i];
                barh_i07a[j][k][i][c] += temp1;
                barh_i07a[k][j][i][c] -= temp1;
                barh_i07a[k][j][i][b] += temp2;
                barh_i07a[j][k][i][b] -= temp2;
            }
            map2+=1;
        }
        map1+=1;
    }
}
} //end [I5]

```

Listing 6.37: implementation of I5 in the amp1 class function ccsd_uncoupled_barh_i07a_store

$$[I6]_{ij}^{kl} = \langle kl|v|ij\rangle + \frac{1}{2}\langle cd|v|kl\rangle t_{ij}^{cd} + \hat{P}_{(ij)}[I5]_{ic}^{kl} t_j^c$$

```

void Amplitudes::ccsd_uncoupled_barh_09_store(){
    //calculating first term of [I6] (barh_09)
    for(alpha=hh_alphamin; alpha<hh_alphamax; alpha++){
        map1=0;
        for(i=0; i<hhbcount[alpha]; i+=2){
            k = B->hhbasis[alpha][i];
            l = B->hhbasis[alpha][i+1];
            map2=0;
            for(j=0; j<hhbcount[alpha]; j+=2){
                i=B->hhbasis[alpha][j];
            }
        }
    }
}

```



```

        j=B->hhbasis[alpha][j+1];
        barh_09[k][l][i][j] = V->hhhh[alpha][map1][map2];
        barh_09[k][l][j][i] = -V->hhhh[alpha][map1][map2];
        barh_09[l][k][i][j] = -V->hhhh[alpha][map1][map2];
        barh_09[l][k][j][i] = V->hhhh[alpha][map1][map2];
        map2+=1;
    }
    map1+=1;
}
}
//calculating the [I5] term of [I6]
for(k=0; k<nh; k++){
    for(l=0; l<nh; l++){
        for(i=0; i<nh; i++){
            for(j=0; j<nh; j++){
                temp = 0.0;
                for(c=0; c<np; c++){
                    temp = temp + (barh_i07a[k][l][i][c]*t1[c][j]
                        - barh_i07a[k][l][j][c]*t1[c][i]);
                }
                barh_09[k][l][i][j] += temp;
            }
        }
    }
}
//calculating second term of [I6]
for(alpha=0; alpha<alphadim; alpha++){
    map1=0;
    for(p=0; p<ppbcount[alpha]; p+=2){
        c = B->ppbasis[alpha][p];
        d = B->ppbasis[alpha][p+1];
        map2=0;
        for(h=0; h<hhbcount[alpha]; h+=2){
            k = B->hhbasis[alpha][h];
            l = B->hhbasis[alpha][h+1];
            for(j=0; j<nh; j++){
                for(i=0; i<nh; i++){
                    temp1 = V->pphh[alpha][map1][map2]*t2[c][d][i][j];
                    barh_09[k][l][i][j] += temp1;
                    barh_09[l][k][i][j] -= temp1;
                }
            }
            map2+=1;
        }
        map1+=1;
    }
}
} //end [I6]

```

Listing 6.38: implementation of I6 in the amp1 class function ccscd_uncoupled_barh_09_store

$$[I7]_d^a = [I1]_d^a - [I2]_d^k t_k^a - \frac{1}{2} \langle dc|v|kl \rangle t_{kl}^{ac}$$

```

void Amplitudes::ccsd_uncoupled_barh_02_store(){

    //initializing barh_02 ([I7]) by including [I1]
    for(int a=0; a<np; a++){
        for(int d=a; d<np; d++){
            barh_02[a][d] = barh_i02a[a][d];
            barh_02[d][a] = barh_i02a[d][a];
        }
    }
    //including the [I2] term
    for(a=0; a<np; a++){
        for(d=0; d<np; d++){
            for(k=0; k<nh; k++){
                barh_02[a][d] = barh_02[a][d] - barh_01[k][d] * t1[a][k];
            }
        }
    }
    //calculating the third term of [I7]
    for(alpha=hh_alphamin; alpha<hh_alphamax; alpha++){
        for(a=0; a<np; a++){
            map1=0;
            for(p=0; p<ppbcount[alpha]; p+=2){
                d = B->ppbasis[alpha][p];
                c = B->ppbasis[alpha][p+1];
                map2=0;
                for(h=0; h<hhbcount[alpha]; h+=2){
                    k = B->hhbasis[alpha][h];
                    l = B->hhbasis[alpha][h+1];
                    temp1= V->pphh[alpha][map1][map2]*t2[a][c][k][l];
                    temp2= V->pphh[alpha][map1][map2]*t2[a][d][k][l];
                    barh_02[a][d] -=temp1;
                    barh_02[a][c] +=temp2;
                    map2+=1;
                }
                map1+=1;
            }
        }
    }
} //end[I7]

```

Listing 6.39: implementation of I7 in the amp1 class function ccsd_uncoupled_barh_02_store

$$[I8]_{cj}^{kb} = [I9]_{cj}^{kb} + \frac{1}{2} \langle dc|v|bk \rangle t_j^d - [I4]_{jc}^{lk} t_l^b + \frac{1}{2} \langle cd|v|kl \rangle t_{jl}^{bd}$$

```

void Amplitudes::ccsd_uncoupled_barh_i10b_store(){

    //initializing barh_i10b, equivalent to calculating [I9]
    for(int k=0; k<nh; k++){
        for(int b=0; b<np; b++){
            for(int c=b; c<np; c++){
                for(int j=k; j<nh; j++){

```

```

        barh_i10b[k][b][c][j] = barh_i10a[k][b][c][j];
        barh_i10b[j][b][c][k] = barh_i10a[j][b][c][k];
        barh_i10b[k][c][b][j] = barh_i10a[k][c][b][j];
        barh_i10b[j][c][b][k] = barh_i10a[j][c][b][k];
    }
}
}
}
//calculating second term of [I8]
for(alpha=ph_alphamin; alpha<ph_alphamax; alpha++){
    map1=0;
    for(p=0; p<ppbcount[alpha]; p+=2){
        d = B->ppbasis[alpha][p];
        c = B->ppbasis[alpha][p+1];
        map2=0;
        for(ph=0; ph<phbcount[alpha]; ph+=2){
            b = B->phbasis[alpha][ph];
            k = B->phbasis[alpha][ph+1];
            temp = 0.5 * V->ppph[alpha][map1][map2];
            for(j=0; j<nh; j++){
                barh_i10b[k][b][c][j] += temp*t1[d][j];
                barh_i10b[k][b][d][j] -= temp*t1[c][j];
            }
            map2+=1;
        }
        map1+=1;
    }
}
//calculating 0.5*[I4]
for(k=0; k<nh; k++){
    for(b=0; b<np; b++){
        for(c=0; c<np; c++){
            for(j=0; j<nh; j++){
                temp1=0.0;
                for(l=0; l<nh; l++){
                    temp1 += 0.5 * barh_07[l][k][j][c]*t1[b][l];
                }
                barh_i10b[k][b][c][j]-=temp1;
            }
        }
    }
}
} //end part of [I8]

void Amplitudes::ccsd_uncoupled_barh_i10c_store(){
    //initializing barh_i10c ([I8]) by including barh_i10b
    for(int k=0; k<nh; k++){
        for(int b=0; b<np; b++){
            for(int c=b; c<np; c++){
                for(int j=k; j<nh; j++){
                    barh_i10c[k][b][c][j] = barh_i10b[k][b][c][j];
                    barh_i10c[j][b][c][k] = barh_i10b[j][b][c][k];
                    barh_i10c[k][c][b][j] = barh_i10b[k][c][b][j];
                    barh_i10c[j][c][b][k] = barh_i10b[j][c][b][k];
                }
            }
        }
    }
}

```

```

    }
  }
}
//calculating 0.5*[I4]
for(k=0; k<nh; k++){
  for(b=0; b<np; b++){
    for(c=0; c<np; c++){
      for(j=0; j<nh; j++){
        temp1=0.0;
        for(l=0; l<nh; l++){
          temp1 += 0.5 * barh_07[l][k][j][c]*t1[b][l];
        }
        barh_i10b[k][b][c][j]-=temp1;
      }
    }
  }
}
//calculating last term of [I8]
for(b=0; b<np; b++){
  for(alpha=hh_alphamin; alpha<hh_alphamax; alpha++){
    map1=0;
    for(p=0; p<ppbcount[alpha]; p+=2){
      d = B->ppbasis[alpha][p];
      c = B->ppbasis[alpha][p+1];
      map2=0;
      for(h=0; h<hhbcount[alpha]; h+=2){
        l = B->hhbasis[alpha][h];
        k = B->hhbasis[alpha][h+1];
        temp1 = 0.5*V->pphh[alpha][map1][map2];
        for(j=0; j<nh; j++){
          barh_i10c[k][b][c][j] += temp1*t2[b][d][j][l];
          barh_i10c[k][b][d][j] -= temp1*t2[b][c][j][l];
          barh_i10c[l][b][c][j] -= temp1*t2[b][d][j][k];
          barh_i10c[l][b][d][j] += temp1*t2[b][c][j][k];
        }
        map2+=1;
      }
      map1+=1;
    }
  }
}
} //end [I8]

```

Listing 6.40: implementation of I8 in the amp1 class function ccscd_uncoupled_barh_i10b_store and ccscd_uncoupled_barh_i10c_store

$$[I9]_{cj}^{kb} = -\langle bk|v|cj\rangle + \frac{1}{2}\langle dc|v|bk\rangle t_j^d$$

```

void Amplitudes::ccscd_uncoupled_barh_i10a_store(){
  //calculating first term of [I9] (barh_i10a)
  for(alpha=ph_alphamin; alpha<ph_alphamax; alpha++){
    map1=0;
    for(ph=0; ph<phbcount[alpha]; ph+=2){
      b = B->phbasis[alpha][ph];

```

```

    k = B->phbasis [ alpha ] [ ph+1];
    map2=0;
    for (ph2=0; ph2<phbcount [ alpha ]; ph2+=2){
        c = B->phbasis [ alpha ] [ ph2];
        j = B->phbasis [ alpha ] [ ph2+1];
        barh_i10a [k] [b] [c] [j] = -V->phph [ alpha ] [ map1 ] [ map2 ];
        map2+=1;
    }
    map1+=1;
}
}
//calculating second term of [I9]
for (alpha=ph_alphamin; alpha<ph_alphamax; alpha++){
    map1=0;
    for (p=0; p<ppbcount [ alpha ]; p+=2){
        d = B->ppbasis [ alpha ] [ p];
        c = B->ppbasis [ alpha ] [ p+1];
        map2=0;
        for (ph=0; ph<phbcount [ alpha ]; ph+=2){
            b = B->phbasis [ alpha ] [ ph];
            k = B->phbasis [ alpha ] [ ph+1];
            temp = 0.5 * V->ppph [ alpha ] [ map1 ] [ map2 ];
            for (j=0; j<nh; j++){
                barh_i10a [k] [b] [c] [j] += temp*t1 [d] [j];
                barh_i10a [k] [b] [d] [j] -= temp*t1 [c] [j];
            }
            map2+=1;
        }
        map1+=1;
    }
}
} //end [I9]

```

Listing 6.41: implementation of I9 in the amp1 class function ccscd_uncoupled_barh_i10a_store

$$[I10]_{ij}^{kb} = -\langle bk|v|ij\rangle - \frac{1}{2}\langle cd|v|bk\rangle t_{ij}^{cd} + \hat{P}_{(ij)}[I9]_{cj}^{kb} t_i^c - \frac{1}{2}[I6]_{ij}^{kl} t_l^b$$

```

void Amplitudes::ccscd_uncoupled_barh_i12a_store(){
    //calculating first term of [I10] (barh_i12a)
    for (alpha=hh_alphamin; alpha<hh_alphamax; alpha++){
        map1=0;
        for (ph=0; ph<phbcount [ alpha ]; ph+=2){
            b = B->phbasis [ alpha ] [ ph];
            k = B->phbasis [ alpha ] [ ph+1];
            map2=0;
            for (h=0; h<hhbcount [ alpha ]; h+=2){
                i = B->hhbasis [ alpha ] [ h];
                j = B->hhbasis [ alpha ] [ h+1];
                barh_i12a [k] [b] [i] [j] = -V->phhh [ alpha ] [ map1 ] [ map2 ];
                barh_i12a [k] [b] [j] [i] = +V->phhh [ alpha ] [ map1 ] [ map2 ];
                map2+=1;
            }
            map1+=1;
        }
    }
}

```

```

}
// calculating the [I9] term of [I10]
for(k=0; k<nh; k++){
  for(b=0; b<np; b++){
    for(j=0; j<nh; j++){
      for(i=0; i<nh; i++){
        temp = 0.0;
        for(c=0; c<np; c++){
          temp = temp + (barh_i10a[k][b][c][j]*t1[c][i]
            - barh_i10a[k][b][c][i]*t1[c][j]);
        }
        barh_i12a[k][b][i][j] = barh_i12a[k][b][i][j] + temp;
      }
    }
  }
}
// calculating the [I6] term of [I10]
for(k=0; k<nh; k++){
  for(b=0; b<np; b++){
    for(j=0; j<nh; j++){
      for(i=0; i<nh; i++){
        temp = 0.0;
        for(l=0; l<nh; l++){
          temp = temp + barh_09[k][l][i][j]*t1[b][l];
        }
        barh_i12a[k][b][i][j] = barh_i12a[k][b][i][j] - 0.5*temp;
      }
    }
  }
}
//calculating second term of [I10]
for(alpha=ph_alphamin; alpha<ph_alphamax; alpha++){
  map1=0;
  for(p=0; p<ppbcount[alpha]; p+=2){
    c = B->ppbasis[alpha][p];
    d = B->ppbasis[alpha][p+1];
    map2=0;
    for(ph=0; ph<phbcount[alpha]; ph+=2){
      b = B->phbasis[alpha][ph];
      k = B->phbasis[alpha][ph+1];
      for(i=0; i<nh; i++){
        for(j=0; j<nh; j++){
          barh_i12a[k][b][i][j] -= V->ppph[alpha][map1][map2]
            *t2[c][d][i][j];
        }
      }
      map2+=1;
    }
    map1+=1;
  }
}
} //end [I10]

```

Listing 6.42: implementation of I10 in the amp1 class function ccsd_uncoupled_barh_i12a_store

$$[I11]_{cj}^{ab} = \langle ab|v|cj\rangle + \frac{1}{2}\langle ab|v|cd\rangle t_j^d$$

```

void Amplitudes::ccsd_uncoupled_barh_i11a_store(){

    //calculating first term of [11] (barh_i11a)
    for(alpha=ph_alphamin; alpha<ph_alphamax; alpha++){
        map1=0;
        for(p=0; p<ppbcount[alpha]; p+=2){
            a = B->ppbasis[alpha][p];
            b = B->ppbasis[alpha][p+1];
            map2=0;
            for(ph=0; ph<phbcount[alpha]; ph+=2){
                c = B->phbasis[alpha][ph];
                j = B->phbasis[alpha][ph+1];
                barh_i11a[a][b][c][j] = V->ppph[alpha][map1][map2];
                barh_i11a[b][a][c][j] = -V->ppph[alpha][map1][map2];
                map2+=1;
            }
            map1+=1;
        }
    }

    //calculating second term of [11]
    for(alpha=0; alpha<alphadim; alpha++){
        for(j=0; j<nh; j++){
            map1=0;
            for(p=0; p<ppbcount[alpha]; p+=2){
                a = B->ppbasis[alpha][p];
                b = B->ppbasis[alpha][p+1];
                map2=0;
                for(p2=0; p2<ppbcount[alpha]; p2+=2){
                    c = B->ppbasis[alpha][p2];
                    d = B->ppbasis[alpha][p2+1];
                    temp3 = 0.5*V->pppp[alpha][pmap][p2map];
                    temp1 = temp3*t1[f][i];
                    temp2 = temp3*t1[e][i];
                    barh_i11a[a][b][c][j] += temp1;
                    barh_i11a[b][a][c][j] -= temp1;
                    barh_i11a[a][b][d][j] -= temp2;
                    barh_i11a[b][a][d][j] += temp2;
                    map2+=1;
                }
                map1+=1;
            }
        }
    }
}
} //end [I11]

```

Listing 6.43: implementation of I11 in the amp1 class function ccsd_uncoupled_barh_i11a_store

In order to get a clearer picture of the efficiency improvements implemented as depicted in listing 6.12-6.43, we refer to the master thesis of M. P. Lohne [2] for comparison.

CCalgo: CLASS implementation

CCalgo is an abstract base class with one derived class *ccsd1*. This class is managing the CCSD algorithm in fig. 6.2, from the class function *ccsd_uncoupled_start*. The implementation of this class function is rendered in listing 6.44. In this listing we observe that the reference energy of eq. (5.37), is calculated and used for initializing the energy in the first iteration. When the energy is initialized the iterative calculations is started. Note that the \hat{T} -amplitudes are initialized to zero in the *Amplitudes* class.

```
void ccsd1::ccsd_uncoupled_start(){
    // set up reference energy  $E_{ref} = \langle \phi_0 | H | \phi_0 \rangle$ 
    ccsd_uncoupled_setup_ref_energy();

    // initialize energy
    E_new = E_ref;
    E_old = 0;

    // start self-consistency procedure
    ccsd_uncoupled_iterate();
} // end ccsd_uncoupled_start
```

Listing 6.44: Implementation of the CCalgo class function *ccsd_uncoupled_start*

The reference energy is calculated in the class function *ccsd_uncoupled_setup_ref_energy*, see listing 6.45. The first term of eq. (5.37) is tabulated in the **s_hh** matrix created in the *Fmatrix* class. When calculating the second term of the equation, we utilise the *hh*-basis of *Basisconfig* to extract the desirable interaction elements from the **hhhh**-matrix of the *Interaction* class.

```
void ccsd1::ccsd_uncoupled_setup_ref_energy(){
    //  $E_{ref} = \langle \phi_0 | H | \phi_0 \rangle = \text{SUM}_i \langle i | h_0 | i \rangle + 0.5 * \text{SUM}_{ij} \langle i j | v | i j \rangle$ 
    E_ref = 0.0;
    for(i=0; i<nh; i++){
        E_ref += F->s_hh[i][i];
    }
    for(alpha=0; alpha<alphadim; alpha++){
        for(i=0; i<hhbcount[alpha]/2; i++){
            E_ref += V->hhhh[alpha][i][i];
        }
    }
} // end ccsd_uncoupled_setup_ref_energy
```

Listing 6.45: Implementation of the CCalgo class function *ccsd_uncoupled_setup_ref_energy*

The iterative process is executed in the class function *ccsd_uncoupled_iterate*, see listing 6.46. The iterative process is continued as long as the difference in energy exceeds a given tolerance, and the number of iteration is less than a given number of max iterations. Both the tolerance and the number of max iterations are input parameters to the CCSD code. First, the function calls the *Amplitudes* class functions for calculating the amplitudes. Then it proceeds by calculating the energy, and the energy difference from the previous iteration. Next it performs a test, which in cases where convergence is not obtainable,

terminates the calculations before max iteration is reached. Last, the amplitudes and the energy from the current iteration are stored, before a new iteration is initiated.

```

void ccscd1::ccsd_uncoupled_iterate(){

    diff = E_new; iter = 0;
    while(abs(diff)>tol && iter<max_iter){

        // update iteration variable
        iter = iter + 1;

        // calculate t1 amplitudes
        T->t1_uncoupled_calc();

        // calculate t2 amplitude
        T->t2_uncoupled_calc();

        // calculate energy
        ccscd_uncoupled_energy();

        // energy difference
        diff = E_new - E_old;

        if((iter>5 && E_new>5*E_old) || (iter>5 && 5*E_new<E_old)){
            break;
        }

        // update t1 and t2 amplitudes
        for(a=0; a<np; a++)
            for(i=0; i<nh; i++)
                T->t1_old[a][i] = T->t1[a][i];
        for(a=0; a<np; a++)
            for(b=0; b<np; b++)
                for(i=0; i<nh; i++)
                    for(j=0; j<nh; j++)
                        T->t2_old[a][b][i][j] = T->t2[a][b][i][j];

        // update old energy variable
        E_old = E_new;
    }

} // end ccscd_uncoupled_iterate

```

Listing 6.46: Implementation of the CCalgo class function `ccsd_uncoupled_iterate`

The CCSD energy is calculated in the class function `ccsd_uncoupled_energy`. The energy is calculated from the algebraic eq. (5.81). Also note the diagrammatic energy expression in eq. (5.96). The first term of the energy equation is calculated from the **h_{hp}** matrix in the *Fmatrix* class, and the *t1* amplitude in the *Amplitudes* class. The second and third term of the energy equation are calculated by utilizing the *pp*-basis and the *hh*-basis of *Basisconfig*, to extract the desirable interaction elements from the **p_{phh}** matrix in the *Interaction* class. The total energy is given by the sum of this CCSD energy and the reference energy, see eq. (5.43).

```

void ccsl::ccsd_uncoupled_energy(){

    //      .....
    //      -()-
    //
    partial1 = 0.0;
    for(i=0; i<nh; i++){
        for(a=0; a<np; a++){
            partial1 = partial1 + F->f_hp[i][a]*T->t1[a][i];
        }
    }

    //      .....
    //      -()- -()- + -()- -()-
    //

    partial2 = 0.0;
    partial3 = 0.0;
    for(alpha=hh_alphamin; alpha<hh_alphamax; alpha++){
        map1=0;
        for(p=0; p<ppbcount[alpha]; p+=2){
            a=B->ppbasis[alpha][p];
            b=B->ppbasis[alpha][p+1];
            map2=0;
            for(h=0; h<hhbcount[alpha]; h+=2){
                i=B->hhbasis[alpha][h];
                j=B->hhbasis[alpha][h+1];
                partial2 += V->pphh[alpha][map1][map2]*T->t1[a][i]*T->t1[b][j];
                partial2 -= V->pphh[alpha][map1][map2]*T->t1[b][i]*T->t1[a][j];
                partial3 += V->pphh[alpha][map1][map2]*T->t2[a][b][i][j];
                map2+=1;
            }
            map1+=1;
        }
    }

    partial2 = partial2;
    partial3 = partial3;

    // total uncoupled ccsl energy
    partial = partial1 + partial2 + partial3;

    // total ground state energy
    E_new = partial + E_ref;

} // end ccsl_uncoupled_energy

```

Listing 6.47: Implementation of the CCalgo class function ccsl_uncoupled_energy

6.2.2 CCSD With HF Basis

In this section we present how we perform CCSD calculations utilizing a Hartree-Fock basis instead of the harmonic oscillator basis (HMO) used so far. The reason for choosing a HF basis is that this basis leads to convergence of the CCSD calculation in a larger

frequency range compared to what we obtain with the HMO basis.

The HF basis is generated by performing a HF calculation as described in chapter 4, and implemented in section 6.1. When conducting the HF calculation we determine the basis set of orthonormal HF orbitals given by

$$\phi_a(\mathbf{r}) = \sum_{\lambda}^{d_{SP}} C_{a\lambda} \psi_{\lambda}(\mathbf{r}), \quad (6.57)$$

where d_{SP} is the dimension of the single-particle space, and

$$\mathcal{B}_{HMO} = \{\psi_{\lambda}(\mathbf{r})\}_{\lambda}^{d_{SP}}, \quad (6.58)$$

constitutes the HMO basis-set. The HF basis-set is thus denoted by

$$\mathcal{B}_{HF} = \{\phi_a(\mathbf{r})\}_{\lambda}^{d_{SP}}. \quad (6.59)$$

Note that the size of \mathcal{B}_{HF} equals the size of \mathcal{B}_{HMO} , and that they span the same single-particle space. With these definitions we obtain the following sp and tp elements

$$\langle a|\hat{h}|b\rangle = \sum_{\alpha\beta}^{d_{SP}} C_{a\alpha}^* C_{b\beta} \langle \alpha|\hat{h}|\beta\rangle, \quad (6.60)$$

and

$$\langle ab|\hat{v}|cd\rangle = \sum_{\alpha\beta\gamma\delta}^{d_{SP}} C_{a\alpha}^* C_{b\beta}^* C_{c\gamma} C_{d\delta} \langle \alpha\beta|\hat{v}|\gamma\delta\rangle, \quad (6.61)$$

where C denotes the expansion coefficients determined by the HF calculation.

In order to utilize the HF basis in the CCSD calculation, we have embedded the HF calculations in a new class *HFbasis*. In this class we perform the HF calculation, which determine the HF energy and the coefficients that enable us to produce the sp and tp elements in eqs. (6.60) and (6.61). When incorporating this new class we made some changes in the *Basisconfig*, *Fmatrix* and *Interaction* class. These changes, in addition to the new class, is presented in the following.

As already mentioned, we have implemented one version of performing the HF calculations. This version is presented in section 6.1. However, in the *HFbasis* class we were forced to make some changes to the implementation. It turns out that the matrix-diagonalization tools used in solving the HF equations in section 6.1 do not produce fully satisfying results. Strangely enough these tools produced satisfying energy results, however when calculating the eigenvectors, corresponding to the coefficients, these tools failed. We therefore conducted a search for a diagonalization tool that was able to provide us with coefficients resulting in satisfactory CCSD results. We performed HF calculations utilizing Jacobi's diagonalization method, we tested three different LAPACK routines; dgeev, zgeev and dsyeev, but they all resulted in the same unsatisfying coefficients. Finally, guided by similar HF and CCSD codes developed by my supervisor M. Hjorth-Jensen and his colleague Gaute Hagen, we developed a code where we perform block-wise diagonalization. From the condition that the quantum numbers m and m_s are conserved, we obtain a HF matrix which is block diagonal in m and m_s values. This means that for each value of (m, m_s) we diagonalize the sub-matrix corresponding to the block of that

(m, m_S) -value. This system is much smaller than the total HF matrix, and the diagonalization tools handle it more accurately. We have implemented this block-diagonal HF calculation utilizing the LAPACK routine dgeev, for asymmetric dense matrix eigenvector problems. The implementation of the iterative HF process is illustrated in listing 6.48.

```

HFbasis::HFbasis(int nh_input, int np_input,
                  basisconfig *B, char* filename, double tol, double iter)
{
    /*Crating dictionary and reading tp elements from file*/
    /*allocate and fill coulomb matrix holding the tp elements*/
    /*allocate and initialize C matrix holding the coefficients*/
    /*allocate total HF-matrix hHF*/
    /*allocate HF-matrices hHF2 holding the blocks of hHF*/
    /*allocate rho and rhon matrix tools for accelerating the convergence*/

    /*performing the iterative HF calculations*/
    while(check && count<iter){
        count++;

        /*calculating both hHF and hHF2 (Hartree-fock matrices)*/
        for(int x=0; x<alphadim_single; x++){

            mkrho(rhon,C);
            for(int i=0; i<num_spfunc; i++){
                for(int j=0; j<num_spfunc; j++){
                    rho[i][j]= 0.8*rho[i][j] + 0.2*rhon[i][j];
                }
            }

            map1=0;
            for(int a=0; a<bc_single[x]; a++){
                alpha=sc[x][a];
                map2=0;
                for(int g=0; g<bc_single[x]; g++){
                    gamma=sc[x][g];
                    if(alpha==gamma)
                        hHF[alpha][gamma] = B->energy[gamma];
                    else
                        hHF[alpha][gamma] = 0;
                    for(int b=0; b<num_spfunc; b++){
                        for(int d=0; d<num_spfunc; d++){
                            sprintf(qn_search, "%d %d %d %d", alpha,b,gamma,d);
                            search_value = v_dictionary.find(qn_search);
                            hHF[alpha][gamma] += rho[b][d]*search_value->second;
                        }
                    }
                    hHF2[x][map1][map2]=hHF[alpha][gamma];
                    map2+=1;
                }
                map1+=1;
            }
        } //end x-loop over (M,Ms) values

        /* diagonalizing the hartree-fock matrix*/
        for(int x=0; x<alphadim_single; x++){

```

```

//initializing LAPACK routine variables corresponding to x-loop (M,Ms)
double *Evals2, **Evecs;
Evals = new double[bc_single[x]];
Evecs = new double*[bc_single[x]];
for(int i=0; i<bc_single[x]; i++)
    Evecs[i] = new double[bc_single[x]];
//diagonalizing
dgeev_diag(hHF2, x, Evecs, Evals2, bc_single[x]);

//updating C
for(int i=0; i<bc_single[x]; i++){
    for(int j=0; j<bc_single[x]; j++){
        C[sc[x][i]][sc[x][j]] = Evecs[i][j];
    }
}

//deallocating local vectors Evals, Evecs
} //end x-loop

//energy check
totalEnergy = HFenergy();
if(abs(totalEnergy-prevEnergy)<tol)
    check=false;
prevEnergy=totalEnergy;
printf("I= %3d \t E_HF=%0.15f \n", count, prevEnergy);
} //end iterative process

/*calculating the final energy from last iteration*/
/*creating new sp and tp elements*/

} //end HFbasis

void HFbasis::mkrho(double **rhon, double **C)
{
    for(i=0; i<num_sfunc; i++)
        for(j=0; j<num_sfunc; j++)
            rhon[i][j]=0.0;
    for(i=0; i<num_sfunc; i++)
        for(j=0; j<num_sfunc; j++)
            for(a=0; a<nh; a++)
                rhon[i][j]=rhon[i][j]+C[i][a]*C[j][a];
} //end mkrho

```

Listing 6.48: Implementation of the HFbasis class

The HF basis first reads the tp elements from file. This file is the same interaction file as before. The implementation is the same as described in listing 6.3, except from the fact that in this implementation all the permutations of the interaction elements are stored in the dictionary. This is necessary in order to calculate the blocks of the HF-matrix. The *coulomb* interaction matrix is exactly the same as in listing 6.3, and is utilized in the energy calculation. The coefficient matrix in this implementation is expanded compared to the implementation in listing 6.4. The number of electrons now equals the number of single-particle basis functions. This is necessary because we need all the eigenvectors of the HF-matrix when we create the new sp and tp elements. Next we allocate the total HF-matrix corresponding to eq. (6.17). In addition to the total HF-matrix, we need a new

HF-matrix containing the sub-matrices of each (m, m_S) -block in the total HF-matrix. We have implemented this new matrix *hHF2* as a three-dimensional array, one dimension for the (m, m_S) -values, and the two other dimensions represents the two-dimensional matrix connecting single-particles corresponding to the (m, m_S) -values. In order to create this matrix we implemented a new configuration system in the *Basisconfig* class, see listing 6.49.

```
//calculating the single-particle max M value
int Mmax_single=(shellnumb-1);
//calculating the number of (M,MS) values
alphadim_single=4*Mmax_single+2;

/*allocating and filling the array containing the number
of single-particle states satisfying the
(M,MS) value, corresponding to the array-index */
bc_single=new int [ alphadim_single ];
alpha=0;
for(int l=-Mmax_single; l<=Mmax_single; l++){
    mvalue=l;
    for(msvalue=-0.5; msvalue<=0.5; msvalue++){
        bsize=0;
        for(int i=0; i<num_spfunc; i++){
            if(mvalue==m[i] && msvalue==ms[i]){
                bsize+=1;
            }
            bc_single [ alpha ]= bsize ;
            alpha+=1;
        }
    }
}
/*allocating and filling the array containing the
quantum numbers of single-particle states satisfying the
(M,MS) value, corresponding to the array-row-number*/
sc=new int * [ alphadim_single ];
for(int i=0; i<alphadim_single; i++){
    sc[i]=new int [ bc_single [ i ] ];
    alpha=0;
    for(int l=-Mmax_single; l<=Mmax_single; l++){
        mvalue=l;
        for(msvalue=-0.5; msvalue<=0.5; msvalue++){
            bsize=0;
            for(int i=0; i<num_spfunc; i++){
                if(mvalue==m[i] && msvalue==ms[i]){
                    sc [ alpha ] [ bsize ]= i ;
                    bsize+=1;
                }
            }
            alpha+=1;
        }
    }
}
```

Listing 6.49: Additional code implementation in the *Basisconfig* class, necessary for the implementation of the *HFbasis* class

First we determine the largest m value the single-particle states can reach with a given shell number. The shell number is already determined in the *Basisconfig* class, see section

6.2.1. We are now dealing with the single particle system in contrast to earlier, when we were considering the two-particle system. The maximal m -value is therefore one half of the eq. (6.13). This is also established by observing fig. 3.1. The number of (m, m_S) -values of the single-particle system is calculated based on the following relations

$$m = 0, \pm 1, \pm 2, \dots, \pm M_{max}, \quad (6.62)$$

$$m_S = \pm \frac{1}{2}. \quad (6.63)$$

When these two variables are determined, we first count the number of single-particles that corresponds to each (m, m_S) -value, and tabulate the number in the basis count array denoted *bc_single*. Next, we tabulate the quantum numbers of these single-particles in the array denoted *sc* (single coupling). This technique is similar to the one we are utilizing for the two-particle basis system.

The single-particle configuration is utilized in constructing and calculating the new HF-matrix. See listing 6.48, where both hHF and hHF2 is calculated. For each single-particle (m, m_S) -value, we calculate the sub-block of the HF-matrix (eq. (4.20)), by using the tabulated block-relation of the single-particle orbitals. Note how we instead of using the coefficient matrix in calculating the HF-matrices, we use *rho*. *Rho* is a composition of itself and *rhon*. *Rhon* is calculated in the class function *mkrho*, and equals the original coefficient multiplication in the HF-matrix expression. This is a practitioner's trick, which we have adopted from Gaute Hagen's HF code. The trick is implemented because it results in a quicker convergence of the code.

Next we diagonalize the sub-matrices, constituting blocks of the HF-matrix, one by one. The sub-matrices are tabulated in hHF2, and they are diagonalized by the LAPACK routine *dgeev* shown in listing 6.50. On input *a* is the HF sub-matrix interpreted as an one-dimensional array. On output *Evals* is the array containing the eigenvalues, and *Evecs* contains the eigenvectors stored column-wise. Note that we sort the eigenvalues and eigenvectors in an ascending order in the class function *mysort*.

```
void HFbasis::dgeev_diag(double ***hHF, int chanel,
                        double **Evecs, double *Evals, int n)
{
    char jobvl, jobvr;
    int info, lda, ldvl, ldvr, lwork;
    double *wi, *vl, *vr, *work, *a;

    jobvr='V'; jobvl='N';
    lda=n; ldvr=n; ldvl=n; lwork=10000;
    wi=new double[n];
    vl=new double[n*n];
    vr=new double[n*n];
    work=new double[lwork];

    a=new double[n*n];
    for(int i=0; i<n; i++){
        for(int j=0; j<n; j++){
            a[i+j*n]=hHF[chanel][i][j];
        }
    }

    dgeev_(&jobvl, &jobvr, &n, a, &lda, Evals, wi,
```

```

        vl , &ldvl , vr , &ldvr , work , &lwork , &info );

    for (int i=0; i<n; i++){
        for (int j=0; j<n; j++){
            Evecs [ i ] [ j ] = vr [ i+j*n ];
        }
    }

    mysort (Evecs , Evals , n );
}

```

Listing 6.50: Illustrates the implementation of the HFbasis class function `dgeev_diag`, which diagonalize the HF-matrix utilizing the LAPACK routine `dgeev`

When the iterative HF process is completed, the HF energy is determined along with the coefficients. The next step is to calculate the new sp and tp elements corresponding to the new HF basis, eq. (6.60) and (6.61), respectively. This is implemented as illustrated in listing 6.51. The sp elements are calculated straightforwardly, and tabulated in the array *new_spenergy*. In this array the indices correspond to the quantum number of the sp state. The tp elements, however, are calculated by performing a matrix multiplication. We observe in eq. (6.61) that if we combine *ab*, *cd*, $\alpha\beta$, and $\gamma\delta$ such that all four pairs are represented by one number, then the matrix elements constitute two-dimensional matrices, and two and two coefficients can be combined to two-dimensional matrices. Thus, eq. (6.61) equals a matrix multiplication of $C[ab][\alpha\beta]$, $C[cd][\gamma\delta]$ and *coulomb* $[\alpha\beta][\gamma\delta]$. The conversion which presents the four pairs of quantum numbers, as four numbers, is already executed in *Basisconfig*, where we have tabulated all pairs of quantum numbers resulting in contributing interaction elements in the matrix *totbasis*. We use *totbasis* when we construct the matrices $C[ab][\alpha\beta]$ and $C[cd][\gamma\delta]$ in *A* and *D* respectively. The matrix multiplication is carried out in two steps, first we multiply $C[ab][\alpha\beta]$ with the interaction matrix *coulomb* $[\alpha\beta][\gamma\delta]$. This multiplication is stored in the *R* matrix, which then is multiplied with $C[cd][\gamma\delta]$. The resulting tp elements are tabulated in a new dictionary *new_vdict*.

```

/*creating the new sp elements*/
new_spenergy=new double [ num_spfunc ];
double new_oscEnergy;
for (int a=0; a<num_spfunc; a++){
    new_oscEnergy=0;
    for (int i=0; i<num_spfunc; i++){
        for (int j=0; j<num_spfunc; j++){
            if (i==j)
                new_oscEnergy += Ccomplete [ i ] [ a ] * Ccomplete [ j ] [ a ] * B->energy [ j ];
            else
                new_oscEnergy += 0.0;
        }
    }
    new_spenergy [ a ] = new_oscEnergy;
}

/*creating the new tp elements*/

//allocating matrix: A[ ][ ][ ][ ], D[ ][ ][ ][ ], R[ ][ ][ ][ ]

```



```

double ***A,***D,***R;
double temp;
A= new double**[alphadim];
D= new double**[alphadim];
R= new double**[alphadim];
for (int i=0; i<alphadim; i++){
  A[i]= new double*[bc[i]];
  D[i]= new double*[bc[i]];
  R[i]= new double*[bc[i]];
  for (int j=0; j<bc[i]; j++){
    A[i][j]= new double[bc[i]/2];
    D[i][j]= new double[bc[i]/2];
    R[i][j]= new double[bc[i]/2];
    for (int k=0; k<bc[i]/2; k++){
      A[i][j][k]= 0.0;
      D[i][j][k]= 0.0;
      R[i][j][k]= 0.0;
    }
  }
}
//filling A matrix
for (int a=0; a<alphadim; a++){
  for (int k=0; k<bc[a]; k+=2){
    map1=0;
    for (int i=0; i<bc[a]; i+=2){
      A[a][k][map1]=C[totbasis[a][i]][totbasis[a][k]]
                    *C[totbasis[a][i+1]][totbasis[a][k+1]];
      A[a][k+1][map1]=C[totbasis[a][i+1]][totbasis[a][k]]
                      *C[totbasis[a][i]][totbasis[a][k+1]];
      map1+=1;
    }
  }
}
//filling D matrix
for (int a=0; a<alphadim; a++){
  for (int l=0; l<bc[a]; l+=2){
    map1=0;
    for (int j=0; j<bc[a]; j+=2){
      D[a][l][map1]=C[totbasis[a][j]][totbasis[a][l]]
                    *C[totbasis[a][j+1]][totbasis[a][l+1]];
      D[a][l+1][map1]=C[totbasis[a][j+1]][totbasis[a][l]]
                      *C[totbasis[a][j]][totbasis[a][l+1]];
      map1+=1;
    }
  }
}
//executing the matrix multiplication
for (int a=0; a<alphadim; a++){
  //R[a][l][k]=A[a][l][k]*coulomb[a][l][k]
  map3=0;
  for (int k=0; k<bc[a]; k+=2){
    map1=0;
    for (int j=0; j<bc[a]; j+=2){
      map2=0;
      for (int i=0; i<bc[a]; i+=2){
        R[a][k][map1]+= A[a][k][map2]*coulomb[a][map2][map1];
      }
    }
  }
}

```

```

        R[a][k+1][map1] += A[a][k+1][map2] * coulomb[a][map2][map1];
        map2 += 1;
    }
    map1 += 1;
}
map3 += 1;
}
//<ab|v|cd>=R[a][l][l]*D[a][l][l]
map1 = 0;
for(int k=0; k<bc[a]; k+=2){
    map2 = 0;
    for(int l=0; l<bc[a]; l+=2){
        temp = 0.0;
        map3 = 0;
        for(int j=0; j<bc[a]; j+=2){
            temp += R[a][k][map3]*D[a][l][map3];
            temp -= R[a][k+1][map3]*D[a][l][map3];
            temp -= R[a][k][map3]*D[a][l+1][map3];
            temp += R[a][k+1][map3]*D[a][l+1][map3];
            map3 += 1;
        }
        sprintf(key, "%d %d %d %d", totbasis[a][k], totbasis[a][k+1],
                    totbasis[a][l], totbasis[a][l+1]);
        new_vdict.insert(MapType::value_type(key, temp));
        map2 += 1;
    }
    map1 += 1;
}
} //end alpha-loop

```

Listing 6.51: Illustrates the implementation of the calculation the new HF basis

When we have tabulated these new sp and tp elements, corresponding to a new HF basis, we utilize them in the *Fmatrix* and *Interaction* class. This results in a CCSD calculation with a HF basis. In order to do this we make the new array of sp elements, and the new dictionary of tp elements accessible to these two classes by embedding the *HFbasis* class in the CCSD code. The main.cpp code is thus implemented as in listing 6.52. We have altered both class functions *read_interaction* and *read_sp_energy* so that they no longer read from file, but fetch the sp and tp elements from the *HFbasis* class. Except from this change, the class functions perform the same operations as presented in section 6.2.1.

```

int main(int argc, char* argv[]){
    ..

    /* Basisconfig object*/
    Basisconfig* B = new Basisconfig(nh,np);

    /* HFbasis object*/
    HFbasis* H = new HFbasis(nh,np,B,tp_energy_file,tol,max_iter);

    /* interaction object*/
    Interaction* V = new int1(nh, np, B,H);
    // read interaction energy elements
    V->read_interaction();
}

```

```

/* f-matrix object*/
Fmatrix* F = new f1(nh, np, B, H);
// read single-particle energy elements
F->read_sp_energy();
// set up f-matrix
F->set_up_fmatrix(V);

/* amplitude object*/
Amplitudes* T = new Amplitudes(nh, np, B, F, V, write3, write4);

/* CCSD algorithm object*/
CCalgo* simulator = new ccsd1(nh, np, max_iter, tol, B,
                              F, V, T, write1, write2);

//// — START SIMULATION — ////
simulator->ccsd_uncoupled_start();

//delete all objects
return 0;
} // end main

```

Listing 6.52: Implementation of main.cpp in the CCSD code utilizing a HF basis

6.2.3 Code Validation

The Configuration Interaction method (CI) is considered the simplest approach to treating electron correlations. In ref. [41] the CI method is elegantly described as follows:

The CI method is perhaps the conceptually simplest of the common many-body techniques based on second quantization. It is the most accurate, in the sense that it converges to the exact solution, and that the other methods are approximations to the full-CI method (FCI). The main drawback of FCI is that the problem scales almost exponentially with the number of particles. This is called the *curse of dimensionality* and is, in fact, the main obstacle and motivation for new many-body methods.

The CI expansion of an N -electron wave function reads

$$\begin{aligned}
 \Psi_{CI} &= \left(1 + \hat{C}_1 + \hat{C}_2 + \dots\right) \Phi_0 \\
 &= \Phi_0 + \sum_{ia} C_i^a \Phi_i^a + \sum_{\substack{i < j \\ a < b}} C_{ij}^{ab} \Phi_{ij}^{ab} + \dots
 \end{aligned} \tag{6.64}$$

where $\{\hat{C}\}$ are excitation operators, Φ_0 is the reference Slater determinant, and $\Phi_{ij,\dots}^{ab,\dots}$ are excited reference Slater determinants. FCI calculations are carried out by including all terms, up to N excitations, in the CI expansion. The FCI provides an exact result within the Hilbert space generated by the chosen basis set. The FCI energy is a variational upper bound to the exact energy, and is determined solely by the selected basis set. For this reason FCI is the standard of comparison when deciding the quality of many-body

correlation methods like CCSD and many-body perturbation theory (MBPT). According to ref. [35] it is even more effective comparing with FCI than experimental data.

In the literature one often encounter what is denoted FCI. The FCI calculation is equivalent with performing an exact diagonalization. In the following we present the diagonalization problem, before we perform an exact diagonalization of the two-electron parabolic quantum dot system in three shells. We compare the result of the exact diagonalization with the CCSD calculation in order to validate the CCSD code.

The Hamiltonian of the N -electron system is defined as

$$\begin{aligned}\hat{H} &= \hat{H}_0 + \hat{V} \\ &= \sum_i \hat{h}_i + \sum_{ij} \hat{v}_{ij}.\end{aligned}\quad (6.65)$$

We define an arbitrary basis set

$$\mathcal{B} = \{|\alpha_i\rangle\}_i^d, \quad (6.66)$$

where d is the dimension of the model space. The time-independent Schrödinger equation reads

$$\hat{H}\psi_\lambda = E_\lambda\psi_\lambda. \quad (6.67)$$

In matrix notation this equation reads

$$\begin{pmatrix} \langle\Phi_0|\hat{H}|\Phi_0\rangle & \langle\Phi_0|\hat{H}|\Phi_1\rangle & \dots & \langle\Phi_0|\hat{H}|\Phi_n\rangle \\ \langle\Phi_1|\hat{H}|\Phi_0\rangle & \langle\Phi_1|\hat{H}|\Phi_1\rangle & \dots & \langle\Phi_1|\hat{H}|\Phi_n\rangle \\ \vdots & \vdots & \ddots & \vdots \\ \langle\Phi_n|\hat{H}|\Phi_0\rangle & \langle\Phi_n|\hat{H}|\Phi_1\rangle & \dots & \langle\Phi_n|\hat{H}|\Phi_n\rangle \end{pmatrix} \begin{pmatrix} c_1^\lambda \\ c_2^\lambda \\ \vdots \\ c_n^\lambda \end{pmatrix} = E_\lambda \begin{pmatrix} c_1^\lambda \\ c_2^\lambda \\ \vdots \\ c_n^\lambda \end{pmatrix}, \quad (6.68)$$

where n is the number of basis functions in the basis set of eq. (6.66), and $|\Phi_i\rangle$ is the N -electron Slater determinant constructed from the basis functions in \mathcal{B} . The connection between \mathbf{c}_λ and ψ_λ reads

$$\psi_\lambda = \sum_i^d c_i^\lambda |\Phi_i\rangle. \quad (6.69)$$

The solution of the eigenvalue eq. (6.68) is exact if $d \rightarrow \infty$. However, truncation is inevitable, and the solution represents a variational upper bound to the energy of the system. Note that if we express the Hamiltonian in second quantized form

$$\hat{H} = \sum_{\alpha\beta} \langle\alpha|\hat{h}|\beta\rangle a_\alpha^\dagger a_\beta + \frac{1}{4} \sum_{\alpha\beta\gamma\delta} \langle\alpha\beta|\hat{v}|\gamma\delta\rangle^{AS} a_\alpha^\dagger a_\beta^\dagger a_\delta a_\gamma, \quad (6.70)$$

then due to Wick's theorem in section 2.4.3, we can express the matrix elements of \hat{H} in terms of $\langle\alpha|\hat{h}|\beta\rangle$ and $\langle\alpha\beta|\hat{v}|\gamma\delta\rangle$.

In the parabolic quantum dot we utilize the harmonic oscillator functions as our single-particle basis. We obtain analytic expressions for the coulomb interaction elements $\langle\alpha\beta|\hat{v}|\gamma\delta\rangle$ in this basis by utilizing the work of ref. [44]. We are therefore able to compute the Hamiltonian of a given model space, and by diagonalizing we determine the upper bound energy and eigenvectors. This upper bound energy constitutes a basis of comparison for the corresponding energy result of the CCSD method. We chose to consider the

two-electron parabolic quantum dot with three shells. This system contains twelve basis functions. The mapping corresponding with eq. (6.4) for these twelve reads

$$\begin{array}{ll}
 |0\rangle \rightarrow |n=0, m=0; ms=-0.5\rangle & |6\rangle \rightarrow |n=0, m=-2; ms=-0.5\rangle \\
 |1\rangle \rightarrow |n=0, m=0; ms=0.5\rangle & |7\rangle \rightarrow |n=0, m=-2; ms=0.5\rangle \\
 |2\rangle \rightarrow |n=0, m=-1; ms=-0.5\rangle & |8\rangle \rightarrow |n=0, m=2; ms=-0.5\rangle \\
 |3\rangle \rightarrow |n=0, m=-1; ms=0.5\rangle & |9\rangle \rightarrow |n=0, m=2; ms=0.5\rangle \\
 |4\rangle \rightarrow |n=0, m=1; ms=-0.5\rangle & |10\rangle \rightarrow |n=1, m=0; ms=-0.5\rangle \\
 |5\rangle \rightarrow |n=0, m=1; ms=0.5\rangle & |11\rangle \rightarrow |n=1, m=0; ms=0.5\rangle.
 \end{array} \tag{6.71}$$

The Coulomb interaction is independent of spin. This property leads to the condition which states that the only nonzero matrix elements are

$$\langle M, M_S | \hat{v} | M, M_S \rangle, \tag{6.72}$$

where

$$M = m_\alpha + m_\beta = m_\gamma + m_\delta, \tag{6.73}$$

$$M_S = ms_\alpha + ms_\beta = ms_\gamma + ms_\delta. \tag{6.74}$$

In order to calculate the ground state energy of this system, we make a guess that the two electrons are present in the lowest shell of this system, thus

$$M = M_S = 0. \tag{6.75}$$

This choice result in seven possible connections of quantum numbers, viz.

$$|0, 1\rangle \quad |0, 11\rangle \quad |1, 10\rangle \quad |2, 5\rangle \quad |3, 4\rangle \quad |6, 9\rangle \quad |7, 8\rangle \quad |10, 11\rangle. \tag{6.76}$$

This results in the Hamiltonian-block matrix

$$\begin{pmatrix}
 \langle \Phi_{0,1} | \hat{H} | \Phi_{0,1} \rangle & \dots & \dots & \dots & \dots & \dots & \dots & \langle \Phi_{0,1} | \hat{H} | \Phi_{10,11} \rangle \\
 \langle \Phi_{0,11} | \hat{H} | \Phi_{0,1} \rangle & \ddots & \dots & \dots & \dots & \dots & \dots & \langle \Phi_{0,11} | \hat{H} | \Phi_{10,11} \rangle \\
 \langle \Phi_{1,10} | \hat{H} | \Phi_{0,1} \rangle & \dots & \ddots & \dots & \dots & \dots & \dots & \langle \Phi_{1,10} | \hat{H} | \Phi_{10,11} \rangle \\
 \langle \Phi_{2,5} | \hat{H} | \Phi_{0,1} \rangle & \dots & \dots & \ddots & \dots & \dots & \dots & \langle \Phi_{2,5} | \hat{H} | \Phi_{10,11} \rangle \\
 \langle \Phi_{3,4} | \hat{H} | \Phi_{0,1} \rangle & \dots & \dots & \dots & \ddots & \dots & \dots & \langle \Phi_{3,4} | \hat{H} | \Phi_{10,11} \rangle \\
 \langle \Phi_{6,9} | \hat{H} | \Phi_{0,1} \rangle & \dots & \dots & \dots & \dots & \ddots & \dots & \langle \Phi_{6,9} | \hat{H} | \Phi_{10,11} \rangle \\
 \langle \Phi_{7,8} | \hat{H} | \Phi_{0,1} \rangle & \dots & \dots & \dots & \dots & \dots & \ddots & \langle \Phi_{7,8} | \hat{H} | \Phi_{10,11} \rangle \\
 \langle \Phi_{10,11} | \hat{H} | \Phi_{0,1} \rangle & \dots & \dots & \dots & \dots & \dots & \dots & \langle \Phi_{10,11} | \hat{H} | \Phi_{10,11} \rangle
 \end{pmatrix}, \tag{6.77}$$

where the Slater determinants are defined as

$$|\Phi_{\alpha\beta}\rangle = \frac{1}{\sqrt{2}} (|\alpha\beta\rangle - |\beta\alpha\rangle). \tag{6.78}$$

By inserting the second quantized Hamiltonian of eq. (6.70) into eq. (6.77), using the dimensionless form of eq. (3.57), we obtain

$$\mathbf{H} = \begin{pmatrix} 2 + \langle 0, 1 | \hat{H} | 0, 1 \rangle & \dots & \dots & \dots & \dots & \dots & \dots & \dots & \langle 0, 1 | \hat{H} | 10, 11 \rangle \\ \langle 0, 11 | \hat{H} | 0, 1 \rangle & 4 + \langle 0, 11 | \hat{H} | 0, 11 \rangle & \dots & \dots & \dots & \dots & \dots & \dots & \langle 0, 11 | \hat{H} | 10, 11 \rangle \\ \langle 1, 10 | \hat{H} | 0, 1 \rangle & \dots & 4 + \langle 1, 10 | \hat{H} | 1, 10 \rangle & \dots & \dots & \dots & \dots & \dots & \langle 1, 10 | \hat{H} | 10, 11 \rangle \\ \langle 2, 5 | \hat{H} | 0, 1 \rangle & \dots & \dots & 4 + \langle 2, 5 | \hat{H} | 2, 5 \rangle & \dots & \dots & \dots & \dots & \langle 2, 5 | \hat{H} | 10, 11 \rangle \\ \langle 3, 4 | \hat{H} | 0, 1 \rangle & \dots & \dots & \dots & 4 + \langle 3, 4 | \hat{H} | 3, 4 \rangle & \dots & \dots & \dots & \langle 3, 4 | \hat{H} | 10, 11 \rangle \\ \langle 6, 9 | \hat{H} | 0, 1 \rangle & \dots & \dots & \dots & \dots & 6 + \langle 6, 9 | \hat{H} | 6, 9 \rangle & \dots & \dots & \langle 6, 9 | \hat{H} | 10, 11 \rangle \\ \langle 7, 8 | \hat{H} | 0, 1 \rangle & \dots & \dots & \dots & \dots & \dots & 6 + \langle 7, 8 | \hat{H} | 7, 8 \rangle & \dots & \langle 7, 8 | \hat{H} | 10, 11 \rangle \\ \langle 10, 11 | \hat{H} | 0, 1 \rangle & \dots & \dots & \dots & \dots & \dots & \dots & 6 + \langle 10, 11 | \hat{H} | 10, 11 \rangle \end{pmatrix} \quad (6.79)$$

$$= \begin{pmatrix} 3.25331 & 0.313329 & -0.313329 & 0.313329 & -0.313329 & 0.117498 & -0.117498 & 0.234996 \\ 0.313329 & 4.86165 & -0.234996 & -0.0783321 & 0.0783321 & -0.0881237 & 0.0881237 & 0.137081 \\ -0.313329 & -0.234996 & 4.86165 & 0.0783321 & -0.0783321 & 0.0881237 & -0.0881237 & -0.137081 \\ 0.313329 & -0.0783321 & 0.0783321 & 4.86165 & -0.234996 & 0.303537 & -0.146873 & 0.137081 \\ -0.313329 & 0.0783321 & -0.0783321 & -0.234996 & 4.86165 & -0.146873 & 0.303537 & -0.137081 \\ 0.117498 & -0.0881237 & 0.0881237 & 0.303537 & -0.146873 & 6.716 & -0.128514 & 0.139529 \\ -0.117498 & 0.0881237 & -0.0881237 & -0.146873 & 0.303537 & -0.128514 & 6.716 & -0.139529 \\ 0.234996 & 0.137081 & -0.137081 & 0.137081 & -0.137081 & 0.139529 & -0.139529 & 6.74905 \end{pmatrix}. \quad (6.80)$$

Note that the matrix elements are antisymmetrized. The interaction elements are calculated utilizing the analytic expression of [44]. We diagonalize this matrix in MATLAB, and obtain the ground state energy

$$E_0 = 3.0386. \quad (6.81)$$

Our CCSD code reproduces this energy result, which indicates that code is valid.

Chapter 7

Computational Results

In this chapter we present the numerical results of the Hartree-Fock (HF) and the Coupled Cluster Singles and Doubles (CCSD) calculations for the two-dimensional parabolic quantum dot. We have performed these calculations utilizing a Harmonic Oscillator (HMO) basis and a Hartree-Fock (HF) basis. We have also conducted these calculations by using two different interactions, which we have defined as a *standard interaction* and an *effective interaction*. These interactions will be introduced in the corresponding sections below, where we also present the corresponding HF and CCSD results. We start by examining the convergence of our energy results in the special case where $\omega = 1$, for two, six and twelve electron-dots. In section 7.3 we extend this convergence study to include the frequencies $\omega = 0.28$ and $\omega = 0.5$. Finally, in section 7.4, we conduct a convergence analysis for the six electron dot with frequencies $\omega = 0.01$ and $\omega = 0.015625$. We compare these results to the corresponding Diffusion Monte Carlo (DMC) and Full Configuration Interaction (FCI) results listed in ref. [45].

7.1 Standard Interaction

In this section we present the results of the HF and CCSD calculations where we have utilized a standard interaction. We have defined the Coulomb interaction as the standard interaction. The reason for selecting the Coulomb interaction as the standard interaction, is that we later introduce an effective interaction which aims to improve the results. This effective interaction is introduced in section 7.2.

The Hamiltonian of the two-dimensional parabolic quantum dot for this standard model reads

$$\hat{H} = -\frac{\hbar^2}{2m^*} \sum_{i=1}^N \nabla_i^2 + \frac{1}{2} m^* \omega^2 \sum_{i=1}^N r_i^2 + \frac{e^2}{4\pi\epsilon_o\epsilon_r} \sum_{i<j}^N \frac{1}{r_{ij}}. \quad (7.1)$$

See section 3.2.4 for more details. In section 3.2.5 we transformed eq. (7.1) into a dimensionless form, viz.

$$\hat{H}' = \frac{1}{2} \sum_{i=1}^N (-\nabla_i'^2 + \omega'^2 r_i'^2) + \sum_{i<j}^N \frac{1}{r_{ij}'}, \quad (7.2)$$

where

$$\hat{H}' = \frac{\kappa^2}{m^*} \hat{H}, \quad (7.3)$$

$$\nabla_i'^2 = l_0^2 \nabla_i^2, \quad (7.4)$$

$$\omega' = \frac{\hbar \kappa^2}{m^*} \omega, \quad (7.5)$$

$$r_i' = \frac{r_i}{l_0}, \quad (7.6)$$

$$r_{ij}' = \frac{r_{ij}}{l_0}. \quad (7.7)$$

In this dimensionless form the length is measured in units of l_0 , and the frequency ω in terms of $\frac{m^*}{\hbar \kappa^2}$. The energy is measured in terms of Hartrees E_H given as

$$E_H = \frac{m^*}{\kappa^2}. \quad (7.8)$$

For the full derivation see section 3.2.5. All the numerical calculations are conducted with the dimensionless Hamiltonian in eq. (7.2), and therefore all the results presented in this chapter correspond to this scaling. The apostrophe notation is neglected in the subsequent text.

From eq. (7.2) we observe that the frequency parameter affects the energy spectrum of the system. This is an expected relation. For example, if the oscillator frequency is increased, then the oscillator potential forces the electrons closer together. This will affect both the electron-electron repulsion and the kinetic energy, and thus change the energy of the system. Experimentally the frequency is a tunable quantity, which means that the system can be analyzed in terms of different frequencies. We have therefore conducted numerical calculations for different values of the frequency. These calculations are conducted with a HMO basis and a HF basis. We start by presenting the results obtained with the HMO basis, and follow up with the results obtained with a HF basis.

7.1.1 Standard Interaction Results: HMO basis

The HMO basis consists of single-particle basis orbitals, which are represented by the eigenfunctions of the time-independent Schrödinger equation

$$\left(-\frac{1}{2} \sum_{i=1}^N \nabla_i^2 + \frac{1}{2} \omega \sum_{i=1}^N r_i^2 \right) \psi_\alpha(\mathbf{r}) = \epsilon_\alpha \psi_\alpha(\mathbf{r}), \quad (7.9)$$

where \mathbf{r} contains both the spatial and the spin degree of freedom. The index α denotes the quantum numbers (n, m, m_s) , see the mapping in eq. (6.4) and table 6.1. If we assume that $N = 1$, eq. (7.9) represents the dimensionless form of the Schrödinger equation of the single-particle parabolic quantum dot, see section 3.2.2. We verify this by multiplying the Hamiltonian of eq. (7.9) with E_H , which yields the Hamiltonian in eq. (3.22).

The total wave function $\psi_\alpha(\mathbf{r})$ reads

$$\psi_\alpha(\mathbf{r}) = \psi_{nm}(x, y) \otimes |\chi_{m_s}\rangle, \quad (7.10)$$

where $\psi_{nm}(x, y)$ is the spatial part, and $|\chi_{m_s}\rangle$ is the spin part of the wave function, see section 1.2.5. The quantum number m_s is associated with the z -projection of the spin, and takes the values

$$m_s = \pm \frac{1}{2}, \quad (7.11)$$

with eigenvectors

$$|m_s = \frac{1}{2}\rangle = |+\rangle, \quad (7.12)$$

$$|m_s = -\frac{1}{2}\rangle = |-\rangle. \quad (7.13)$$

These eigenvectors are referred to as spin-up and spin-down, respectively, see section 1.2.4. The spatial part of the wave function satisfies

$$\left(-\frac{1}{2} \sum_{i=1}^N \nabla_i^2 + \frac{1}{2} \omega \sum_{i=1}^N r_i^2 \right) \psi_{nm}(x, y) = \epsilon_{nm} \psi_{nm}(x, y), \quad (7.14)$$

where n and m are quantum numbers, and ϵ_{nm} is the corresponding eigenvalue. The eigenvalues ϵ_{nm} depend on the frequency as follows

$$\epsilon_{nm} = (1 + |m| + 2n)\omega, \quad (7.15)$$

which corresponds to the energy in eq. (3.57). The spatial part of the wave function in eq. (7.14), is given in eq. (3.55) where $m^* = \hbar = 1$. The total wave function in eq. (7.10) constitutes the basis functions of our HMO basis.

In our calculations the single-electron Hamiltonian \hat{h} is given by the Hamiltonian in eq. (7.14). This means that our basis leads to a diagonal single-particle matrix

$$\langle \alpha | \hat{h} | \beta \rangle = \delta_{\alpha\beta} \epsilon_{\alpha}. \quad (7.16)$$

Remember that $\alpha = (n, m, m_s)$, and that the single-particle elements and the interaction elements $\langle \alpha\beta | \hat{v} | \gamma\delta \rangle$ are provided as input files to our program, see chapter 6.

All the calculations in this thesis, either with standard interaction or effective interaction, HMO basis or HF basis, are performed in what we call the *direct product space* \mathcal{P}_{DP}

$$\mathcal{P}_{DP} \subset \mathcal{H}_N^{AS}, \quad (7.17)$$

where \mathcal{H}_N^{AS} is the N -electron Hilbert space. The basis of \mathcal{P}_{DP} reads

$$\mathcal{B}_{DP} = \mathcal{B}_{DP}(R) = \{ |\Phi_{\alpha_1, \alpha_2, \dots, \alpha_N}\rangle : \max\{\epsilon_i\} \leq R \}, \quad (7.18)$$

where $|\Phi_{\alpha_1, \alpha_2, \dots, \alpha_N}\rangle$ is a Slater determinant with HMO basis functions as single-particle orbitals, and ϵ_i is the unscaled energy, i.e. the energy in eq. (7.15) with ω neglected. The variable R represents the shell number of the quantum dot, see fig. 3.1 or table 3.1. In this basis there are no restrictions on which single-particle orbital that can be occupied. The single-particle HMO-basis used in building the N -particle basis is denoted

$$\mathcal{B}_{sp}(R) = \{ |\alpha\rangle \}_{\alpha=0}^{\alpha_{\max}(R)}, \quad (7.19)$$

where $\alpha_{\max}(R)$ denotes the number of single-particle orbitals that fills all the shells up to shell R , e.g. 2, 6 and 12 corresponds to $R = 1$, $R = 2$ and $R = 3$ respectively.

Tables 7.1-7.3 display the HF and CCSD results of the two-dimensional parabolic quantum dot with two, six, twelve and twenty electrons in frequency range $\omega = [0.1 - 1]$. Note that only selected frequencies are presented for the twelve- and twenty-electron dots because no convergence is obtained for frequencies below $\omega = 0.9$. The HF results are obtained by the HF-code described in section 6.1. The CCSD results are obtained by utilizing a HMO-basis, i.e. the code presented in section 6.2.1. In the tables, x denotes that the energy result was not obtained because convergence was not reached. Note that these CCSD results are also rendered in table 7.21, where results obtained with both standard and effective interaction are displayed.

ω	R	$N = 2$		$N = 6$	
		HF	CCSD	HF	CCSD
0.1	10	0.525635	0.4411357	3.852394	x
	11	0.525635	0.4410973	3.691474	x
	12	0.525635	0.4410662	3.690394	x
	13	0.525635	0.4410406	3.691461	x
	14	0.474354	0.4410191	3.690389	x
	15	0.525635	0.4410009	3.691457	x
	16	0.525635	0.4409852	3.691457	x
	17	0.525635	0.4409716	3.691457	x
	18	0.525635	0.4409597	3.691456	x
	19	0.525635	0.4409492	3.691455	x
	20	0.525635	0.4409399	3.691456	x
0.2	10	0.882293	0.7740851	6.162264	x
	11	0.882293	0.7750155	6.162241	x
	12	0.882293	0.7749068	6.293543	x
	13	0.882293	0.7748177	6.162226	x
	14	0.882293	0.7747435	6.293541	x
	15	0.882293	0.7746807	6.293542	x
	16	0.882293	0.7746270	6.162222	x
	17	0.882293	0.7745805	6.162222	x
	18	0.882293	0.7745400	6.162222	x
	19	0.882293	0.7745042	6.293541	x
	20	0.882293	0.7744725	6.293541	x
0.3	10	1.204351	1.0839642	8.337021	x
	11	1.204350	1.0837248	8.337003	x
	12	1.204350	1.0835326	8.431396	x
	13	1.204350	1.0833753	8.431394	x
	14	1.204350	1.0832442	8.336988	x
	15	1.204350	1.0831333	8.336988	x
	16	1.204350	1.0830385	8.431395	x
	17	1.204350	1.0829565	8.431395	x
	18	1.204350	1.0828849	8.431395	x
	19	1.204350	1.0828219	8.431395	x
	20	1.204350	1.0827661	8.336987	x
0.4	10	1.508011	1.3785506	10.405170	9.9630316
	11	1.508010	1.3782124	10.405170	9.96066012
	12	1.508010	1.3779410	10.405164	9.95882140
	13	1.508010	1.3777187	10.405165	9.95736001
	14	1.508010	1.3775335	10.343706	9.95617041
	15	1.508010	1.3773769	10.343705	9.95518395
	16	1.508010	1.3772428	10.343705	9.95435347
	17	1.508010	1.3771269	10.405165	9.95364590
	18	1.508010	1.3770257	10.405166	9.95303565
	19	1.508010	1.3769366	10.405166	9.95250444
	20	1.508010	1.3768576	10.405166	9.95203531
0.5	10	1.799741	1.6635345	12.271310	11.8097742
	11	1.799740	1.6631055	12.271308	11.8067720
	12	1.799740	1.6627612	12.271304	11.8044422
	13	1.799740	1.6624790	12.271304	11.8025849
	14	1.799740	1.6622438	12.271304	11.8010730
	15	1.799740	1.6620449	12.271303	11.7998177
	16	1.799740	1.6618746	12.271303	11.7987615
	17	1.799740	1.6617272	12.271304	11.7978667
	18	1.799740	1.6615985	12.271304	11.7970859
	19	1.799740	1.6614852	12.271303	11.7964033
	20	1.799740	1.6613847	12.271304	11.7958063

Table 7.1: HF and CCSD results for the parabolic quantum dot with 2 and 6 electrons, where we have used standard interaction. Furthermore the CCSD results are obtained by the use of a HMO basis. The oscillator frequency is given by ω , and R denotes the size of the model space. We use x to denote that convergence was not reached. Frequency and energy are given in units of Hartrees [E_H].

ω	R	$N = 2$		$N = 6$	
		HF	CCSD	HF	CCSD
0.6	10	2.082921	1.9414355	14.059672	13.5830163
	11	2.082920	1.9409237	14.059670	13.5794387
	12	2.082920	1.9405126	14.059667	13.5766596
	13	2.082920	1.9401757	14.059666	13.5744445
	14	2.082920	1.9398947	14.059666	13.5726375
	15	2.082920	1.9396570	14.059667	13.5711389
	16	2.082920	1.9394534	14.059667	13.5698737
	17	2.082920	1.9392772	14.059665	13.5687966
	18	2.082920	1.9391232	14.059666	13.5678598
	19	2.082920	1.9389876	14.059666	13.5670465
	20	2.082920	1.9388674	14.059666	13.5663312
0.7	10	2.359584	2.2138170	15.788364	15.2994967
	11	2.359583	2.2132295	15.788360	15.2953928
	12	2.359583	2.2127575	15.788358	15.2922076
	13	2.359583	2.2123704	15.788357	15.2896616
	14	2.359583	2.2120475	15.788358	15.2875859
	15	2.359583	2.2117742	15.788358	15.2858615
	16	2.359583	2.2115401	15.788357	15.2844087
	17	2.359583	2.2113374	15.788358	15.2831656
	18	2.359583	2.2111603	15.788357	15.2820916
	19	2.359583	2.2110043	15.788357	15.2811532
	20	2.359583	2.2108658	15.788357	15.2803347
0.8	10	2.631050	2.4766317	17.469226	16.9702520
	11	2.631050	2.4765209	17.469224	16.9656660
	12	2.631050	2.4764356	17.469224	16.9621042
	13	2.631050	2.4763683	17.469224	16.9592623
	14	2.631050	2.4763141	17.469222	16.9569381
	15	2.631050	2.4762697	17.469222	16.9550082
	16	2.631050	2.4762328	17.469222	16.9533793
	17	2.631050	2.4762017	17.469224	16.9519870
	18	2.631050	2.4761752	17.469223	16.9507836
	19	2.631050	2.4761524	17.469223	16.9497362
	20	2.631050	2.4761327	17.469222	16.9488122
0.9	10	2.898266	2.7459092	19.110793	18.6032695
	11	2.898266	2.7451890	19.110792	18.5982402
	12	2.898266	2.7446098	19.110793	18.5943353
	13	2.898265	2.7441344	19.110792	18.5912138
	14	2.898265	2.7437375	19.110793	18.5886689
	15	2.898266	2.7434015	19.110791	18.5865462
	16	2.898266	2.7431134	19.110792	18.5847570
	17	2.898266	2.7428639	19.110792	18.5832271
	18	2.898265	2.7426457	19.110792	18.5819043
	19	2.898266	2.7424535	19.110792	18.5807499
	20	2.898266	2.7422828	19.110792	18.5797339
1.0	10	3.161909	3.0069378	20.719217	20.2043451
	11	3.161909	3.0061589	20.719215	20.1989070
	12	3.161909	3.0055324	20.719216	20.1946825
	13	3.161909	3.0050178	20.719215	20.1913062
	14	3.161909	3.0045882	20.719215	20.1885503
	15	3.161908	3.0042243	20.719215	20.1862564
	16	3.161909	3.0039123	20.719214	20.1843190
	17	3.161908	3.0036420	20.719215	20.1826592
	18	3.161908	3.0034056	20.719214	20.1812261
	19	3.161908	3.0031972	20.719214	20.1799750
	20	3.161908	3.0030122	20.719216	20.1788722

Table 7.2: HF and CCSD results for the parabolic quantum dot with 2 and 6 electrons, where we have used standard interaction. Furthermore the CCSD results are obtained by the use of a HMO basis. The oscillator frequency is given by ω , and R denotes the size of the model space. Frequency and energy are given in units of Hartrees [E_H].

ω	R	$N = 12$		$N = 20$	
		HF	CCSD	HF	CCSD
0.5	10	40.216196	x	133.573994	x
	11	40.165991	x	133.243889	x
	12	40.216110	x	133.177845	x
	13	40.165874	x	133.174234	x
	14	40.165867	x	133.174194	x
	15	40.165857	x	133.174200	x
	16	40.165857	x	133.174218	x
	17	40.165857	x	133.174215	x
	18	40.165854	x	133.174208	x
	19	40.216094	x	133.174204	x
	20	40.165855	x	133.174208	x
0.9	10	61.866124	67.5217413	194.017825	x
	11	61.865572	67.4984203	193.883910	x
	12	61.865569	67.4810303	193.874972	x
	13	61.865550	67.4677383	193.874423	x
	14	61.865545	67.4572599	193.874133	x
	15	61.865547	67.4487472	193.874102	x
	16	61.865547	67.4417244	193.874042	x
	17	61.865544	67.4358049	193.874076	x
	18	61.865540	67.4307674	193.874083	x
	19	61.865545	-	193.874074	x
	20	61.865544	-	193.874052	x
1.0	10	66.912039	65.8065392	158.017678	x
	11	66.911369	65.7841408	158.010275	x
	12	66.911363	65.7673051	158.004950	x
	13	66.911328	65.7544540	158.004758	x
	14	66.911326	65.7442987	158.004584	x
	15	66.911320	65.7360500	158.004315	x
	16	66.911321	65.7292334	158.004586	x
	17	66.911320	65.7234980	158.004270	x
	18	66.911323	65.7186088	158.004278	x
	19	66.911320	-	158.004270	x
	20	66.911318	-	158.004269	x

Table 7.3: HF and CCSD results for the parabolic quantum dot with 12 and 20 electrons, where we have used standard interaction. Furthermore the CCSD results are obtained by the use of a HMO basis. The oscillator frequency is given by ω , and R denotes the size of the model space. We use x to denote that convergence was not reached. Frequency and energy are given in units of Hartrees [E_H].

First we consider the HF results for the two-electron quantum dot ($N = 2$) in table 7.1 and 7.2. In our calculations we observe that when exceeding $R = 10$, i.e. ten shells, we obtain energy convergence. From this we can conclude that the HF calculations have a quick convergence rate. Thus the number of basis orbitals necessary in order to reach convergence are limited to around hundred. However, if we observe the development in convergence starting at lower shells, we can extract a system behavior which is common for all frequencies. As an example we present the energy results of lower shell numbers for the frequency $\omega = 1$, see table 7.4. In this table we observe that the transition from

ω	R	$N = 2$	
		HF	CCSD
1.0	1	3.253314	3.253314
	2	3.253314	3.152328
	3	3.162691	3.038605
	4	3.162691	3.025231
	5	3.161921	3.017606
	6	3.161921	3.013626
	7	3.161909	3.011020
	8	3.161909	3.009236
	9	3.161909	3.007930
	10	3.161909	3.006938

Table 7.4: HF and CCSD results for a 2-electron parabolic quantum dot, where we have used standard interaction and a HMO basis. The model space is in range $R = [1 - 9]$, for the oscillator frequency $\omega = 1$. Frequency and energy are given in units of Hartrees $[E_H]$. These are the results plotted in fig. 7.1.

one odd to the next even shell number does not change the energy. The reason for this behavior is clarified by the following derivation. The HF ansatz for a two-electron system reads

$$\begin{aligned}
 \Psi_{HF}(\mathbf{r}_1, \mathbf{r}_2) &= \frac{1}{\sqrt{2!}} \begin{vmatrix} \varphi_a(\mathbf{r}_1) & \varphi_a(\mathbf{r}_2) \\ \varphi_b(\mathbf{r}_1) & \varphi_b(\mathbf{r}_2) \end{vmatrix} \\
 &= \frac{1}{\sqrt{2!}} \sum_{p=0}^1 (-1)^p \hat{P} \varphi_a(\mathbf{r}_1) \varphi_b(\mathbf{r}_2),
 \end{aligned} \tag{7.20}$$

where

$$\varphi_a(\mathbf{r}) = \sum_{\alpha=1}^d C_{a\alpha} \psi_{\alpha}(\mathbf{r}), \tag{7.21}$$

is the HF orbitals, and $\{\psi_{\alpha}(\mathbf{r})\}_{\alpha=1}^d$ is the set of single-particle orbitals constituting the HMO basis. Note that α represents the mapping of the quantum numbers n , m and m_s , see eq. (6.4) and table 6.1. A more thorough review of the HF theory is given in chapter 4. Note that the HF ansatz represents a linear combination of 2×2 determinants due to the linear expansion of the HF orbitals. The HF ansatz also results in the fact that only one-particle one-hole (1p1h) excited determinants can occur, i.e. only one electron per determinant is excited from a hole state to a particle state. This fact applies in general to all N -electron systems. With this in mind we examine the transition from $R = 1$ to $R = 2$ for the two-electron system.

In the case of $R = 1$ we have that $R = R_f$, where R_f is the Fermi shell in which all possible orbitals are occupied hole states. This means that the HF wave function in eq. (7.20) is the non-interacting ground state, viz.

$$\Psi_{HF}(\mathbf{r}_1, \mathbf{r}_2) = \Psi_0(\mathbf{r}_1, \mathbf{r}_2), \quad (7.22)$$

and the HF energy reads

$$E_{HF} = E_{\text{ref}} = \langle \Psi_0 | \hat{H} | \Psi_0 \rangle = 3.253314, \quad (7.23)$$

where E_{ref} denotes the non-interacting ground state energy. In the transition to $R = 2$, we are given the possibility of including 1p1h excited determinants in the HF wave function. The ground state of the two-particle system reads

$$\Psi_0(\mathbf{r}_1, \mathbf{r}_2) = \begin{vmatrix} \psi_0(\mathbf{r}_1) & \psi_0(\mathbf{r}_2) \\ \psi_1(\mathbf{r}_1) & \psi_1(\mathbf{r}_2) \end{vmatrix}, \quad (7.24)$$

where the hole states ψ_0 and ψ_1 in bra-ket notation reads

$$|0\rangle = |n = 0, m = 0, m_s = -1/2\rangle, \quad (7.25)$$

$$|1\rangle = |n = 0, m = 0, m_s = 1/2\rangle. \quad (7.26)$$

When $R = 2$ we include additional single-particle states in the basis, viz.

$$|2\rangle = |n = 0, m = -1, m_s = -1/2\rangle, \quad (7.27)$$

$$|3\rangle = |n = 0, m = -1, m_s = 1/2\rangle, \quad (7.28)$$

$$|4\rangle = |n = 0, m = 1, m_s = -1/2\rangle, \quad (7.29)$$

$$|5\rangle = |n = 0, m = 1, m_s = 1/2\rangle. \quad (7.30)$$

We repeat that the Coulomb interaction is independent of angular momentum and spin, thus the total angular momentum $M = m_\alpha + m_\beta$ and the total spin $M_S = m_{s_\alpha} + m_{s_\beta}$ is conserved. If we now imagine that the electrons occupy the ground state in eq. (7.24), then total angular momentum and total spin are given by the ground state orbitals in eqs. (7.25) and (7.26), which yield $M = 0$ and $M_S = 0$. We then try to include the 1p1h excited determinant

$$\Psi_0(\mathbf{r}_1, \mathbf{r}_2) = \begin{vmatrix} \psi_1(\mathbf{r}_1) & \psi_1(\mathbf{r}_2) \\ \psi_5(\mathbf{r}_1) & \psi_5(\mathbf{r}_2) \end{vmatrix}. \quad (7.31)$$

This determinant has a total angular momentum $M = 1$ and spin $M_S = 1$. This excitation is not allowed since it does not satisfy the condition of M and M_S conservation. In fact none of the possible 1p1h excited determinants satisfy the conservation condition. Thus in the transition from $R = 1$ to $R = 2$, no more correlations are included in the wave function, and the energy is therefore the same. This behavior is also clear from the shell structure in fig. 3.1. In this figure we observe that for the two-particle case we can draw vertical conservation-lines through each m value. These conservation lines cross all the basis orbitals which are possible to combine in a 1p1h determinant. From one odd shell number to the next even shell number we observe that no new orbitals are included, i.e. crossed by the vertical line.

The behavior of the two-particle system reviewed above cannot be extended to the system of six, twelve or twenty particles. In Tables 7.1-7.3, we observe that the HF energy

of $N = 6, 12, 20$ changes from one odd shell to the next even shell. We can convince ourselves of this fact by observing the transition from one shell to another, similar as for the two-particle case above. When we do this, we see that in such transitions allowed 1p1h excitations exists, and thus results in new correlations and changed energies.

Further, we compare the HF results in tables 7.1-7.3, with the corresponding standard interaction results in tables 7.16-7.19. Remember that these two sets of HF results are obtained in two different ways, one performing a block-wise diagonalization of the HF-matrix, while the other diagonalizes the full HF-matrix, see section 6.2.2 and 6.1.1, respectively. In the case of the two-electron quantum dot we observe that the two results are in agreement with each other. If we turn the attention to the six-electron quantum dot, we observe that in the lowest frequency range $\omega = [0.1 - 0.3]$, the HF energies are not in agreement with each other. This is also the frequency specter in which we obtain no convergence in the CCSD results, however without connection. For the twelve-electron quantum dot we observe that for the selected frequencies the HF results are in agreement within fifth decimal, however the twenty-electron dot is not in agreement for other frequencies than $\omega = 1$. From this we draw the conclusion that for low frequencies, and more than two electrons, the HF method which diagonalize the full HF-matrix does not produce satisfying results. Also, the fact that the CCSD method does not converge when we utilize the HMO basis for low frequencies and electron numbers exceeding two, implies that other basis choices could be a better starting point for the CCSD method.

The HF method is *variational*, which means that the HF energy is an overestimate of the exact ground state energy. In table 7.4 we observe that the energy is improving with increasing values of R , the same is observed in tables 7.1-7.3. This is expected, i.e.

$$E_0 < E_{\text{HF}}(R + 1) \leq E_{\text{HF}}(R). \quad (7.32)$$

In the two-particle quantum dot, where the frequency equals $\omega = 1$, we know the exact ground state energy, see section 3.2.3. This value reads

$$E_0 = 3E_H, \quad (7.33)$$

where E_H is the Hartrees defined in eq. (7.8). In table 7.2 and 7.4 we observe, as expected, that the HF calculations overshoot the exact result. If we turn the attention to the CCSD calculations, we observe that these results tend to be lower than the HF results, viz.

$$E_{\text{CCSD}}(R) \leq E_{\text{HF}}(R). \quad (7.34)$$

This is a pattern not only valid for the two-particle case, or the value of the frequency.

The CCSD method is not variational, which means that the CCSD energy can both overestimate and underestimate the exact energy. Therefore, without knowledge of the exact energy, one cannot determine whether the HF or the CCSD results yield the best energy estimate. The best estimate naturally refers to the energy which is closest to the exact energy. In order to conclude which energy estimate is the best, one commonly compares the results with the results of other variational many-body methods, e.g. Variational Monte Carlo [25], Diffusion Monte Carlo [25], or Full Configuration Interaction. However, in the two-electron system with $\omega = 1$, we can conclude that the CCSD energy is the best estimate. In this case the disagreement of the CCSD method is in the order of 10^{-2} . Theoretically we expect the CCSD method to perform better than the HF

method because it includes higher excitation levels than 1p1h in the determinant, thus more correlation is included.

In the following we examine the assumption that the CCSD method performs better than the HF method by making plots of both energy results as a function of shell number R , for the selected frequency $\omega = 1$. In order to determine which method is the better one, we also plot the *relative error* as a function of R given by

$$\epsilon_{\text{error}}(R) = \left| \frac{E_{\text{exact}} - E(R)}{E_{\text{exact}}} \right|, \quad (7.35)$$

where E_{exact} is the exact energy of the system. When the exact energy is unknown, E_{exact} is exchanged by energy results of other many-body methods. In our calculations where the exact energy is unknown, we insert the Diffusion Monte Carlo (DMC) energy E_{DMC} reported by ref. [43] into eq. (7.35).

We start by analysing the energy and the relative error plot of the two-electron system in fig. 7.1. As already mentioned, the exact energy of this system is known and equals

$$E_{\text{exact}} = 3. \quad (7.36)$$

In the energy plot we observe that the CCSD energy is lower than the HF energy. We also observe that the CCSD energy overshoots the exact energy. In the relative error plot we observe that the CCSD method has a lower relative error compared to the HF method. The relative error plot thus confirms that the CCSD method performs better than the HF method. Another fact which becomes obvious in the energy plot, is that the HF energy flattens out almost immediately after $R = 2$. This means that the most important correlation contributions possible for the HF method, are included when $R = 3$. When $R = 2$ the CCSD method has already achieved a better energy than the HF method do with $R = 20$. This means that the correlation contribution from the 2p2h excitations are more important than the combined 1p1h excitations in $R = [2 - 20]$. Thus, beyond $R = 3$ the HF method contributes very little, and is practically converged. Correspondingly, we see that the CCSD method obtains the most important contributions within the first five shells. As an illustration we can calculate the difference in the CCSD energy of $R = 10$ and $R = 20$

$$E_{\text{CCSD}}(R = 20) - E_{\text{CCSD}}(R = 10) \approx 0.004. \quad (7.37)$$

The energy and relative error of the HF and CCSD method for the six-electron quantum dot is also displayed in fig. 7.1. Again we observe that the energy and relative error of the CCSD method is lower than the HF method. For this system we do not know the exact energy. However, when calculating the relative error we use the assumed exact DMC energy

$$E_{\text{DMC}} = 20.1597. \quad (7.38)$$

Similar to the two-electron quantum dot, the most important correlation contributions of both methods are obtained within the first few shells. The HF energy flattens out at $R = 4$, and at this stage the CCSD method has already achieved an energy better than what the HF method achieves at $R = 20$.

Finally, the energy and relative error of the twelve-electron quantum dot, are displayed in fig. 7.1. The DMC energy used in calculating the relative error for this system reads

$$E_{\text{DMC}} = 65.700. \quad (7.39)$$

The HF energy flattens out at $R = 7$. The CCSD method obtains a better energy for $R = 6$ than the HF method obtains at $R = 20$. Tables 7.4 and 7.5 display the energy results plotted in shell range $R = [1 - 9]$.

ω	CCSD	$N = 6$		$N = 12$	
		HF	CCSD	HF	CCSD
1.0	1	-	-	-	-
	2	22.2198128	22.2198128	-	-
	3	21.5931984	21.4198874	73.765549	73.7655491
	4	20.7669198	20.4213206	70.673850	70.2975271
	5	20.7484027	20.3197149	67.569929	66.9899114
	6	20.7202575	20.2608927	67.296870	66.4520049
	7	20.7201312	20.2367594	66.934743	65.9716865
	8	20.7192482	20.2217499	66.923094	65.8893232
	9	20.7192487	20.2115900	66.912245	65.8389318

Table 7.5: HF and CCSD results for a 6-electron and a 12-electron parabolic quantum dot, where we have used standard interaction and a HMO basis. The model space is in range $R = [1 - 9]$, for the oscillator frequency $\omega = 1$. Frequency and energy are given in units of Hartrees $[E_H]$. These are the results plotted in fig. 7.1.

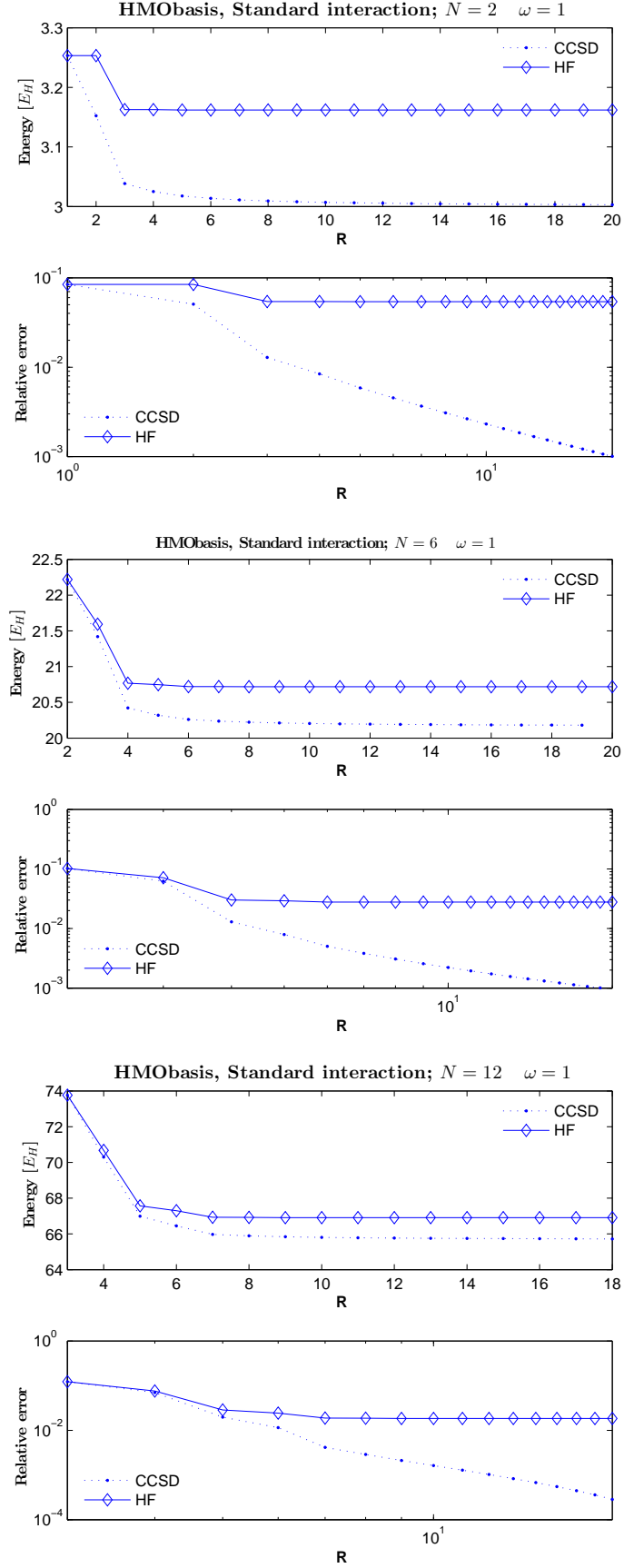


Figure 7.1: Energy and relative error as functions of R for the parabolic quantum dot with 2, 6 and 12 electrons, where we have used standard interaction and a HMO basis. The oscillator frequency takes the value $w = 1$. The energy is given in units of Hartrees [E_H].

7.1.2 Standard Interaction Results: HF basis

In this section we present the CCSD and HF results obtained by utilizing a HF-basis in the CCSD calculations. The HF results presented here are calculated with the code which diagonalize the HF-matrix block-wise, see section 6.2.2. The HF basis is reviewed in detail in section 6.2.2, we therefore refer to this section for more reading on the HF basis.

Tables 7.16-7.19 display the standard interaction results of the HF and the CCSD method in frequency range $\omega = [0.1 - 1]$, and shell range $R = [10 - 20]$. In these tables, x denotes that convergence was not reached, and $-$ denotes that no calculations have been done, mainly due to convergence problems and high run-times.

If we consider the CCSD results, we see that all the presented CCSD results are lower than the corresponding HF results. We also notice that for all frequencies the CCSD energies of $R = 10$ are lower than the HF energies of $R = 20$. We also notice that the CCSD results obtained with the effective interaction, in all our calculations, are lower than the corresponding standard interaction results. Similar as above, we examine the performance of the two methods HF and CCSD by plotting the energy and the relative error of the two, six, and twelve-electron dot. We plot these entities for $\omega = 1$, in shell range $R = [1 - 20]$. Table 7.6 displays the energy results in shell range $R = [1 - 9]$, and the corresponding plots are shown in fig. 7.2.

ω	R	$N = 2$		$N = 6$		$N = 12$	
		HF	CCSD	HF	CCSD	HF	CCSD
1.0	1	3.2533141	3.2533141	-	-	-	-
	2	3.2533141	3.1523281	22.2198128	22.2198128	-	-
	3	3.1626914	2.9669847	21.5931985	21.0241121	73.7655490	73.7655490
	4	3.1626914	2.9734696	20.7669195	19.8213687	70.6738492	69.1024870
	5	3.1619214	2.9761152	20.7484023	19.6466395	67.5699302	65.1301189
	6	3.1619214	2.9748429	20.7202571	19.4803667	67.2968693	64.0936717
	7	3.1619090	2.9736287	20.7201316	19.4837809	66.9347449	63.0575380
	8	3.1619090	2.9726967	20.7192484	19.4923071	66.9230945	62.8249571
	9	3.1619089	2.9719410	20.7192482	19.4892288	66.9122442	62.6349819

Table 7.6: HF and CCSD results for a 2, 6 and 12-electron parabolic quantum dot, where we have used standard interaction and a HF basis. The model space is in range $R = [1 - 9]$, for the oscillator frequency $\omega = 1$. Frequency and energy are given in units of Hartrees $[E_H]$. These are the results plotted in fig. 7.2.

The energy plot and the relative error plot of the two-electron quantum dot in fig. 7.2 exhibit the expected behavior, where the CCSD energy performs better compared to the HF energy, i.e. the CCSD energy and relative error is lower than the corresponding HF energy and relative error. However, for the six and twelve-electron, we observe a discrepancy in this tendency. The CCSD energy is lower compared to the HF energy, but the relative error reveals that the CCSD result underestimates the energy by an amount which is greater than the amount the HF method overestimates the energy. Because of this unsatisfying result we consider the corresponding CCSD and HF results obtained with Gaute Hagen's code. These results are given for selected frequencies in table 7.22. We observe that our CCSD energy consistently underestimates the energy by a percentage in range 3%-6%, compared with Hagen's CCSD energy. However, our HF energy equals Hagen's HF energy to a minimum of six decimals. In fig. 7.3 we plot Hagen's HF and

CCSD energies in addition to the relative error, for the six and twelve-electron quantum dot. From this figure we see that we obtain the expected results, which implies that the CCSD method performs better than the HF method.

In order to interpret the discrepancy in our CCSD code utilizing a HF basis and standard interaction, we note the following: The method of our CCSD code is based on a more *Newton-method-like* minimization of the energy, while Hagen uses a *conjugate gradient* method in order to determine the energy. In general we know that the Newtonian method of finding a minimum depends on a first guess which lies not too far from the actually minimum. If the first guess does not satisfy the criteria, there is a relatively good chance that the method does not find the minimum, or possibly gets stuck in a local minimum. The conjugate gradient method is however not correspondingly dependent on the first guess, and thus constitutes a better method in some cases. This may be the source of the bad performance of our CCSD code. However, another source of error in our code is the HF basis we feed to the CCSD method. If the HF method for some reason miscalculates or do not converge properly, then this affects our CCSD results. Though, it must be said that numerous comparisons are made between the two codes in order to avoid such errors.

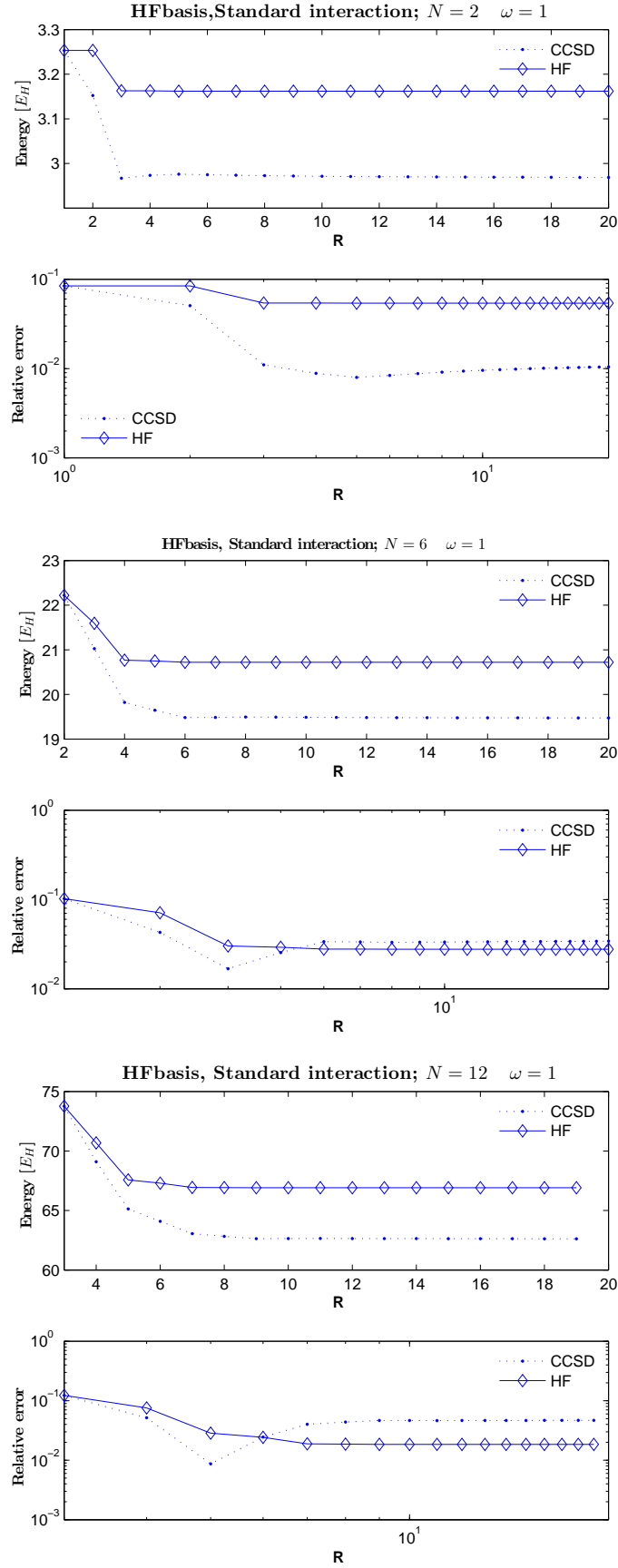


Figure 7.2: Energy and relative error as functions of R for the parabolic quantum dot with 2, 6 and 12 electrons, where we have used standard interaction and a HF basis. The oscillator frequency takes the value $w = 1$. The energy is given in units of Hartrees $[E_H]$.

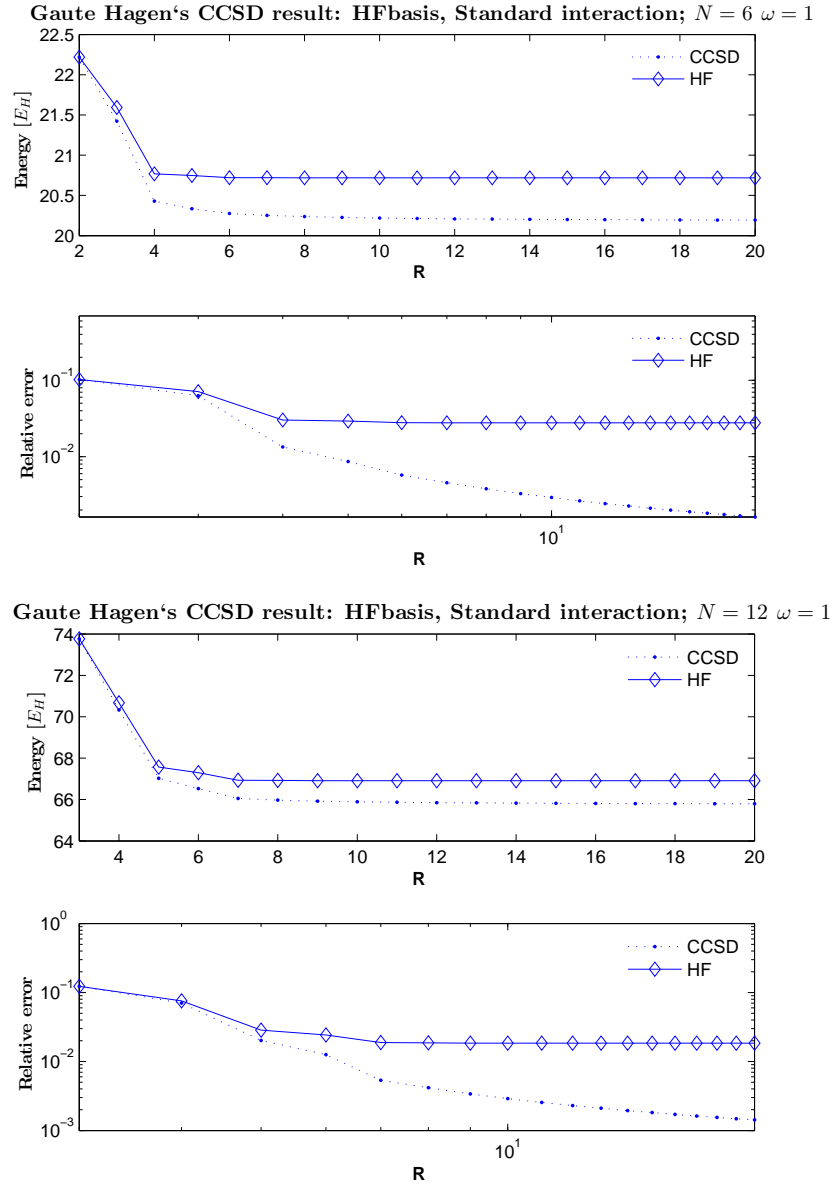


Figure 7.3: Energy and relative error as functions of R for the parabolic quantum dot with 6 and 12 electrons, where we have used standard interaction and a HF basis. These results are obtained with Gaute Hagen's code. The oscillator frequency takes the value $\omega = 1$. The energy is given in units of Hartrees [E_H].

7.2 Effective Interaction

In this section we introduce the effective interaction, and we present the HF and CCSD results obtained by utilizing this interaction.

The effective interaction is adopted because of the slow convergence rate of the CCSD results, when utilizing standard interaction as a function of R . This technique is widely used in nuclear physics [46, 47, 48]. The goal of effective interaction theory is to devise an "effective" Hamiltonian \hat{H}_{eff} in a model space \mathcal{P} of smaller dimension m than the dimension n of Hilbert space \mathcal{H} , and with m exact eigenvalues of the original Hamiltonian $\hat{H} = \hat{H}_0 + \hat{H}_1$, see [49]. The model space \mathcal{P} is usually spanned by a few eigenvectors of \hat{H}_0 , i.e. the non-interacting Hamiltonian. The effective Hamiltonian of an A -body system is usually approximated by a sub-cluster approximation approach, [46]. This approach involves the computation of the exact Hermitian effective Hamiltonian of an a -body system, where $a < A$. The effective a -body interactions are extracted and applied to the A -body system. In the following we present the basics of effective interaction theory. For a more detailed review see for example ref. [49].

Basics of effective interaction theory

We first assume that we have a finite Hilbert space \mathcal{H} , where $n = \dim(\mathcal{H})$. The spectral decomposition of the Hamiltonian then reads

$$\hat{H} = \sum_{k=1}^n E_k |\psi_k\rangle \langle \psi_k|, \quad (7.40)$$

where $\{E_k\}_{k=1}^n$ are the real eigenvalues corresponding to the orthonormal set of eigenvectors $\{|\psi_k\rangle\}_{k=1}^n$ satisfying

$$\hat{H}|\psi_k\rangle = E_k |\psi_k\rangle. \quad (7.41)$$

Within this Hilbert space we define a model space, which constitutes the subspace $\mathcal{P} \subset \mathcal{H}$ with $m = \dim(\mathcal{P}) \leq n$. This subspace is spanned by the orthonormal basis $\{|e\rangle\}_{k=1}^m$, viz.

$$\mathcal{P} \equiv \text{span}\{|e_k\rangle : k = 1, \dots, m\}. \quad (7.42)$$

The basis $\{|e\rangle\}_{k=1}^m$ is usually taken to be the eigenvectors of the non-interacting Hamiltonian H_0 . We define the orthogonal projector \hat{P} of the model space as

$$\hat{P} = \sum_{i=1}^m |e_i\rangle \langle e_i|. \quad (7.43)$$

The orthogonal complement of the model space \mathcal{P} is the excluded space $\mathcal{Q} \subset \mathcal{H}$. The orthogonal projector \hat{Q} of the excluded space is defined as

$$\begin{aligned} \hat{Q} &= 1 - \sum_{i=1}^m |e_i\rangle \langle e_i| \\ &= \sum_{i=m+1}^n |e_i\rangle \langle e_i|. \end{aligned} \quad (7.44)$$

This subdivision of the Hilbert space leads to the following relation for the Hamiltonian operator, and also any other arbitrary operator in that Hilbert space.

$$\begin{aligned}\hat{H} &= (\hat{P} + \hat{Q}) \hat{H} (\hat{P} + \hat{Q}) \\ &= \hat{P} \hat{H} \hat{P} + \hat{P} \hat{H} \hat{Q} + \hat{Q} \hat{H} \hat{P} + \hat{Q} \hat{H} \hat{Q}\end{aligned}\quad (7.45)$$

This is possible since

$$\hat{P} + \hat{Q} = 1 \quad (7.46)$$

This means that \hat{H} can be expressed in a block matrix form, viz.

$$\hat{H} = \begin{pmatrix} \hat{P} \hat{H} \hat{P} & \hat{P} \hat{H} \hat{Q} \\ \hat{Q} \hat{H} \hat{P} & \hat{Q} \hat{H} \hat{Q} \end{pmatrix}. \quad (7.47)$$

Further, the idea of effective interaction theory is to find a unitary transformation of the Hamiltonian

$$\hat{H}' = e^{-s} \hat{H} e^s, \quad (7.48)$$

such that

$$\hat{P} \hat{H}' \hat{Q} = \hat{Q} \hat{H}' \hat{P} = 0. \quad (7.49)$$

This is referred to as the de-coupling of the model space \mathcal{P} and its complement space \mathcal{Q} . Remember that a unitary transformation preserves the eigenvalues of the operator. The fact that \hat{H}_{eff} has eigenvalues identical to m of the eigenvalues of \hat{H} , and operates only in the model space \mathcal{P} , leads to an effective Hamiltonian given by

$$\hat{H}_{\text{eff}} = \hat{P} \hat{H}' \hat{P}. \quad (7.50)$$

We assume that the arrangement of the eigenvalues in eq. (7.40) corresponds to the E_k $k = 1, \dots, m$ values reproduced by \hat{H}_{eff} , and define the effective interaction by

$$\hat{V}_{\text{eff}} = \hat{H}_{\text{eff}} - \hat{P} \hat{H}_0 \hat{P}, \quad (7.51)$$

where \hat{H}_0 is the Hamiltonian of the non-interacting system.

In our calculations we have utilized effective interaction elements produced by the algorithm in ref. [50]. The effective interaction in this algorithm is produced by a uniform transformation of the two-body Hamiltonian. The CCSD method is exact in a finite number of shells (R) for the two-electron quantum dot, since it includes all possible excitations of that system. For higher quantum dots with more electrons, the CCSD method is not exact. For the two-electron quantum dot we should therefore obtain the exact result, or at least a result close to the exact, when we use the effective interaction in the CCSD calculations. For systems where $N > 2$, the effective interaction will never give an exact result, however it performs better than the bare standard interaction. The CCSD results obtained with HMO basis and HF basis are presented below.

7.2.1 Effective Interaction Results: HMO basis

In this section we present CCSD results obtained by the use of the HMO-basis. The HF results, which we present, are calculated with the code presented in section 6.1.1, and the CCSD results are obtained by using the code presented in section 6.2.1.

Tables 7.7-7.9 display the energy results for the two-electron, six-electron, twelve electron and twenty-electron quantum dot in the frequency range $\omega = [0.1 - 1]$, and shell range $R = [10 - 20]$. Note that only selected frequencies in this range are displayed for the twelve- and twenty-electron quantum dot. The reason for this can be viewed in tables 7.20-7.21. In these tables we observe that the CCSD energies do not converge for frequencies below $\omega = 0.9$ for the twelve-electron dot, and the twenty-electron dot obtains no convergence in shell range $R = 10 - 20$.

ω	R	$N = 2$		$N = 6$	
		HF	CCSD	HF	CCSD
0.1	10	0.513823	0.4408192	3.799144	x
	11	0.514865	0.4408153	3.67778	x
	12	0.515737	0.4408123	3.67910	x
	13	0.516478	0.4408099	3.68019	x
	14	0.517116	0.4408080	3.68110	x
	15	0.517671	0.4408064	3.68187	x
	16	0.518157	0.4408050	3.68254	x
	17	0.518588	0.4408038	3.82284	x
	18	0.518971	0.4408029	3.68362	x
	19	0.519315	0.4408020	3.68407	x
	20	0.519625	0.4408013	3.68447	x
0.2	10	0.868121	0.7740851	6.229692	x
	11	0.869392	0.7740678	6.236240	x
	12	0.870454	0.7740545	6.136989	x
	13	0.871355	0.7740439	6.245981	x
	14	0.872129	0.7740355	6.249704	x
	15	0.872801	0.7740286	6.142590	x
	16	0.873390	0.7740228	6.255637	x
	17	0.873910	0.7740180	6.258038	x
	18	0.874373	0.7740139	6.260154	x
	19	0.874787	0.7740103	6.262032	x
	20	0.875161	0.7740072	6.147887	x
0.3	10	1.188837	1.0820986	8.361069	x
	11	1.190241	1.0820647	8.368267	x
	12	1.191412	1.0820387	8.374125	x
	13	1.192404	1.0820182	8.378986	x
	14	1.193256	1.0820017	8.306997	x
	15	1.193995	1.0819883	8.386598	x
	16	1.194641	1.0819769	8.389631	x
	17	1.195212	1.0819675	8.312779	x
	18	1.195720	1.0819595	8.394613	x
	19	1.196174	1.0819526	8.315537	x
	20	1.196583	1.0819467	8.398533	x
0.4	10	1.491584	1.3759256	10.330185	9.9454069
	11	1.493078	1.3758748	10.337852	9.9452608
	12	1.494324	1.3758358	10.344095	9.9451599
	13	1.495378	1.3758051	10.349281	9.9450917
	14	1.496283	1.3757804	10.353656	9.9450442
	15	1.497067	1.3757602	10.357397	9.9450098
	16	1.497753	1.3757434	10.360631	9.9449857
	17	1.498358	1.3757293	10.363457	9.9449673
	18	1.498896	1.3757173	10.365945	9.9449553
	19	1.499378	1.3757070	10.368154	9.9449508
	20	1.499811	1.3756980	10.370128	9.9449386
0.5	10	1.782633	1.6602102	12.192703	11.7877088
	11	1.784193	1.6601430	12.200736	11.7874660
	12	1.785495	1.6600914	12.207280	11.7872934
	13	1.786596	1.6600507	12.212716	11.7871723
	14	1.787539	1.6600180	12.217304	11.7870871
	15	1.788357	1.6599913	12.221226	11.7870153
	16	1.789072	1.6599688	12.224617	11.7869654
	17	1.789703	1.6599501	12.227580	11.7869253
	18	1.790264	1.6599342	12.230189	11.7868967
	19	1.790766	1.6599205	12.232505	11.7868681
	20	1.791217	1.6599087	12.234575	11.7868562

Table 7.7: HF and CCSD results for the parabolic quantum dot with 2 and 6 electrons, where we have used effective interaction. Furthermore the CCSD results are obtained by the use of a HF basis. The oscillator frequency is given by ω , and R denotes the size of the model space. We use x to denote that convergence was not reached. Frequency and energy are given in units of Hartrees [E_H].

ω	R	$N = 2$		$N = 6$	
		HF	CCSD	HF	CCSD
0.6	10	2.065276	1.9374704	13.978111	13.5569972
	11	2.066890	1.9373877	13.986446	13.5566484
	12	2.068235	1.9373242	13.993236	13.5563989
	13	2.069372	1.9372742	13.998876	13.5562198
	14	2.070347	1.9372339	14.003636	13.5560972
	15	2.071191	1.9372009	14.007706	13.5559808
	16	2.071930	1.9371735	14.011226	13.5558996
	17	2.072581	1.9371504	14.014300	13.5558350
	18	2.073159	1.9371308	14.017007	13.5557830
	19	2.073677	1.9371139	14.019411	13.5557391
	20	2.074142	1.9370993	14.021558	13.5557087
0.7	10	2.341500	2.2092656	15.704314	15.2699298
	11	2.343157	2.2091684	15.712902	15.2694719
	12	2.344538	2.2090937	15.719900	15.2691427
	13	2.345705	2.2090347	15.725714	15.2689039
	14	2.346705	2.2089873	15.730618	15.2687276
	15	2.347571	2.2089484	15.734813	15.2685909
	16	2.348328	2.2089161	15.738440	15.2684681
	17	2.348996	2.2088889	15.741608	15.2683781
	18	2.349589	2.2088658	15.744399	15.2683047
	19	2.350120	2.2088458	15.746875	15.2682441
	20	2.350597	2.2088286	15.749088	15.2681936
0.8	10	2.612597	2.4766317	17.383039	16.9374786
	11	2.614292	2.4765209	17.391846	16.9369117
	12	2.615702	2.4764356	17.399023	16.9365032
	13	2.616895	2.4763683	17.404986	16.9362049
	14	2.617916	2.4763141	17.410016	16.9359775
	15	2.618800	2.4762697	17.414316	16.9357964
	16	2.619573	2.4762328	17.418037	16.9356538
	17	2.620255	2.4762017	17.421285	16.9355383
	18	2.620860	2.4761752	17.424147	16.9354434
	19	2.621401	2.4761524	17.426686	16.9353645
	20	2.621888	2.4761327	17.428955	16.9352983
0.9	10	2.879496	2.7403243	19.022731	18.5675774
	11	2.881222	2.7402008	19.031730	18.5669036
	12	2.882659	2.7401057	19.039064	18.5664180
	13	2.883873	2.7400306	19.045156	18.5660594
	14	2.884912	2.7399700	19.050296	18.5657850
	15	2.885812	2.7399204	19.054690	18.5655828
	16	2.886598	2.7398791	19.058492	18.5654299
	17	2.887292	2.7398444	19.061812	18.5652569
	18	2.887907	2.7398148	19.064735	18.5651374
	19	2.888458	2.7397893	19.067332	18.5650404
	20	2.888953	2.7397672	19.069649	18.5651041
1.0	10	3.142864	3.0008954	20.629488	20.1659808
	11	3.144617	3.0007599	20.638659	20.1652034
	12	3.146076	3.0006555	20.646131	20.1646430
	13	3.147308	3.0005730	20.652339	20.1642277
	14	3.148363	3.0005065	20.657576	20.1639098
	15	3.149277	3.0004520	20.662054	20.1636642
	16	3.150076	3.0004067	20.665928	20.1634524
	17	3.150779	3.0003684	20.669311	20.1632922
	18	3.151404	3.0003359	20.672289	20.1631504
	19	3.151963	3.0003068	20.674934	20.1630322
	20	3.152465	3.0002825	20.677297	-

Table 7.8: HF and CCSD results for the parabolic quantum dot with 2 and 6 electrons, where we have used effective interaction. Furthermore the CCSD results are obtained by the use of a HF basis. The oscillator frequency is given by ω , and R denotes the size of the model space. Frequency and energy are given in units of Hartrees [E_H].

ω	R	$N = 12$		$N = 20$	
		HF	CCSD	HF	CCSD
0.5	10	39.966822	x	131.764728	x
	11	39.990131	x	131.782935	x
	12	40.040808	x	131.938984	x
	13	40.057265	x	132.093393	x
	14	40.070878	x	132.214286	x
	15	40.082324	x	132.310309	x
	16	40.054730	x	132.388510	x
	17	40.062323	x	132.453543	x
	18	40.107895	x	132.508490	x
	19	40.074764	x	132.555572	x
	20	40.079921	x	132.596373	x
0.9	10	61.618529	60.6547962	145.731066	x
	11	61.646288	60.6502211	192.299468	x
	12	61.668703	60.6469217	171.115485	x
	13	61.686916	60.6445654	192.665350	x
	14	61.702051	60.6428248	192.791274	x
	15	61.714813	60.6414659	192.893099	x
	16	61.725722	60.6403942	192.977086	x
	17	61.735156	60.6395259	193.047683	x
	18	61.743402	60.6388116	193.107851	x
	19	61.750665	-	193.159771	x
	20	61.757110	-	193.205040	x
1.0	10	66.659618	65.6830761	157.435628	
	11	66.687758	65.6781550	157.507135	x
	12	66.710564	65.6745247	157.561246	x
	13	66.729091	65.6719555	157.606935	x
	14	66.744498	65.6700471	157.643679	x
	15	66.757510	65.6685641	157.674349	x
	16	66.768626	65.6673961	157.700169	x
	17	66.778250	65.6664502	157.722204	x
	18	66.786653	65.6656707	157.741251	x
	19	66.794059	-	157.757880	x
	20	66.800629	-	157.772512	x

Table 7.9: HF and CCSD results for the parabolic quantum dot with 12 and 20 electrons, where we have used effective interaction. Furthermore the CCSD results are obtained by the use of a HF basis. The oscillator frequency is given by ω , and R denotes the size of the model space. We use x to denote that convergence was not reached. Frequency and energy are given in units of Hartrees [E_H].

First we consider the HF results in tables 7.7-7.9. We observe that the two-electron behavior observed in section 7.1.1, where the energy from one odd shell to the next even shell was unchanged, no longer applies. We also observe that the HF energies for the quantum dots with more than two electrons are increasing as the shell number R increase. This does not break with the fact that the HF method is variational, it only means that the method is variational within each shell. In section 7.1.1 we anticipated the course of action, and noticed that the energy calculated with the effective interaction for both HF and CCSD is lower than the corresponding energies calculated with standard interaction. This is what we expected since the reason for introducing effective interaction was speed-up in convergence, thus reaching the minimum faster as a function of R .

Further, we examine the energy convergence as a function of R for the two, six and twelve-electron quantum dot by plotting the energy and relative error in eq. (7.35) as a function of R , see fig. 7.4. Table 7.10 presents the plotted HF and CCSD results in shell range $R = [1 - 9]$.

ω	R	$N = 2$		$N = 6$		$N = 12$	
		HF	CCSD	HF	CCSD	HF	CCSD
1.0	1	3.000000	3.000000	-	-	-	-
	2	3.121868	3.0634405	20.8122102	20.8122102	-	-
	3	3.098370	3.0086025	20.9823009	20.8619718	70.313660	70.3136599
	4	3.114506	3.0055190	20.4641400	20.2131001	69.103569	68.8011012
	5	3.123489	3.0031994	20.5318841	20.1964929	66.706794	66.2726313
	6	3.129965	3.0022793	20.5555247	20.1765083	66.708320	66.0451838
	7	3.134571	3.0016914	20.5838199	20.1717164	66.514457	65.7253574
	8	3.138031	3.0013277	20.6030929	20.1688708	66.580016	65.7043516
	9	3.140718	3.0010753	20.6179994	20.1671102	66.622511	65.6909130

Table 7.10: HF and CCSD results for a 2, 6 and 12-electron parabolic quantum dot, where we have used effective interaction and a HMO basis. The model space is in range $R = [1 - 9]$, for the oscillator frequency $\omega = 1$. Frequency and energy are given in units of Hartrees [E_H]. These are the results plotted in fig. 7.4.

In fig. 7.4, we observe that the CCSD results perform better than the HF results in all three cases of two, six and twelve-electrons. The relative errors are found in the same manner as in section 7.1.1, with the same DMC energy estimates representing the exact energy. We emphasize that these calculations utilize the HMO-basis, and give the expected result regarding the performance of HF and CCSD. The same performance results are reported when we utilise standard interaction and HMO-basis.

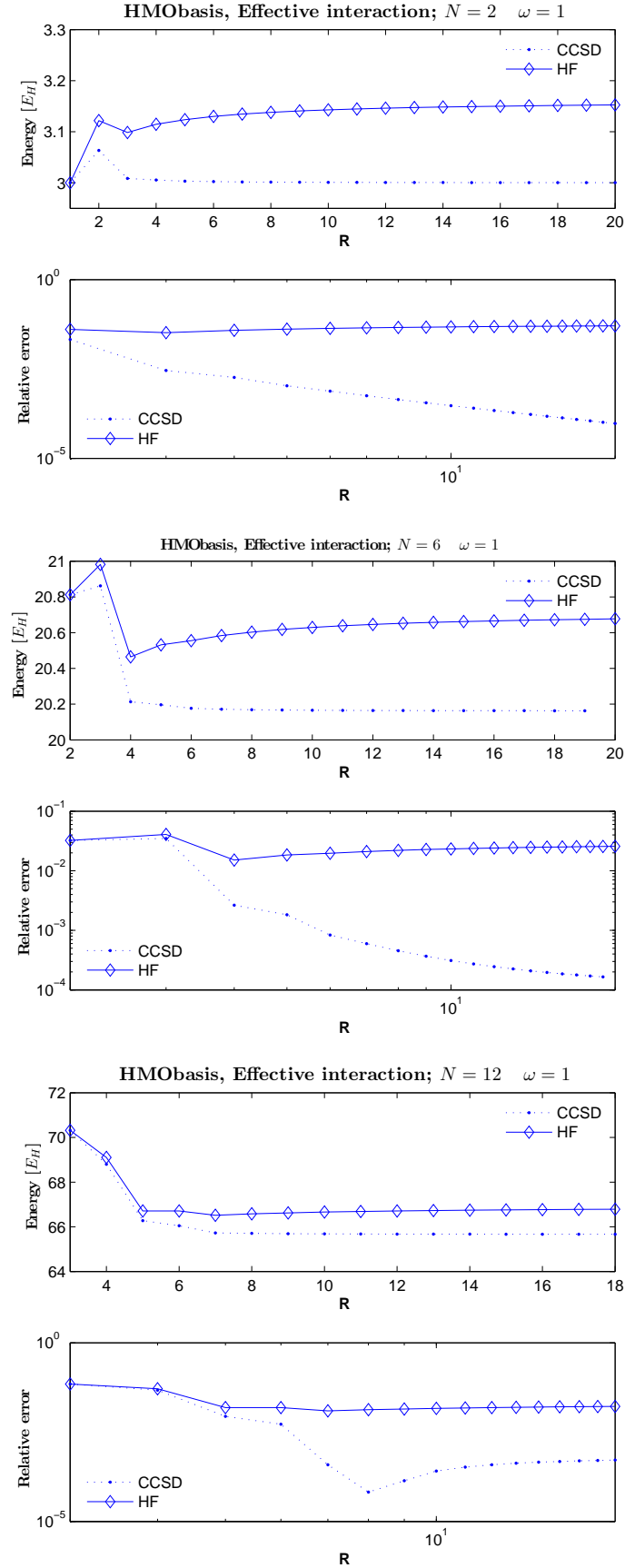


Figure 7.4: Energy and relative error as functions of R for the parabolic quantum dot with 2, 6 and 12 electrons, where we have used effective interaction and a HMO basis. The oscillator frequency takes the value $\omega = 1$. The energy is given in units of Hartrees $[E_H]$.

7.2.2 Effective Interaction Results: HF basis

In this section we present the CCSD result obtained with an effective interaction and the HF basis, presented in section 6.2.2. We also present HF results calculated with the code introduced in that same section.

Tables 7.16-7.19 display the HF results and the CCSD energy results obtained with a HF-basis for the two, six, twelve and twenty-electron quantum dot in frequency range $\omega = [0.1 - 1]$ and shell range $R = [10 - 20]$. The energy results for the two and six-electron dots are complete. However, for the two other dots this list is incomplete. In the tables, x denotes that convergence was not reached, and $-$ denotes that no calculations have been done, mainly due to convergence problems and high run-times.

If we compare both the HF and CCSD energies with the corresponding results obtained in section 7.1.2, we can conclude that the effective interaction leads to lower energies than what we obtain with the standard interaction. This suggests that the introduction of the effective interaction yields better convergence of the energy. It is also interesting to compare the CCSD results with the corresponding CCSD results obtained by the use of HMO-basis and effective interaction. Our CCSD results in tables 7.16-7.19, give lower energies compared to the HMO-CCSD results in tables 7.20-7.21. However, in section 7.1.2, we experienced that the introduction of the HF basis gave rise to energies lower than what we desired. Therefore we turn to Hagen's effective interaction CCSD results in table 7.22. If we compare these results with the corresponding HMO-CCSD energies, we observe that the introduction of the HF-basis leads to a higher energy than the HMO-basis. This fact does not necessarily mean that the HMO-basis performs better than the HF-basis. Remember that the CCSD method can underestimate the energy. If we consider $\omega = 1$ and $N = 6$ as an example, we have the DMC result $E_{\text{DMC}} = 20.1597$, which we know is an overestimate of the energy. In this case the HMO- and HF-basis results read

$$\begin{aligned} E_{\text{CCSD}}^{\text{HF}} &= 20.1786331, \\ E_{\text{CCSD}}^{\text{HMO}} &= 20.1659808. \end{aligned} \tag{7.52}$$

We see that the result connected to the HF basis is the highest, thus performance-wise this is the less favorable choice. This, however, does not alter the fact that the HF basis opens the possibility of exploring a larger frequency range. We reach convergence for lower frequencies when the HF basis is used.

We consider the convergence of the HF and CCSD energy for $\omega = 1$ as before. We plot the energy and the relative error of the two, six, and twelve-electron dots in fig. 7.6. The energy results in shell range $R = [1 - 9]$, are displayed in table 7.11. Again we observe that our CCSD energy for the six-electron and the twelve-electron dots underestimates the energy such that the HF-method performs better. In fig. 7.6 we plot the corresponding results of Hagen, and obtain the desirable result where the CCSD method is the favourable. In section 7.1.2 we discussed briefly the possible error-sources to this effect. We refer to this section for details, but make one notice here. Our CCSD code utilizing the HF basis do not converge for the twenty-electron dot in large parts of the frequency range in tables 7.17- 7.18. One of the exceptions to this tendency of no-convergence is the energy in shell $R = 10$ for frequency $\omega = 0.5$. We observe that the HF energy of $R = 10$ is significantly different from the values of higher shells. In ref. [43], Gaute Hagen's code is utilized

ω	R	$N = 2$		$N = 6$		$N = 12$	
		HF	CCSD	HF	CCSD	HF	CCSD
1.0	1	3.0000000	3.0000000	-	-	-	-
	2	3.1218683	3.0634405	20.8122102	20.8122102	-	-
	3	3.0983696	2.9468994	20.9823009	20.4335720	70.3136599	70.3136599
	4	3.1145058	2.9563780	20.4641404	19.5833698	69.1035677	67.4759916
	5	3.1234889	2.9622458	20.5318834	19.5219107	66.7067953	64.2245970
	6	3.1299651	2.9635122	20.5555241	19.4097806	66.7083189	63.5700686
	7	3.1345705	2.9641346	20.5838190	19.4260387	66.5144583	62.7456563
	8	3.1380311	2.9645401	20.6030921	19.4430711	66.5800133	62.6230566
	9	3.1407182	2.9648067	20.6179981	19.4470102	66.6225098	62.4980079

Table 7.11: HF and CCSD results for a 2, 6 and 12-electron parabolic quantum dot, where we have used effective interaction and a HF basis. The model space is in range $R = [1 - 9]$, for the oscillator frequency $\omega = 1$. Frequency and energy are given in units of Hartrees $[E_H]$. These are the results plotted in fig. 7.5.

to calculate this system of twenty-electron dots. Compared to this HF result, our HF energy is in agreement to the third decimal. Our CCSD energy though, is much lower than Hagen's. In the higher shells where the HF energy obviously is wrong, we obtain no convergence. This fact suggest that the source of error in our CCSD code lies in the HF calculations.

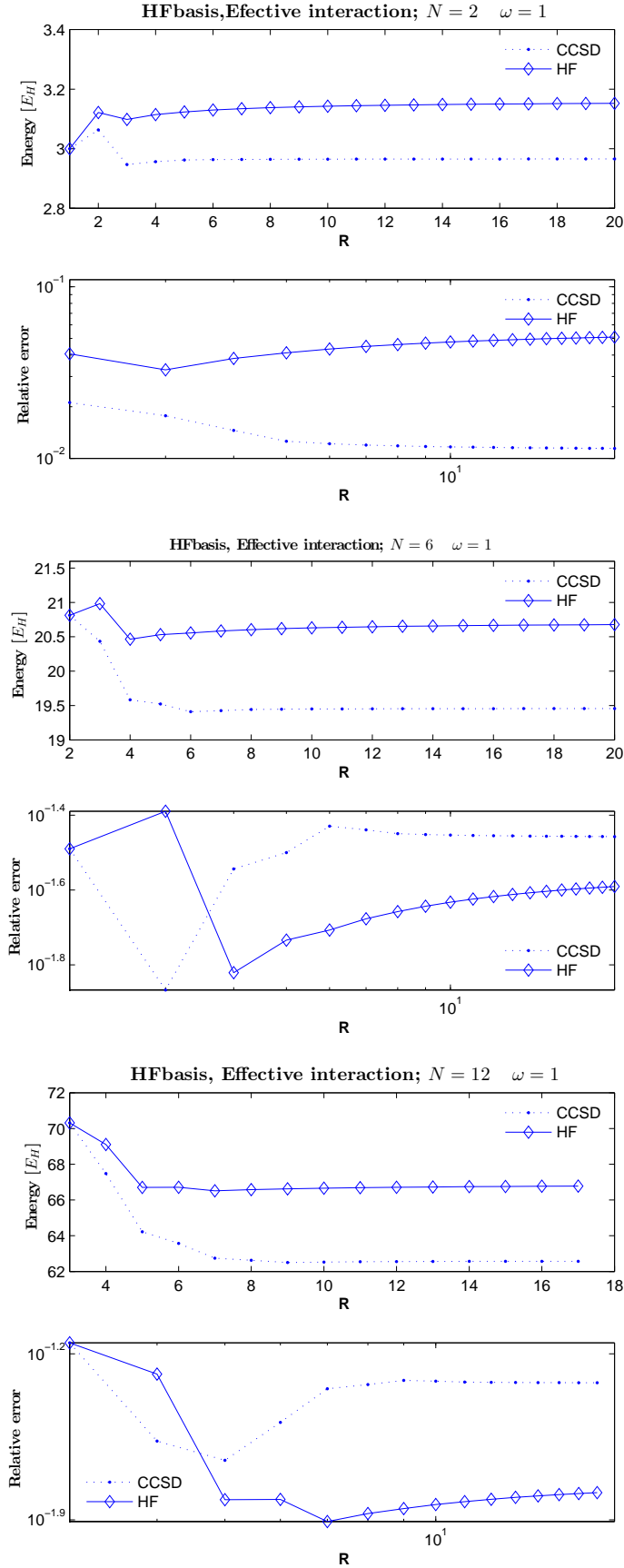


Figure 7.5: Energy and relative error as functions of R for the parabolic quantum dot with 2, 6 and 12 electrons, where we have used effective interaction and a HF basis. The oscillator frequency takes the value $w = 1$. The energy is given in units of Hartrees $[E_H]$.

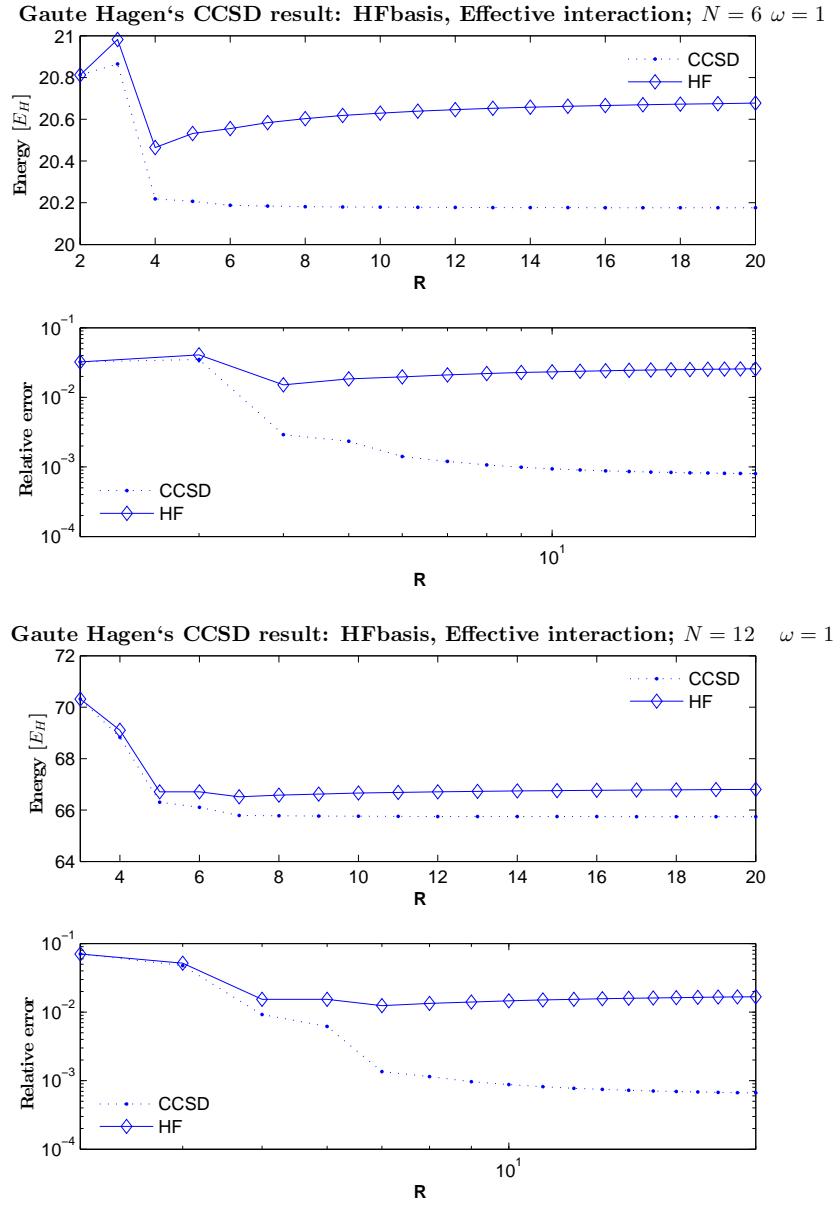


Figure 7.6: Energy and relative error as functions of R for the parabolic quantum dot with 6 and 12 electrons, where we have used effective interaction and a HF basis. These results are obtained with Gaite Hagen's code. The oscillator frequency takes the value $w = 1$. The energy is given in units of Hartrees [E_H].

7.3 Frequency Analysis

In this section we extend our analysis of the energy and the relative error as functions of shell number R . We now plot these two functions for lower frequencies. We select the two frequencies $\omega = 0.28$ and $\omega = 0.5$, since we have corresponding DMC energies reported in ref. [43]. We consider the results obtained with both HF basis and HMO basis, when possible, for the six and twelve-electron quantum dots. In each illustration we plot the effective interaction together with the standard interaction results. In addition we perform a linear fit of the relative errors in order to determine if the convergence rate of the CCSD method is universal, meaning independent of frequency.

In fig. 7.7 we plot the energy and relative error of the six-electron with HMO and HF basis for the selected frequencies. Note that for the HMO basis the energy do not converge for $\omega = 0.28$. We also plot the corresponding results of Hagen's CCSD code in fig. 7.8. The reason for considering Hagen's code, as discussed earlier, is that for the six and twelve-electron dot our CCSD code does not produce fully satisfying results. For the six-electron quantum dot we observe that the CCSD energy flattens out at $R = 6$ for all the frequencies, and independent of which basis we use. This means that all important correlation contributions are included when we reach $R = 6$. Therefore we consider the energy difference

$$E_{\text{diff}} = E_{\text{CCSD}}(\omega, R = 2) - E_{\text{CCSD}}(\omega, R = 6), \quad (7.53)$$

for each frequency $\omega = 0.28, 0.5, 1.0$. Table 7.12 displays the energy difference in eq. (7.53), for the results of our CCSD code and Hagen's CCSD code. In the table we observe a general tendency that the energy differences increase when the frequency is increased. Also note that if we compare the corresponding differences obtained with standard and effective interaction, the differences are larger when we use the standard interaction. Intuitively this is reasonable since the effective interaction is expected to increase the convergence of the CCSD energy as a function of R . From our results we observe that the effective interaction produces lower energies than what we obtain with standard interaction within same shell numbers. Therefore, for the effective interaction the range which leads to convergence is smaller, and thus the energy differences are smaller. For the results obtained with Hagen's code, we extend this study of energy differences to include the difference from one shell to the next in the shell range $R = [3 - 9]$. We expect that good convergence is reflected in small energy differences for higher shell numbers. The energy differences we observe show that the energy of the lowest shell numbers increases with the decrease of frequency, while higher lying shells experience a decrease in the energy difference when the frequency decreases. *Thus, an increase in the frequency leads to a slower convergence rate.*

The energy and relative error as a function of R for the twelve-electron quantum dot with the two frequencies in question, are plotted in fig. 7.9. The corresponding plot of Hagen's results are displayed in fig. 7.10. Note that HMO basis results are not obtained for the twelve-electron quantum dot, thus only HF basis results are presented. In the energy plot we observe that the most important correlation contributions are included for $R = 9$. Therefore, in table 7.13 we tabulate the energy difference

$$E_{\text{diff}} = E_{\text{CCSD}}(\omega, R = 3) - E_{\text{CCSD}}(\omega, R = 9), \quad (7.54)$$

for the frequency values $\omega = 0.28, 0.5, 1.0$. The general tendency is that for increasing frequencies, the energy differences increase. However, if we study the energy differences

from one shell to the next, in shell range $R = [3-12]$, we observe that the energy of higher shells increase when the frequency increases. *Thus, the convergence rate is expected to decrease when the frequency is increased.*

Guided by the convergence analysis of refs. [43] and [51], we examine the slope of the CCSD energy results. We assume the parametrization

$$\log_{10}\epsilon \approx \alpha \log_{10}R + c, \quad (7.55)$$

where R is the shell number and $\log_{10}\epsilon$ reads

$$\log_{10}\epsilon(R) = \log_{10} \left| \frac{E_{\text{DMC}} - E_{\text{CCSD}}(R)}{E_{\text{DMC}}} \right|. \quad (7.56)$$

The resulting slopes α of this parametrization for the six and twelve-electron dot, calculated with Hagen's CCSD code, are given in table 7.14. This slope is a measure on the convergence rate, where a high slope denotes fast convergence, and a low slope denotes slow convergence. In the table we observe that generally the convergence increases when the frequency increases, for the six-electron dot. This is what we expected from the consideration of energy differences above. However, note that these two cases are not directly comparable since we here consider the convergence related to the relative error, which is related to the DMC energy. For the twelve-electron quantum dots we observe that the convergence decreases when the frequency increases. In order to conclude with a general behavior for the convergence rate, we depend on extending this type of study including more frequencies and more electrons. What we can conclude with, is that from the relative errors plots in fig. 7.7-7.10, we see that the errors lie in a range $10^2 - 10^3$. If we compare these results with the results of the CCSD calculations in ref. [43], we conclude that we obtain results which correspond with what we can expect of the CCSD method.

E_{diff} for $N = 6$						
ω	CCSD HMObasis		CCSD HFbasis		Hagen HFbasis	
	std	eff	std	eff	std	eff
0.28	-	-	2.0164	0.8941	1.6055	0.4702
0.5	1.7990	0.5629	2.3556	1.1238	1.7744	0.5443
1.0	1.9589	0.6357	2.7394	1.4024	2.7394	1.4024

Table 7.12: Energy difference in eq. (7.53) for the 6-electron quantum dot. Eff denotes effective interaction and std denotes standard interaction. The difference is calculated for the results obtained with our CCSD code using both HMO and HF basis, and with Hagen's code using the HF basis. Energy is given in terms of Hartrees $[E_H]$

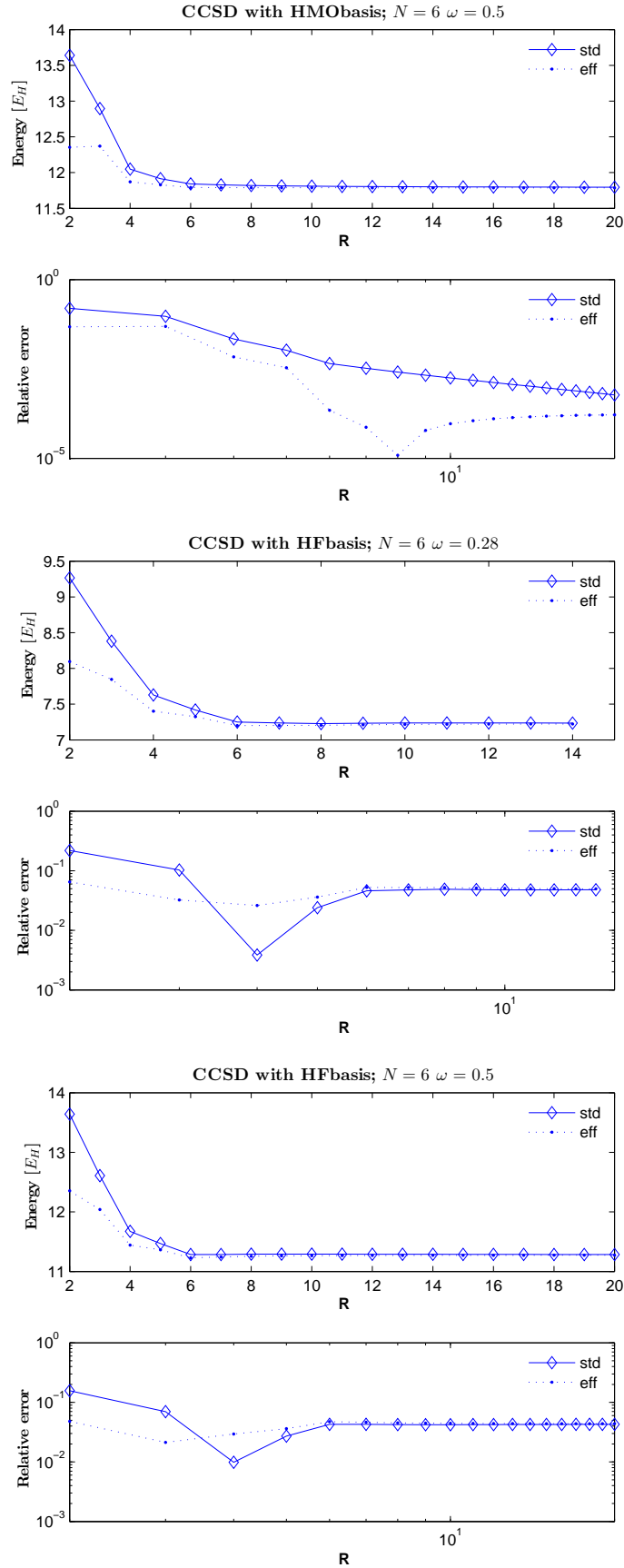


Figure 7.7: CCSD energy and relative error as functions of R for the 6-electron quantum dot, where we have used both HMO and HF basis. The oscillator frequency takes the values $\omega = 0.28, 0.5$. The calculations are conducted with both standard and effective interaction, denoted std and eff respectively. Energy is given in terms of Hartrees [E_H].

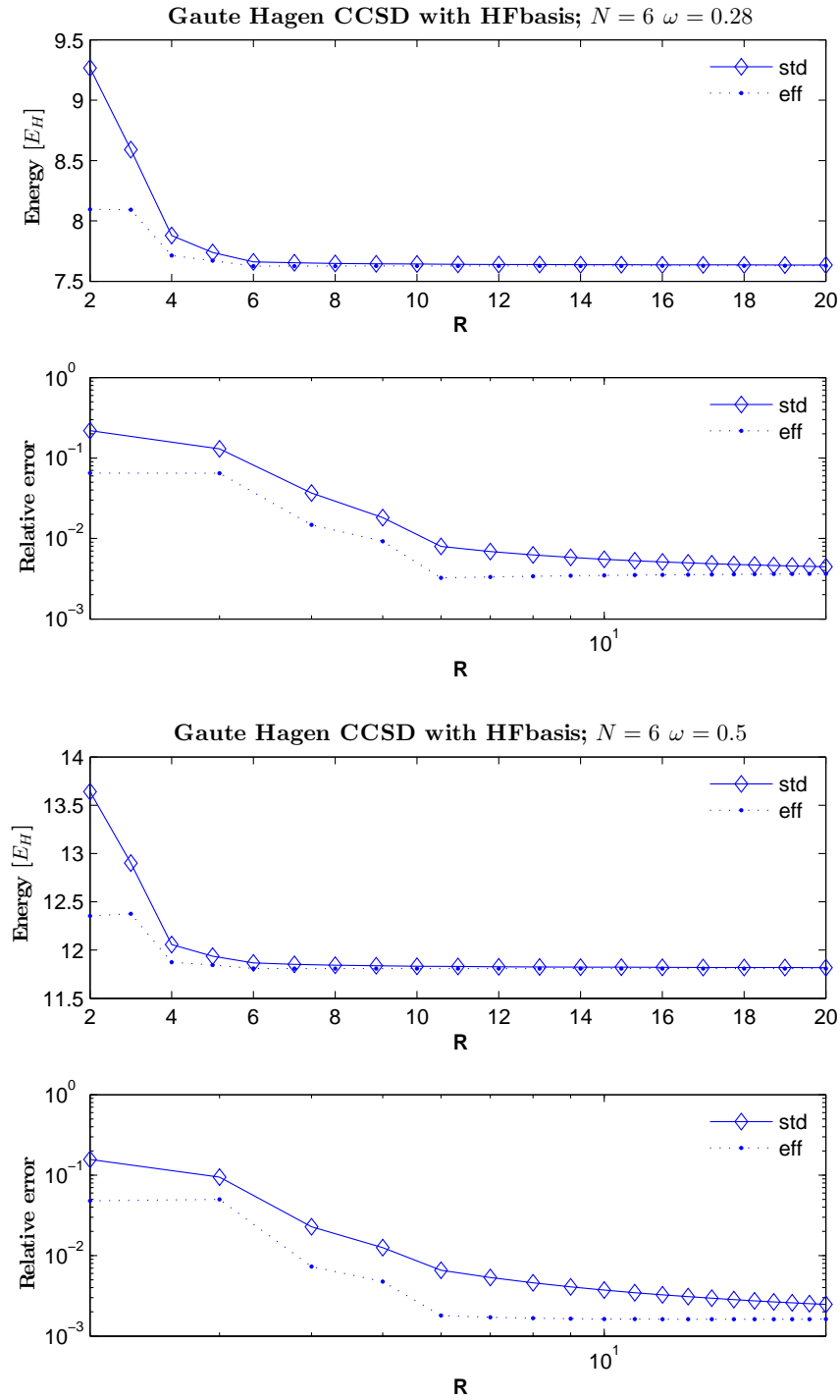


Figure 7.8: CCSD energy and relative error as functions of R for the 6-electron quantum dot, where we have used a HF basis. These results are obtained with Gaute Hagen's CCSD code. The oscillator frequency takes the values $\omega = 0.28, 0.5$. The calculations are conducted for both standard and effective interaction denoted std and eff, respectively. Energy is given in terms of Hartrees [E_H].

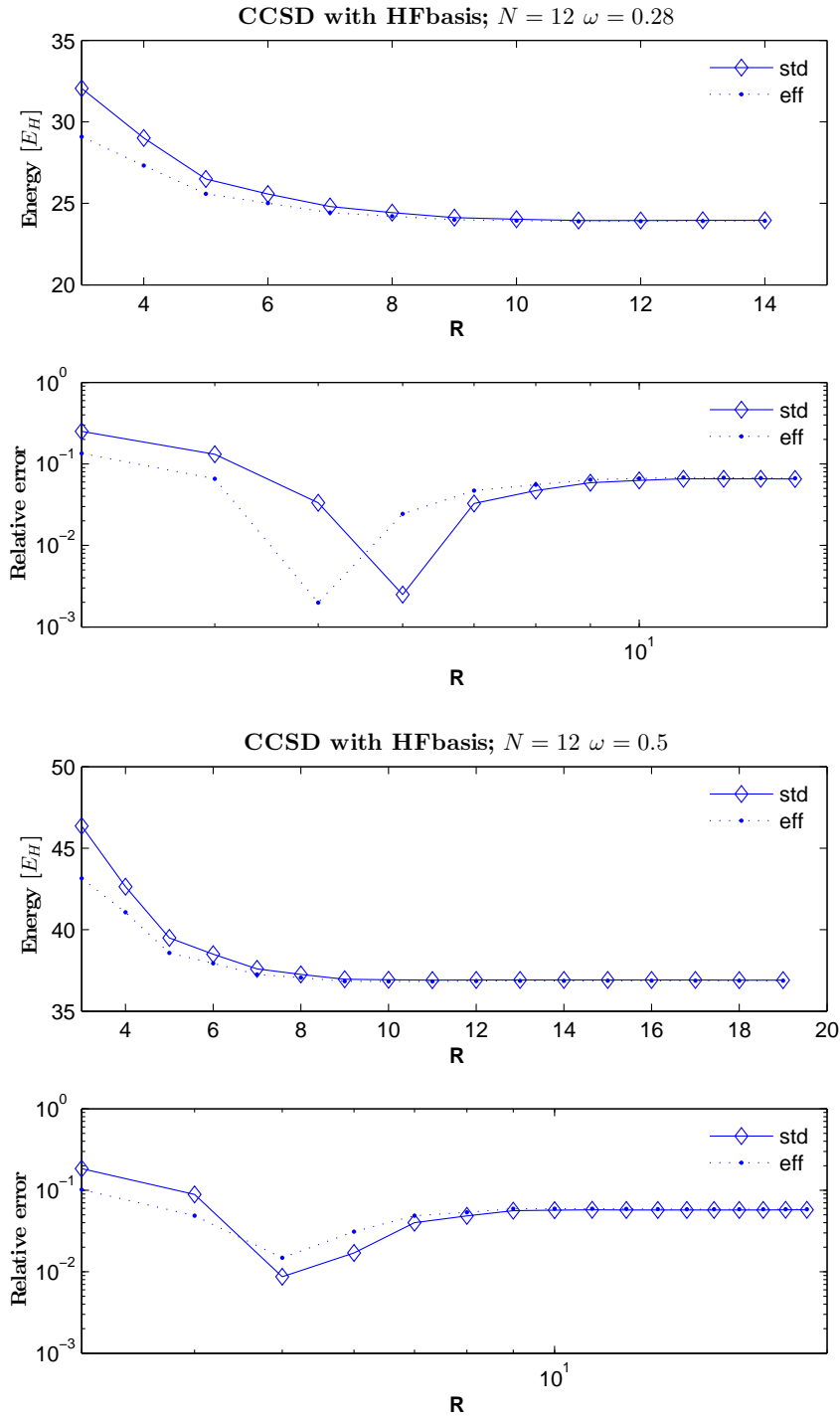


Figure 7.9: CCSD energy and relative error as functions of R for the 12-electron quantum dot, where we have used a HF-basis. Results of the HMO-basis do not converge for the 12-electron quantum dot with frequencies below $\omega = 0.9$. The calculations are conducted for both standard and effective interaction denoted std and eff, respectively. Energy is given in terms of Hartrees [E_H].

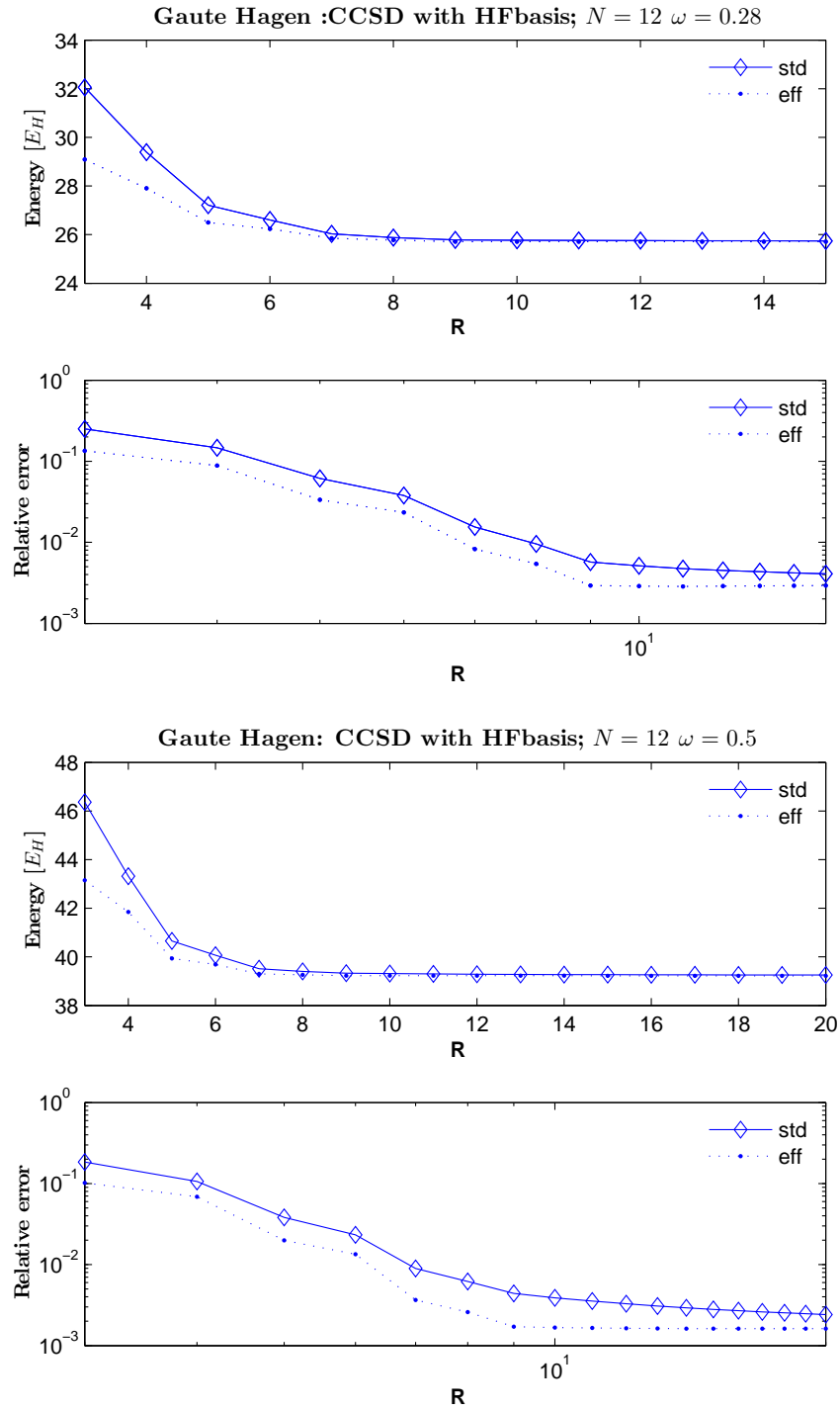


Figure 7.10: CCSD energy and relative error as functions of R for the 12-electron quantum dot, where we have used a HF basis. These results are obtained with Gaute Hagen's CCSD code. The oscillator frequency takes the values $\omega = 0.28, 0.5$. The calculations are conducted for both standard and effective interaction denoted std and eff, respectively. Energy is given in terms of Hartrees [E_H].

E_{diff} for $N = 12$				
ω	CCSD HFbasis		Hagen HFbasis	
	std	eff	std	eff
0.28	7.9274	5.0975	6.2750	3.3774
0.5	9.3983	6.3136	7.0293	3.9272
1.0	11.1306	7.8157	7.8427	4.5501

Table 7.13: Energy difference in eq. (7.54) for the 12-electron quantum dot. Eff denotes effective interaction and std denotes standard interaction. The difference is calculated for the results obtained with our CCSD code using the HF basis, and with Hagen’s code using the HF basis. Energy is given in terms of Hartrees [E_H].

ω	$N = 6$		$N = 12$	
	α std	α eff	α std	α eff
0.28	-0.263	0.061	-0.353	0.066
0.5	-0.531	0.005	-0.593	-0.023
1.0	-0.786	-0.177	0.059	0.007

Table 7.14: The slope of the parametrization in eq. (7.55) for the quantum dot with 6 and 12 electrons. The results are obtained by using both standard (std) and effective (eff) interaction.

7.4 The Wigner Crystal Limit

Wigner crystal is the name of the solid phase of electrons, which is formed when the electron density is less than a critical value. The reason for crystallization is that for low electron-densities the potential energy dominates the kinetic energy. This leads to a localisation of the electrons, since the spatial arrangement of the electrons gains importance. The drive towards a minimum in potential energy leads to crystallization. According to the article in ref. [45], features associated with correlation appear to develop very differently in quantum dots and bulk systems, and therefore it is of interest to study the properties of quantum dots in such strongly correlated settings. Remember from chapter 3 that quantum dots constitute an accessible laboratory of analogues to unexplored physics, thus the great interest for studying features of these systems. The article highlights the broken translation symmetries seen in the quantum dots, as the reason for the difference between the quantum dots and the bulk systems. The broken symmetries lead to a reduced ability to delocalize the electrons. Therefore the quantum dots possess the property of constituting an ”incipient” Wigner crystal for numerous frequencies. If we lower the frequency, which is the same as broadening our harmonic oscillator potential, the electron density is decreased. For low enough frequencies we start to see the effects of Wigner crystallization. In light of the low frequencies required in the Wigner crystal, we can justify the theoretical interest of examining the CCSD theory of these quantum dots. Low frequencies lead to a smaller distance between the Fermi-level of the system and the particle space. This means that the probability of excitation is much higher, and thus weakens the theoretical assumption that the ground state wave function is represented by one Slater determinant comprised of hole states. Therefore, it is interesting to investigate if or when the current CCSD theory breaks down. According to the article referred to above, Wigner effects occur for the frequencies $\omega = 0.01$ and $\omega = 0.015625$. The article presents both DMC and FCI results for the six-electron quantum dot with these selected

frequencies. Therefore, in this section we examine the CCSD-energy convergence of the six-electron quantum dots for the two frequencies above. We conduct energy calculations on this system with Gaute Hagen's CCSD code, where we have use both effective and standard interaction. Note that for frequencies in this range, we are forced to utilize the HF-basis in order to reach convergence. The reason for not performing these calculations with our CCSD code is the fact, discussed earlier, that for the six and twelve-electron quantum dots it produces much too low energies.

Table 7.15 present the HF and CCSD energies of the six-electron quantum dot, for the two frequencies of interest, and in shell range $R = [1 - 20]$. The calculations are conducted for both standard and effective interaction. In fig. 7.11 we plot the CCSD energy, the relative error related to the DMC result, and the relative error related to the FCI result. The DMC and FCI result are listed in ref. [45]. The DMC energies reads

$$\begin{aligned} E_{\text{DMC}}(\omega = 0.1) &= 0.6892, \\ E_{\text{DMC}}(\omega = 0.015625) &= 0.9426, \end{aligned} \tag{7.57}$$

and the FCI energies reads

$$\begin{aligned} E_{\text{FCI}}(\omega = 0.1) &= 0.6974, \\ E_{\text{FCI}}(\omega = 0.015625) &= 0.9475. \end{aligned} \tag{7.58}$$

We observe that the DMC method, which results in a variational upper bound to the exact energy, produces better results compared with the FCI method. This agrees with the opinion of the article above, which states that a Variational Monte Carlo (VMC) calculation followed by the DMC calculation, is the most accurate method for treating the strongly interacting quantum dots in the Wigner crystal limit. It is therefore interesting to see if the CCSD results agrees with the DMC results. Good agreement serves as support and validation of the CCSD theory. In fig. 7.11 we observe that the energy calculated with effective interaction in lower shells, for both frequencies, are lower than the corresponding energy of standard interaction. This demonstrates that the use of effective interaction improves the energy convergence as a function of R . We also observe from the relative errors related to DMC, that the energy differences lie in range $10^{-2} - 10^{-3}$. In ref. [43], the same relative error analysis is performed for two, six, twelve, and twenty-electron dots with different frequencies, where DMC results were calculated. This article obtains the same energy differences related to DMC results, as we do. This fact suggests that the CCSD method is incapable of producing results with relative errors lower than $10^{-2} - 10^{-3}$. The same article conducts calculations where triples are included, i.e. CCSDT. In these calculations the article obtains more correlation contributions, and thus obtains a relative error estimate of lower magnitude. However, the fact that we obtained results in good agreement with DMC for such low frequencies, implies that the theory of CCSD holds.

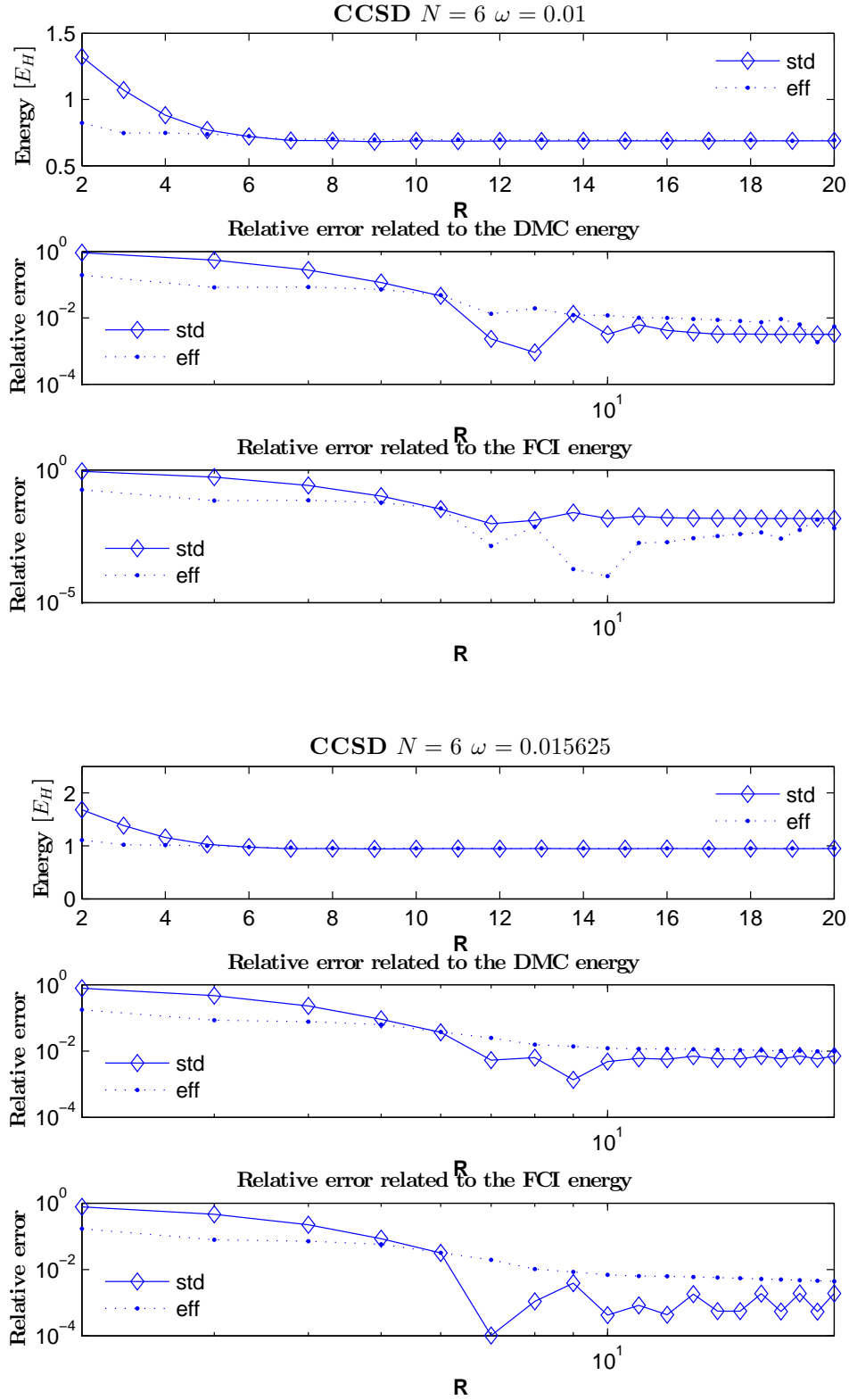


Figure 7.11: CCSD energy and relative errors as functions of R for the 6-electron quantum dot, with the oscillator frequencies $\omega = 0.01$ and $\omega = 0.015625$. The relative errors are related to DMC and FCI results given in ref. [45]. Results are shown for both the standard and the effective interaction denoted std and eff, respectively. Energy is given in terms of Hartrees [E_H].

$N = 6$								
R	$\omega = 0.01$				$\omega = 0.015625$			
	Standard interaction		Effective interaction		Standard interaction		Effective interaction	
	HF	CCSD	HF	CCSD	HF	CCSD	HF	CCSD
1	-	-	-	-	-	-	-	-
2	1.3219813	1.3219813	0.8225111	0.8225111	1.6837266	1.6837266	1.1089280	1.1089280
3	1.1362292	1.0708663	0.8336548	0.7465426	1.4599213	1.3833295	1.1216041	1.0224716
4	0.9539356	0.8808231	0.7542907	0.7476640	1.2488615	1.1583886	1.0285171	1.0152543
5	0.9183190	0.7695779	0.7745741	0.7386484	1.2029785	1.0277548	1.0527979	1.0018531
6	0.8565072	0.7207833	0.7584758	0.7224630	1.1318844	0.9771990	1.0334078	0.9778346
7	0.8404033	0.6907901	0.7663359	0.6983549	1.1155077	0.9475969	1.0413433	0.9659666
8	0.8155698	0.6885757	0.7616912	0.7025371	1.0902574	0.9485382	1.0362814	0.9572823
9	0.7576972	0.6801434	0.7658745	0.6975275	1.0852148	0.9438478	1.0413838	0.9554845
10	0.7460973	0.6870071	0.7658555	0.6973308	1.0770239	0.9471012	1.0423726	0.9540487
11	0.7433483	0.6849744	0.7688028	0.6961490	1.0118983	0.9482834	1.0457492	0.9534760
12	0.7947480	0.6863313	0.7703819	0.6960672	1.0739756	0.9479094	1.0480464	0.9534473
13	0.7407353	0.6867240	0.7725492	0.6955366	1.0109796	0.9492025	1.0504329	0.9531623
14	0.7405519	0.6869753	0.7742362	0.6951491	1.0736228	0.9480285	1.0523914	0.9529134
15	0.7405368	0.6869726	0.7758143	0.6947044	1.0736171	0.9480234	1.0540805	0.9526607
16	0.7405302	0.6869978	0.7771534	0.6942951	1.0109505	0.9492728	1.0555204	0.9524275
17	0.7405299	0.6870055	0.7783180	0.6955834	1.0736151	0.9480114	1.0567620	0.9522134
18	0.7405299	0.6869930	0.7793303	0.6935637	1.0109503	0.9492880	1.0578430	0.9520179
19	0.7405299	0.6870037	0.7397413	0.6879288	1.0736150	0.9480081	1.0587924	0.9518381
20	0.7405298	0.6870060	0.7810021	0.6929473	1.0109502	0.9492937	1.0596326	0.9516728

Table 7.15: HF and CCSD energy of the 6-electron quantum dot, for the oscillator frequencies $\omega = 0.01$ and $\omega = 0.015625$, in shell range $R = [1 - 20]$. These results are obtained with Gaute Hagen's CCSD code, where we use the HF-basis when we calculate the CCSD energy. Results are obtained for both standard and effective interaction. The frequency and the energy is given in terms of Hartrees $[E_H]$. These are the results plotted in fig. 7.11

7.5 Tables

This section holds the tables 7.16-7.22. These tables contain energy results obtained with both Hagen's and our CCSD code. The tables are placed here only of aesthetic reasons.

ω	R	$N = 2$				$N = 6$			
		Standard interaction		Effective interaction		Standard interaction		Effective interaction	
		HF	CCSD	HF	CCSD	HF	CCSD	HF	CCSD
0.1	10	0.5256350	0.4406740	0.5138235	0.4377957	3.7925546	3.4054820	3.7687268	3.3512448
	11	0.5256349	0.4406536	0.5148648	0.4380389	3.7925510	3.4095970	3.7715519	3.3589624
	12	0.5256349	0.4406332	0.5157371	0.4382388	3.7925493	3.4163351	3.7737762	3.3684649
	13	0.5256349	0.4406137	0.5164783	0.4384060	3.7925474	3.4176445	3.7755720	3.3730899
	14	0.5256349	0.4405957	0.5171160	0.4385481	3.7925465	3.4182917	3.7770533	3.3767182
	15	0.5256349	0.4405794	0.5176705	0.4386705	3.7925460	3.4184209	3.7782959	3.3795383
	16	0.5256349	0.4405646	0.5181571	0.4387770	3.7925456	3.4184442	3.7793533	3.3819700
	17	0.5256349	0.4405513	0.5185876	0.4388706	3.7925454	3.4184463	3.7802642	3.3841126
	18	0.5256349	0.4405392	0.5189711	0.4389535	3.7925453	3.4184414	3.7810571	3.3860124
	19	0.5256349	0.4405283	0.5193150	0.4390274	3.7925452	3.4184389	3.7817536	3.3877112
	20	0.5256349	0.4405184	0.5196251	0.4390938	3.7925452	3.4184363	3.8275516	3.3551721
0.2	10	0.8822933	0.7676319	0.8681207	0.7642631	6.2784783	5.6111171	6.2296935	5.5977295
	11	0.8822930	0.7675562	0.8693917	0.7645117	6.2784779	5.6127131	6.2362397	5.6001864
	12	0.8822930	0.7674888	0.8704542	0.7647131	6.2784752	5.6131697	6.2415643	5.6018535
	13	0.8822930	0.7674296	0.8713553	0.7648802	6.2935421	5.6150892	6.2459807	5.6028446
	14	0.8822930	0.7673777	0.8721293	0.7650213	6.2935409	5.6148320	6.2497036	5.6036208
	15	0.8822930	0.7673321	0.8728012	0.7651420	6.2935408	5.6145766	6.2528856	5.6042248
	16	0.8822930	0.7672919	0.8733899	0.7652466	6.2935405	5.6143412	6.2556363	5.6047445
	17	0.8822930	0.7672562	0.8739101	0.7653381	6.2935405	5.6141249	6.2580384	5.6051837
	18	0.8822930	0.7672244	0.8743729	0.7654188	6.2935405	5.6139293	6.2601541	5.6055619
	19	0.8822930	0.7671959	0.8747874	0.7654905	6.2935405	5.6137524	6.2620319	5.6058910
	20	0.8822930	0.7671702	0.8751608	0.7655547	6.2935405	5.6135925	6.2637097	5.6061803
0.3	10	1.2043507	1.0707137	1.1888375	1.0669088	8.4313973	7.6264958	8.3610693	7.6060779
	11	1.2043501	1.0705786	1.1902406	1.0671488	8.4313973	7.6263021	8.3682664	7.6080897
	12	1.2043501	1.0704613	1.1914120	1.0673413	8.4313960	7.6258846	8.3741245	7.6094960
	13	1.2043500	1.0703602	1.1924045	1.0675003	8.4313956	7.6253749	8.3789884	7.6105075
	14	1.2043500	1.0702727	1.1932560	1.0676338	8.4313954	7.6248983	8.3830910	7.6113053
	15	1.2043500	1.0701964	1.1939946	1.0677476	8.4313953	7.6244651	8.3865981	7.6119736
	16	1.2043500	1.0701295	1.1946413	1.0678458	8.4313950	7.6240777	8.3896307	7.6125136
	17	1.2043500	1.0700705	1.1952122	1.0679315	8.4313950	7.6237312	8.3922792	7.6129701
	18	1.2043500	1.0700181	1.1957198	1.0680068	8.4313949	7.6234225	8.3946122	7.6133627
	19	1.2043500	1.0699713	1.1961742	1.0680737	8.4313949	7.6231458	8.3966830	7.6137036
	20	1.2043500	1.0699293	1.1965833	1.0681333	8.4313949	7.6228975	8.3985333	7.6140030
0.4	10	1.5080112	1.3605689	1.4915844	1.3563465	10.4051703	9.5038991	10.3301854	9.4802831
	11	1.5080104	1.3603742	1.4930778	1.3565736	10.4051695	9.5031638	10.3378525	9.4822003
	12	1.5080104	1.3602079	1.4943236	1.3567551	10.4051657	9.5023737	10.3440952	9.4835463
	13	1.5080103	1.3600660	1.4953783	1.3569044	10.4051657	9.5016142	10.3492812	9.4845616
	14	1.5080103	1.3599437	1.4962826	1.3570292	10.4051657	9.5009377	10.3536562	9.4853661
	15	1.5080103	1.3598376	1.4970666	1.3571353	10.4051656	9.5003387	10.3573968	9.4860186
	16	1.5080103	1.3597449	1.4977526	1.3572266	10.4051654	9.4998100	10.3606316	9.4865608
	17	1.5080103	1.3596632	1.4983580	1.3573060	10.4051654	9.4993428	10.3634567	9.4870194
	18	1.5080103	1.3595909	1.4988961	1.3573758	10.4051653	9.4989285	10.3659453	9.4874130
	19	1.5080103	1.3595263	1.4993775	1.3574375	10.4051653	9.4985590	10.3681542	9.4877544
	20	1.5080103	1.3594685	1.4998108	1.3574926	10.4051653	9.4982284	10.3701279	9.4880537
0.5	10	1.7997408	1.6415581	1.7826326	1.6369365	12.2713101	11.2919940	12.1927030	11.2655842
	11	1.7997400	1.6413060	1.7841934	1.6371499	12.2713082	11.2908782	12.2007369	11.2674626
	12	1.7997400	1.6410929	1.7854948	1.6373198	12.2713041	11.2897994	12.2072806	11.2689476
	13	1.7997398	1.6409120	1.7865958	1.6374593	12.2713041	11.2888197	12.2127172	11.2698153
	14	1.7997398	1.6407567	1.7875394	1.6375754	12.2713038	11.2879633	12.2173038	11.2706170
	15	1.7997398	1.6406223	1.7883571	1.6376740	12.2713038	11.2872122	12.2212257	11.2712663
	16	1.7997398	1.6405050	1.7890725	1.6377586	12.2713038	11.2865540	12.2246175	11.2718056
	17	1.7997398	1.6404018	1.7897035	1.6378321	12.2713037	11.2859752	12.2275797	11.2722615
	18	1.7997398	1.6403106	1.7902643	1.6378965	12.2713037	11.2854632	12.2301891	11.2726316
	19	1.7997398	1.6402292	1.7907659	1.6379534	12.2713037	11.2850077	12.2325052	11.2729693
	20	1.7997398	1.6401563	1.7912172	1.6380041	12.2713036	11.2846007	12.2345748	11.2732651

Table 7.16: Results of Hartree-Fock calculations and Coupled Cluster Singles and Doubles calculations using a HF basis, for a 2-dimensional parabolic quantum dot with 2 and 6 electrons. The oscillator frequency is given by ω , and the size of the model space is given by R . The results are obtained with both the standard and the effective interaction. The frequency and the energy are given in terms of Hartrees [E_H].

ω	R	$N = 2$				$N = 6$			
		Standard interaction		Effective interaction		Standard interaction		Effective interaction	
		HF	CCSD	HF	CCSD	HF	CCSD	HF	CCSD
0.6	10	2.0829208	1.9160210	2.0652756	1.9110197	14.0596725	13.0149234	13.9781112	12.9860219
	11	2.0829201	1.9157145	2.0668897	1.9112193	14.0596700	13.0134795	13.9864455	12.9878641
	12	2.0829201	1.9154572	2.0682347	1.9113780	14.0596667	13.0121397	13.9932358	12.9891747
	13	2.0829199	1.9152394	2.0693722	1.9115079	14.0596666	13.0109607	13.9988768	12.9901710
	14	2.0829199	1.9150529	2.0703469	1.9116158	14.0596662	13.0099388	14.0036361	12.9909601
	15	2.0829199	1.9148918	2.0711911	1.9117071	14.0596662	13.0090474	14.0077058	12.9915982
	16	2.0829199	1.9147513	2.0719295	1.9117854	14.0596662	13.0082695	14.0112255	12.9921280
	17	2.0829199	1.9146280	2.0725808	1.9118533	14.0596662	13.0075868	14.0142994	12.9925751
	18	2.0829199	1.9145189	2.0731593	1.9119128	14.0596661	13.0069839	14.0170072	12.9929577
	19	2.0829199	1.9144217	2.0736768	1.9119653	14.0596661	13.0064484	14.0194106	12.9932891
	20	2.0829199	1.9143347	2.0741423	1.9120119	14.0596661	13.0059702	14.0215582	21.6559650
0.7	10	2.3595839	2.1853974	2.3414996	2.1800358	15.7883627	14.6873757	15.7043143	14.6562269
	11	2.3595833	2.1850397	2.3431572	2.1802222	15.7883601	14.6856243	15.7129023	14.6580217
	12	2.3595833	2.1847407	2.3445379	2.1803701	15.7883581	14.6840377	15.7199008	14.6593088
	13	2.3595832	2.1844883	2.3457052	2.1804909	15.7883579	14.6826719	15.7257141	14.6602860
	14	2.3595832	2.1842724	2.3467052	2.1805910	15.7883574	14.6814938	15.7306188	14.6610578
	15	2.3595831	2.1840862	2.3475712	2.1806756	15.7883574	14.6804710	15.7348130	14.6616816
	16	2.3595831	2.1839240	2.3483284	2.1807480	15.7883574	14.6795808	15.7384402	14.6621990
	17	2.3595831	2.1837816	2.3489961	2.1808107	15.7883573	14.6788007	15.7416081	14.6626349
	18	2.3595831	2.1836557	2.3495893	2.1808655	15.7883573	14.6781126	15.7443988	14.6630076
	19	2.3595831	2.1835437	2.3501197	2.1809138	15.7883573	14.6775021	15.7468756	14.6633302
	20	2.3595831	2.1834433	2.3505968	2.1809568	15.7883573	14.6769572	15.7490888	14.6636120
0.8	10	2.6310505	2.4506428	2.6125974	2.4449396	17.4692271	16.3190577	17.3830383	16.2858657
	11	2.6310499	2.4502369	2.6142916	2.4451135	17.4692246	16.3170177	17.3918452	16.2876117
	12	2.6310499	2.4498987	2.6157023	2.4452514	17.4692237	16.3152003	17.3990231	16.2888407
	13	2.6310498	2.4496136	2.6168946	2.4453634	17.4692235	16.3136596	17.4049847	16.2897930
	14	2.6310498	2.4493701	2.6179158	2.4454562	17.4692230	16.3123345	17.4100147	16.2905426
	15	2.6310497	2.4491602	2.6188000	2.4455344	17.4692230	16.3111886	17.4143159	16.2911657
	16	2.6310497	2.4489776	2.6195730	2.4456013	17.4692229	16.3101932	17.4180358	16.2916689
	17	2.6310497	2.4488173	2.6202546	2.4456591	17.4692229	16.3093217	17.4212846	16.2920922
	18	2.6310497	2.4486757	2.6208600	2.4457096	17.4692229	16.3085537	17.4241464	16.2924537
	19	2.6310497	2.4485496	2.6214012	2.4457541	17.4692229	16.3078728	17.4266864	16.2927663
	20	2.6310497	2.4484368	2.6218880	2.4457937	17.4692229	16.3072653	17.4289560	16.2930393
0.9	10	2.8982660	2.7124535	2.8794968	2.7064271	19.1107946	17.9169735	19.0227302	17.8819079
	11	2.8982656	2.7120022	2.8812224	2.7065889	19.1107926	17.9146593	19.0317295	17.8836013
	12	2.8982656	2.7116270	2.8826587	2.7067168	19.1107924	17.9126245	19.0390644	17.8847890
	13	2.8982655	2.7113111	2.8838725	2.7068207	19.1107920	17.9109356	19.0451561	17.8857160
	14	2.8982655	2.7110416	2.8849119	2.7069065	19.1107916	17.9094716	19.0502959	17.8864431
	15	2.8982654	2.7108094	2.8858117	2.7069788	19.1107916	17.9082101	19.0546910	17.8870318
	16	2.8982654	2.7106075	2.8865983	2.7070404	19.1107916	17.9071154	19.0584920	17.8875188
	17	2.8982654	2.7104304	2.8872917	2.7070937	19.1107916	17.9061579	19.0618116	17.8879280
	18	2.8982654	2.7102739	2.8879075	2.7071402	19.1107915	17.9053148	19.0647358	17.8882772
	19	2.8982654	2.7101347	2.8884581	2.7071812	19.1107915	17.9045676	19.0673311	17.8885788
	20	2.8982654	2.7100101	2.8889533	2.7072176	19.1107915	17.9039011	19.0696501	17.8888420
1	10	3.1619089	2.9713381	3.1428642	2.9650049	20.7192171	19.4862464	20.629487	19.4494262
	11	3.1619086	2.9708440	3.1446171	2.9651554	20.7192154	19.4836774	20.6386575	19.4510653
	12	3.1619086	2.9704340	3.1460758	2.9652740	20.7192154	19.4814424	20.6461315	19.4522123
	13	3.1619085	2.9700890	3.1473083	2.9653701	20.7192151	19.4795789	20.6523388	19.4531118
	14	3.1619085	2.9697950	3.1483635	2.9654494	20.7192148	19.4779827	20.6575763	19.4538149
	15	3.1619084	2.9695418	3.1492769	2.9655161	20.7192148	19.4766115	20.6620548	19.4543850
	16	3.1619084	2.9693217	3.1500753	2.9655729	20.7192147	19.4754228	20.6659278	19.4548559
	17	3.1619084	2.9691287	3.1507790	2.9656219	20.7192147	19.4743839	20.6693103	19.4552512
	18	3.1619084	2.9689582	3.1514040	2.9656647	20.7192147	19.4734696	20.6722898	19.4555882
	19	3.1619084	2.9688065	3.1519627	2.9657023	20.7192147	19.4726597	20.6749343	19.4558791
	20	3.1619084	2.9686708	3.1524651	2.9657357	20.7192147	19.4719375	20.6772971	19.4561326

Table 7.17: Results of Hartree-Fock calculations and Coupled Cluster Singles and Doubles calculations using a HF basis, for a 2-dimensional parabolic quantum dot with 2 and 6 electrons. The oscillator frequency is given by ω , and the size of the model space is given by R . The results are obtained with both the standard and the effective interaction. The frequency and the energy are given in terms of Hartrees $[E_H]$.

ω	R	$N = 12$				$N = 20$			
		Standard interaction		Effective interaction		Standard interaction		Effective interaction	
		HF	CCSD	HF	CCSD	HF	CCSD	HF	CCSD
0.1	10	14.1515353	x	13.7019376	x	33.9086498	x	32.8422263	x
	11	14.4056810	x	14.1237291	x	34.0059882	x	33.2885034	x
	12	14.4381374	x	14.2122652	x	34.2159996	74.8122094	33.6081384	70.6897177
	13	14.5353978	x	14.3455896	x	34.3416211	x	33.8414801	x
	14	14.5406114	x	14.3764171	x	34.5854719	x	34.1516063	77.0044410
	15	14.5521422	x	-	-	-	-	-	-
	16	14.5546698	x	-	-	-	-	-	-
	17	14.5559995	x	-	-	-	-	-	-
	18	14.5570461	x	-	-	-	-	-	-
	19	-	-	-	-	-	-	-	-
	20	-	-	-	-	-	-	-	-
0.2	10	20.9239242	18.7870461	20.7635551	18.7312124	54.2748013	x	53.2009178	x
	11	22.5694931	x	20.7783127	18.6678743	54.7134917	x	53.9235847	x
	12	22.6509802	x	20.7957819	18.6655976	55.3126708	x	54.6479233	x
	13	22.7238257	x	20.8097782	18.6695711	55.6073512	x	55.0563578	x
	14	22.7513136	x	22.1274054	x	55.9454490	x	55.4772296	x
	15	22.7685744	x	-	-	-	-	-	-
	16	22.7794689	x	-	-	-	-	-	-
	17	22.7863870	x	-	-	-	-	-	-
	18	22.7907901	x	-	-	-	-	-	-
	19	22.7935993	x	-	-	-	-	-	-
	20	22.7953929	x	-	-	-	-	-	-
0.3	10	27.8860797	25.2692227	27.6848635	25.1808651	71.7936870	x	70.5719047	x
	11	27.8827086	25.2026044	27.7065931	25.1441561	72.5197927	x	71.6155285	x
	12	27.8827075	25.2049891	27.7253041	25.1558310	73.2957263	x	72.5428679	x
	13	27.8826965	25.2108975	27.7403501	25.1683174	73.5940421	x	72.9536627	x
	14	27.8826933	25.2149814	27.7527424	25.1760507	73.8288416	x	73.2730674	x
	15	27.8826926	25.2171950	27.7631306	25.1814151	-	-	-	-
	16	27.8826919	25.2165910	27.7719682	25.1837628	-	-	-	-
	17	27.8826906	25.2157920	27.7795810	25.1854913	-	-	-	-
	18	27.8826906	25.2148897	27.7862098	25.1869886	-	-	-	-
	19	27.8826905	25.2140380	27.7920342	25.1880660	-	-	-	-
	20	27.8826905	25.2132475	27.7971932	25.1889643	-	-	-	-
0.4	10	34.2425692	31.2501180	34.0303819	31.1620241	87.4415394	x	85.8823287	x
	11	34.2418372	31.2121779	34.0548788	31.1481297	88.4296120	x	87.3501728	x
	12	34.2418183	31.2202974	34.0744561	31.1639098	89.2746140	x	88.3877161	x
	13	34.2417851	31.2277278	34.0902633	31.1772846	89.5322096	x	88.7669000	x
	14	34.2417850	31.2285573	34.1033328	31.1828059	89.6808510	x	89.0089407	x
	15	34.2417836	31.2285026	34.1143105	31.1867108	-	-	-	-
	16	34.2417830	31.2271622	34.1236670	31.1886897	-	-	-	-
	17	34.2417827	31.2258248	34.1317383	31.1903195	-	-	-	-
	18	34.2417826	31.2245706	34.1387736	31.1916191	-	-	-	-
	19	34.2417824	31.2234240	34.1449609	31.1926891	-	-	-	-
	20	34.2417824	31.2223792	34.1504456	31.1935855	-	-	-	-
0.5	10	40.2161958	36.9217464	39.9947475	36.8304403	101.2266452	x	95.2870386	88.2896591
	11	40.2161389	36.9042339	40.0205019	36.8330914	102.7763096	x	101.3495483	x
	12	40.2161093	36.9117459	40.0408077	36.8486643	103.6977017	x	102.6067275	x
	13	40.2160881	36.9173124	40.0572591	36.8604514	103.9346780	x	102.9933387	x
	14	40.2160871	36.9162527	40.0708750	36.8648908	104.0504061	x	103.2202505	x
	15	40.2160833	36.9148145	40.0823267	36.8680398	-	-	-	-
	16	40.2160832	36.9129738	40.0920995	36.8701204	-	-	-	-
	17	40.2160831	36.9112545	40.1005371	36.8717412	-	-	-	-
	18	40.2160830	36.9096913	40.1078968	36.8730501	-	-	-	-
	19	40.2160828	36.9082788	40.1143733	36.8739546	-	-	-	-
	20	-	-	40.1201172	36.8748575	-	-	-	-

Table 7.18: Results of Hartree-Fock calculations and Coupled Cluster Singles and Doubles calculations using a HF basis, for a 2-dimensional parabolic quantum dot with 12 and 20 electrons. The oscillator frequency is given by ω , and the size of the model space is given by R . The results are obtained with both the standard and the effective interaction. We use x to denote that convergence was not reached, and $-$ denotes that no calculation was done, mainly due to convergence problems and high run-times. The frequency and the energy are given in terms of Hartrees $[E_H]$.

ω	R	$N = 12$				$N = 20$			
		Standard interaction		Effective interaction		Standard interaction		Effective interaction	
		HF	CCSD	HF	CCSD	HF	CCSD	HF	CCSD
0.6	10	45.9113802	42.3644307	45.6820229	42.2690307	109.1449650	101.3459788	108.5930074	100.8407273
	11	45.9113435	42.3604829	45.7084777	42.2824630	114.7683642	x	108.6438109	100.4997756
	12	45.9113201	42.3656059	45.7294155	42.2962144	116.5597276	x	114.4403301	x
	13	45.9113147	42.3688585	45.7464134	42.3060667	116.8587328	x	115.4025926	x
	14	45.9113121	42.3667309	45.7604885	42.3100018	116.9982602	x	115.7727095	x
	15	45.9113081	42.3644942	45.7723387	42.3128056	-	-	-	-
	16	45.9113081	42.3622442	45.7824590	42.3148193	-	-	-	-
	17	45.9113078	42.3601989	45.7912018	42.3164050	-	-	-	-
	18	45.9113078	42.3583622	45.7988315	42.3176924	-	-	-	-
	19	45.9113077	42.3567123	45.8055486	42.3187586	-	-	-	-
	20	45.9113077	42.3552307	45.8115079	42.3196587	-	-	-	-
0.7	10	51.3920032	47.6285621	51.1557897	47.5280224	121.9318374	113.4333003	121.3727947	112.9517103
	11	51.3917987	47.6327988	51.1827379	47.5479424	121.9092014	112.9746044	121.4315411	112.6503465
	12	51.3917859	47.6352663	51.2042292	47.5598021	121.8876083	112.5942132	121.4707793	112.3727079
	13	51.3917857	47.6361098	51.2216925	47.5683697	121.8875930	112.5348264	121.5148301	112.3609701
	14	51.3917824	47.6332659	51.2361642	47.5720823	121.8875262	112.5133424	121.5501969	112.3689294
	15	51.3917796	47.6304756	51.2483584	47.5747398	-	-	-	-
	16	51.3917795	47.6278594	51.2587770	47.5767167	-	-	-	-
	17	51.3917791	47.6255140	51.2677814	47.5782829	-	-	-	-
	18	51.3917790	47.6232556	51.2756425	47.5795595	-	-	-	-
	19	51.3917790	47.6213849	51.2825654	47.5806195	-	-	-	-
	20	51.3917790	47.6197113	51.2887088	47.5815166	-	-	-	-
0.8	10	56.7001166	52.7468143	56.4578814	52.6413931	134.2941652	125.1723041	133.7275188	124.7085755
	11	56.6997216	52.7554936	56.4852467	52.6649946	134.2785137	124.7618181	133.7919164	124.4458046
	12	56.6997171	52.7555289	56.5072262	52.6751428	134.2647094	124.4294216	133.8380389	124.2087518
	13	56.6997106	52.7545217	56.5250904	52.6823763	134.2646867	124.3949573	133.8826911	124.2149477
	14	56.6997074	52.7512595	56.5399120	52.6859301	134.2644626	124.3891845	133.9185244	124.2366245
	15	56.6997062	52.7480262	56.5524068	52.6884814	-	-	-	-
	16	56.6997060	52.7450779	56.5630864	52.6904061	-	-	-	-
	17	56.6997054	52.7424540	56.5723195	52.6919334	-	-	-	-
	18	56.6997054	52.7401258	56.5803827	52.6931811	-	-	-	-
	19	56.6997054	52.7380516	56.5874852	52.6942190	-	-	-	-
	20	56.6997054	52.7362002	-	-	-	-	-	-
0.9	10	61.8661252	57.7440521	61.6185310	57.6334083	146.3050433	136.6235236	145.7306575	136.1745284
	11	61.8655708	57.7546429	61.6462870	57.6586726	146.2942527	136.2576889	145.7991502	135.9469918
	12	61.8655703	57.7526906	61.6687013	57.6676930	146.2855755	135.9708047	145.8499917	135.7485083
	13	61.8655492	57.7502575	61.6869164	57.6740717	146.2854688	135.9531884	145.8951702	135.7675354
	14	61.8655467	57.7463569	61.7020484	57.6775239	146.2851105	135.9578975	145.9314535	135.7956216
	15	61.8655464	57.7427367	61.7148123	57.6800145	-	-	-	-
	16	61.8655461	57.7394834	61.7257240	57.6819067	-	-	-	-
	17	61.8655456	57.7365998	61.7351604	57.6834081	-	-	-	-
	18	61.8655456	57.7340497	61.7434030	57.6846364	-	-	-	-
	19	61.8655456	57.7317837	61.7506647	57.6855187	-	-	-	-
	20	61.8655456	-	61.7571113	57.6863836	-	-	-	-
1.0	10	66.9120351	62.6377109	66.6596230	62.5221049	158.0176668	147.8304975	157.4356291	147.3924484
	11	66.9113645	62.6488248	66.6877593	62.5477216	158.0102763	147.5060487	157.5071434	147.1974772
	12	66.9113640	62.6452817	66.7105645	62.5558738	158.0049514	147.2594864	157.5612507	147.0338217
	13	66.9113232	62.6417508	66.7290914	62.5616230	158.0047567	147.2526261	157.6069274	147.0608675
	14	66.9113215	62.6374118	66.7445043	62.5649638	158.0043170	147.2631296	157.6436679	147.0936463
	15	66.9113214	62.6334491	66.7575087	62.5673862	-	-	-	-
	16	66.9113210	62.6299189	66.7686291	62.5692341	-	-	-	-
	17	66.9113206	62.6267964	66.7782484	62.5706983	-	-	-	-
	18	66.9113206	62.6240410	66.7866520	62.5718977	-	-	-	-
	19	66.9113206	62.6215965	66.7940568	62.5728975	-	-	-	-
	20	66.9113206	62.6194204	66.8006313	62.5737466	-	-	-	-

Table 7.19: Results of Hartree-Fock calculations and Coupled Cluster Singles and Doubles calculations using a HF basis, for a 2-dimensional parabolic quantum dot with 12 and 20 electrons. The oscillator frequency is given by ω , and the size of the model space is given by R . The results are obtained with both the standard and the effective interaction. We use x to denote that convergence was not reached, and $-$ denotes that no calculation was done, mainly due to convergence problems and high run-times. The frequency and the energy are given in terms of Hartrees [E_H].

ω	R	$N = 2$		$N = 6$		$N = 12$		$N = 20$	
		Std CCSD	Eff CCSD	Std CCSD	Eff CCSD	Std CCSD	Eff CCSD	Std CCSD	Eff CCSD
0.1	10	0.4411357	0.4408192	x	x	x	x	x	x
	11	0.4410973	0.4408153	x	x	x	x	x	x
	12	0.4410662	0.4408123	x	x	x	x	x	x
	13	0.4410406	0.4408099	x	x	x	x	x	x
	14	0.4410191	0.4408080	x	x	x	x	x	x
	15	0.4410009	0.4408064	x	x	x	x	x	x
	16	0.4409852	0.4408050	x	x	x	x	x	x
	17	0.4409716	0.4408038	x	x	x	x	x	x
	18	0.4409597	0.4408029	x	x	x	x	x	x
	19	0.4409492	0.4408020	x	x	x	x	x	x
	20	0.4409399	0.4408013	x	x	x	x	x	x
0.2	10	0.7751508	0.7740851	x	x	x	x	x	x
	11	0.7750155	0.7740678	x	x	x	x	x	x
	12	0.7749068	0.7740545	x	x	x	x	x	x
	13	0.7748177	0.7740439	x	x	x	x	x	x
	14	0.7747435	0.7740355	x	x	x	x	x	x
	15	0.7746807	0.7740286	x	x	x	x	x	x
	16	0.7746270	0.7740228	x	x	x	x	x	x
	17	0.7745805	0.7740180	x	x	x	x	x	x
	18	0.7745400	0.7740139	x	x	x	x	x	x
	19	0.7745042	0.7740103	x	x	x	x	x	x
	20	0.7744725	0.7740072	x	x	x	x	x	x
0.3	10	1.0839642	1.0820986	x	x	x	x	x	x
	11	1.0837248	1.0820647	x	x	x	x	x	x
	12	1.0835326	1.0820387	x	x	x	x	x	x
	13	1.0833753	1.0820182	x	x	x	x	x	x
	14	1.0832442	1.0820017	x	x	x	x	x	x
	15	1.0831333	1.0819883	x	x	x	x	x	x
	16	1.0830385	1.0819769	x	x	x	x	x	x
	17	1.0829565	1.0819675	x	x	x	x	x	x
	18	1.0828849	1.0819595	x	x	x	x	x	x
	19	1.0828219	1.0819526	x	x	x	x	x	x
	20	1.0827661	1.0819467	x	x	x	x	x	x
0.4	10	1.3785506	1.3759256	9.9630316	9.9454069	x	x	x	x
	11	1.3782124	1.3758748	9.96066012	9.9452608	x	x	x	x
	12	1.3779410	1.3758358	9.95882140	9.9451599	x	x	x	x
	13	1.3777187	1.3758051	9.95736001	9.9450917	x	x	x	x
	14	1.3775335	1.3757804	9.95617041	9.9450442	x	x	x	x
	15	1.3773769	1.3757602	9.95518395	9.9450098	x	x	x	x
	16	1.3772428	1.3757434	9.95435347	9.9449857	x	x	x	x
	17	1.3771269	1.3757293	9.95364590	9.9449673	x	x	x	x
	18	1.3770257	1.3757173	9.95303565	9.9449553	x	x	x	x
	19	1.3769366	1.3757070	9.95250444	9.9449508	x	x	x	x
	20	1.3768576	1.3756980	9.95203531	9.9449386	x	x	x	x
0.5	10	1.6635345	1.6602102	11.8097742	11.7877088	x	x	x	x
	11	1.6631055	1.6601430	11.8067720	11.7874660	x	x	x	x
	12	1.6627612	1.6600914	11.8044422	11.7872934	x	x	x	x
	13	1.6624790	1.6600507	11.8025849	11.7871723	x	x	x	x
	14	1.6622438	1.6600180	11.8010730	11.7870871	x	x	x	x
	15	1.6620449	1.6599913	11.7998177	11.7870153	x	x	x	x
	16	1.6618746	1.6599688	11.7987615	11.7869654	x	x	x	x
	17	1.6617272	1.6599501	11.7978667	11.7869253	x	x	x	x
	18	1.6615985	1.6599342	11.7970859	11.7868967	x	x	x	x
	19	1.6614852	1.6599205	11.7964033	11.7868681	x	x	x	x
	20	1.6613847	1.6599087	11.7958063	11.7868562	x	x	x	x

Table 7.20: Results of Coupled Cluster Singles and Doubles calculations with a HMO basis, for the 2-dimensional parabolic quantum dot with 2, 6, 12, and 20 electrons. Calculations utilizing both effective and standard interaction are performed. The oscillator frequency is given by ω , and the size of the model space is given by R . We use x to denote that convergence was not reached, and $-$ denotes that no calculation was done, mainly due to convergence problems and high run-times. The frequency and the energy are given in terms of Hartrees [E_H].

ω	R	$N = 2$		$N = 6$		$N = 12$		$N = 20$	
		Std CCSD	Eff CCSD	Std CCSD	Eff CCSD	Std CCSD	Eff CCSD	Std CCSD	Eff CCSD
0.6	10	1.9414355	1.9374704	13.5830163	13.5569972	x	x	x	x
	11	1.9409237	1.9373877	13.5794387	13.5566484	x	x	x	x
	12	1.9405126	1.9373242	13.5766596	13.5563989	x	x	x	x
	13	1.9401757	1.9372742	13.5744445	13.5562198	x	x	x	x
	14	1.9398947	1.9372339	13.5726375	13.5560972	x	x	x	x
	15	1.9396570	1.9372009	13.5711389	13.5559808	x	x	x	x
	16	1.9394534	1.9371735	13.5698737	13.5558996	x	x	x	x
	17	1.9392772	1.9371504	13.5687966	13.5558350	x	x	x	x
	18	1.9391232	1.9371308	13.5678598	13.5557830	x	x	x	x
	19	1.9389876	1.9371139	13.5670465	13.5557391	x	x	x	x
	20	1.9388674	1.9370993	13.5663312	13.5557087	x	x	x	x
0.7	10	2.2138170	2.2092656	15.2994967	15.2699298	x	x	x	x
	11	2.2132295	2.2091684	15.2953928	15.2694719	x	x	x	x
	12	2.2127575	2.2090937	15.2922076	15.2691427	x	x	x	x
	13	2.2123704	2.2090347	15.2896616	15.2689039	x	x	x	x
	14	2.2120475	2.2089873	15.2875859	15.2687276	x	x	x	x
	15	2.2117742	2.2089484	15.2858615	15.2685909	x	x	x	x
	16	2.2115401	2.2089161	15.2844087	15.2684681	x	x	x	x
	17	2.2113374	2.2088889	15.2831656	15.2683781	x	x	x	x
	18	2.2111603	2.2088658	15.2820916	15.2683047	x	x	x	x
	19	2.2110043	2.2088458	15.2811532	15.2682441	x	x	x	x
	20	2.2108658	2.2088286	15.2803347	15.2681936	x	x	x	x
0.8	10	2.4817210	2.4766317	16.9702520	16.9374786	55.6142541	x	x	x
	11	2.4810643	2.4765209	16.9656660	16.9369117	x	x	x	x
	12	2.4805365	2.4764356	16.9621042	16.9365032	x	x	x	x
	13	2.4801034	2.4763683	16.9592623	16.9362049	x	x	x	x
	14	2.4797420	2.4763141	16.9569381	16.9359775	x	x	x	x
	15	2.4794361	2.4762697	16.9550082	16.9357964	x	55.4970044	x	x
	16	2.4791739	2.4762328	16.9533793	16.9356538	x	55.4960295	x	x
	17	2.4789468	2.4762017	16.9519870	16.9355383	x	55.4952400	x	x
	18	2.4787484	2.4761752	16.9507836	16.9354434	x	55.4945887	x	x
	19	2.4785735	2.4761524	16.9497362	16.9353645	x	x	x	x
	20	2.4784183	2.4761327	16.9488122	16.9352983	x	x	x	x
0.9	10	2.7459092	2.7403243	18.6032695	18.5675774	67.5217413	60.6547962	x	x
	11	2.7451890	2.7402008	18.5982402	18.5669036	67.4984203	60.6502211	x	x
	12	2.7446098	2.7401057	18.5943353	18.5664180	67.4810303	60.6469217	x	x
	13	2.7441344	2.7400306	18.5912138	18.5660594	67.4677383	60.6445654	x	x
	14	2.7437375	2.7399700	18.5886689	18.5657850	67.4572599	60.6428248	x	x
	15	2.7434015	2.7399204	18.5865462	18.5655828	67.4487472	60.6414659	x	x
	16	2.7431134	2.7398791	18.5847570	18.5654299	67.4417244	60.6403942	x	x
	17	2.7428639	2.7398444	18.5832271	18.5652569	67.4358049	60.6395259	x	x
	18	2.7426457	2.7398148	18.5819043	18.5651374	67.4307674	60.6388116	x	x
	19	2.7424535	2.7397893	18.5807499	18.5650404	-	-	x	x
	20	2.7422828	2.7397672	18.5797339	18.5651041	-	-	x	x
1.0	10	3.0069378	3.0008954	20.2043451	20.1659808	65.8065392	65.6830761	x	x
	11	3.0061589	3.0007599	20.1989070	20.1652034	65.7841408	65.6781550	x	x
	12	3.0055324	3.0006555	20.1946825	20.1646430	65.7673051	65.6745247	x	x
	13	3.0050178	3.0005730	20.1913062	20.1642277	65.7544540	65.6719555	x	x
	14	3.0045882	3.0005065	20.1885503	20.1639098	65.7442987	65.6700471	x	x
	15	3.0042243	3.0004520	20.1862564	20.1636642	65.7360500	65.6685641	x	x
	16	3.0039123	3.0004067	20.1843190	20.1634524	65.7292334	65.6673961	x	x
	17	3.0036420	3.0003684	20.1826592	20.1632922	65.7234980	65.6664502	x	x
	18	3.0034056	3.0003359	20.1812261	20.1631504	65.7186088	65.6656707	x	x
	19	3.0031972	3.0003068	20.1799750	20.1630322	-	-	x	x
	20	3.0030122	3.0002825	20.1788722	-	-	-	x	x

Table 7.21: Results of Coupled Cluster Singles and Doubles calculations with a HMO basis, for the 2-dimensional parabolic quantum dot with 2, 6, 12, and 20 electrons. Calculations utilizing both effective and standard interaction are performed. The oscillator frequency is given by ω , and the size of the model space is given by R . We use x to denote that convergence was not reached, and $-$ denotes that no calculation was done, mainly due to convergence problems and high run-times. The frequency and the energy are given in terms of Hartrees [E_H].

ω	R	$N = 6$				$N = 12$			
		Standard interaction		Effective interaction		Standard interaction		Effective interaction	
		HF	CCSD	HF	CCSD	HF	CCSD	HF	CCSD
0.28	10	8.0195654	7.6420217	7.9503486	7.6265198	26.5544123	25.7671981	26.3556216	25.7097047
	11	8.0195654	7.6402821	7.9574337	7.6267528	26.5500256	25.7571863	26.3764354	25.7089637
	12	8.0195646	7.6389390	7.9632003	7.6269465	26.5500161	25.7512192	26.3949453	25.7095597
	13	8.0195641	7.6378740	7.9679873	7.6271116	26.5500115	25.7467104	26.4098190	25.7100520
	14	8.0195638	7.6370090	7.9720248	7.6272531	26.5500073	25.7431822	26.4220543	25.7104662
	15	8.0195637	7.6362936	7.9754762	7.6273760	26.5500056	25.7403589	26.4323047	25.7108287
	16	8.0195634	7.6356919	7.9784605	7.6274830	26.5500050	25.7380486	26.4410213	25.7111467
	17	8.0195634	7.6351796	7.9810669	7.6275772	26.5500037	25.7361228	26.4485269	25.7114264
	18	8.0195633	7.6347380	7.9833626	7.6276606	26.5500037	25.7344940	26.4550604	25.7116747
	19	8.0195633	7.6343539	7.9854003	7.6277355	26.5500036	25.7330989	26.4607996	25.7118960
	20	8.0195633	7.6340166	7.9872211	7.6278024	26.5500035	25.7318909	26.4658820	25.7120944
0.5	10	12.2713101	11.8328624	12.1927030	11.8080467	40.2161958	39.3115046	39.9947475	39.2245629
	11	12.2713082	11.8296765	12.2007369	11.8079634	40.2161389	39.2977500	40.0205019	39.2237324
	12	12.2713041	11.8272035	12.2072806	11.8079183	40.2161093	39.2875904	40.0408076	39.2231854
	13	12.2713041	11.8252330	12.2127172	11.8078980	40.2160881	39.2798074	40.0572591	39.2228307
	14	12.2713038	11.8236274	12.2173038	11.8078924	40.2160871	39.2736814	40.0708750	39.2226161
	15	12.2713038	11.8222954	12.2212257	11.8078958	40.2160833	39.2687321	40.0823267	39.2224826
	16	12.2713038	11.8211733	12.2246175	11.8079048	40.2160832	39.2646537	40.0920995	39.2224029
	17	12.2713037	11.8202157	12.2275797	11.8079164	40.2160831	39.2612375	40.1005371	39.2223594
	18	12.2713037	11.8193893	12.2301891	11.8079312	40.2160830	39.2583354	40.1078968	39.2223399
	19	12.2713037	11.8186692	12.2325052	11.8079463	40.2160828	39.2558401	40.1143733	39.2223362
	20	12.2713036	11.8180363	12.2345748	11.8079618	40.2160828	39.2536726	40.1201172	39.2223434
1.0	10	20.7192171	20.2184888	20.6294870	20.1786331	66.9120351	65.8908799	66.6596230	65.7576419
	11	20.7192154	20.2129241	20.6386575	20.1779127	66.9113645	65.8682547	66.6877593	65.7537409
	12	20.7192154	20.2085938	20.6461315	20.1773944	66.9113640	65.8512672	66.7105645	65.7509230
	13	20.7192151	20.2051315	20.6523388	20.1770091	66.9113232	65.8382374	66.7290914	65.7489566
	14	20.7192148	20.2023012	20.6575763	20.1767132	66.9113215	65.8279084	66.7445043	65.7475162
	15	20.7192147	20.1999464	20.6620548	20.1764813	66.9113214	65.8195199	66.7575087	65.7464249
	16	20.7192147	20.1979574	20.6659278	20.1762959	66.9113209	65.8125770	66.7686291	65.7455804
	17	20.7192147	20.1962562	20.6693103	20.1761453	66.9113206	65.8067336	66.7782484	65.7449093
	18	20.7192147	20.1947851	20.6722898	20.1760214	66.9113206	65.8017498	66.7866520	65.7443670
	19	20.7192147	20.1935008	20.6749343	20.1759181	66.9113206	65.7974502	66.7940568	65.7439223
	20	20.7192147	20.1923706	20.6772971	20.1758311	66.9113205	65.7937039	66.8006313	65.7435531

Table 7.22: HF and CCSD results for the 2-dimensional parabolic quantum dot with 6 and 12 electrons. These results are obtained with Gaute Hagen's CCSD code. We used a HF basis in the CCSD calculations, which were performed with standard and effective interaction. The oscillator frequency is given by ω , and the size of the model space is given by R . The frequency and the energy are given in terms of Hartrees $[E_H]$.

Chapter 8

Conclusion

In this thesis we have conducted numerical studies of systems consisting of several interacting electrons in two dimensions. These systems are known as quantum dots. We have focused on the closed shell parabolic quantum dots, where the electrons are trapped in a harmonic oscillator potential, and interact through the standard Coulomb interaction or a renormalized effective Coulomb interaction. The goal of this thesis was to improve the Coupled Cluster Singles and Doubles (CCSD) C++ code developed by Magnus Pedersen Lohne in his thesis work [2]. By improving this code we aimed to expand the model in which we could examine the quantum dots. M. P. Lohne's code was restricted to handle a maximum of 10 shells and oscillator frequencies no lower than $\omega = 0.4$. For twenty-electron quantum dots these calculations took roughly three days. Our objective was to expand the limitation of 10 shells by implementing memory-saving handling of the interaction elements, and also to implementing calculation techniques which would speed up the code. In addition to improving the CCSD machinery, we developed a Restricted Hartree-Fock (RHF) C++ code, which served to create a new basis-input and starting point for the CCSD calculations. This Hartree-Fock basis was a necessity in order to obtain energy convergence in the CCSD code for lower oscillator frequencies than $\omega = 0.4$. The overall meaning of further development of this CCSD code, was to study the reliability of the CCSD method when calculating the ground state energy of parabolic quantum dots in two dimensions. Another important goal was to consider the accuracy of the CCSD method for different sizes of the single-particle model space and for different strengths, i.e. different frequencies, of the oscillator potential.

We have studied the parabolic quantum dots under the limitations of a closed shell system. We have thus considered only the two-, six-, twelve- and twenty-electron quantum dots, with main focus on the six- and twelve-electron systems. We have calculated the ground state energies of these systems for frequencies in the range $\omega \in [0.1 - 1]$, using both the HF and the CCSD method. The frequencies $\omega = 0.28, 0.5, 1.0$ are given special attention. For the six-electron quantum dots we conducted, in addition, calculations for the two selected frequencies $\omega = 0.01$ and $\omega = 0.015625$, in order to compare with the corresponding results of other many-body methods in ref. [45]. All calculations are conducted with both the standard Coulomb interaction and the renormalized effective Coulomb interaction. We have also considered two different basis choices in our CCSD calculation. We utilized both a harmonic oscillator (HMO) basis and a Hartree-Fock (HF) basis as the basis spanning the single-particle Hilbert space.

In our analysis we found that in general we obtain better energy results when we use

the effective interaction instead of the standard Coulomb interaction. In both cases we observed that the size of the model space, i.e. the number of shells R , affects the accuracy of our result. Generally the most important correlation contributions are included in the first number of shells, a number which increases with the number of electrons in the quantum dots. However, higher shells do contribute in regard to the accuracy, but after the 20 shells we have considered, the contributions from higher-lying excitations to the CCSD method saturate. The difference between our converged CCSD results and the assumed exact DMC results, is in the range $10^{-2} - 10^{-3}$. These results agree with the CCSD results of ref. [43]. Thus, we conclude that in order to obtain better accuracy we must include higher excitations like three-particle three-hole ($3p3h$) excitations.

Our analysis also revealed that a basis change is required in order to obtain converged energy results for weak confinement potentials. The use of HMO basis did not produce converged energy results for $R \geq 10$ when $\omega < 0.4$ for the six-electron quantum dots, and $\omega < 0.9$ for the twelve-electron quantum dots. The convergence with HMO basis deteriorates with increasing electron numbers. Therefore we used a HF basis instead, which gave us converged solutions for weak confinement potentials. The HF basis allowed us to conduct calculations for confinement potentials with low frequencies in the limit of the Wigner crystal [45]. In this limit the weak potential leads to localization of the electrons, and the fear is that this will alter the Coupled Cluster ansatz for the ground state wave function. Meaning that we must perform multi-reference Coupled Cluster theory instead. However, for the frequencies $\omega = 0.01$ and $\omega = 0.015625$ we obtained CCSD energies which compare well with both the DMC and FCI results listed in ref. [45]. The differences are in the same range as above.

Future Prospects

One possible improvement of this work would be to include triples correlations, and thus expand our CCSD code to a CCSDT code. We expect that the triples yield significant better energies and error estimates compared to our CCSD results, see for example ref. [43].

An implementation of the Equation-of-Motion Coupled Cluster (EOMCC) would enable the consideration of a particle attached or removed. This would be an interesting field to explore since the limitation of closed shell systems no longer applies. If we could consider systems where one particle is added or one is removed from the closed shell, we would be able to calculate chemical potentials. Chemical potentials can be extracted from experiments, and the theoretical consideration of these systems therefore gives rise to new grounds of comparison. For example refs. [52] and [53] report experimental research on this field.

Another field of interest would be to consider the time-dependent CC theory, where one adds the external influence of for example an electromagnetic field. It is crucial to develop a proper theory that can handle these features for a better and fundamental understanding of how matter reacts to external influences.

Bibliography

- [1] T. D. Crawford and H. F. S. III, "An introduction to coupled cluster theory for computational chemists," *Reviews in Computational Chemistry*, vol. 14.
- [2] M. P. Lohne, "Coupled-cluster studies of quantum dots," Master's thesis, Department of Physics, University of Oslo, 2010.
- [3] R. H. Dicke and J. P. Wittke, *Introduction to quantum mechanics*. Addison-Wesley publishing company, INC., 1960.
- [4] A. Messiah, *Quantum Mechanics*, vol. 1. North-Holland publishing company, Amsterdam, 1961.
- [5] P. A. M. Dirac, *The principles of quantum mechanics*. Oxford University Press, second ed., 1935.
- [6] P. Hemmer, *Kvante mekanikk*. Tapir Akademiske Forlag, Tondheim, fifth ed., 2005.
- [7] R. Shankar, *Principles of Quantum Mechanics*. Plenum Press, New York, second ed., 1994.
- [8] J. M. Leinaas, "Non relativistic quantum mechanics," lecture notes, Department of Physics, University of Oslo, 2009.
- [9] D. J. Griffiths, *Introduction to Quantum Mechanics*. Pearson Education, INC., second ed., 2005.
- [10] R. D. Mattuck, *A guide to Feynman diagrams in the many-body problem*. McGraw-Hill Inc., second ed., 1976.
- [11] E. K. U. Gross, E. Runge, and O. Heinonen, *Many-Particle Theory*. Adam Hilger, 1991.
- [12] H. Anton and C. Rorres, *Elementary Linear Algebra*. John Wiley and Sons, INC, ninth ed., 2000.
- [13] W. Nolting, *Springer-verlag, Berlin*. Fundamentals of Many-Body Physics, 2009.
- [14] S. Raimes, *Many-Electron Theory*. North-Holland Publishing Company, 1972.
- [15] R. W. Knoss, ed., *Quantum Dots*. Nova science publisher, 2009.

- [16] L. Kouwenhoven and C. Marcus, "Quantum dots," *Physics World*, vol. 11, no. 6, 1998.
- [17] L. E. Lervaag, "Vmc calculations of two-dimensional quantum dots," Master's thesis, Department of Physics, University of Oslo, 2010.
- [18] E. Waltersson and E. Lindroth, "Many-body perturbation theory calculations on circular quantum dots," *Phys. Rev. B*, vol. 76, no. 045314, 2007.
- [19] P. Matagne, J. P. Leburton, D. G. Austing, and S. Tarucha, "Shell charging and spin-filling sequences in realistic vertical quantum dots," *Phys. Rev. B*, vol. 65, no. 085325, 2002.
- [20] A. Kumar, S. E. Laux, and F. Stern, "Electron states in a gaas quantum dot in magnetic field," *Phys. Rev. B*, vol. 42, no. 5166, 1990.
- [21] J. M. Leinaas, "Lecture notes fys3120." Department of Physics, University of Oslo, 2011.
- [22] S. M. Reimann and M. Manninen, "Electronic structure of quantum dots," *Rev. Mod. Phys.*, vol. 74, no. 1283, 2002.
- [23] M. Taut, "Two electrons in a homogeneous magnetic field: particular analytic solution," *J. Phys. A: Math. Gen.*, vol. 27, no. 1045, 1994.
- [24] M. B. Tavernier, E. Anisimovas, F. M. Peeters, B. Szafran, J. Adamowski, and S. Bednarek, "Four-electron quntum dot in magnetic fiels," *Phys. Rev. B*, vol. 68, no. 205305, 2003.
- [25] J. M. Thijssen, *Computational Physics*. Cambridge University Press, second ed., 2007.
- [26] R. A. Adams, *Calculus*. Pearson Educating Canada Inc., fifth ed., 2003.
- [27] J. Čížek, "On the correlation problems in atom and molecular systems," *Journal of Chemical Physics*, vol. 45, no. 4256, 1966.
- [28] J. Čížek, "On the use of the cluster expansion and the technique of diagrams in calculations of correlation effects in atoms and molecules," *Advances in Chemical Physics*, vol. 14, no. 35, 1969.
- [29] J. Čížek and J. Paldus, "Correlation problems in atomic and molecular systems iii. rederivation of the coupled-pair many-electron theory using the traditional quantum chemical methodst," *Int. J. quantum chem.*, vol. 5, no. 359, 1971.
- [30] A. C. Hurley, *Electron correlation in small molecules*. Academic Press, London, 1976.
- [31] H. J. Monkhorst *Int. J. quantum chem. Symp.*, vol. 11, no. 421, 1977.
- [32] J. A. Pople, R. Krishnan, H. B. Schlegeland, and J. S. Binkley *Int. J. quantum chem. Symp.*, vol. 14, no. 545, 1978.

-
- [33] R. J. Bartlett and G. D. Purvis *Int. J. quantum chem.*, vol. 14, no. 561, 1978.
- [34] G. D. Purvis and R. J. Bartlett *J. Chem. Phys.*, vol. 76, no. 1910, 1982.
- [35] I. Shavitt and R. J. Bartlett, *Many-body methods in chemistry and physics*, ch. 9-13. Cambridge University Press, New York, 2009.
- [36] F. E. Harris, H. J. Monkhorst, and D. L. Freeman, *Algebraic and Diagrammatic Methods in Many-Fermion Theory*. Oxford University Press, 1992.
- [37] A. Szabo and N. S. Ostlund, *Modern Quantum Chemistry*. No. 68, Dover Publications, 1996.
- [38] S. A. Kucharski and R. J. Bartlett, “Fifth-order many-body perturbation theory and its relations to various coupled cluster approaches,” *Adv. Quantum Chem*, vol. 18, no. 281, 1986.
- [39] B. Stroustrup, *The C++ Programming Language*. Addison Wesley, special ed., 2009.
- [40] H. P. Langtangen, *Python Scripting in Computational Science*. Springer, 2001.
- [41] S. Kvaal, *Analysis of many-body methods for quantum dots*. PhD thesis, University of Oslo, 2009.
- [42] W. H. Press, S. A. Teukolsky, W. T. Vetterling, and B. P. Flannery, *Numerical Recipes*. Cambridge University Press.
- [43] M. P. Lohne, G. Hagen, M. Hjorth-Jensen, S. Kvaal, and F. Pedervia, “Ab initio computation of circular quantum dots.” Unpublished, 2010.
- [44] M. Rontani. PhD thesis, Università degli Studi di Modena e Reggio Emilia, 1999.
- [45] A. Ghosal and et al., “Incipient wigner localization in circular quantum dots,” *Phys. rev. B*, vol. 76, no. 085341, 2007.
- [46] P. Navrátil, J. P. Vary, and B. R. Barrett *Phys. Rev. C*, vol. 62, no. 054311, 2000.
- [47] D. Dean, T. Engeland, M. Hjorth-Jensen, M. Kartamyshev, and E. Osnes *Prog. Part. Nucl. Phys.*, vol. 53, no. 419, 2004.
- [48] E. Caurier, G. Martinez-Pinedo, F. Nowacki, A. Poves, and A. P. Zuker *Rev. Mod. Phys.*, vol. 77, no. 427, 2005.
- [49] S. Kvaal, “Geometry of effective hamiltonians,” *Phys. Rev. C*, vol. 78, no. 044330, 2008.
- [50] S. Kvaal, “Open source fci code for quantum dots and effective interactions,” *ArXiv e-prints*, no. arXiv:0810.2644v1, 2008.
- [51] S. Kvaal *Phys. Rev. B*, vol. 80, no. 045321, 2009.
- [52] S. Sasaki, D. G. Austing, and S. Tarucha *Physica B*, vol. 256, no. 157, 1998.
- [53] S. Tarucha, D. G. Austing, T. Honda, R. J. van der Hage, and L. P. Kouwenhoven *Phys. Rev. Lett.*, vol. 77, no. 3613, 1996.